Role of Tau and NRF2 in Oxidative Stress Responses

Belinda Ameyaw
Magdalen College

A thesis submitted for the degree of
Doctor of Philosophy
Hilary Term 2024

DECLARATION

This studentship was funded by the Medical Research Council as an iCase project in collaboration and co-funded with the Novo Nordisk Research Centre Oxford. Unless otherwise stated, the projects were undertaken at the Centre for Human Genetics (CHG; until November 2023, the Wellcome Centre for Human Genetics) and its core facilities, within the Nuffield Department of Medicine, at the University of Oxford. The data presented here is my work with the support of the following:

The fluorescent in situ hybridisation of the SH-SY5Y cells was performed by Dr Daniela Moralli. Flow cytometric sorting of the CRISPR-CAS9 edits in the SH-SY5Y was performed under the supervision of Dr Ruddy Montandon, with the whole genome sequencing data generated by the CHG core facility. Analyses of the sequence data was undertaken by the DPhil student, Jia-Yuan Zhang. The proteomic data was generated by the Rasler laboratory at the Universitätsmedizin Berlin and analysed by me.

Transcriptomic sequencing data was generated from the podocytes by the CHG core facility and analysed by Dr Fiona Hamey. The proteomic data from CRISPR-dCAS9 gene editing of the podocytes was generated by the Discovery Proteomics Facility of the Target Discovery Institute, which is also part of the Nuffield Department of Medicine, and analysed by me.

Both the wildtype and *MAPT* knockout kidney organoids were produced by Dr Phalguni Rath with the immunofluorescent validations undertaken by me. The 232P cell lines were a gift from The Laboratory of Aging Disorders at the Ente Ospedaliero Cantonale, Switzerland.

The thesis is 51,000 words and has been submitted to the University of Oxford for the degree of Doctor of Philosophy in Clinical Medicine and no part has been submitted for any other degree at this or any other university.

ACKNOWLEDGEMENTS

I am grateful to my supervisors – Professor John Todd and Dr Katherine Bull – for their support during the course of my DPhil. Their continuous patience and encouragement have been instrumental in my progress.

I am also grateful to the MRC, Novo Nordisk and the JDRF/Wellcome Diabetes and Inflammation Laboratory for the funding to undertake this project.

I would also like to thank both past and present members of the Todd/Wicker, Bull, Cornall and O'Callaghan laboratories: Aneesha, Rose, Jessica, Tanya, Tom, Jie, Jianwei, Jenny, Mukta, Shannah and Ailsa. It was always reassuring to know that you were available to answer any questions I had.

Finally, I would like to thank my family and friends: John, Irene, Thomas, Audrey, Teddy, Ese, Seugnet and Richard for your constant encouragement without which I could not have made it this far.

ABSTRACT

Diabetic kidney disease (DKD) is a complication of diabetes with significant morbidity and limited therapeutic options. With increasing diabetes prevalence there is an urgent need for better understanding of DKD pathogenesis with the goal of identifying more effective treatments and prevention approaches. Oxidative stress is a known contributor to DKD, but efforts to target this by pharmacological upregulation of the antioxidant transcription factor Nuclear factor-erythroid factor 2-related factor 2 (NRF2) in DKD clinical trials have not led to new therapeutics. This project investigated how oxidative stress influences DKD, with three key objectives and findings:

a) **I characterised the effects of oxidative stress in podocytes**, finding evidence for a bimodal effect of NRF2, and the identification of new candidate NRF2-regulated genes. Pharmacological induction of NRF2 in the podocytes using NRF2 agonist CDDO-Im or NRF2 activation/inhibition with CRISPR-dCAS9 were assessed for their effect on tBHP-induced stress induction: both a 50% inhibition of NRF2 expression or exposure to 30 nM CDDO-Im for 6 hours were found to be protective.

b) **I identified a novel role for the Microtubulin Associated Protein Tau (*MAPT)* gene in protection against oxidative stress.** In immortalised human podocytes, *MAPT* transcriptomic expression increased with tBHP-induced oxidative stress. In the neuroblastoma cell line SH-SY5Y, which expresses high levels of Tau, Tau KO led to increased oxidative stress, reversible by re-expressing Tau, but not fully rescued by NRF2 upregulation or microtubule stabilisation.

c) I began to develop **a more physiological model for the analysis of Tau-associated oxidative stress**, by deletion of *MAPT* in induced pluripotent stem cells (iPSC), and optimisation of my oxidative stress assay in human iPSC-derived kidney organoids.

LIST OF ABBREVIATIONS

ACE Angiotensin Converting Enzyme
ACTA1 Actin alpha 1
ACTB Actin beta
AD Alzheimer's Disease
ADAM17 A disintegrin and metalloprotease 17
AGE Advanced Glycation End-products
ALDOA Aldolase fructose bisphosphate A
ARE Antioxidant Response Elements
ARPC3 Actin related protein 2/3 complex subunit 3
ATXN7L3B Ataxin 7 like 3B
BSA Bovine Serum Albumin
CDDO-Im 2-cyano-3,12 dioxooleana-1,9 diene-28-imidazolide
CDH1 Cadherin 1
CDH2 Cadherin 2
cDNA complementary deoxyribonucleic acid
CEBPB CCAAT enhancer binding protein
CHG Centre for Human Genetics
CKD Chronic Kidney Disease
COL2A1 Collagen, type II, alpha 1
COL4A3 Collagen type IV alpha 3 chain
CRISPR Clustered regularly interspaced short palindromic repeats
CRISPR KRAB Clustered regularly interspaced short palindromic repeats Kruppel-associated box
CRISPR SAM Clustered regularly interspaced short palindromic repeats synergistic activation mediator system
Ct Cycle threshold
DAMPS Damage associated molecular patterns
DAPI 4′,6-diamidino-2-phenylindole
DCLK1 Doublecortin like kinase 1
DDX17 Dead box helicase 17
DEPC Diethyl pyrocarbonate
DIA Data independent acquisition
DKD Diabetic Kidney Disease
DLGAP4 Disc large homology associated protein 4
DM Diabetes mellitus
DMEM Dulbecco's Modified Eagle's Medium
DMSO Dimethyl sulfoxide
DN Diabetic nephropathy
DNA Deoxyribonucleic acid
DNPH 2,4-Dinitrophenylhydrazine
EDTA Ethylenediaminetetraacetic acid
eGFR Estimated Glomerular Filtration Rate
eNOS Endothelial Nitric Oxide Synthase
EPCAM Epithelial cellular adhesion molecule
FAIM Fas apoptotic inhibitory molecule
FAM98A Family with sequence similarity 98-member A
FBLIM1 Filamin binding LIM 1

FCS Foetal cattle serum
FDR False discovery rate
FP Foot Process
FUS Fused in sarcoma
GABRR1 Gamma aminobutyric acid type A receptor
GAPDH Glyceraldehyde 3-phosphate dehydrogenase
GATA 3 GATA Binding Protein 3
GBM Glomerular Basement Membrane
GCLM Glutamate-Cysteine Ligase Modifier Subunit.
GCLM Glutamate cysteine ligase modifier
GCS γ-Glutamine Cysteine Synthase
GO Gene Ontology
HIF1A Hypoxia inducible factor 1 subunit alpha
HINT1 histidine triad nucleotide binding protein 1
HMGCR 3-hydroxy-3-methylglutaryl-CoA reductase
HMOX1 Heme Oxygenase 1
hnRNP U Heterogeneous nuclear ribonucleoprotein particle U
ID1 DNA binding protein inhibitor 1
IF Immunofluorescence
IL6 Interleukin 6
iPSC Induced Pluripotent Stem Cell
IR Insulin Receptor
ITGB1 Integrin subunit beta 1
KEAP-1 Kelch-like ECH-Associated Protein 1
KIF1A Kinesin family member 1A
KIF21B Kinesin family member 21 B
KKS kallikrein-kinin system
KLHL13 Kelch Like Family Member 13
KLHL13 Kelch like family member 13
KLHL9 Kelch Like Family Member 9
KLHL9 Kelch like family members9
KO Knockout
KRT1 Keratin 1
LCP1 Lymphocyte cytosolic protein 1
LRP2 Low density lipoprotein receptor-related protein 2
MACF1 microtubule actin crosslinking factor 1
MAPT Microtubulin Associated Protein Tau
MDA Malondialdehyde
MMP2 Matrix Metalloprotease 2
MS Mass spectrometry
MYH9 Myosin heavy polypeptide 9
NADH Nicotinamide adenine dinucleotide
NADPH Nicotinamide adenine dinucleotide phosphate
NFE2L2 Nuclear factor erythroid 2-related factor 2
NLRP3 NOD-like receptor pyrin domain 3
NO Nitric Oxide
NOD Non-Obese Diabetic
NOS Nitric Oxide Synthase
NOX Nicotinamide adenine dinucleotide phosphate oxidase
NQO1 NAD(P)H Quinone Dehydrogenase 1

NRF2 Nuclear factor-erythroid factor 2-related factor 2
PCA Principal component analysis
PCR polymerase chain reaction
PFH Protein free hybridoma
PKC Protein Kinase C
PVDF Polyvinylidene difluoride
PVDF Polyvinylidene difluoride
qPCR Quantitative polymerase chain reaction
RAAS Renin Angiotensin Aldosterone System
RAB1A Ras-related protein Rab-1A
RAGE Receptors for Advanced Glycosylation End-products
RIPA Radioimmunoprecipitation assay
RNA Ribonucleic acid
RNA-Seq Ribonucleic acid sequencing
ROS Reactive Oxygen Species
SD Slit Diaphragm
SDS sodium dodecyl sulphate
SEM standard error of the mean
SEPTIN2 Septin 2
SERPINA 1 Serpin family A member 1
SFN Stratifin
SGLT2 Sodium Glucose Co-Transporter 2
SHMT1 Serine hydroxymethyltransferase 1
snRNP70 U1 small nuclear ribonucleoprotein
SOX 17 SRY-box transcription factor 17
SQLE Squalene
SREBF2 Sterol regulatory element binding transcription factor 2
SRSF2 Serine and arginine rich splicing factor 2
SRSF2 Serine and arginine rich splicing factor 2
STAT3 Signal transducer and activator of transcription 3
SYNPO Synaptopodin
T1D Type 1 diabetes
T2D Type 2 diabetes
Tau Tubulin Associated Unit
tBHP Tert-butyl hydroperoxide
TBS Tris-buffered saline
TBST Tris-buffered saline (TBS) supplemented with 0.1% Tween-20
TCA Trichloroacetic Acid
TENM2 Teneurin Transmembrane Protein 1
TGFβ Transforming Growth Factor Beta
TLR Toll Like Receptor
TNFR1 Tumour Necrosis Factor Receptor 1
TUBB1 Tubulin beta 1 chain
TUBB4A Tubulin beta 4 chain
TXNRD1 Thioredoxin reductase 1
TXNRD1 Thioredoxin reductase 1
UMOD Uromodulin
WT Wild type
WT1 Wilms' tumour gene 1
ZNF90 Zinc finger protein 90

Chapter 1
Introduction

Diabetes is a chronic metabolic disorder characterised by defects in the body's ability to regulate glucose and maintain insulin homeostasis (Gupta et al., 2023). Over 500 million adults were living with diabetes as of 2021, an increase of approximately 29% from 2015, though as many as half these people are unaware of their diagnosis (Collaborators, 2023).

There are two main subtypes of diabetes, type 1 diabetes (T1D), classified as a failure of insulin production due to autoimmune damage to the pancreatic β cells, and type 2 diabetes (T2D), due to insulin resistance and failure of β-cell insulin production. T2D accounts for 90% or more of all cases (Galicia-Garcia et al., 2020). While the aetiology and management of T1D and T2D differ, diabetic kidney disease (DKD) is a chronic complication affecting 30-40% of people with both T1D and T2D.

Enhancing our understanding of the physiological changes occurring in a diabetic milieu, such as haemodynamic alterations, hormonal imbalances and protein glycation, is thus a crucial focus for research, as insights into the pathogenesis of diabetic complications can identify new avenues for treatment and disease management.

In this thesis, I focus on the role of oxidative stress, a key characteristic of a diabetic tissue environment and linked to DKD. I explore the pathways involved in oxidative damage in renal podocytes, with particular focus on the antioxidant transcription factor Nuclear factor-erythroid factor 2-related factor 2 (NRF2), and characterise a new role for the microtubule binding protein Tau in oxidative injury.

1.1 Definition and diagnosis of diabetic kidney disease

Most of the burden of diabetes, 80% of cases, is borne by lower- and middle-income countries, where prevalence is rising faster than in high-income regions, often in the context

of limited resources to manage diabetes and its complications. By 2045, 1 in 8 adults, or nearly 800 million people will be living with diabetes, with the rise in T2D driven by increasing levels of obesity (Sun et al., 2022) (Koye et al., 2018).

With this increasing prevalence comes an increase in complications such as diabetic retinopathy, cardiovascular disease and DKD (Gheith et al., 2016b) (Teo et al., 2021) (Wei et al., 1998). The 10-year mortality with diabetes is estimated at 11.5%, rising to 31.1% with chronic kidney disease (CKD) alongside diabetes (Afkarian et al., 2013). A large prospective study in Mexico City, where access to diabetic drugs is limited, showed that people living with diabetes for more than 10 years have a 12-fold increase in mortality compared to the general population, with the steepest increase in deaths due to renal disease (Herrington et al., 2018). In the UK, despite access to drugs for glycaemic control, there are nearly 14,000 deaths related to diabetes annually, with over 22,000 people living with diabetes requiring dialysis or a kidney transplant, and diabetes responsible for 530 myocardial infarctions every week. Diabetes is estimated to cost the NHS at least £10 billion per year, equivalent to 10% of its entire budget (Whicher et al., 2020) (UK Renal Registry, 2022).

DKD is the most common cause of renal failure worldwide. Diagnosis is usually clinical, defined by the presence of albuminuria (≥3.4 mg/mmol) and progressive reduction in estimated glomerular filtration rate (eGFR) in the context of diabetes (> 10 yrs duration of T1D, may be present at diagnosis in T2D) and in the absence of signs or symptoms of other primary causes of kidney disease (American Diabetes Association, 2022). In most cases therefore a renal biopsy for histological diagnosis is not performed (Sugahara et al., 2021). The calculation of eGFR uses the reciprocal of serum creatinine and factors such as age, gender and historically ethnicity (Levey et al., 2009) (Gama et al., 2021)

1.2 The structure and function of the renal glomerulus

The human kidney contains around 1 million nephrons. Each nephron comprises a renal corpuscle, made up of a glomerulus containing a bundle of capillaries surrounded by Bowman's capsule, and a renal tubule (Figure 1.1). The glomerular filtration barrier is a tripartite structure consisting of a basement membrane, fenestrated endothelial cells and the interdigitating podocyte cells (Pollak et al., 2014) (Haraldsson et al., 2008). Within the glomerular structure, there are also mesangial cells which form the vascular pole, and parietal epithelial cells lining Bowman's capsule. The glomerular filtration unit functions to allow the passage of water, electrolytes and small molecules into the urinary space or filtrate, while preventing the loss of larger proteins from the blood space.

1.1

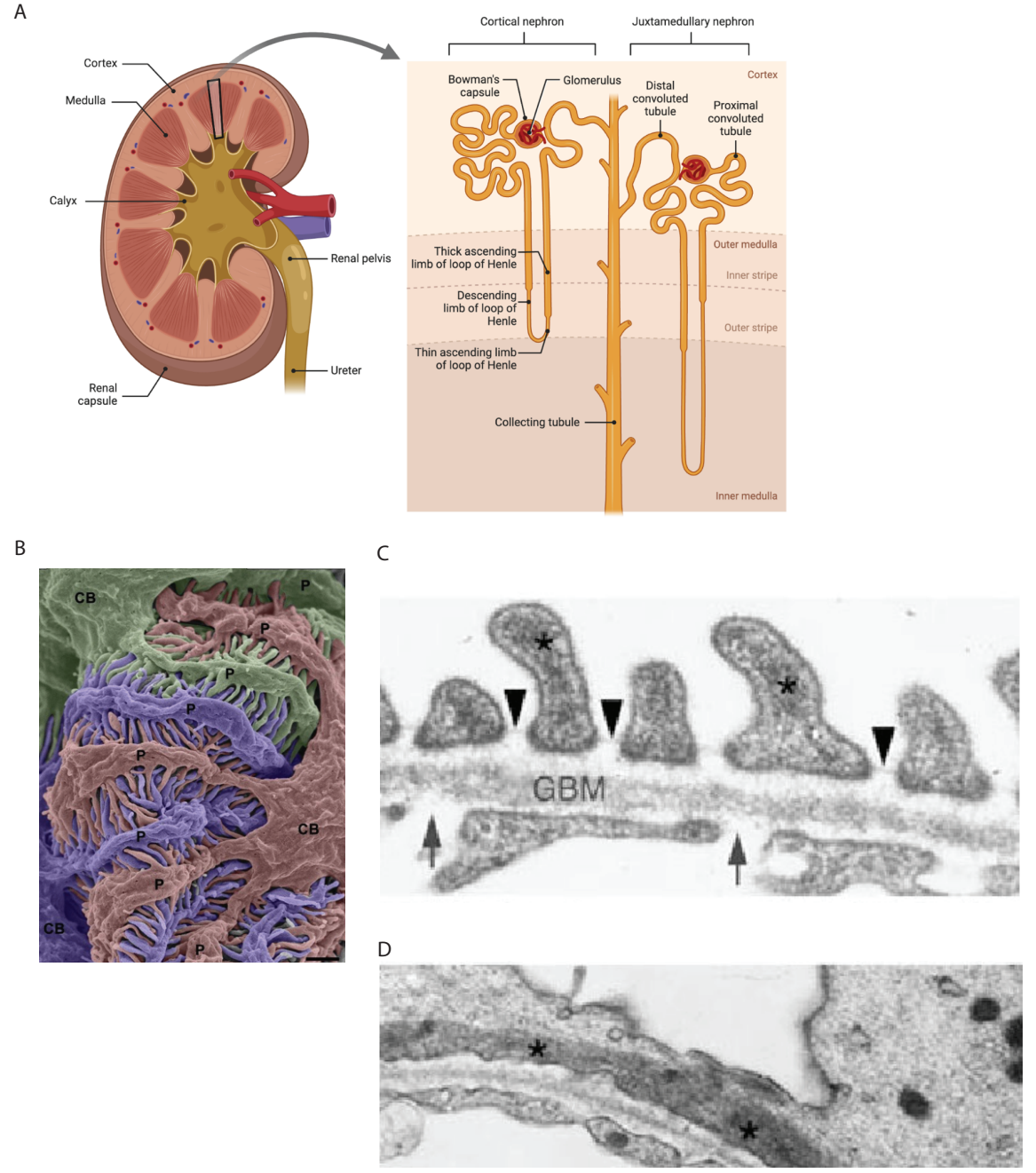

Figure 1.1 A. Gross anatomy of the human kidney and structure of the nephron **Source**: (Dewangan, 2023) **B.** Scanning electron micrograph showing podocyte morphology. **Source:** (Ichimura et al., 2015). CB = Cell body; P – primary process. **C-D** Transmission electron micrographs of the human glomerular capillary wall. **C** Healthy kidney with arrows indicating endothelial fenestrations, arrowheads represent filtration slits between podocyte foot processes and asterisks indicate actin filaments in podocyte cytoplasm. **D** Proteinuric kidney with podocytes undergoing effacement and flattening of the actin filaments – indicated with asterisks. GBM – glomerular basement membrane **Source**: (Mathieson, 2012)

1.2.1 Glomerular endothelial cells

The first part of the glomerular filtration barrier is the endothelial cells lining the glomerular capillaries. These are fenestrated, with 60-80 nm transcellular holes for water permeability, and coated in a negatively-charged glycocalyx which is thought to contribute to the charge selectivity of the glomerular filtration barrier (Bohrer et al., 1978). Molecules that cross this barrier must then navigate the thick extracellular glomerular basement membrane (GBM) comprised of type 4 collagen, laminins, nidogen and heparin sulphate proteoglycans. This extracellular material is synthesised by both endothelial cells and the podocytes.

1.2.2 Podocytes

Podocytes are highly specialised, terminally differentiated visceral epithelial cells that form a layer around the glomerular capillaries due to their complex network of long interdigitating foot processes (FP) (Figure 1.1B).

Under physiological conditions, podocytes show minimal expression of proliferation-associated markers such as Ki-67, Cyclin A and Cyclin B1 and an instead express cyclin-dependent kinase inhibitor p57 (Nagata et al., 1998) (Shankland and Wolf, 2000) (Pavenstadt et al., 2003). However, the conventional idea that podocytes do not regenerate in adults has been challenged by evidence from genetic fate mapping studies in mice suggesting that following injury and podocyte loss, podocytes can partially be replaced by the parietal epithelial cells that populate Bowman's capsule (Wanner et al., 2014). Differentiated podocytes consist of a cell body and major processes that extend outward to form interdigitating FPs encircling the glomerular capillaries. Differentiated podocytes have both cytoplasmic microtubules and actin-like microfilaments. Between the interdigitating FPs lies the slit diaphragm (SD), essential for solute efflux across the glomerular wall (Andrews, 1981) (Kriz et al., 1994). This SD is made up of key podocyte-specific proteins including

Nephrin, Podocin, Synaptopodin and Neph1 (Boute et al., 2000) (Lenkkeri et al., 1999) (Mundel et al., 1991) (Kestilä et al., 1998) (Mundel et al., 1997). The SD is a critical component of the filtration barrier, such that genetic absence of nephrin or podocin results in severe early-onset proteinuric kidney disease (Welsh and Saleem, 2011) (Martin and Jones, 2018). Nephrin, encoded by *NPHS1,* is the main extracellular SD protein (Ruotsalainen et al., 1999), and via phosphorylation it complexes with binding partners such as CD2AP as a signalling scaffold (Shih et al., 2001). This signalling is supported by direct interactions with the lipid raft-associated podocin, encoded by *NPHS2,* which multimerises to recruit lipids to the plasma membrane (Schwarz et al., 2001). Transmembrane Neph1 similarly contributes to both the SD and intracellular actin signalling, and interacts with junctional protein ZO-1, supporting SD integrity (Sagar et al., 2017) (Ning et al., 2020) Actin-binding synaptopodin may regulate podocyte actin-cytoskeletal dynamics via Rho GTPase, although the lack of phenotype in unchallenged synaptopodin knock-out mice suggests this function may be required only in the context of renal injury (Ning et al., 2020).

1.2.3 Mesangial cells

The mesangial cells are specialised pericytes that maintain the single nephron glomerular filtration rate due to their contractile properties and contribute to the function of the nephron via phagocytosis, clearing macromolecules that have managed to cross the endothelial barrier (Ziegler et al., 2021) (He et al., 2021). Thus, contributing to the glomerular charge and size selective barrier, filtering blood while preventing the loss of molecules larger than 70 kDa.

1.2.4 The renal tubules

Approximately 150 L of urinary filtrate are generated per day, so the renal tubule must reabsorb most of the filtered salt and water, this occurs predominantly in the proximal tubule. More distally in the tubule, further salt and water reabsorption is precisely modulated to

maintain fluid and electrolyte homeostasis, and the tubule also provides metabolic regulation of acid base balance.

1.3 Risk factors for diabetic kidney disease

DKD develops in 30- 40% of people with both T1D and T2D and the risk is higher with duration of diabetes, poor glycaemic control, hypertension, smoking or family history (Brancati et al., 1997). Genome-wide association studies have identified a small number of genes associated with DKD, for example *TENM2*, *DCLK1* and *GABRR1* (Sandholm et al., 2022) (van Zuydam et al., 2018). These associations include genes linked to known basement membrane disease such as *COL4A3,* and tubulointerstitial disease, such as *UMOD* (van Zuydam et al., 2018) (Salem et al., 2019).

1.4 Renal Glomerular changes in diabetic kidney disease

In this section current understanding of the roles of specific renal structures in diabetic renal damage is described.

1.4.1 Histological changes in diabetic kidney disease

The diabetic milieu alters renal morphology, generating a distinct constellation of structural changes, even if individually these changes could be observed in other renal disorders (Fioretto and Mauer, 2007). Some of these alterations, such as basement membrane thickening and podocyte effacement, are postulated to underlie renal insufficiency due to their importance in maintaining the integrity of the kidney filtration barrier. Others, such as the appearance of Kimmelstiel-Wilson nodules and mesangial expansion impact the overall integrity of the glomeruli with or without directly affecting the morphology of a component of the filtration barrier (Zhou et al., 2022) (Fioretto et al., 1994).

1.4.2 The glomerular basement membrane in diabetic kidney disease

Disruptions to the GBM are an early indicator of renal damage. Dysfunction or loss of GBM proteins including laminin and Collagen 4 are known causes of monogenic proteinuric kidney disease (Bull et al., 2014) (Barker, 1990). Basement membrane components including collagenous (type IV collagen) and non-collagenous (glycoproteins laminin and nidogen and the heparan sulfate proteoglycan agrin) molecules are altered in diabetes. For instance, there is an overproduction of the collagen amino acid hydroxylysine and decreased expression of laminin and heparan sulfate in people living with diabetes relative to those not living with diabetes (Beisswenger and Spiro, 1973) (Shimomura and Spiro, 1987). Basement membrane thickening can precede albuminuria – in T1D, glomerular basement thickening can be observed as early as 1.5 to 2 years from disease onset despite normoalbuminuria (Østerby, 1972) (Saxena et al., 2008), suggesting that GBM changes may be very early step in DKD pathogenesis, but a causative mechanism is not fully understood.

1.4.3 Glomerular endothelial cells in diabetic kidney disease

Glomerular endothelial cells have a negatively charged glycocalyx layer on their luminal surface consisting of proteoglycans bound to the glycosaminoglycans heparan sulphate, and hyaluronan that is suggested to aid permselectivity (Oohira et al., 1983) (Dane et al., 2015) (Florian et al., 2003) (Bohrer et al., 1978). In both T1D and T2D, evidence of decreased endothelial fenestration has been observed, alongside the development of proteinuria and decreased GFR (Weil et al., 2012) (Toyoda et al., 2007) , and it has been suggested that a deviation in the net charge of the epithelial cells could be an important component of disease pathology, due to impaired repulsion of polyanions including albumin (Chang et al., 1975) (Guimarães et al., 2003) (Osicka et al., 1996). Experimental data on immortalised glomerular endothelial cells exposed to high glucose concentrations showed they had decreased

expression of heparan sulfate with an associated increase in albumin permeability (Singh et al., 2011). However, although murine conditional KOs of the heparan sulfate agrin gene have severe glomerular basement membrane charge defects, they show no abnormalities in filtration (Harvey et al., 2007).

1.4.4 Podocytes and diabetic kidney disease

Since podocytes are largely irreplaceable, podocyte loss is a key contributor to renal damage in proteinuric diseases. Indeed, most monogenic forms of nephrotic syndrome, a severe form of proteinuria, are due to mutations in podocyte-specific genes (Preston et al., 2019). In both T1D and T2D with microalbuminuria, the expression of the podocyte slit diaphragm-specific protein nephrin in the kidney is lower than in healthy controls and changes from a punctate to a granular cellular distribution (Doublier et al., 2003). Podocin and synaptopodin are also less abundant in biopsies of T2D patients with DKD (Langham et al., 2002), while urinary podocyte mRNAs are detectable in T2D prior to the development of microalbuminuria (Fukuda et al., 2020). Observational data, initially in Pima Indians with T2D, shows a correlation between podocyte loss, proteinuria and glomerulosclerosis (Pagtalunan et al., 1997). Taken together these findings indicate that podocyte damage and loss are early changes in DKD and contribute to progression and renal damage.

In DKD podocytes undergo effacement. This term describes a flattening, retraction, widening and shortening of foot processes. A gradual simplification of interdigitation results in a loss of the slit diaphragms, by electron microscopy these changes result in replacement of distinct foot process architecture with a flat cytoplasmic layer (Fig 1.1C and D). Effacement involves several changes in the podocytes which limit their normal function as part of the filtration barrier. For example, involving de-differentiation, sometimes considered as an epithelial to

mesenchymal transition, with reduced expression of specific markers such as nephrin, and an increase in mesenchymal markers such as vimentin and nestin, alongside an increase in cellular proliferation (Herman-Edelstein et al., 2011). These changes disrupt the slit diaphragm, and thus the integrity of the selective filtration barrier. Additionally, effacing podocytes exhibit increased apoptosis, dependent on an increase in TGF-beta (TGF- β) expression, via increased expression of both mitogen-activated protein kinase p38 and caspase-3 (Schiffer et al., 2001) (Li et al., 2004).

1.4.4.1 Effects of hyperglycaemia and insulin on podocytes

In vitro models offer some insights into the mechanism by which a hyperglycaemic environment could induce podocyte effacement: in cultured mouse podocytes hyperglycaemia-dependent hypertrophy is itself dependent on parathyroid hormone-related protein (PTHrP) (Romero et al., 2010). Cultured human podocytes exposed to high glucose (20 mM) undergo de-differentiation and a switch from oxidative phosphorylation to lactic acidosis, with altered expression of regulators of oxidative metabolism. This is dependent on reduced expression of myocyte-specific enhancer factor 2C (MEF2C) and myogenic factor (MYF5), with a similar profile observed in the human diabetic kidney (Imasawa et al., 2017). Podocytes express insulin receptor (IR) and are insulin sensitive, able to rapidly increase cellular glucose uptake via GLUT1 and GLUT4 in response to insulin (Coward et al., 2005). Prolonged exposure of both human conditionally immortalised and primary murine podocytes to a 'diabetic' environment *in vitro*, with high glucose plus high insulin, TNF and IL-6, results in insulin resistance via IR protein degradation (Lay et al., 2017). Podocyte-specific deficiency in GLUT4 in db/db mice, a diabetic mouse model that is protected from glomerular hypertrophy, suggests a direct role for hyperglycaemia in DKD via the podocyte (Guzman et al., 2014).

In addition to the central role for podocytopathy, the development of DKD may also be influenced by adaptation and sclerosis of mesangial cells, and later in disease progression may depend in part on the extent of tubular damage (Alsaad and Herzenberg, 2007). However, given the central role podocyte loss has in DKD I chose to initially focus on these cells for the research presented in this thesis.

1.5 The pathogenic basis of diabetic kidney disease

Diabetes is associated with microvascular and macrovascular damage affecting the muscle, skin, eyes, heart, brain and kidneys. Nearly all patients with T1D and two thirds of T2D patients develop retinopathy (Scanlon, 2008) (Mathur et al., 2004). In comparison, between 20% and 40% of people living with diabetes develop DKD (Gheith et al., 2016a) (Jefferson et al., 2008). Hyperglycaemia induces specific metabolic and non-metabolic changes affecting both the vasculature and tissues directly and underlying DKD pathology. These can be broadly divided into haemodynamic changes, inflammation and metabolic factors including oxidative stress. Whilst acknowledging that these factors overlap and interact, I will here consider them in turn with an emphasis on oxidative stress given its relevance to the aims of this thesis.

Understanding these factors is could be essential in identifying novel DKD treatments and in the repurposing of existing ones for DKD management.

1.5.1 Haemodynamic changes – hypertension and hyperfiltration

Atherosclerosis, vascular inflammation, endothelial dysfunction and structural remodelling lead to micro- and macrovascular complications (Petrie et al., 2018). This vascular injury is itself driven by hyperglycaemia via reactive oxygen species (ROS), intracellular production

of advanced glycation end-products (AGE) and protein kinase C (PKC) (Brownlee, 2005). Oxidative injury will be discussed in more detail in section 1.5.3.

High blood pressure promotes the loss of kidney function while DKD enhances the likelihood of increased blood pressure (BP) (Harjutsalo and Groop, 2014).

The latter is due to the central role of the kidneys in BP regulation, controlling sodium handling and thus intravascular volume via mechanisms including the renin-angiotensin-aldosterone system (RAAS). RAAS blockade is an established treatment that reduces proteinuria and slows the progression of diabetic nephropathy (Brenner et al., 2001).

Both systemic hypertension and raised intraglomerular pressure contribute to kidney damage in diabetes. Systemic hypertension commonly co-exists with diabetes, with both diseases sharing risk factors including obesity and dyslipidaemia. Hypertension promotes hyperfiltration, one of the earliest signs of DKD. Glomerular hyperfiltration refers to either a filtration rate of between 125 ml/min/1.73m^2 to 175 ml/min/1.73m^2 or a filtration fraction of above 18.7± 3.2% depending on whether the emphasis is on the whole kidney or single nephron hyperfiltration (Huang et al., 2011) (Helal et al., 2012) (Tonneijck et al., 2017). In animal studies, glomerular hypertrophy precedes hyperfiltration, associated with hyperglycaemic induction of somatostatin, insulin growth factors and insulin growth factor binding proteins (Flyvbjerg et al., 1999) (Flyvbjerg et al., 1989). In T2D, hyperfiltration, inferred by initially high eGFR, is associated with later DKD progression and an increase in all-cause mortality (Penno et al., 2020) (Magee et al., 2009) (Cherney et al., 2014) (Ruggenenti et al., 2012).

The pathogenesis of glomerular hyperfiltration is complex but can occur due to either a net reduction in the afferent glomerular arteriolar resistance or a net increase in the efferent

arteriolar resistance, in either case resulting in increased intraglomerular pressure. This is influenced by angiotensin II, the difference between the mean pressures of the glomerular capillary and the proximal tubule (transmembrane hydraulic pressure gradient) and the permeability and area of the filtration surface as determined by the ultrafiltration coefficient (Cherney et al., 2014).

Reductions in proinsulin C-peptide, indiscriminate opening of the ATP-sensitive K+ channels, nitric oxide (NO) bioavailability, increases in angiotensin II and increases in COX-2 prostanoids brought on by hyperglycaemia can promote a net increase in glomerular pressure (Carmines et al., 1996) (Troncoso Brindeiro et al., 2008) (Cherney et al., 2008) (Nordquist et al., 2008). For example, the RAAS system is chronically activated in long-standing diabetes, and angiotensin II promotes efferent and afferent vasoconstriction leading to increased renovascular resistance (Lovshin et al., 2018). This vascular theory for hyperfiltration sits alongside the tubular theory, which postulates that hyperfiltration occurs due to a combination of an enhanced proximal tubular sodium and glucose reabsorption, with upregulation of sodium-glucose cotransporters and sodium-hydrogen exchangers. Increased proximal sodium reabsorption leads to lower sodium delivery to the juxtaglomerular macula densa located in the distal convoluted tubule. As low sodium here can indicate low circulating volume, the macula densa cells respond via a system of tubuloglomerular feedback, by reducing adenosine signalling, which lowers afferent arteriolar resistance, in addition to promoting renin release and thus RAAS activation (Tonneijck et al., 2017). Currently, the mainstays of treatment for DKD target these pathways, namely RAAS inhibition with ACE inhibitors, Angiotensin II receptor blockers or mineralocorticoid receptor antagonism and inhibition of proximal sodium (and glucose) reabsorption via the sodium glucose co-transporter 2 (SGLT2) (The et al., 2023) (Brenner et al., 2001) (Bakris et al., 2020)

1.5.2 Inflammation

Although renal immune infiltration is not a central hallmark of DKD histology, systemic inflammation occurs early in disease, preceding microalbuminuria (Scurt et al., 2019)

Immune involvement in DKD includes both innate and adaptive responses. Inflammatory markers including tumour necrosis factor receptor 1 (TNFR1) correlate with mortality in people with DKD and are emerging as new biomarkers or potential therapeutic targets. For example, proteinuria directly increases expression of the chemokine IL-8 in proximal tubular cells, orchestrating immune infiltration by promoting neutrophil chemotaxis (Tang et al., 2003, Leto and Geiszt, 2006) (Wada et al., 1994) (Saulnier et al., 2014). Chronic damage to cells by high glucose or glycation leads to apoptosis and the release of damage-associated molecular patterns (DAMPS) recognised by innate pattern recognition receptors including Toll like receptors (TLRs), overexpressed in glomeruli with DKD (Verzola et al., 2014). TLRs trigger production of intracellular reactive oxygen species (ROS) and mediate an NF-kB driven pro-inflammatory response with release of TNF-α, IL-6 and IL-1β, which contribute to fibrosis (Tang and Yiu, 2020). Kidney injury also promotes monocyte recruitment and differentiation. Macrophages are present in the glomeruli and interstitium in DKD, and animal models implicate CCR2 mediated macrophage recruitment in pathogenesis (Awad et al., 2011) (Klessens et al., 2017).

While innate immune dysfunction is well characterised in DKD, the role of the adaptive immune system is less well understood. However, renal T cell infiltration is increased in people with T2D, and in a transgenic CD8 T cell model (OT1), podocytes stimulated by cytokines can present peptide and stimulate T-cell activation (Li et al., 2020) (Liu et al., 2023) .

1.5.3 Oxidative stress

The term oxidative stress was initially described by Helmut Sies as the imbalance between oxidants and antioxidants in favour of the former, with the potential of causing damage (Sies, 2000). Within the body, oxidants such as superoxides, hydroxyls and hypochlorous acid can be a protective mechanism against infection. For instance, neutrophils undergoing phagocytosis transfer electrons from nicotinamide adenine dinucleotide phosphate (NADPH) to molecular oxygen, via NADPH oxidase, to form superoxides. Superoxides are then converted to other oxidants that kill microorganisms (DeLeo and Quinn, 1996) (Dahlgren and Karlsson, 1999) (Leto and Geiszt, 2006).

Microsomal and mitochondrial electron transport chains generate hydrogen peroxide (Boveris et al., 1972). Peroxides, superoxides and other highly reactive oxidants are collectively called ROS, a subgroup of free radicals with an unpaired electron in their atomic orbital rendering them unstable (Lobo et al., 2010). Modulation of ROS to establish an equilibrium with antioxidants involves an array of metabolic processes. For example, superoxide dismutase converts superoxides into hydrogen peroxides that are then mopped up by either catalases or glutathione reductases. Likewise, α-tocopherol and urate block ROS activity by retarding lipid peroxidation chain reactions and scavenging free radicals. However, if unchecked, the high reactivity of ROS allows these molecules to setup a chain reaction that modifies lipoproteins, membranes and DNA with ramifications for the pathophysiology of diseases (Betteridge, 2000). Excessive production of free radicals and subsequent oxidative stress are thus hallmarks of cancer, diabetes and neurological disease.

1.5.3.1 Oxidative stress as a driver of diabetic vascular disease

Oxidative stress has been proposed as a common factor contributing to the associated disorders of insulin resistance, dyslipidaemia and cardiovascular risk (Ceriello and Motz, 2004). (Lee et al., 2017). The state of hyperglycaemia in diabetes results in increased production of mitochondrial ROS and oxidative stress via disruption of mitochondrial respiratory chain enzymes including xanthine oxidases, lipoxygenases, cyclooxygenases, nitric oxide synthases, and peroxidases, with upregulation of NADH oxidases (Yu et al., 2006) (Volpe et al., 2018). Autooxidation of excessive glucose can also stimulate oxidative stress (Wolff and Dean, 1987), as can free radical generation by non-enzymatic glycation products or the production of AGE and their interactions with their receptors (RAGE) (Yim et al., 2001) (Mullarkey et al., 1990). Glycation can also worsen oxidative injury by inactivating antioxidant enzymes such as superoxide dismutase (Morgan et al., 2002). Under conditions of high glucose, there is increased activity of the aldose reductase dependent polyol pathway, whereby glucose is converted to sorbitol and then fructose. This process depletes NADPH, consequently reducing synthesis of the intracellular antioxidant glutathione, and instead generates nicotinamide adenine dinucleotide (NADH), a substrate for NADH oxidase, promoting super oxide production (Tang et al., 2012).

Endothelial dysfunction is an early event in atherosclerosis, and ultimately contributing to micro- and macrovascular complications in diabetes (Johnstone et al., 1993) (Shi and Vanhoutte, 2017). This endothelial damage appears to be mediated directly and indirectly via oxidative stress. Endothelial cell apoptosis can be induced *in vitro* by fluctuating glucose levels via protein kinase C (PKC) dependent NADPH oxidase activation, while *in vivo* endothelial nitric oxide synthase (eNOS) deficiency exacerbates rodent diabetes models, inducing earlier onset and more pronounced renal damage (Zhao et al., 2006).

The expression of AGE and RAGE are elevated in atherosclerotic plaques from diabetic compared to non-diabetic subjects and associated with increased inflammation**,** and the accumulation of advanced oxidation products including oxidised low-density lipoprotein may trigger endothelial activation via RAGE (Burke et al., 2004) (Guo et al., 2008)**.** Oxidative stress may cause vascular damage via increased lipid peroxidation, since inhibition of this pathway ameliorates wound healing defects in diabetic mice (Altavilla et al., 2001).

A further driver of diabetic endothelial damage is activation of the NOD-like receptor pyrin domain 3 (NLRP3) inflammasome that leads to the generation of IL-1β and IL-18 and is linked to atherosclerosis (Abderrazak et al., 2015). This occurs in direct response to high glucose, but also due to increases in mitochondrial ROS and AGE, with depletion of intracellular potassium identified as a possible shared final pathway of NLRP3 activation (Wang et al., 2020) (He et al., 2016).

1.5.3.2 Oxidative stress and diabetic kidney disease

The nephron is often considered particularly vulnerable to oxidative injury owing to the high mitochondrial content of proximal tubular cells and podocytes (Duann and Lin, 2017). In diabetes, as unregulated increased glucose uptake occurs in renal cells including podocytes it fuels the mitochondrial respiratory chain via oxidative phosphorylation, with resultant production of ROS by partial reduction of O_2 to the reactive superoxide (Coward et al., 2005) (Nishikawa et al., 2000). While both superoxide and NO may have functional signalling roles in the healthy kidney, for example in tubulo-glomerular feedback, elevated levels of ROS and NADPH oxidase (NOX) are thought to lead to oxidative stress with DNA damage and cell death in DKD (Liu et al., 2004). These free radicals promote increased activity of the renin-angiotensin signalling pathway via the proximal tubule AT1 receptor, which results in sodium retention and hypertension, and increased expression of inflammatory and fibrotic

markers including TGF-β, ultimately contributing to fibrosis and loss of renal function (Banday and Lokhandwala, 2011) (Gray et al., 2013). In addition to the generation of new ROS, there may be defects in the antioxidant response. For example, cultured fibroblasts from people with T1D and DKD fail to increase production of antioxidant enzymes, including catalase and glutathione peroxidase, in response to high glucose, compared to healthy controls or T1D without DKD (Ceriello et al., 2000).

Despite the accepted dogma that oxidative stress is central to DKD, clinical trials of antioxidant therapies have had only mixed results. While NOX4 inhibition protected from renal damage in the T1D streptozocin-induced mouse diabetic model, phase II clinical trials of a NOX1/4 inhibitor in T2D did not reduce albuminuria, with the outcome of a similar trial in T1D awaited (Jha et al., 2014) (Elbatreek et al., 2019) (Reutens et al., 2020). High-dose folic acid has been trialled, with the objective of providing co-factor so that NOS can drive production of NO rather than superoxides. However, this failed to show a benefit in a phase III trial in T2D (Elbatreek et al., 2019).

Inhibition of the renin angiotensin pathway is the mainstay of treatment for DKD, reducing protein leak and slowing the decline in eGFR, beyond their effects on blood pressure (Lewis et al., 1993). While these drugs have pleiotropic effects, they have long been known to have antioxidant properties, which may contribute to their reported efficacy (Chopra et al., 1992). Similarly, SGLT2 inhibition is effective in slowing progression of DKD, providing a much-needed new tool in the treatment of DKD, and may reduce free radical generation or promote antioxidant activity, in addition to blood pressure lowering and anti-hyperglycaemic effects (The et al., 2023) (Yaribeygi et al., 2019).

NRF2 is a transcription factor that regulates the expression of over 1,000 genes involved in antioxidant defence, detoxification and metabolism (Zang et al., 2020). Under physiological

1.2

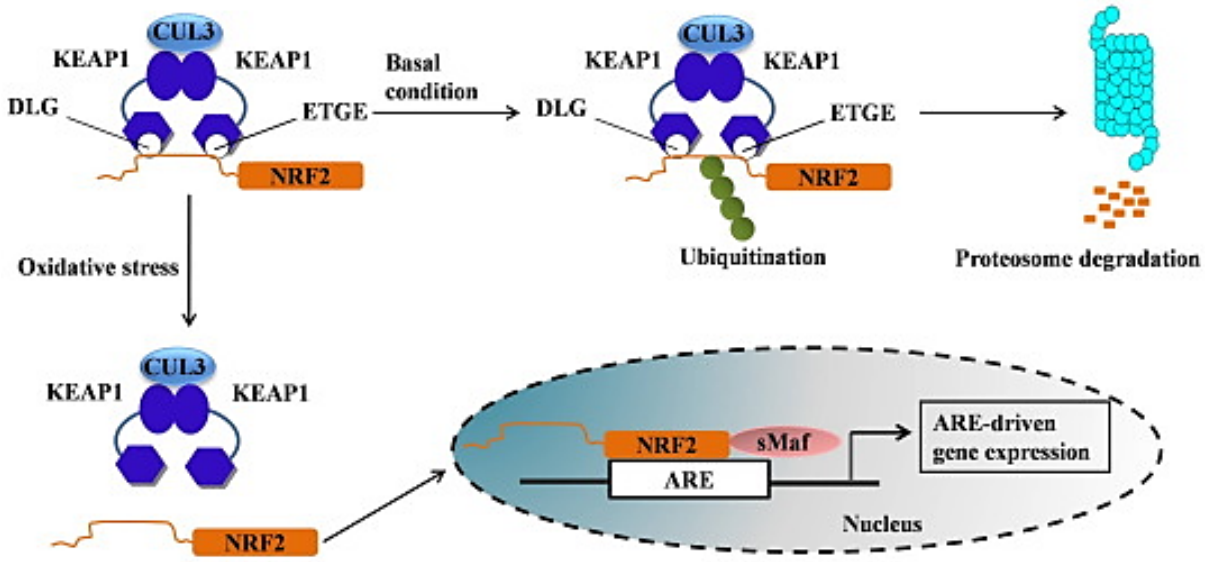

Figure 1.2 NRF2/KEAP 1 pathway. KEAP1-NRF2 complex leads to degradation of NRF2 under basal conditions. In response to oxidative stress or following exposure to NRF2 agonists, de novo NRF2 migrates to the nucleus, binds to genes with antioxidant response elements (ARE) and activates their expression. Source: (Ahmed et al., 2017)

conditions, NRF2 complexes with Kelch-like ECH-associated protein 1 (KEAP-1) in the cytoplasm, leading to the transcription factor's ubiquitination and degradation (Figure 1.2). Modifications to cysteine residues of KEAP-1 in response to oxidative stress or NRF2 pathway activators result in *de novo* NRF2 migrating to the nucleus where it heterodimerises with bZIP proteins. Thus, it forms a transactivation complex that binds to and induces genes with antioxidant response elements (ARE), including heme oxygenase 1 (*HMOX1*) and NAD(P)H quinone dehydrogenase 1 (*NQO1*) (Wang et al., 2016a, Reichard et al., 2007). Activation of these downstream effectors promotes antioxidant pathways to avert the redox imbalance. As a key regulator of antioxidant response NRF2 has, therefore, been considered an attractive therapeutic target in DKD. While a phase III clinical trial of the NRF2-activating drug bardoxolone methyl was terminated early due to increased risk of heart failure, the earlier phase II study had demonstrated a promising increase in estimated glomerular filtration rate (eGFR) (de Zeeuw et al., 2013) (Pergola et al., 2011). Moreover, KEAP-1, as the principal negative regulator of NRF2 has been considered a possible target for drugs in

chronic diseases such as cancers, metabolic and inflammatory and autoimmune diseases (Cuadrado et al., 2019). Inhibitors of KEAP1 such as naphthalene bis-sulfonamide compounds could be novel drug targets but progress into clinical trials has been limited (Marcotte et al., 2013).

The mixed results in trials of drugs targeting oxidative pathways may reflect our as yet limited comprehension of the essential drivers of DKD. Better understanding of the complex cellular responses to oxidative stress is a critical first step towards the design of therapies linked to mechanism. In this context, the role of NRF2 in oxidative stress will be considered in more detail, with reference to existing evidence of a link to the microtubule associated Tau protein.

1.6 Tau, oxidative stress and NRF2

1.6.1 Tau protein in neurodegenerative disease

The microtubule-associated protein tau (*MAPT*) gene encodes the protein, tubulin associated unit (Tau). Tau's canonical role is to bind tubulin to facilitate the assembly and stabilisation of microtubule structure (Weingarten et al., 1975). In humans, the Tau gene is located on chromosome 17q31.21 and contains 14 exons assigned to its four core domains: exons 1, 2 and 3 are part of the N-terminal domain, exons 4, 4a, 5, 6, 7, 8 constitute the proline-rich domain, 9, 10, 11 and 12 make up the microtubule-binding domain while finally, exons 13 and 14 encode the C-terminal domain (Mukrasch et al., 2009). The human MAPT gene undergoes alternative splicing. Currently, based largely on work in the brain, there are six well-validated isoforms that vary in the number of N-terminal inserts (0N, 1N or 2N) and C-terminal repeat domains (3R or 4R) (Figure 1.3). Isoform expression patterns are influenced by factors including developmental stage and disease (Bachmann et al., 2021). In addition, Tau undergoes many post-translational modifications such as phosphorylation, truncation and acetylation with hyperphosphorylation observed in neurological disease (Bramblett et al., 1993).

The development of hyperphosphorylated, insoluble and filamentous Tau is a hallmark of human neurodegenerative diseases collectively called tauopathies. These diseases, which include Alzheimer's disease (AD), frontotemporal dementia, corticobasal degeneration and progressive supranuclear palsy, have distinct clinical and biological manifestations such as the accumulation of amyloid beta protein in Alzheimer's patients (Zhang et al., 2022). However, they are grouped together as they feature alterations in Tau's isoform balance and / or post-translational modifications leading to Tau aggregates. For example, in AD and Parkinson's disease, abnormally phosphorylated Tau aggregates in neurons lose their

physiological microtubulin-binding and stabilising functions (Alonso et al., 1994b). Despite this apparent loss of function, clinical trials with drugs that stabilise the microtubule have been unsuccessful (Hung and Fu, 2017) (Tsai et al., 2020) An alternate hypothesis is that altered Tau is pathogenic due to a gain of function, supported by evidence in mice that the injection of abnormal Tau can trigger 'propagation' or spreading Tau aggregation (Clavaguera et al., 2009).

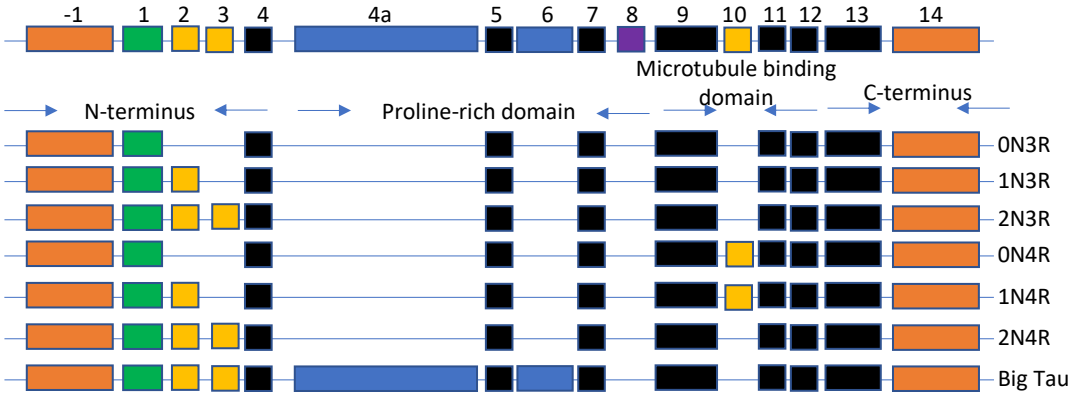

Figure 1.3 The *MAPT* gene, the six known isoforms and big Tau generated through alternate splicing.

1.6.2 Association between Tau and oxidative stress with reference to NRF2

Tauopathy severity correlates with upregulation of oxidative stress markers in the brain (Castellani et al., 1995, Smith et al., 1996) and cerebrospinal fluid (Pratico et al., 2000a). Elevated lipid peroxidation and decreased antioxidant activity are also early features of murine AD models, in which combined amyloid beta and tau protein modification, mimicking frontotemporal dementia and AD, results in deregulation of the oxidative phosphorylation system, with reduced NADH ubiquinone oxidoreductase activity linked to mutant Tau (Resende et al., 2008, Rhein et al., 2009b). Transgenic mice homozygous for the rare human pathogenic Tau mutation P301L are an established model for frontotemporal dementia; aged P301L mice have mitochondrial dysfunction with modified lipid

peroxidation, increased antioxidant activity and higher levels of ROS than WT (David et al., 2005). Finally, overexpression of Tau in cultured neurons impairs peroxisome transport and increases sensitivity to oxidative stress (Wang et al., 2016b). These findings indicate an association between altered Tau and oxidative stress. However, deletion of *Mapt* in mice, while altering microtubule stability, was not associated with any neurological phenotype except in aged mice as might be expected (Harada et al., 1994b) (Ikegami et al., 2000).

In vitro Tau binds to complexes involved in both RNA processing and translation, and in chromatin remodelling and splicing (Geeth Gunawardana et al., 2015) (Montalbano et al., 2021). Tau also appears to protect neuronal genomic DNA from damage (Sultan et al., 2011), and this appears to hold *in vivo*: when hippocampal segments of *Mapt*$^{-/-}$ mice were compared to WT mice, impaired hippocampal neuron DNA and RNA integrity under hyperthermia-induced oxidative stress was observed (Violet et al., 2014). Alongside this stress increase, the mRNA levels of Nrf2, as well as its downstream effectors Hmox1 and γ-glutamine cysteine synthase (GES) increased in the *Mapt*$^{-/-}$ mice relative to the control (Jara et al., 2018). NRF2 deficiency in AD prone mice exacerbates both neuronal oxidative stress and learning and memory. (Rojo et al., 2017).

Nrf2 binds to an antioxidant response element (ARE) within intron 1 of the *MAPT* gene and induces *MAPT* transcription in response to hypoxia. Human polymorphisms in this ARE are associated with altered *MAPT* mRNA levels, with SNP rs242561 associated with increased *MAPT* expression and protection from supranuclear palsy, Parkinson's disease, and corticobasal degeneration (Wang et al., 2016b). These data would suggest that at least in mice, and perhaps also in humans, Tau could have a physiological functional role in oxidative stress response. The broadening of Tau's role into biological processes ubiquitous to all living cells has promoted research into Tau beyond non-neurodegenerative diseases.

However, despite findings in Tau deletion models, most work has focused on post-translationally modified Tau, and loss of the protein remains under explored in human cells (Sola et al., 2020b). The role of Tau in oxidative stress in human cells is untested, and it is not known whether this is dependent on NRF2.

1.7 Models to study diabetic kidney disease

1.7.1 *In vivo* models

While there are numerous rodent models of diabetes, many of these do not develop advanced renal disease. Kidney injury is strain dependent, with C57BL/6J mice relatively resistant to diabetic and indeed non-diabetic kidney disease (Qi et al., 2005). Some of the more commonly used models are discussed below.

1.7.1.1 DKD in T1D murine models

Non-obese diabetic (NOD) mice, a model for T1D in which the disease develops spontaneously and results from autoimmune destruction of the pancreatic islet beta cells, develop early kidney damage, with albuminuria, matrix mesangial expansion, and podocyte loss at 40 days after diabetes onset (Doi et al., 1990). Akita mice, carrying a spontaneous mutation in the pre-pro insulin gene, *Ins1*, likewise develop mesangial expansion and albuminuria similar to early human DKD, but without mesangiolysis or nodular sclerosis. There is strain-dependent phenotypic variability with some IgA deposition described that may be contributing to non-DM related renal injury (Chang and Gurley, 2012). Streptozocin is toxic to β cells, and the streptozocin-induced model of T1D is commonly used and develops mainly tubular injury. When combined with genetic deletion of endothelial nitric oxide synthase (eNOS) these animals develop more mesangial damage with nodules and

mesangiolysis. However, there is likely some direct contribution from streptozocin to renal toxicity (Leiter, 1982).

1.7.1.2 Diabetic kidney disease in T2D murine models

The db/db leptin deficient mouse is commonly used to model obese, insulin-resistant T2D (Szabadfi et al., 2014). Early diabetic nephropathy can take over a year to develop, though when combined with eNOS (through gene mutation) in the susceptible C57Bl/6 KS strain (containing a DBA2 strain region), more pronounced renal disease develops by week 26 with albuminuria, podocyte loss and mesangial expansion, making this one of the few *in vivo* models of more advanced kidney disease (Zhao et al., 2006). Ob/Ob insulin-resistant mice, when bred on the black and tan brachyuric strain background, show rapidly progressive disease, with proteinuria and podocyte loss by 8 weeks, mesangial expansion by 10 weeks, and advanced DN by 18 weeks including some interstitial fibrosis. This rapid progression may make this strain amenable to treatment to try to reverse renal damage. However, leptin-deficient mice are infertile, making breeding time consuming and complex (Hudkins et al., 2010) (Alpers and Hudkins, 2011).

1.7.1.3 Limitations of current in vivo models

Pathways or genes highlighted in murine models do not always translate to human disease, in part because of the genetic divergence between our species, the inbred nature of the laboratory animal compared to human genetic heterogeneity, and the failure of models to fully recapitulate human disease mechanisms. Experimental work *in vivo* can be slow and costly, and accurately measuring cellular responses *in vivo* is complex. While rodent models of DKD have been important experimental tools, they often exhibit only relatively mild or late onset renal involvement, and this is typically background strain dependent. In some models, renal damage may be at least in part due to non-diabetic mechanisms or toxicity. *In*

vitro models can address some of these limitations by providing more rapid and flexible methods to study and manipulate human cells.

1.7.2 *In vitro* models

1.7.2.1 Cell lines

Tubulointerstitial fibrosis is a final common pathway in kidney disease, and in DKD, the extent of interstitial fibrosis correlates with risk of progression (Nath, 1992)**.** Proximal tubular epithelial cells can be subjected to high glucose, TGF- β, glycated proteins, angiotensin II or hypoxia in order to mimic the diabetic milieu (Slyne et al., 2015). For example, rat renal proximal tubular epithelial cells exposed to AGE-modified bovine serum albumin (BSA) exhibit increased matrix metalloprotease (MMP2) activity and ROS which could be reversed by angiotensin II inhibition (Fukami et al., 2014)**.**

Podocyte injury is a central event in DKD development and experiments in podocytes under high glucose conditions have demonstrated release of ROS species that trigger p36MAPK and NADPH oxidase signalling pathways, leading to podocyte apoptosis (Eid et al., 2009) (Susztak et al., 2006). *In vitro* study of podocyte injury has progressed owing to the availability of immortalised human and murine podocyte cell lines. These cells express a temperature sensitive SV40 promotor, such that they proliferate at 33^{o}C, permitting routine culture, with a fibroblast like morphology, but on transfer to 37^{o}C for 10-12 days, cease proliferation and differentiate to adopt an enlarged flattened morphology, expressing key podocyte-specific markers including nephrin and podocin (Saleem et al., 2002)**.**

Human mesangial cells similarly apoptose under high glucose conditions, but glucose can also promote mesangial cell proliferation, via inhibition of hydrogen sulphide synthesis (Mishra et al., 2005) (Ding et al., 2017)**.**

However, standard culture medium already contains supraphysiological levels of glucose, making the relevance of high glucose *in vitro* systems to the human diabetic environment questionable. Very high glucose concentrations (25 mmol/L or more) will exert an osmotic effect that may explain some observed *in vitro* cellular injury. Exposure to a combination of high glucose, insulin and proinflammatory cytokines may provide a more disease-informative system (Lay et al., 2017).

Much of the work in proximal tubular cells is in cells of non-human origin and may be less applicable to clinical disease. Primary cells can dedifferentiate very quickly, and immortalised cell lines can lose characteristics of the parent lines. Causing perturbations in cell physiology by environmental or genetic manipulation does not necessarily imply *in vivo* causation, and carefully designed rescue experiments are required to demonstrate specificity of effects. Cell monocultures also fail to replicate the complex cellular cross talk and structure of the glomerulus or tubule. Thus, there is a need for more sophisticated models to better represent human kidney pathology.

1.7.2.2 Kidney-on-a-chip

Organ-on-a-chip technology uses microfluidic and microchannel cell co-culture systems to replicate tissue and organ level function. Fluid flow, pressure and chemical gradients can be controlled to modulate cellular organisation and function. Using podocytes differentiated from induced pluripotent stem cells (iPSCs) co-cultured with endothelial cells, separated by a laminin membrane, a 'glomerulus-on-a-chip' system, differential clearance of albumin and inulin can be demonstrated, mimicking the free filtration of inulin but not the large molecule albumin by the glomerular filtration barrier (Musah et al., 2017)**.** Exposure of such a system to high glucose results in increased permeability of the barrier to albumin, endothelial dysfunction and production of ROS (Wang et al., 2017)**.**

1.7.2.3 Kidney organoids

Organoids are miniaturised 3-dimensional *in vitro* models that mimic some of the biological and functional complexity of the organ, due to self-organising multicellular structure. Typically, organoids are derived from stem cells (pluripotent, foetal or adult) and differentiated by culturing with tissue specific combinations of growth factors and extracellular components (Hofer and Lutolf, 2021). Organoids offer advantages over animal models: they are faster and less expensive to generate, may be easier to manipulate, are generated from human cells, and provide an ethical opportunity to reduce and replace animal work.

However, *in vitro* cell and tissue engineering approaches still face limitations. Most organoids represent a foetal-like developmental stage rather than adult cellular physiology, and complex structures and functions may not be replicated. Additionally, heterogeneity presents challenges with reproducibility and scale (Yi et al., 2021). Human kidney organoids, for example, share some transcriptomic similarity with the foetal kidney, but do not replicate renal filtration or develop a vasculature (Combes et al., 2019). Nevertheless, recent experiments with subcapsular transplantation of organoids in immunodeficient mice suggest size-selective glomerular sieving of dextrans and formation of a vascular network (van den Berg et al., 2020) (Low et al., 2019)**.** Kidney organoids have been particularly useful to explore renal developmental patterning, but when combined with iPSC gene editing can also recapitulate renal genetic disease such as polycystic kidney disease due to PKD1 mutations (Freedman et al., 2015). Kidney injury models using renal organoids have also been developed, typically for nephrotoxin-mediated injury with a view to drug screening, e.g. using cisplatin (Digby et al., 2020). A recent paper described exposure of organoids to hemin, to model haemolysis-induced oxidative stress, such as might occur in sickle cell disease, and used this to identify the anti-fibrotic 4-(phenylthio) butanoic acid as a possible therapeutic

agent for hemin induced oxidative stress (Przepiorski et al., 2022). To date, an established kidney organoid model for DKD has not been fully developed, though this is an active area of research: for example, a model in which organoids are exposed to high oscillating glucose levels leads to increased extracellular matrix deposition (Garreta et al., 2022).

1.8 Summary

In this thesis I use *in vitro* models to study oxidative stress pathways relevant to DKD. I aimed to answer three key questions:

1. How does oxidative stress alter RNA and protein level pathways in renal podocytes, and how does NRF2 influence this?
2. Does Tau have a functional role in the oxidative stress response?
3. Can better models be developed to study renal oxidative stress?

To address these questions, in Chapter 3 I describe NRF2-dependent and independent transcriptomic and proteomic signatures of oxidative stress in human podocytes. In Chapter 4 I applied gene editing to define a role for Tau in protection from oxidative injury in a neuronal cell line, and in Chapter 5 I established tools to explore the function of Tau in a multicellular context using kidney organoids.

Chapter 2
Materials and Methods

2.1 Cell Culture and Maintenance

SH-SY5Y cells (from ATCC) were maintained in culture flasks in a complete media of Dulbecco's Modified Eagle's Medium (DMEM) (Gibco), 100 international units (U/ml) penicillin, 100 μg/ml streptomycin (Sigma-Aldrich), 1% L-glutamine (Sigma-Aldrich) and 10% foetal bovine serum (FCS) (Sigma-Aldrich). Cells were passaged every three days by washing with phosphate buffered saline (PBS) (Sigma-Aldrich), incubated with trypsin-ethylenediaminetetraacetic acid (EDTA) (Sigma-Aldrich) at 37°C for 5 minutes followed by neutralisation with 10% FCS in PBS. They were centrifuged at 500 g for minutes and pellets resuspended in complete media. Cell counting was performed using a haemocytometer and reseeding at 20,000 cells per cm^2. Cells were maintained at 37°C and 5% CO_2.

Podocytes used in this work were a gift from Professor Moin Saleem, University of Bristol. These cells were created from human podocytes derived from a nephrectomy specimen and transfected with temperature-sensitive T antigen transgene tsA58 T (Saleem et al., 2002). This transgene allows cell proliferation at the permissive temperature of 33°C but induces cell differentiation at 37°C. The cells were cultured as described in the original publication such that either at the permissive or non-permissive temperatures, they were incubated with 5% CO_2 in a complete media containing RPMI1640 (Gibco) with 10% fetal calf serum (FCS), 100 U/ml penicillin and 100 μg/ml streptomycin (Gibco) with 1% insulin-transferrin-selenium (Gibco). Proliferating cells were passaged every three days in a similar manner to the SH-SY5Y cells. For differentiation, cells were moved to a 37°C incubator and showed markers of differentiated podocytes such as nephrin and synaptopodin after 12 days at this non-permissive temperature.

LentiX-293T (Takarabio) were cultured in high glucose DMEM (Sigma-Aldrich) with 10% FBS. Cells were passaged twice a week and split in a 1:20 ratio.

2.2 Genomic DNA Analysis

2.2.1 DNA extraction for routine PCR

500 µl of QuickExtract (Lucigen) solution was added to 10^6 cells, vortexed for 15 seconds and incubated at 65°C for six minutes. The solution was then vortexed for 15 seconds, incubated at 98°C for two minutes and quantified using a Nanodrop ND-1000 UV/VIS Spectrophotometer (Thermo Fisher Scientific).

2.2.2 DNA extraction for Whole Genome Sequencing (WGS)

Gentra Puregene Kit (Qiagen) was used to extract DNA from 5 x 10^6 cells according to the manufacturer's protocol. Concentration of DNA yielded was between 300 ng/µl and 700 ng/µl, with A260/280 absorbance ratio of 1.8 and A260/230 ratio of 2. 17 µl of each sample was submitted for long range WGS in our Centre. Further experimental details on whole genome sequencing can be found in 2.7.4.4.

2.2.3 PCR amplification and gel electrophoresis

Unless otherwise described, polymerase chain reactions (PCR) were performed using 500 ng of DNA in a total reaction volume of 25 µl together with water, 5 µl 5x OneTaq reaction buffer (NEB), 0.5µl 10mM dNTP (Thermo Fisher Scientific), 0.5µl of 10 υM forward primer and 0.5µl of 10µM reverse primer and 0.125µl OneTaq DNA polymerase (NEB). Thermocycling conditions were as follows: 30 seconds initial denaturation at 94°C 34 cycles of 94°C for 30 seconds, annealing at 50-70°C (primer specific) for 30 seconds, and 68°C for 60 seconds. The final extension was at 68°C for 5 minutes. The final holding temperature was at 4°C. Samples were run on 1% agarose gels with SybrSafe stain (Thermo Fisher

Scientific) for 45 minutes at 100z V. Visualisation was performed using GelDoc transilluminator system (Bio-Rad).

2.2.4 Sanger sequencing

Amplicons of interest were cut and cleaned up using the Qiaquick gel extraction kit (Qiagen) according to the manufacturer's instruction. Following quantification of DNA concentration, 5µl of PCR product at 10ng/µl was submitted for sequencing with 5 µl of primers at 3.2pmol/µl. Sequencing was performed by Source Bioscience.

2.3 Gene Expression Studies

2.3.1 RNA extraction

One ml of TRIzol (Invitrogen) was added to 1 – 5 x 10^6 cells and incubated at room temperature (RT) for 5 minutes followed by 200 µl of Chloroform. Samples were vortexed for 15 seconds and incubated at RT for 3 minutes before centrifugation at 12000 g for 15 minutes at 4°C. The top-most aqueous phase was collected and added to 500 µl of isopropanol. The resulting solution was centrifuged for 10 minutes at 12000 g at 4°C and the pellet washed twice with 75% ethanol, then dried and resuspended in diethyl pyrocarbonate (DEPC)- treated water. RNA was quantified using Nanodrop ND-1000 UV/VIS Spectrophotometer (Thermo Fisher Scientific) with A260/280 absorbance ratio of ~ 2 and A260/230 ratio of >2. For each 1 ug of RNA, 1 ul of 10x reaction buffer with $MgCl_2$ 1 ul of DNase I and 10 ul of DEPC-treated water as provided by Thermo Fisher Scientific's DNase I (EN0521)) was mixed and incubated at 37°C for 30 minutes. 1 ul of 50 mM EDTA (Thermo Fisher Scientific) was added to the RNA solution and incubated for a further 65°C for 10 minutes. The final concentration of the RNA was then quantified before use for experimentation.

2.3.2 cDNA synthesis

A reaction mix of 4 µl 5x LunaScript RT Supermix (NEB) and 800 ng RNA, made up to 20 µl with DEPC-water, was incubated at 25°C for 2 minutes, 55°C for 10 minutes and 95°C for 1 minute.

2.3.3 Quantitative PCR (qPCR)

Gene expression was measured using PowerTrack SYBR Green qPCR master mix (Thermo Fisher Scientific) comprising 5 µl master mix, 0.5 µl of reverse and forward primers at 10 µM concentrations and 5ng of cDNA in a 10 µl reaction volume with water. The thermocycling conditions were 95°C for 2 mins, and 40 cycles of 95°C for 5 seconds plus 60°C for 30 seconds in a QuantStudio 6 Flex real-time PCR system (Thermo Fisher Scientific). Cycle threshold (Ct) values were analysed using the $2^{-\Delta\Delta Ct}$ method with normalisation performed against two housekeeping genes – GAPDH and Beta actin.

2.4 Protein Expression Studies

2.4.1 Cell Lysis and protein quantification

Five to ten million cells washed in cold PBS were lysed on ice for 10 minutes using a cocktail of radioimmunoprecipitation assay (RIPA) buffer (Sigma-Aldrich), 0.1% sodium dodecyl sulphate (SDS) (Thermo Fisher Scientific) and cOMPLETE protease inhibitor (Roche). Samples were then sonicated for 10 minutes – 30 seconds on and 30 seconds off – using Bioruptor Pico sonicator (Diagenode) and centrifuged at 13,000 rpm for 5 minutes. The supernatant was collected and quantified using Qubit 4 fluorometer (Thermo Fisher Scientific).

2.4.2 Western blotting

Loading buffer was prepared using 4x Laemmli buffer (Bio-Rad) and 10% 2-mercaptoethanol. Lysates were diluted in loading buffer and incubated at 99°C for 10

minutes. Samples were loaded into wells of 4-20% Mini-Protean gels (Bio-Rad) alongside a protein ladder (Cell Signal). Gels were run for 20 minutes at 100 V then at 130 V for 60 minutes. The gels were activated using ultraviolet light on a ChemiDoC MP Imaging System (Bio-Rad) before performing a wet transfer at 100 V for 40 minutes onto a 0.2 μm polyvinylidene difluoride (PVDF) membrane. Blots were blocked with 5% Amersham ECL blocking agent (Cytiva) in tris-buffered saline (TBS) supplemented with 0.1% Tween-20 (TBST) (Sigma Aldrich) for 1 hour at RT. Blots were incubated overnight in antibody dissolved in blocking solution before three ten-minute washes with TBST. Blots were incubated at RT in secondary antibodies solutions for an hour and washed as described. Membranes were visualised using LI-COR's Odyssey CLx.

2.4.3 Immunofluorescence

Unless otherwise stated, immunofluorescence images were obtained as follows: cells were seeded onto cover slips in 24-well plates overnight, fixed with 2% paraformaldehyde for 20 minutes at RT and washed three times with PBS. A permeabilization solution of PBS with 0.1% Triton-X 100 (Thermo Fisher Scientific) was added to the cells and incubated at RT for 10 minutes. The cells were blocked in 1% bovine serum albumin (BSA) (Thermo Fisher Scientific) in PBS for 1 hour. Primary and secondary antibody solutions were prepared in blocking solutions with an hour incubation for each. Three washes of 10 minutes each between antibody incubation were performed using PBS supplemented with 0.1% Tween-20 (PBST). Nuclear staining was performed at RT for 5 minutes using 4′,6-diamidino-2-phenylindole (DAPI) (Thermo Fisher Scientific) diluted in PBS followed by a PBST wash. Cover slips were mounted using VECTASHIELD antifade mounting medium (Vectorlabs). Imaging was performed on Leica SP8 SMD X Confocal Microscope.

2.4.3 Flow cytometry

One to five million cells were harvested and washed with PBS. Live cell staining was performed by diluting cells in a 100 µl solution of Zombie NIR fixable stain in PBS (BioLegend) at RT for 20 minutes. Cells were washed three times in PBS with 5% FCS and ultracentrifuged at 2,000 rpm for 2 minutes. The cells were then fixed in ice cold methanol on ice for 20 minutes and washed three times with PBS with 5% FCS. Primary and secondary antibody solutions were prepared in PBS with 5% FCS with each incubation lasting 30 minutes. Cells were sorted using a BD FACSCANTO flow cytometry system and analysed using Flowjo (BD).

2.5 Lentiviral Transduction

Lentiviral production was performed using Lenti-HEK293T cells cultured without antibiotics to 80 – 85% confluence. Two hours before transfection, the medium was replaced with Opti-MEM reduced serum media (Thermo Fisher Scientific). The packaging plasmids pMD2.G (Addgene #12259) and psPAX2 (Addgene #12260) and the plasmid of interest were used at a ratio of 1:3:4 with the Lipofectamine transfection reagent (Thermo Fisher Scientific) according to the manufacturer's instruction. Lentiviral supernatant was harvested from the cells 48 and 72 hours after transfection and stored at 4°C before ultracentrifugation at 22,000 rpm for 2 hours at 4°C in a swinging-bucket rotor. The pellet was resuspended in 50 µl of ice-cold PBS. Transduction of cells was carried out as follows: the 50 µl lentiviral resuspension was added to 60 cm dish. One million cells were resuspended in complete media supplemented with 10 µg/ml protamine sulfate were added and cultured for three days before antibiotic selection if necessary (puromycin selection was performed at 10 µg/ml).

2.6 Chapter 3- Specific Methods

2.6.1 Induction of oxidative stress in podocytes using tBHP

Podocytes were differentiated at 37°C for 13-14 days with a media change every three days. Five hundred thousand differentiated cells were then treated with 100 µM of tert-Butyl hydroperoxide (tBHP), as Luperox tBH70X (Millipore, 458139-25 ml) or water control. Subsequently, the cells were harvested and assayed.

2.6.2 Live cell and peroxidised lipid quantification

Cell culture media was removed, and the cells were washed with cold PBS to remove dead cells and debris. The remaining cells were dissociated with 5 ml trypsin with EDTA (Thermo Fisher Scientific, 25200056) and the trypsin neutralised with culture media. The live cells were washed with PBS and counted by haemocytometer, stained with trypan blue to exclude dead cells. Lipid peroxidation or malondialdehyde (MDA) assay kit (Abcam, AB118970) was used following the manufacturer's protocol for calorimetry quantification as follows. Harvested, counted cells were lysed using 300 µl of malondialdehyde lysis buffer with 3µl butylated hydroxytoluene (BHT) and sonicated at 4°C for 10 minutes, cycling 10 seconds on and 10 seconds off. The cell solution was then centrifuged at 13,000 g for 10 minutes to remove insoluble material. Supernatant was collected and stored at 4°C until ready to use. Standard solutions of MDA from 0 –100 µm were prepared in double deionised water. Two hundred µl of each of the standards and the lysed cell supernatant were added to 96-well plates. 600 µl of thiobarbituric acid (TBA) was added to each well and the resulting solution incubated for 60 minutes at 95°C to form the MDA-TBA adduct. The solution was then cooled to room temperature in an ice bath for 10 minutes. Two hundred µl of each of the MDA-TBA adduct solutions was aliquoted to create a triplicate set for each of the conditions and the absorbance measured immediately on a microplate reader at OD 532 nM. The mean

average reading for each triplicate set was calculated. The mean value of standard 1 (0 µM background) was subtracted from all the standard and lysate samples. Using the concentration of the standards and the corrected values, a line of best fit was plotted and used to calculate the concentration for the cell lysate samples. To calculate the MDA concentration per number of live cells, the MDA concentration extrapolated from the standard curve was multiplied by four giving the total MDA concentration in nmol. Then this value was divided by the number of live cells used for the assay giving a unit of nmol/cell.

2.6.3 Quantifying carbonylated protein expression with carbonyl assay kit

Five hundred thousand cells suspended in 150 µl of water were homogenised by sonication with Bioruptor Pico sonicator (Diagenode) for 10 minutes, cycling 30 seconds on and 30 seconds off. The cell lysates were treated with 15 µl of streptozocin at RT for 15 minutes before centrifuging at 12,000 g for 5 minutes, and the supernatant collected. This supernatant containing the total protein was then quantified using Qubit 4 fluorometer (Thermo Fisher Scientific). One hundred µl of sample containing 0.5 – 2 mg protein was used per assay. A reagent background control of 100 µl of water was also used. Each 100 µl lysate was added to 10 0µl 0.1% 2,4-Dinitrophenylhydrazine (DNPH) and vortexed and incubated for 10 minutes at room temperature. Thirty µl of Trichloroacetic Acid (TCA) was added to each sample, vortexed and placed on ice for 5 minutes before spinning at 12,000 g for 2 minutes. The supernatant was discarded, and the pellet was kept undisturbed. 500µl of cold acetone was added to each sample, placed at -20°C for 5 minutes to wash the pellet. The acetone was then removed from the pellet. This step was repeated before adding 200 µl of guanidine solution and sonicating for 1 minute to dissolve the protein. One hundred µl of the resulting solution was added to a 96-well plate and the OD at 375 nm was measured using a microplate reader. The reagent background solution OD was also quantified. The precise amount of total

protein in each guanidine-dissolved protein was quantified using Qubit 4 fluorometer (Thermo Fisher Scientific). For the analysis, the OD reading for the reagent background solution was subtracted from the readings for each sample of interest. The carbonylated protein in the sample was calculated using the formula:

$$C = [(OD\ 375\ nm)/6.364) \times (100)]\ nmol/well$$

where:

OD 375 nm is the optical density reading of the sample of interest following reagent background solution deduction.

6.364 is the extinction coefficient using the enclosed 96 well plate.

in mM (= 22 mM-1 cm-1 x 0.2893 cm path length in well)

C is the Carbonyl in your sample well (nmol)

To calculate the amount of carbonylated protein per total protein CP:

$$CP = nmol\ carbonyl\ per\ mg\ protein$$

$$= (C/P) \times 1000 \times D$$

where:

P is the total protein per sample

D is the dilution or concentration step applied to sample

1000 is the factor to convert μg to mg.

2.6.4 qPCR for podocyte-specific markers

The qPCR was performed according to the procedure described in 2.3.3 using the list of primers below:

Oligonucleotide name	Sequence
Nephrin_F (Navarro-Munoz et al., 2011)	AGGAGAGCGGGACACTCAGA
Nephrin_R (Navarro-Munoz et al., 2011)	CCTCAGGGAGCGGTAATACG
Podocin_F (Navarro-Munoz et al., 2011)	TCACTGAAATTCTTCTAGAGAGGAAGAG
Podocin_R (Navarro-Munoz et al., 2011)	CCCAAATACAGGTCACTGAATCC
Synaptopodin_F (Sun et al., 2019)	CATTGACATCCAGCCCAACACC
Synaptopodin_R (Sun et al., 2019)	TGGCCGTCCTGTTGACCACT
GAPDH_F (Du et al., 2015)	GTCTCCTCTGACTTCAACAGCG
GAPDH_R (Du et al., 2015)	ACCACCCTGTTGCTGTAGCCAA
Beta actin_F (Zhang et al., 2017)	CACCATTGGCAATGAGCGGTTC
Beta actin_R (Zhang et al., 2017)	AGGTCTTTGCGGATGTCCACGT

The primers were designed based on previously reported publications as shown in the table above. Both GAPDH and beta actin were used as qPCR housekeeping genes for each experiment comparing the tBHP-treated cells with those cells treated with water to ensure the appropriate baseline was set in response to the experimental condition. This was in line with previous studies using qPCR to assess the effect of oxidative stress on the expression of genes of interest (Junaid et al., 2021) (Zainuddin et al., 2010).

2.6.5 Immunofluorescence

Following treatment with either tBHP or the water vehicle, the harvested cells were washed with PBS. They were then fixed and permeabilised with ice cold methanol on ice for 20 minutes. The cells were derivatised with DNPH (Phillip Harris) for 20 minutes at room temperature. The cells were washed five times with TBST. The cells were blocked in 1% bovine serum albumin (BSA) (Thermo Fisher Scientific) in PBS for an hour. Primary and secondary antibody solutions were prepared in blocking solutions with an hour incubation for each. Three washes of 10 minutes each between antibody incubation was performed using PBS supplemented with 0.1% Tween-20 (PBST). Nuclear staining was performed at room temperature for 5 minutes using DAPI (Thermo Fisher Scientific) diluted in PBS followed by a PBST wash. The following antibodies were used for immunofluorescence: anti-nephrin (AF4269-SP), anti-synaptopodin (SC-515842), anti-DNP (A150-117A).

2.6.7 Transcriptomic experiment for tBHP treatment of podocytes

Following treatment with tBHP or vehicle control for 24 hours, 5 x 10^6 cells differentiated podocytes were treated with 1 ml of TRIzol (Invitrogen) and incubated at room temperature for 5 minutes after which 200 µl of chloroform was added. Samples were vortexed for 15 seconds and incubated at room temperature for 3 minutes before centrifugation at 12,000 g for 15 minutes at 4°C. The top-most aqueous phase was collected and added to 500 µl of isopropanol. The resulting solution was centrifuged for 10 minutes at 12,000 g at 4°C and the pellet washed twice with 75% ethanol. The pellet was dried and resuspended in DEPC-treated water. RNA was quantified using Nanodrop ND-1000 UV/VIS Spectrophotometer (Thermo Fisher Scientific) with A260/280 absorbance ratio of ~ 2 and A260/230 ratio of >2.

The integrity of the RNA was also measured using RNA ScreenTape (Agilent) with all values above 8. Thirty μl of RNA was submitted to Oxford Genomic Centre for RNA sequencing at concentrations between 10 and 30 ng/μλ RNA.

Fifty million reads were obtained for each sample. The total reads per sample were mapped onto the Hg38 genome build to identify the region of sequence mapping. An assessment of the clustering between the samples was performed and a PCA plot of the top 500 variable genes generated. Differentially expressed genes were identified between groups using the DESeq2 Bioconductor package (Love et al., 2014). The list of upregulated genes was identified as those with an adjusted p value of < 0.05 and a $\log_2$foldchange of ≤ 1 the downregulated genes were populated as those with an adjusted p value of < 0.5 and a $\log_2$foldchange of ≥ -1. These were the recommended thresholds for the DeSeq2 Bioconductor package which while stringent eliminated the possibility of noise being mistaken as experimental differences (Love et al., 2014). The differentially expressed genes were analysed for their biological and molecular pathways using EnrichR which identifies those pathways in which a significant proportion of differentially expressed genes are represented. (Xie et al., 2021) (Chen et al., 2013b) (Kuleshov et al., 2016)

1

2.6.8 NRF2 induction with 1-2-Cyano-3,12-dioxooleana-1,9 (11)-dien-28-oyl] imidazole (CDDO-Im)

Two and hundred fifty thousand differentiated podocytes were seeded onto 60 cm dishes overnight. The cells were treated with 10 nM, 20 nM, 30 nM and 40 nM CDDO-Im or 40 nM of DMSO in cell culture media and incubated for 6 hours. The cells were then harvested and

assayed. For those experiments in which cells were primed with CDDO-Im and then treated with tBHP, the CDDO-Im or the DMSO was removed after six hours of treatment followed by a rinsing of the cells with fresh media three times before tBHP at 100 μM or water prepared in media was added to the cells for 24 hours.

2.6.9 CRISPR-dCAS9 activation and inhibition of NRF2

Guide RNAs were selected from published CRISPRi and CRISPRa libraries (Horlbeck et al., 2016). The top five guide RNAs, as ranked by features predicted to optimise efficacy and reduce off target effects, were selected for *NFE2L2* (NRF2) activation inhibition. None of the guides selected overlapped. The table below details the guides used for activation and inhibition:

Guide Name	Protospacer sequence	dCRISPR activation or inhibition
LentiSamv2_NRF2_0	GTGTCGTGATGCGTAGACGG	Negative control
LentiSamv2_NRF2_1	GGCAAGAAGCTCGCGGTCCG	Activation
LentiSamv2_NRF2_2	GCAGGCGGGGGCCTAGAGG	Activation
LentiSamv2_NRF2_3	GGGAGGGCAAACTGAACGC	Activation
LentiSamv2_NRF2_4	GCCAACCTGTCCCTTGGCCC	Activation
LentiSamv2_NRF2_5	GGCAGGAAAGGGCCAACCGA	Activation
LentiKRAB_NRF2_0	GCTGCATGGGGCGCGAATCA	Negative control
LentiKRAB_NRF2_1	GAGCCCGAGGGCGAACGGGT	Inhibition
LentiKRAB_NRF2_2	GCACGAGCCCGAGGGCGAAC	Inhibition
LentiKRAB_NRF2_3	GAGGCGCGGCGCGGACAGGG	Inhibition
LentiKRAB_NRF2_4	GACATATATAAAGTACTCAG	Inhibition
LentiKRAB_NRF2_5	GATTCTCTTCTGTGCTGTCA	Inhibition

Both negative controls were scrambled sequences which did not target regions within the human genome (Ruf et al., 2021) (Tripathi et al., 2021).

2.6.9.1 Cloning of guide RNAs

Equimolar amounts of oligonucleotide pairs for each guide RNA were annealed by incubation at 95°C for 5 minutes in a thermocycler and slow cooling to RT in an annealing buffer consisting of 50 mM Tris-HCl pH 7.5 (Thermo Fisher Scientific), 10 mM $MgCl_2$ (Sigma Aldrich), 1 mM ATP (Sigma Aldrich) and 10 mM Dithiothreitol (DTT) (Sigma Aldrich). A combined digestion ligation was performed using T7 ligase buffer (NEB), fast digest enzyme BSMBI (Thermo Fisher Scientific), 100mM DTT (Thermo Fisher Scientific), T7 ligase (NEB), Bovine serum albumin (BSA) (Thermo Fisher Scientific) annealed oligonucleotides (diluted at 1:10), LentiSamV2 plasmid (Addgene #75112) or pLV hU6-sgRNA hUbC-dCas9-KRAB-T2a-Puro (Addgene #71236). The resulting solution was incubated at 37°C and 20°C for 5 minutes for 15 cycles in a thermocycler. Then the product of the digestion ligation was used to transform SURE2 supercompetent E. coli cells (Agilent) according to the manufacturer's instructions. For selection, the transformed cells were cultured on Luria broth agar plates prepared with 100µg/ml ampicillin (Thermo Fisher Scientific) overnight at 37°C. Colony PCR was performed from the resulting clones using CPPT/CTS FWD standard primer (AGAAAAGGGGGGATTGGGGGGTAC) and the reverse sequence of the guide RNA oligos at an annealing temperature of 61°C following the PCR protocol detailed in 2.2.3.

2.6.9.2 Transfection of HEK293T with positive clones and packaging plasmids to make lentivirus.

The packaging plasmids pMD2.G and psPAX2 and the LentiSAMv2 or pLV hU6-sgRNA hUbC-dCas9-KRAB-T2a-Puro with the guide RNA inserts were used at a ratio of 1:3:4 with the Lipofectamine transfection reagent (Thermo Fisher Scientific), Harvesting and transduction was as described in 2.5 Lentiviral Transduction.

2.6.9.3 qPCR for KEAP1 and NRF2 expression following CRISPR-dCAS9 activation and inhibition

RNA extraction and qPCR were performed as described in 2.3 with the following primers:

Oligonucleotide name	Sequence
KEAP 1_F (Lan et al., 2020)	TTCGCCTACACGGCCTC
KEAP 1_F (Lan et al., 2020)	GAAGTTGGCGATGCCGATG
NRF2_F (Fan et al., 2017)	TCTGACTCCGGCATTTCACT
NRF2_R(Fan et al., 2017)	GGCACTGTCTAGCTCTTCCA
GAPDH_F (Du et al., 2015)	GTCTCCTCTGACTTCAACAGCG
GAPDH_R (Du et al., 2015)	ACCACCCTGTTGCTGTAGCCAA
Beta actin_F (Zhang et al., 2017)	CACCATTGGCAATGAGCGGTTC
Beta actin_R (Zhang et al., 2017)	AGGTCTTTGCGGATGTCCACGT

The primers were used under the conditions for which their publications suggested.

2.6.10 Performing Oxyblot

Loading buffer was prepared using 4x Laemmli buffer (Bio-Rad) and 10% 2-mercaptoethanol. Lysates were diluted in loading buffer and incubated at 99°C for 10 minutes. Samples were loaded into wells of 4-20% Mini-Protean gels (Bio-Rad) alongside a protein ladder (Cell Signal). Gels were run for 20 minutes at 100 V then at 130 V for 60 minutes. The gels were activated using ultraviolet light on a ChemiDoC MP Imaging System (Bio-Rad) before performing a wet transfer at 100 V for 40 minutes onto a 0.2 μm PVDF membrane.

The blots were blocked with 5% Amersham ECL blocking agent (Cytiva) in TBST for 1 hour at RT. Blots were incubated in a housekeeping antibody (either GAPDH or Cyclophilin-B; product numbers in 2.6.11) for 1 hour at RT and washed three times with TBST. The blots were then incubated with the appropriate LI-COR IRDYE secondary antibody for the housekeeping primary antibody for an hour at room temperature and washed three times in

TBST (2.6.11). Then the blot was derivatised in 1% DNPH prepared in 2 N HCl for 10 minutes at room temperature and washed three times with 2 N HCl before being blocked in 5% Amersham ECL blocking agent for 1 hour. Finally, the blot was incubated for 1 hour with anti-DNP antibody (A150-117A) prepared in blocking solution, washed three times with TBST and incubated with anti-goat secondary antibody (LI-COR 926-32214). The blot was washed three times antibody dissolved in blocking solution before three ten-minute washes and visualised using LI-COR's Odyssey CLx.

2.6.11 Western blot

The western blots were performed as described in 2.4.2 with the following antibodies:

Antibody	Source
NRF2	Abcam (Ab62352)
HMOX1	Thermo Fisher Scientific (MA1-112)
Cyclophilin-B	Abcam (ab236760)
GAPDH	Santa Cruz (SC-365062)
LI-COR 680RD goat anti mouse secondary antibody	926-68070
LI-COR 800CW goat anti rabbit secondary antibody	925-32211

2.6.12 Flow cytometric quantification of oxidative stress

Following treatment with tBHP or the water vehicle control, media was removed, and cells washed with cold PBS and trypsinised as described previously. The trypsin digest was neutralised using media and the resuspended cells centrifuged at 500 g for 5 minutes and the supernatant discarded. The cell pellet was resuspended and transferred to a 96-well plate. Cells were incubated with NIR Zombie live/dead stain (BioLegend) for 15 minutes at room temperature and washed three times with 5% FCS (Thermo Fisher Scientific) in PBS. An unstained control well was incubated with 5% FCS in PBS without stain. For each wash, the cells were centrifuged at 500 g for 5 minutes. The cells were then fixed in ice cold methanol

on ice for an hour and washed three times with 5% FCS in PBS. They were then derivatised using 0.1% DNPH in HCl at room temperature for 20 minutes and washed five times with 5% FCS in PBS. A control well for derivatisation was also prepared in which the cells were treated with 0.1% HCl. Following derivatisation, the cells were incubated with anti-DNP antibody (A150-117A) for 30 minutes on ice and washed with 5% FCS in PBS. They were then incubated with anti-goat secondary antibody (A-11055) for 30 minutes and washed three times with 5% FCS in PBS. In total there were four control wells: unstained, live/dead stain only, primary with secondary antibodies but no live-dead stain and secondary only. In those cases where other antibodies were tested together with the anti-DNP antibody in the same well of cells, the single stains for each antibody were also used for control. Cells were sorted using BD FACSCANTO flow cytometry system and analysed using the Flowjo software (BD).

2.6.14 Mass spectrometry proteomics experiment for podocytes

For the proteomics study with the podocytes, the following conditions were tested simultaneously:

Cell line	Experimental Condition 1	Experimental Condition 2
WT podocytes	CDDO-Im treated	Water treated
WT podocytes	CDDO-Im treated	tBHP treated
WT podocytes	DMSO treated	Water treated
LentiKrab_NRF2_0	DMSO treated	tBHP treated
LentiKrab_NRF2_1	DMSO treated	tBHP treated

The cells were harvested following treatment by removing the culture media and washing with PBS and trypsinised. The cells were centrifuged at 500 g for 5 minutes, the supernatant was removed, and the cells were lysed using 1% SDS, centrifuged 12,000 g for 5 minutes at

4°C and the supernatant collected. The amount of protein was quantified using Qubit 4 fluorometer and 10 µl of each sample was run on a protean gel as follows:
Loading buffer was prepared using 4x Laemmli buffer (Bio-Rad) and 10% 2-mercaptoethanol. Lysates were diluted in loading buffer and incubated at 99°C for 10 minutes. Samples were loaded into wells of 4-20% Mini-Protean gels (Bio-Rad) alongside a protein ladder (Cell Signal). Gels were run for 20 minutes at 100 V then at 130 V for 60 minutes. The gels were imaged using ultraviolet light on a ChemiDoC MP Imaging System (Bio-Rad). Each sample had a minimum of 15 µg of protein submitted for the proteomic experiment. The samples were enzymatically digested and analysed by liquid chromatography-tandem mass spectrometry (LC-MS/MS) using an Ultimate 3000 UHPLC coupled to an Orbitrap Fusion Lumos Mass Spectrometer as previously described (Dellar et al., 2023): The data was acquired in a data-independent acquisition (DIA) mode such that the MS1 scans were acquired with 120,000 resolution and an m/z of 350-1650, an AGC target of 5e5 and a maximum injection time of 20 ms. MS/MS scans were obtained at 30,000 resolution and the normalised higher energy collisional dissociation was set at 30%. The raw mass spectrometry files were analysed in DIA-NN v8 using automatically generated precursor ions produced in silico from a protein sequence database. To obtain differentially expressed proteins between the groups, the output from DIA-NN was analysed in R using the Bioconductor workflow package DEP1.25.0. Proteins with missing values were filtered out unless identified in 2/3 replicates of at least one condition. Data was background corrected and normalisation performed using variance stabilising transformation, and remaining missing values imputed using k-nearest neighbour before differential expression analysis. To identify differentially expressed proteins *'test_diff'* which performs a differential enrichment test based on protein-wise linear models and empirical Bayes statistics using limma was used (Ritchie et al., 2015). False discovery rate was estimated using 'fdrtool' package which

works by calculating both tail-area based FDR values (p values) and density-based local FDR (z-scores and t-scores) (Strimmer, 2008).

2.7 Chapter 4- Specific Methods

2.7.1 Establishing a stable inducible CAS9-expressing SH-SY5Y cell line.

2.7.1.1 Lentiviral transduction of SH-SY5Y neuroblastoma cells

The packaging plasmids pMD2.G (Addgene #12259) and psPAX2 (Addgene #12260) and the inducible CAS9 plasmid pCW-CAS9 (Addgene #50661) were used at a ratio of 1:3:4 with the Lipofectamine transfection reagent (Thermo Fisher Scientific) and lentivirus harvested and added to cells for transduction as described earlier before antibiotic selection with puromycin at 10ug/ml for a week. To induce CAS9 expression, the cells were treated with doxycycline at 0.75 µg/ml for 72 hours.

2.7.1.2 Quantification of CAS9 expression in the inducible CAS9-expressing SH-SY5Y cell line

qPCR was performed using the conditions described in 2.3 using the primers:

Primer Name	Sequence
GAPDH_F (Du et al., 2015)	5'GTCTCCTCTGACTTCAACAGCG
GAPDH_F (Du et al., 2015)	5'ACCACCCTGTTGCTGTAGCCAA
Beta Actin Forward (Zhang et al., 2017)	5'CACCATTGGCAATGAGCGGTTC
Beta Actin Reverse (Zhang et al., 2017)	5'AGGTCTTTGCGGATGTCCACGT
CAS9 Forward (Yang et al., 2018)	5'GAAAGTTCGACAATCTGACCAAGG
CAS9 Reverse (Yang et al., 2018)	5'TGCCACGTGCTTTGTGATCTG

2.7.2 Transfection of SH-SY5Y-CAS9 cells with *MAPT* sgRNA

sgRNA for exon 1 and exon 4a were obtained from Synthego at a concentration of 1 µg/µl. Sequence for exon 1 was 5'GACACGGACGCUGGCCUGAA and for exon 4a 5' UGGAGAGGAAAUCCACAGGG. These two guides were selected because they had the lowest off-target effect and highest target efficiency using algorithm from three primer design platforms: Benchling, CHOPCHOP and IDT. The control sequence was a proprietry product from Synthego which is a scrambled sequence which cannot target human genome (Negative Control sgRNA (mod) #1).

Reverse transfection of cells was performed using RNAimax transfection reagent (Thermo Fisher Scientific) according to the manufacturer's instruction. After 72 hours, single cells were sorted into wells of a 96-well plate using a Sony SH800z Cell Sorter and cultured in complete SH-SY5Y culture media to confluence.

2.7.3 Induction of oxidative stress with tert-butyl hydroperoxide (tBHP)

For SH-SY5Y cells, 3 x 10^6 cells were seeded on 60 cm dishes and treated with 15 µM Luperox tBHP (Sigma Aldrich) or water control for 24 hours. After 24 hours, the medial was removed and the cells washed with PBS. Cells were then scraped and collected into a 10 ml Falcon tube, centrifuged at 500 g and the supernatant removed. The pellet was then collected for subsequent assays.

2.7.4 Genomic DNA analyses

2.7.4.1 Long range PCR between exon 1 and 4a

Following DNA extraction and quantification, the exon 1 forward primer 5'GGATGGGCGGCCAACTGTTAGAGAG and the exon 4a reverse primer 5'AAACAAGGTGGGTAGCACGG were used at an annealing temperature of 66°C following the protocol of NEB's Phusion high fidelity DNA polymerase. The PCR product was run on a 1% gel and the amplicons of interest cleaned up as described earlier before sending for Sanger sequencing.

2.7.4.2 Exon 1 and exon 4a specific PCRs

PCR was performed as described in 2.23 using the following primers: 5' CGAAGTGATGGAAGATCACG and 5' AAACAAGGTGGGTAGCACGG in exon 1 and

5’ GCTTCTAGGAGACCTGCACC and 5’ TTTTGTGTCCTCTCCCAAAG in exon 4a at an annealing temperature of 51°C.

2.7.4.3 Analysis of Sanger sequencing traces

Sanger sequence traces were visualised on the Snapgene Software (version 6.1). Alignment of WT and edited traces was performed using Synthego’s ICE analysis platform (Synthego, 2019)

2.7.4.4 Whole genome sequencing

PacBio HiFi long range WGS library preparation and sequencing were performed by the Oxford Genomics Core. For each cell line sample, one SMRT (8 M) flow cell was used. Sequencing was performed on the PacBio Sequel IIe platform. For the WT cell line, 23.45 Gb HiFi reads were generated (mean read length 9.23 Mb). For the *MAPT* $^{-/-A2}$ cell line, 26.91 Gb HiFi reads were generated (mean read length 12.79 Mb). Analysis of WGS was performed by Jia-uan Zhang in the Todd/Wicker group as follows: HiFi sequencing reads for each cell line were separately aligned to the GRCh38 reference genome (without fix patches and alternative haplotypes) using pbmm2 (https://github.com/PacificBiosciences/pbmm2) with parameter --preset ccs. Joint structural variant calling was subsequently performed using pbsv (https://github.com/PacificBiosciences/pbsv) with parameter --ccs and tandem repeat annotation. Identified variants meeting all of the following criteria were selected for subsequent analyses: (i) located on chromosome 1-22 or chromosome X; (ii) genotypes available for both samples; (iii) not annotated as being imprecise or involving tandem repeats; (iv) sequencing depth (DP).

2.7.5 Gene expression analysis

2.7.5.1 Reverse Transcriptase PCR for MAPT isoforms

cDNA from the cell lines were produced as described in 2.3.2 and used in a reverse transcriptase PCR with the primers below using Taq DNA polymerase (NEB) according to the protocol detailed in 2.2.3 and the stated annealing temperatures.

2.7.6 Protein Analysis

2.7.6.1 Western blotting

This was performed according to the protocol described in 2.4.2. Three µl Tau recombinant protein (Sigma Aldrich) was run alongside all sample. Tau 12 (MAB2241) and Tau 46 (SC-32274) antibodies were used at concentrations of 1:1,000 and 1:250, respectively. Cyclophilin-B antibody (ab236760) was used at a concentration of 1:1000 or GAPDH antibody (SC-365062) at 1:500 as the loading controls. The secondary antibodies IRDye 680LT Goat anti-rabbit IgG (926-68071) and IRDye 800CW Goat anti-mouse IgG (926-32210) were used at a concentration of 1:10,000.

Isoform	**Forward (5'-3')**	**Reverse (5'-3')**	**T_m**
0N	CTTCTCCTCCTCCGCTGTC	CTGCTTCTTCAGCCTTTCAGG	54°C
1N	CTTCTCCTCCTCCGCTGTC	ATGCCTGCTTCTTCAGCTTC	53°C
2N	CTTCTCCTCCTCCGCTGTC	GAGCTCCCTCATCCACTAAGG	55°C
232rtPCR	CTTCTCCTCCTCCGCTGTC	TCACAAACCCTGCTTGGC	56°C
232gPCR	GGATGGGCGGCCAACTGTTAGAGAG	GGCCTCAAGGGATCCTCCTGCCTG	61°C

For free tubulin and polymerised tubulin, the SH-SY5Y cells were washed twice with 1 ml of buffer A (containing 0.1 M MES (pH 6.75), 1 mM MgSO4, 2 mM EGTA, 0.1 mM EDTA, and 4 M glycerol) at 37 °C. After incubating the cells at 37 °C for 5 min in 400 ml of free tubulin extraction buffer (buffer A plus 0.1% Triton X-100 and pro- tease inhibitors), the extracts were centrifuged at 37 °C for 2 min at 16,000 g. The supernatant fractions contained

free tubulin that had been extracted from the cytosol. The cell pellet and lysed cells in a culture dish were dissolved in 400 ml of 25 mM Tris (pH 6.8) with 0.5% SDS, which contained tubulin in its original polymerized state (i.e., microtubules). Equal amounts of total proteins from the free and polymerized tubulin fractions were analysed by Western blot analysis using an anti-tubulin antibody (ATN02) at 1:200.

2.7.6.2 Immunofluorescence

Antibodies used for immunofluorescence are shown below and were used at a concentration of 1:50. For standard immunofluorescence, the protocol is as in 2.4.3. For the polymerised tubulin immunofluorescent assay, cells were washed in extraction buffer (80 mM PIPES/KOH, pH 6.8, 1 mM MgC12, 1 mM EGTA, 30% glycerol, 1 mM GTP), incubated for 30 seconds with extraction buffer containing 0.02% (wt/vol) saponin, and washed with extraction buffer, with each step at 37°C. This was to remove the free tubulin. Subsequently, the immunofluorescence staining protocol described in 2.4.3 was followed.

Antibody	**Source**
Tau 46	Santa Cruz (SC-32274)
NRF2	Abcam (Ab62352)
HMOX1	Thermo Fisher Scientific (MA1-112)
KEAP1	Thermo Fisher Scientific (TA502059)
Tubulin polyclonal antibody	Cytoskeleton (ATN02)
Anti-DNP antibody	Bethyl Laboratory (A150-117A)
LI-COR 680RD goat anti mouse secondary antibody	926-68070
LI-COR 800CW goat anti rabbit secondary antibody	925-32211
LI-COR 800CW anti-goat secondary antibody	926-32214

2.7.6.3 Mass Spectrometry Proteomics

The following cell lines and test conditions were included in the mass spectrometry proteomics experiment, carried out as described previously in 2.7.3:

Cell line	Experimental Condition
WT SH-SY5Y	Water control
WT SH-SY5Y	tBHP treated
MAPT $^{-/-A2}$	Water control
MAPT $^{-/-A2}$	tBHP treated
MAPT $^{-/-A4}$	Water control
MAPT $^{-/-A4}$	tBHP treated

Four replicates were tested for each cell line/condition combination. After 24 hours of treatment with either tBHP or water vehicle control, the culture media was removed, and the cells were washed with PBS and trypsinised. The cells were centrifuged at 500 g for 5 minutes, the supernatant was removed. The cells were washed three times with PBS and the pellet of cells stored at -80°C until they were dispatched frozen to the Ralser laboratory in Berlin for testing. The sample preparation and data processing used was identical to that which was previously described in section 2.6.14.

2.7.7 Fluorescent In-situ Hybridisation (FISH)

FISH was performed by Daniela Moralli at the CHG. BAC RP11-782E1 (localised at chr17: 43,983,233-44,203,399, hg19), overlapping the *MAPT* locus was used as probe. In addition, a probe for the centromere of chromosome 17 (RP11-227J24) and BAC RP11-579A4 mapping to the band distal to *MAPT* (chr17: 56594950-56914115, hg19) were used to position the *MAPT* locus on chr17. The probes were hybridised to metaphase spreads from 100 SH-SY5Y cells (metaphases and interphases). As a control for the FISH experiment, the BACs were labelled and hybridised to metaphase spreads from a diploid control cell line.

2.7.8 Oxidative Stress Flow Cytometry

Each treatment condition was performed in triplicates as described in 2.7.3. Oxidative stress was measured in live cells as described in:

2.6.12 Flow cytometric quantification of oxidative stress.

2.7.9 Transfection of *MAPT* KO cells with pInducer20-Tau or pInducer 20

2.7.9.1 Lentiviral transduction of MAPT $^{-/-A2}$ and MAPT $^{-/-A4}$

The packaging plasmids pMD2.G (Addgene #12259) and psPAX2 (Addgene #12260) and the plasmids pInducer20 Tau (Addgene #92201) or the control plasmid pInducer20 (#44012) were used at a ratio of 1:3:4 with the Lipofectamine transfection reagent (Thermo Fisher Scientific) according to the manufacturer's instruction. Lentiviral supernatant was harvested from the cells 48 and 72 hours after transfection and stored at 4°C before ultracentrifugation at 22,000 rpm for 2 hours at 4°C in a swinging-bucket rotor. The pellet was resuspended in 50 µl of ice-cold PBS. Transduction of cells was done as follows: Fifty µl lentiviral resuspension was added to a 60 cm dish. One million cells were resuspended in complete media supplemented with 10 µg/ml protamine sulfate and added to the lentivirus and cultured for three days. The cells were not selected with antibiotics.

2.7.9.2 Western blot for MAPT $^{-/-A2}$ and MAPT $^{-/-A4}$ transduced with pInducer20 Tau or pInducer20.

This was carried out as described in section 2.7.6.1 using Tau 12 antibody (MAB2241) and GAPDH 12 (SC-365062). IRDye 800CW Goat anti-mouse IgG (926-32210) was used for detection.

2.7.10 CDDO-Im treatment of SH-SY5Y cells as a primer before tBHP treatment

Three million WT SH-SY5Y, *MAPT* $^{-/-A2}$ and *MAPT* $^{-/-A4}$ cells were seeded onto 60 cm dishes overnight. The cells were treated with 100 nM CDDO-Im or 100 nM of DMSO in cell culture media and incubated for 6 hours before treatment with 15 µM tBHP Luperox (Sigma Aldrich) for 18 hours. The cells were then harvested and assayed according to the flow cytometry protocol described in 2.7.8.

2.8 Chapter 5 – Specific Methods

2.8.1 Differentiation of kidney organoids

The timeline for the differentiation of the kidney organoids is shown below:

	hiPSC Diff Protocol Self-Organization 3D Organoids					
-7 Seed hiPSCs onto 24 well plates **E8** **200 to 300ul media**	**-6** Change media **APEL with PFH and CHIR99021**	**-5** Change media **APEL with PFH and CHIR99021**	**-4** Change media **APEL with PFH and CHIR99021**	**-3** Change media **APEL with PFH and CHIR99021**	**-2** Change media **APEL with PFH and FGF9/Heparin**	**-1** change media half and half **APEL with PFH and FGF9/Heparin**
7+0 3d day 1ml media 6 well plate DISSOCIATION CHIR PULSE 5 µM 1h Apel FGF9/Heparin	**7+1**	**7+2** **APEL with PFH and FGF9/Heparin**	**7+3** Patterning starts	**7+4** **APEL with PFH and FGF9/Heparin**	**7+5** Can swap APEL for E6 From this point change media every other day **No FGF9/HEPARIN**	**7+6**
7+7 MEDIA CHANGE	**7+8**	**7+9** MEDIA CHANGE	**7+10**	**7+11** MEDIA CHANGE	**7+12**	**7+13** MEDIA CHANGE
7+14	**7+15** MEDIA CHANGE	**7+16**	**7+17** MEDIA CHANGE	**7+18** FIX (FOR ICC, IHC)	**7+19 Prolonged** MEDIA CHANGE	**7+20 Prolonged**
7+21 Prolonged MEDIA CHANGE	**7+22 Prolonged**	**7+23 Prolonged** MEDIA CHANGE	**7+24 Prolonged**	**7+25 Prolonged** MEDIA CHANGE FIX (FOR ICC, IHC)		

2D

3D

For 2D differentiation 80,000 cells were seeded on 24-well plates in 300 µl of E8 media (day -7). On the next day, 300 µl of APEL2 medium (STEMCELL Technologies) was added with 8 µM CHIR99021(Tocris) and protein-free hybridoma (PFH) (Thermo Fisher Scientific 12040-0770), titrated for each batch between 1% and 10%. On day -5, -4 and -3 media was refreshed with APEL2 with CHIR99021. This step keeps the cells on the glomerular pathway of differentiation.

On day -2, 200 ng/ml of FGF9 (RnD systems) and 1 µg/ml Heparin (Thermo Fisher Scientific) in APEL 2 media were added to the cells. On day -1 media is refreshed by replacing half of the spent media with fresh APEL 2 with FGF9. On Day 0 cells are dissociated in preparation for 3D differentiation.

3D Differentiation – Day 7+0

A transwell plate (PICM03050-CM) was prepared by adding 1 ml of APEL 2 media with PFH and 5 µM CHIR99021 and submerging the filter in the media, ensuring no bubbles between the filter and the media and leaving the plate with the transwell in an incubator to equilibrate. Cells were then gently washed cells in a 24-well plate with PBS. One ml of TryplE (Thermo Fisher Scientific) was added and incubated at 37°C for 1 minute. Following this, cells were observed under a microscope for clumps, the cells should not be single celled at this stage. Following APEL 2 with PFH neutralisation cells were gently pipetted up and down to break up large clamps, transferred cells into 15 ml falcon tubes and centrifuged at 1,400 rpm for 4 minutes leaving an aliquot for cell counting. Next cells were resuspended in APEL 2 media with PFH and aliquoted into 500,000 cells per Eppendorf tube.

The tubes were centrifuged at 400 g for 1 minute rotated 180° and centrifuged again. This step was repeated for a total of four spins changing the orientation of the tube each time. A Pasteur pipette was used to suck up the pellet and place on the transwell, excess media from the Pasteur pickup was also collected with a P200 pipette. Four to five organoids were placed per transwell and incubated in CHIR99021 media for an hour. After 1 hour, organoids were transferred to a fresh 6-well plate with 1 ml of APEL 2 media with 200 ng/ml FGF9, PFH and 1ug/ml heparin and equilibrate at 37°C. Media was changed on day 7+2 and 7+4. On day 7+5, the media was changed from APEL 2 to E6 (Thermo Fisher Scientific) without heparin and FGF9. This media was refreshed every other day until day 7+18 or 7+25.

2.8.3 Immunofluorescence for podocytes and hiPSCs

Two hundred and fifty thousand 13-day differentiated podocytes and 500,000 hiPSCs were seeded onto cover slips within 24-well plates. Staining was performed as described in 2.4.3 Immunofluorescence. All the antibodies tested are listed in section 2.8.2.

2.8.2 Immunofluorescence for kidney-specific organoids

After differentiation, the organoids were transferred to glass bottom Ibidi plates (Thistle Scientific) and fixed with 2% paraformaldehyde (PFA) at 4°C for 20 minutes. The PFA was removed, and the organoids were washed three times with PBS. One hundred and fifty µl of blocking buffer (10% donkey serum (Sigma Aldrich)/0.3% TritonX (Thermo Fisher Scientific) / PBS) into the Ibidi plates containing organoids. The organoids were then blocked at RT for 2-3 hours, gently keep shaking the dish using a rocker during incubation. The primary antibodies (listed below) were prepared in blocking buffer at 1:200 and the organoids were incubated at 4°C overnight.

Antibody	Source
Nephrin	BioTechne (AF4269-SP)
Synaptopodin	Santa Cruz (SC-515842)
GATA 3	Cell signalling Technology (5852S)
E-Cadherin	BD Biosciences (610182)
SOX 17	BioTechne (AF1924-SP)
WT 1	Santa Cruz (SC-7385)
LRP2	Sapphire Bioscience (NBP2-39033)
Tau 46	Santa Cruz (SC-32274)
Alexa fluor anti-mouse 546	Thermo Fisher Scientific (A-11003)
Alexa fluor anti-goat 488	Thermo Fisher Scientific (A-11055)
Alexa fluor anti-sheep 594	Thermo Fisher Scientific (A-11016)
Alexa fluor anti-rabbit 488	Thermo Fisher Scientific (A-11008)

The primary antibody solution was then aspirated off the dish and organoids were washed with PBTX (0.3% TritonX/PBS) six times, 10 minutes each with gentle shaking. Then they were incubated with secondary antibodies (1:400) of choice in PBTX at 4°C overnight.
The secondary antibody solution was then aspirated off and the organoids were incubated with DAPI (1:1,000 dilution) in PBS for 5 mins. The organoids were washed with PBS for 10 minutes, three times and dehydrated by incubating in 25%, 50% ,75% and 100% methanol solutions for 5 minutes. They were then cleared using 1:2 benzyl alcohol to benzyl benzoate solution for 24 hours and imaged using a Leica SP8 SMD X Confocal microscope.

2.8.3 Oxidative stress induction in organoids

Fully differentiated kidney organoids (7+25 days of differentiation) were treated with either 50 µM or 200 µM tBHP (Luperox) for 24 hours in APEL 2 media. The control organoids were treated with water vehicle. After 24 hours, the media was aspirated and the organoids were washed with PBS.

2.8.4 Immunofluorescence for oxidative stress in organoids

Following treatment with either tBHP or water, the organoids were transferred to glass bottom Ibidi plates (Thistle Scientific) and fixed with 2% paraformaldehyde (PFA) at 4°C for 20 minutes. The PFA was removed, and the organoids were washed three times with PBS. One hundred and fifty µl of blocking buffer (10% donkey serum (Sigma Aldrich) /0.3% TritonX (Thermo Fisher Scientific) / PBS) was added to the Ibidi plates containing organoids. The organoids were derivatised with 0.1% DNPH for 20 minutes and washed five times (10 minutes each) with TBST. The organoids were then blocked at room temperature for 2-3 hours, with gentle shaking using a rocker during incubation. The primary antibodies were prepared in blocking buffer at 1:200 and the organoids were incubated at 4°C overnight. The primary antibody solution, Nephrin, E-Cadherin, DNP, was then aspirated off the dish and organoids were washed with PBTX (0.3% TritonX/PBS) six times, 10 minutes each with gentle shaking. Then they were incubated with secondary antibodies (1:400) of choice in PBTX at 4°C overnight. The secondary antibody solution was then aspirated off. The organoids were washed with PBS for 10 minutes, three times and dehydrated by incubating in 25%, 50% ,75% and 100% methanol solutions for 5 minutes. They were then cleared using 1:2 benzyl alcohol to benzyl benzoate solution for 24 hours and imaged using Leica SP8 SMD X confocal microscope.

2.8.5 *MAPT* KO in hIPS cells

The *MAPT* KO cells were generated by Dr Phalguni Rath using the forward sgRNA GAUCACGCUGGGACGUACG in exon 1 and the reverse sgRNA in exon 9 UCGGCUCCACUGAGAACCUGA using electroporation as follows: 50 µl vitronectin (Thermo Fisher Scientific) was added to 48-well plates and incubated for an hour at room temperature. A transfection mix of 1µl sgRNA (Synthego), 0.6 µl CAS9 RNP (Synthego) and

4.4 µl of buffer R (Thermo Fisher Scientific) was mixed by pipetting followed by a short spin and incubated at room temperature for 15 minutes. The cells were prepared for electroporation during this time: spent media was removed, and TrypLE (0.5µl/6-well plate) was added and incubated for 5 minutes at 37°C. DMEM/F12 (2 ml/well of 6-well plate; 5 ml per T25 flask) was added to the cells to dilute TrypLE and all the cells were collected and centrifuged at 100 g for 5 minutes at room temperature. The supernatant was discarded and the cells resuspended in 10 ml DMEM/F12. The cells were again centrifuged at 100 g for 5 minutes at room temperature, the medium was discarded and the cells resuspended in 1 ml E8 medium. Cell viability was checked using Trypan Blue. Ten thousand cells/transfection prepared in E8 medium were collected into a falcon tube, centrifuged at 100 g and following removal of the E8 media resuspended in 7 µl of buffer R. Then the cell suspension was added to the RNP mix and kept on ice for 5 minutes. The cells were electroporated using following parameters for KOLFC2 hIPS cells) – 1200 volts, 30 ms, 2 pulses and seeded directly in one well of vitronectin coated 48-well plate containing 200 µl E8 media with RevitaCell supplement. After 24 hours, the cells were checked for viability. Media was then changed and the cells grown for a further 48 hours. The cells were dissociated using TrypLE and seeded in ultra-low density (2,000-5,000 cells in 60 mm dish) for single-cell cloning. Collect remaining cells for genomic DNA isolation to verify cutting efficiency. Expanded single cell clones and PCR performed using the following primers: forward 5'CAGAACTTATCCTCTCCTCT and reverse 5'GGTCCGTGTCGGGATGGGG and sequence amplicon.

2.8.6 Nuclei isolation from human renal biopsy

Nuclei isolation from healthy human renal biopsy was performed by Jessica Kepple as follows: single nuclei were isolated from fresh or liquid nitrogen flash frozen renal biopsies using the 10X Genomics Chromium Nuclei Isolation Kit with RNase Inhibitor 16 rxns (PN-

1000494), with protocol modifications including supplemented RNase inhibitor and FACS sorting. The day prior to the nuclei isolation, polypropylene 1.5 ml Eppendorf tubes were coated with 10% BSA (MACS BSA Stock Solution, Miltenyi Biotec, 130-091-376) overnight at 4°C to be used during nuclear isolation experiment. Human renal biopsies (5-12 mg) were homogenized using kits pestle on ice in 200 µl of chilled lysis buffer supplemented with additional 0.2 U/µl RNase inhibitor. The samples were incubated on ice from 10 minutes in additional 300 µl of lysis buffer with 0.2 U/µl RNase inhibitor. The homogenate was transferred to a Nuclei Isolation Column in a 10%BSA precoated collection tube and centrifuged at 16,000 rpm for 20 seconds at 4°C. The column was then discarded and the supernatant was resuspended with gentle mixing 15x times with a pipet, then centrifuged at 500 g for 3 min at 4°C. The pellet was resuspended and washed with 500 µl of the Debris Removal Buffer with 0.2 U/µl of RNase inhibitor and mixed by gently pipetting fifteen times. The resuspension was then centrifuged at 700 rpm for 10 minutes at 4°C and supernatant was discarded. The pellet was resuspended in 200 µl of Wash Buffer and filtered through a 40-µm FLOWMI cell strainer (SP Bel-Art, 136800040) and counted using a haemocytometer. Samples with more than 1 million nuclei were then FACS sorted to clean up the sample using Sytox-7AAD Live dead staining. Samples with below 1 million nuclei after washing were filtered a second time with the 40-µm FLOWMI cell strainer.

Single cell RNA-sequencing

Gene libraries from isolated human renal single nuclei were constructed with droplet-based single-cell RNA sequencing (scRNA-seq) using the Chromium Next Gen Single Cell 3' Reagent v3.1 Dual Index Kit. Single nuclei were loaded at 1,000 nuclei/µl for a targeted 10,000 nuclei per sample depending on starting biopsy weight. Libraries were then sent to the Oxford Genomics Centre for Illumina NovoSeq6000 Sequencing. Subsequent Illumina runs

were demultiplexed and the resulting fastq files were processed through the 10X Genomics Cellranger pipeline on the command line. Filtered gene matrix data was then analysed in R using the Seurat package.

2.9 Statistical Analysis

Statistical analyses were performed using Prism 9 (GraphPad Software). Unless otherwise stated, data is shown as mean with standard error of the mean (SEM). Comparisons between two groups for continuous data have been undertaken using Student's T-test. Where more than two groups are compared, p-values for multiple T-tests were corrected for multiple comparisons using the Holm-Šídák method. Results were reported as significant if $P_{\text{corrected}} < 0.05$ and uncorrected P values are also shown. Statistical analysis of proteomic data is described in section 2.6.14 Mass spectrometry proteomics experiment for podocytes.

Chapter 3

A Multiomic Investigation of Oxidative Stress in Podocytes

3.1 Introduction and Aims

In this Chapter, I investigated the role of the transcription factor nuclear factor erythroid 2-related factor 2 (NRF2; encoded by the NFE2L2 gene) in the response to oxidative stress in a human podocyte cell line, with the following aims:

a. Establish an oxidative stress induction protocol in immortalised podocyte cells and determine the consequent global changes in gene expression and protein abundance.
b. Define how suppression or upregulation of NRF2 expression alters the oxidative stress response in podocytes.
c. Assess the proteins and biological pathways disrupted in response to oxidative stress, with NRF2 modulation. In particular:
    I. Proteins that are modulated in response to NRF2 overexpression and inhibition, suggesting that they are NRF2-regulated genes
    II. Conversely, proteins altered in response to oxidative stress but not modified by NRF2 manipulation, suggesting non-NRF2 related oxidative stress pathways.

Given current understanding of the role of NRF2, I hypothesised that if a credible method of inducing oxidative stress in the podocytes was developed, upregulating NRF2 would protect the podocytes from oxidative stress induction. I proposed that an assessment of pathways from a proteomic or transcriptomic dataset, this observation would be explainable with the activation of genes involved in the NRF2/KEAP1 pathway such as HMOX1 and NQO1.

Overall, this approach aimed to define novel NRF2-dependent or -independent genes or pathways of relevance to oxidative stress response and DKD, as potential future therapeutic targets.

3.2 Results

Aim 3a: Establish an oxidative stress induction protocol in immortalised podocyte cells and determine the consequent global changes in gene expression and protein abundance

3.2.1 Four-hour treatment of podocytes with Tert-Butyl hydroperoxide increases peroxidised lipids but does not change expression of podocyte-specific markers

As previously described, there is an assortment of ways of inducing oxidative stress within cell lines. I wanted a method which ensured sufficient cell viability for live cells to be interrogated, induced oxidative stress in the live cells sufficiently to show a quantifiable difference in peroxidised lipid and carbonylated protein in treated cells compared with control and crucially affected the expression of podocyte-specific markers in a manner that reflected their expression in DKD patient. I began by assessing the effect of a variety of reagents on podocyte viability. As shown in Table 1, okadaic acid at 5 nM had the most significant effect on cell death with minimal effect on cell viability from the five glucose concentrations and from 4-hour treatment with 100 uM tBHP. As is described in the appendix 1.3, further exploration of the glucose conditions for their comparison with mannitol showed no significicant difference between oxidative stress levels hence these conditions were not explored further despite the high cell viability. Instead I focused on tBHP.

Table 1: Effect of oxidative stress induction condition on podocyte viability

	Condition						
	5 nM okadaic acid	10 mM glucose	20 mM glucose	30 mM glucose	40 mM glucose	50 mM glucose	4-hour 100 uM tBHP
Cell viability	<10%	99%	97%	95%	93%	91%	93%

Tert-Butyl hydroperoxide (tBHP) is an established model substance for the induction and evaluation of oxidative stress in cells and tissues, promoting lipoperoxidation of membrane phospholipids via peroxyl and alkoxyl radicals and depleting reduced glutathione by oxidation (Davies, 1989) (Schnellmann, 1988). However, the effect of tBHP on oxidative stress in podocytes *in vitro* has not been studied. To establish a protocol to induce oxidative stress in the human podocyte LY line, an initial 100 μM concentration of tBHP was chosen, based on its ability to induce oxidative stress in kidney proximal tubular cells – tBHP-treated cells showed increased amounts of glutathione disulphide and peroxidised lipids (Schnellmann, 1988). Exposure of the AB podocyte line – a human immortalised podocyte cell also produced by Saleem et al using an identical process as the LY cells (Methods): at this concentration of tBHP for 2 hours did not alter intracellular Ca^{2+}, suggesting podocytes remain viable with 100 μM tBHP, although oxidative injury was not assessed (Schenk et al., 2018).

Following exposure to 100 μM tBHP cytotoxicity was assessed and levels of peroxidised lipid in podocytes measured as a read out for oxidative stress. Because the expression of podocyte-specific markers is altered in DKD patients, these markers were also measured in the stressed podocytes (Wang et al., 2008, Kostovska et al., 2020).

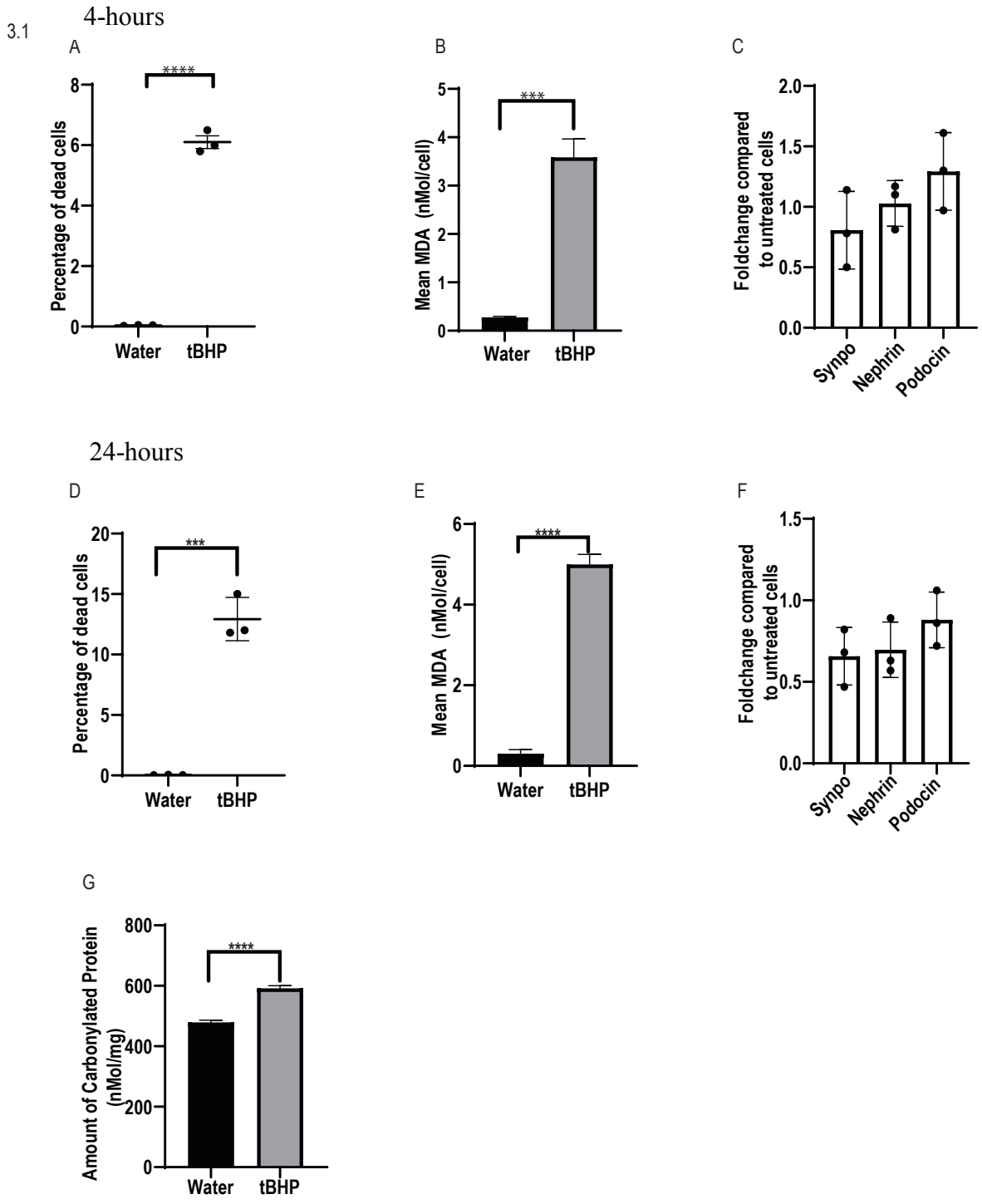

Figure 3.1 Effect of 100 μM tBHP for 4 hours (A-C) and 24 hours (D-G) on podocyte viability, expression of podocyte-specific markers and on peroxidised lipids. **A** Percentage of dead cells for water-treated and tert-butyl hydroperoxide (tBHP)-treated cells, measured by haemocytometer with trypan blue staining. **B** Mean malondialdehyde (MDA) per cell for water-treated and tBHP treated podocytes by colorimetric quantification of supernatant. **C** Quantitative polymerase chain reaction (qPCR) measurement of cDNA. Fold change in expression with tBHP relative to water treated cells is shown for podocyte specific markers as indicated using 2-ddCt. **D** Percentage of dead cells in water-treated and tBHP-treated cells

by trypan blue staining. **E** MDA concentration per cell for water-treated and tBHP-treated podocytes by colorimetric quantification of supernatant. **F** Fold change in expression by qPCR for podocyte specific markers following treatment of cells with tBHP compared to water. **G** Carbonylated protein measured by carbonyl content assay ***p<0.001, **** p<0.0001. Error bars represent the standard deviation. Results for A and C are from data obtained from three independent repeats.

An initial treatment duration of 4 hours was selected based on published data in a murine lens epithelia cell line, in which 130 μM tBHP was eliminated by cells in culture after 4-6 hours (Spector et al., 2002). In response to 100 μM tBHP for 4 hours, mean average podocyte cell death was 7% versus 0.04% in water-treated controls (Figure 3.1A). Exposure to tBHP resulted in an increase in peroxidised lipid, as measured by elevated MDA (Figure 3.1B) but no difference was detectable in the expression of three podocyte-specific markers, synaptopodin, nephrin and podocin (Figure 3.1C).

3.2.2 24-hour treatment of podocytes with tBHP decreases expression of synaptopodin and nephrin while increasing levels of peroxidised lipids

To establish if longer exposure to tBHP could induce changes in podocyte gene expression, the time in culture was increased to 24 hours. After 24 hours of tBHP treatment, the mean percentage of dead cells was 13% compared to 0.037% in control cells (Figure 3.1D). Oxidative stress increased compared to control, as measured by both peroxidised lipid (MDA assay) (Figure 3.1E), and carbonylated protein level (Figure 3.1G). The expression of both synaptopodin and nephrin was lower after 24 hours tBHP exposure relative to control as measured by quantitative polymerase chain reaction (qPCR), though podocin expression was not altered (Figure 3.1G).

In summary, following exposure to 100 μM tBHP for 24 hours, oxidative stress is induced, and expression of podocyte-specific markers reflects observations in DKD, suggesting a

pathologically relevant response, while maintaining an acceptable high level of cell viability. This treatment protocol was used for all subsequent oxidative stress experiments on podocytes including the transcriptomic and proteomic experiments described in this Chapter.

3.2.3 Perturbations in biological pathways in tBHP-treated podocytes

In order to assess the biological pathways altered in the podocytes in the context of oxidative stress, RNA sequencing (RNA-Seq) and mass spectrometry (MS) proteomics were performed. In the transcriptomic experiment, triplicates of 24-hour 100 µM tBHP-treated podocytes and water-treated control podocytes were compared. For the proteomic study, the effect of tBHP treatment on podocytes formed part of a larger experiment in which other conditions were investigated (explained in detail later in the Chapter).

3.2.3.1 Podocyte transcriptomic changes with oxidative stress

RNA-seq data per sample clustered by condition (tBHP versus control) based on both principal component analysis (PCA) multidimensional scaling and pairwise comparisons of all the transcripts (Figure 3.2A and B). All three samples for each condition were used for the subsequent analyses.

To account for genes with very low expression and improve the reliability of log fold change estimates, shrinkage was performed. Shrinkage considers the fact that some genes such as stress-induced genes have greater deviations from their mean independent of experimental conditions while others – including housekeeping genes – have tighter controls. Thus, it ensures that such deviations are not mistaken as experimental differential expression (Wu et al., 2013). After shrinkage was performed, 2,525 genes were upregulated while 2,696 were downregulated.

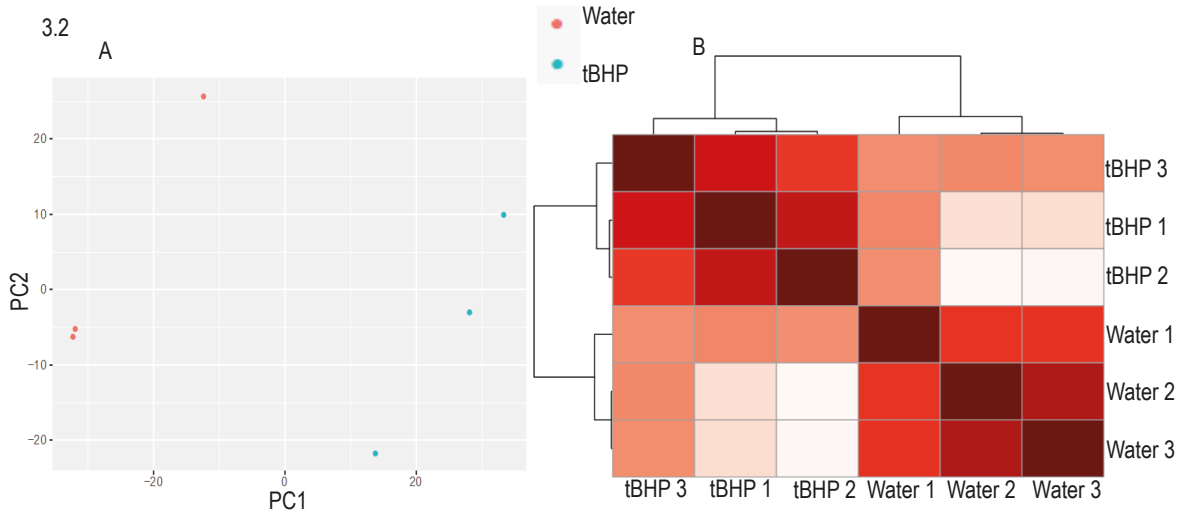

Figure 3.2 Comparison of genes expressed in podocytes with or without tBHP treatment. **A** Multidimensional scaling principal component analysis showing variance in expressed genes in triplicates of water-treated and tBHP-treated podocytes. **B** Heatmap showing the results of pairwise comparisons between the samples treated with either tBHP or water (Analysis by Fiona Hamey).

3.2.3.2 Genes upregulated with oxidative stress in podocytes

To identify molecular functions, biological pathways and cellular structures most perturbed by oxidative stress, I determined the overlap between the differentially-expressed genes and pathway databases including Gene Ontology (GO) Molecular function 2021 and Reactome 2022 (Xie et al., 2021, Kuleshov et al., 2016, Chen et al., 2013a). The enrichment analysis is performed for the input up- and down-regulated gene lists, against a selected background library to generate the graphs. Volcano plots were generated based on the corresponding odds ratio (x-position) and p-value (y-position) from the results. Significantly enriched gene sets are highlighted in colour.

Statistically, the most different GO molecular function term was RNA-binding (GO:0003723) in tBHP-treated podocytes versus control with 253/1,406 genes in the RNA-binding set upregulated (18% overlap) (Figure 3.3A). These include the fused in sarcoma (*FUS*) gene involved in the regulation of transcription, splicing and transport of RNA, U1

small nuclear ribonucleoprotein 70 kDa (*snRNP70*), which is critical for the formation of the U1snRNP component of the spliceosome, and heterogeneous nuclear ribonucleoprotein particle U (*hnRNP U*), important for the normal splicing of pre-mRNA (Ye et al., 2015) (Spritz et al., 1987) (Kwiatkowski et al., 2009).

MAPT, encoding the microtubule protein Tau, was also amongst the RNA-binding genes upregulated in response to oxidative stress (Figure 3.3D). Four GO terms associated with DNA binding also upregulated with high probability (Figure 3.3A): 155 genes were upregulated in GO:0003677 DNA binding (2,510 genes in term, 6.2% overlap), 132 for GO:0043565 sequence-specific DNA binding (1,678 genes in term, 7.9% overlap), 123 for GO:0003690 double-stranded DNA binding (1,660 genes in term, 7.4% overlap) and 132 for GO:1990837 sequence-specific double-stranded DNA binding (1,567 genes in term, 8.4% overlap). Fifty-two genes were shared amongst all these four DNA binding GOs indicating that these ontologies are overlapping subsets of DNA binding. Consistent with RNA and DNA binding related-pathway modulation, the nucleus is the top cellular location for proteins encoded by upregulated genes in podocyte oxidative stress by p value (Figure 3.3B). Regarding molecular functions, upregulated genes include known microtubular beta tubulin genes, *TUBB1* and *TUBB4A,* Kinesin-like proteins *KIF1A* and *KIF21B)*, and mitochondrial genes, cytochrome c1 *CYC1* and NADH ubiquinone oxidoreductase subunit *NDUFA11*.

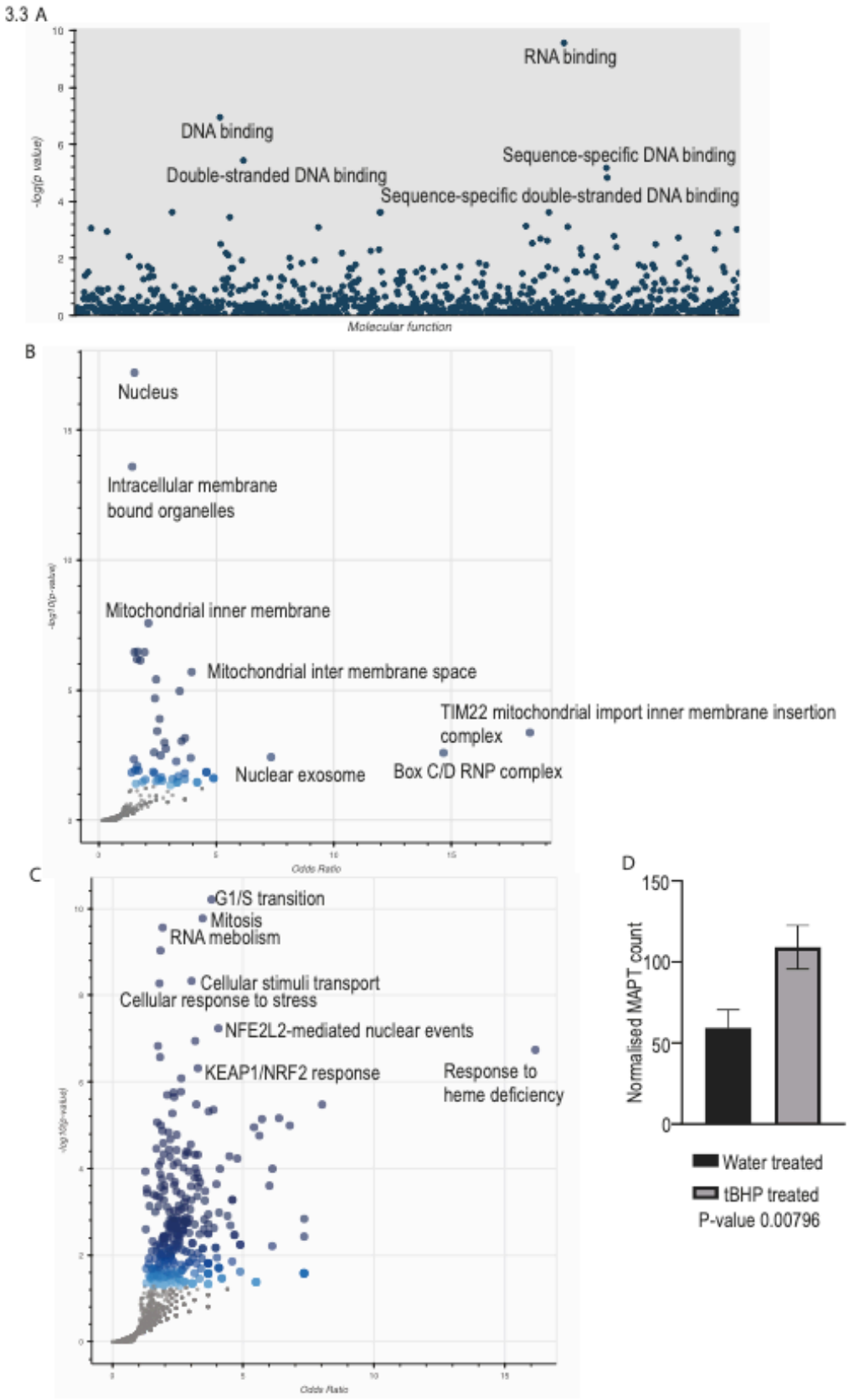

Figure 3.3 Upregulated genes in response to tBHP treatment of podocytes for 24 hours **A** Manhattan plot showing molecular functions enriched for upregulated genes in podocytes with tBHP. **B** Top cellular components within which upregulated genes are expressed. **C** Top

biological pathways perturbed in podocytes with tBHP. **D** Normalised MAPT expression in podocytes treated with or without tBHP. **p<0.01.

I then investigated the biological pathways that overlap with the set of upregulated genes using an alternative pathway analysis tool (Xie et al., 2021) (Chen et al., 2013b) (Kuleshov et al., 2016). I interrogated the upregulated genes against the current database on Enrichr, Reactome 2022. Three of the top ten pathways related to cellular stress and the NRF2/NFE2L2/KEAP1 pathway (Figure 3.3C). Thirty-five genes specifically overlapped between the upregulated gene set and the KEAP1/NRF2 pathway ((31% overlap) while 28 overlapped between the upregulated genes and the nuclear events mediated by NRF2/*NFE2L2* pathway (35% overlap), amongst which are downstream effectors of NRF2 such as heme oxygenase 1 (*HMOX1)* and NADPH quinone dehydrogenase 1 (*NQO1*). Altered G1/S transition and mitosis (Figure 3.3C) may reflect terminally-differentiated podocytes attempting to re-enter the cell cycle under stress and consequently undergoing mitotic cell death (Lasagni et al., 2013).

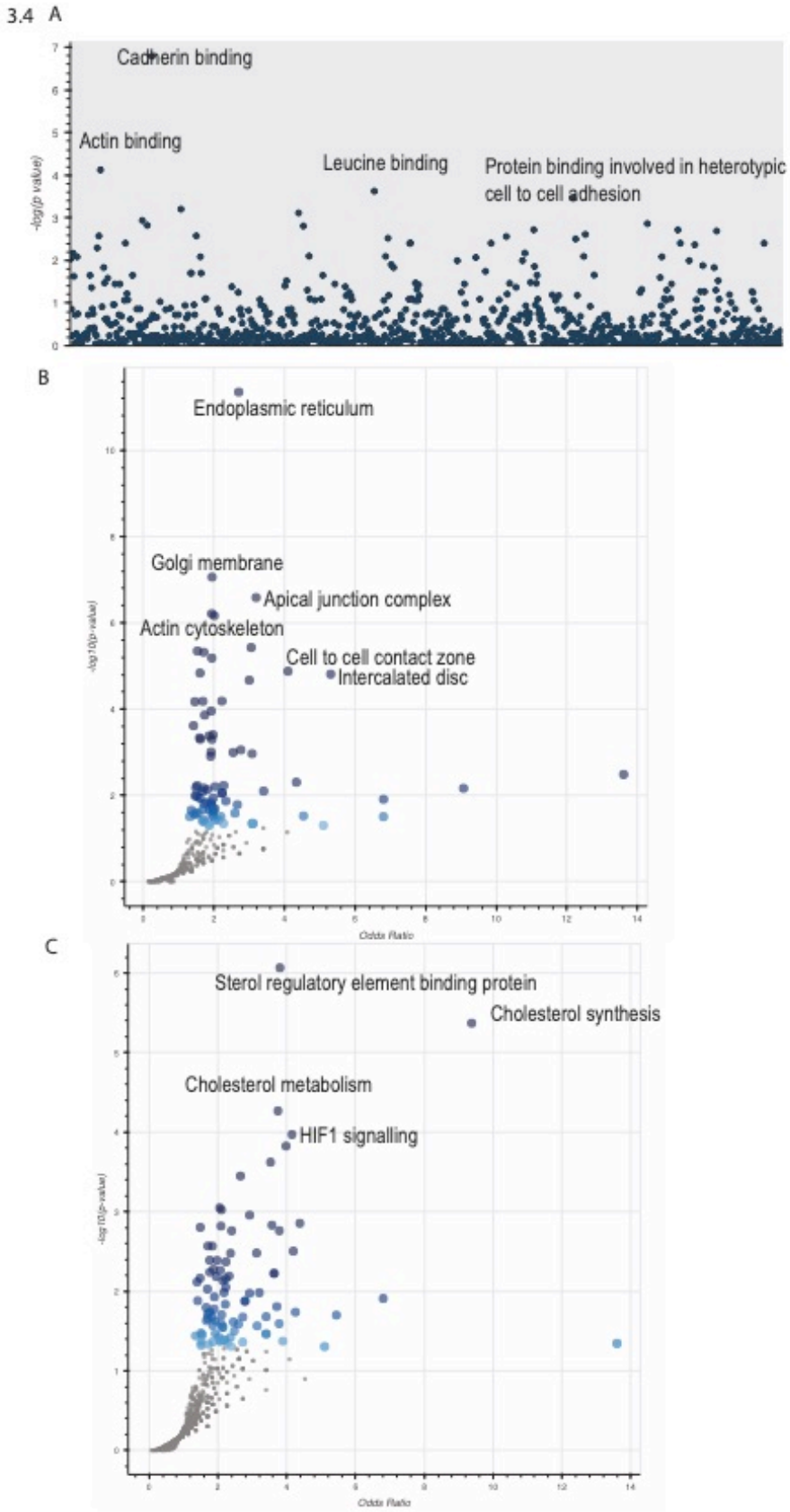

Figure 3.4 Downregulated genes in response to tBHP treatment of podocytes for 24 hours **A** Manhattan plot for molecular functions perturbed in podocytes with tBHP. **B** Volcano plot identifying cellular components within which downregulated genes are expressed. **C** Volcano plot illustrating biological pathways most of the downregulated genes contribute to.

3.2.3.3 Genes downregulated with oxidative stress in podocytes

RNA-seq analysis of podocytes treated with tBHP versus control podocytes identified 2,696 downregulated genes. The GO molecular function most disrupted based on p value was cadherin binding, *CDH1*, encoding E-cadherin, and *CDH2*, encoding N-cadherin were downregulated alongside *MYH9*, *ITGB1* and *EPCAM* (Figure 3.4A). De-differentiation in diseased podocytes features a transition from P-cadherin to N-cadherin (May et al., 2014). The top predicted cellular location of proteins encoded by downregulated genes was the endoplasmic reticulum lumen by p value (Figure 3.4B), including reduced expression of *ADAM17,* encoding a disintegrin and metalloproteinase linked to renal fibrosis and previously described as activated by oxidative stress or mitochondrial damage (Mulder et al., 2012) (Brill et al., 2009). *COL2A1*, a type 1 collagen found in embryonic kidney and *SERPINA1,* encoding the serine protease alpha 1 antitrypsin, was also downregulated.

Sterol biosynthesis was the top pathway in five databases, including Reactome 2022, Bioplanet 2019, Wikipathway 2021and Kegg 2021 (Figure 3.4C). This was due to decreased expression of genes encoding enzymes involved in sterol or cholesterol synthesis including *SQLE, IDI1, SREBF2* and *HMGCR.* Of the podocyte-specific markers previously queried with qPCR (Figure 3.1F), only *SYNPO,* but not *NPHS1*, was detectable as downregulated in response to oxidative stress, highlighting that while RNA-seq provides an unbiased overview it can be less sensitive than methods such as qPCR for individual genes.

3.2.3.4 Changes in the podocyte proteome in response to oxidative stress

Mass spectrometry (MS) proteomics to assess the effect of tBHP on podocytes formed part of a larger experiment including WT and NRF2-modulated podocyte lines, described in detail later in this Chapter. A full list of these conditions is provided in Table 3.1. Here, Conditions 1 and 2 were compared. These cells were treated for 6 hours with 30 nM dimethyl sulphoxide (DMSO) control followed by 18 hours exposure to water control (Condition 1) or 100 μM tBHP Condition 2). This duration was slightly shorter than the 24 hours used for the transcriptomics experiment in order to standardise to subsequent conditions.

Table 3.1 Proteomics conditions for human immortalised podocytes

Condition	Cell line	0-6 hours	6-24 hours
1	Wildtype	30 nM DMSO	water
2	Wildtype	30 nM DMSO	100 μM tBHP
3	Wildtype	30 nM CDDO-Im	water
4	Wildtype	30 nM CDDO-Im	100 μM tBHP
5	LentiKRAB_NRF2_0 control	30 nM DMSO	water
6	LentiKRAB_NRF2_0 control	30 nM DMSO	100 μM tBHP
7	LentiKRAB_NRF2_1	30 nM DMSO	100 μM water
8	LentiKRAB_NRF2_1	30 nM DMSO	100 μM tBHP

Across the six samples within these two conditions (three replicates per condition), similar numbers of peptides were detected with a mean of 6,750 unique proteins identified (SD = 99) (Figure 3.5A). The variance between samples explained by principal component 1 (PC1) was 54.9% and distinguished Condition 1 from Condition 2 (Figure 3.5B).

Twenty-four proteins were upregulated under Condition 2 (oxidative stress) in comparison with Condition 1 (control) (log_2 fold change cut off of + 0.58 and adjusted p-value ≤ 0.05) (Figure 3.5C), with the NRF2-regulated heme oxygenase HMOX1 the top upregulated protein by fold change and p-value. Over one third (37.5%) were broadly involved in protein metabolism and modification (Table 3.2).

Table 3.2 Proteins upregulated in tBHP-treated wildtype podocytes versus control by gene ontology biological process

GO Biological Process	Overlapping Genes
Post-translational protein modification (GO:0043687)	C4A, TF, IL6, ITIH2, AFP, SERPINC1, MFGE8, APOB, F5
Cellular protein metabolic process (GO:0044267)	C4A, TF, IL6, ITIH2, AFP, SERPINC1, MFGE8, APOB, F5
Acute phase response (GO:0006953)	ITIH4, CEBPB, IL6
Cellular protein modification process (0006464)	C4A, TF, IL6, ITIH2, AFP, SERPINC1, MFGE8, APOB, F5
Acute inflammatory response (GO:0002526)	ITIH4, CEBPB, IL6
Platelet degranulation (GO:0002576	ITIH4, TF, A2M, F5
Response to hydrogen peroxide (GO:0042542	IL6, HMOX1, HBA1
Regulation of neurogenesis (GO:0050767	IL6, SERPINF1, FAIM
Regulated exocytosis (GO:0045055	ITIH4, TF, A2M, F5
Regulation of lipid storage (GO:0010883)	IL6, APOB

Of the 24 proteins upregulated under Condition 2, five were also upregulated in the transcriptomic dataset: interleukin 6 (*IL6),* which plays an important role in inflammation in addition to B cell maturation*;* the transcription factor CCAAT enhancer binding protein (CEBPB), which has proinflammatory genes including *IL6* as its targets*;* FAS apoptotic inhibitory molecule FAIM*,* which reduces oxidative stress-dependent loss of cell viability by

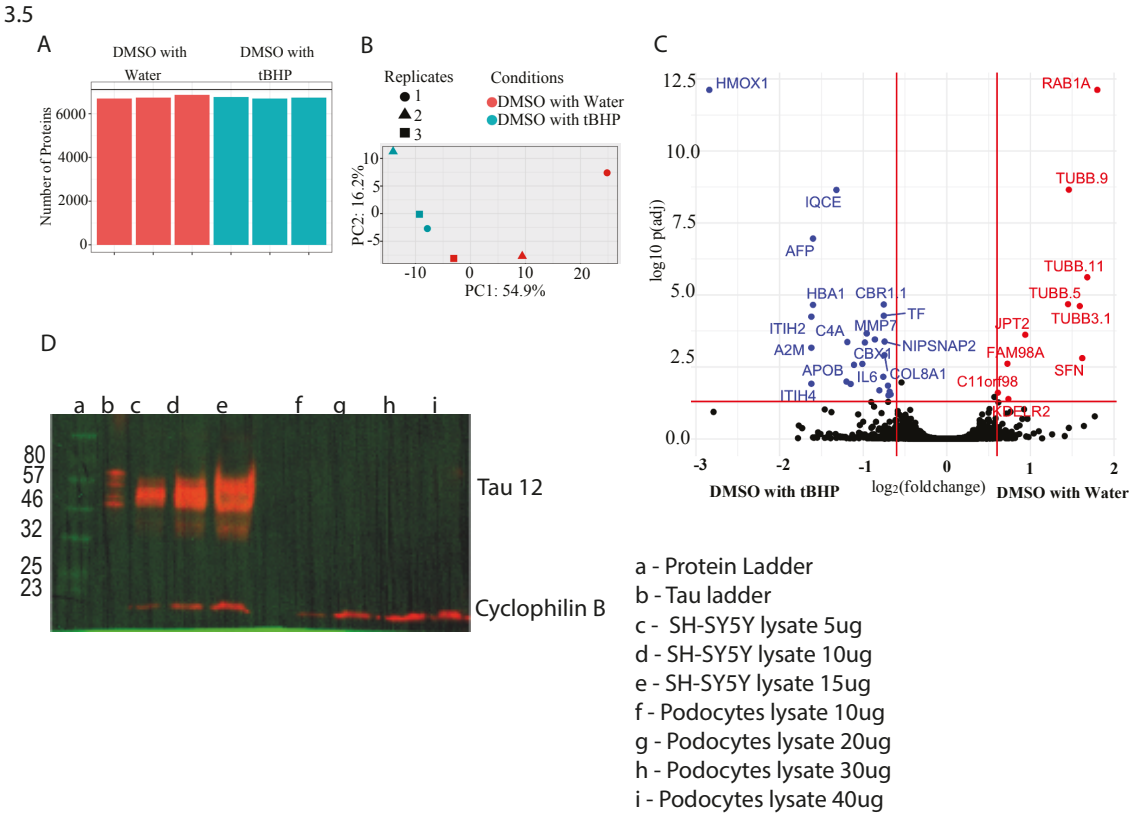

Figure 3.5 Proteomic analyses of differentially expressed genes in response to tBHP. **A** Number of proteins detected per replicate in podocytes treated with water control or tBHP after DMSO control (Conditions 1 and 2 in Table 3.1). **B** PCA plot for variance within replicates and between conditions for the top 5,000 proteins. **C** Differentially-expressed genes between tBHP treated cells versus water-treated cells. Blue labels are upregulated in tBHP-treated cells and red labels are downregulated in tBHP-treated cells. Vertical and horizontal red lines represent cut offs for $\log_2$ fold change of +/- 0.58 while the horizontal line represents a cut-off of 0.05 for p(adjusted) values. **D** Western blot showing expression of Tau protein in SH-SY5Y lysates at increasing total protein concentration and in differentiated podocytes using Tau 12 antibody

decreasing protein aggregation; DLG associated-protein 4, DLGAP4, which has a role in actin cytoskeleton dynamics and the formation of adherens junctions; and HMOX1 (Romero et al., 2022) (Stein and Yang, 1995, Maeda et al., 2010, Kaku and Rothstein, 2020). Podocytes express IL-6 receptors, and also express the proinflammatory cytokine IL-6, with increased expression in podocytes exposed to stress or lipopolysaccharides. IL-6 signalling to podocytes leads to increased cell motility via Signal transducer and activator of transcription 3 (STAT3) and myosin light chain (Lee et al., 2012) (He et al., 2018).

Eight proteins were downregulated with oxidative stress (log_2 fold change cut off of - 0.58 and adjusted p value ≤ 0.05), with Ras-related protein Rab-1A (RAB1A) showing the greatest fold change and the lowest p value (Figure 3.5C). RAB1A is a small GTPase with a role in vesicle transport and membrane trafficking from the endoplasmic reticulum to the Golgi, and may also have a role in signal transduction and autophagy (Schöppner et al., 2016). In rat podocytes, bradykinin promotes RAB1A expression (Tan et al., 2005), suggesting a link between RAB1A and the kallikrein-kinin system (KKS), which triggers release of bradykinin. KKS activity has been implicated in DKD, correlating with risk of diabetic nephropathy in patients with type 1 diabetes (Harvey et al., 1992).

In contrast to the transcriptomic data, Tau was not detected at the protein level by MS, although Tau-associated tubulin proteins, TUBB3, TUBB, SFN and FAM98A, were the most frequent proteins downregulated with oxidative stress (Barbier et al., 2019). Moreover, as shown in 3.5D, lysates from 12-day differentiated LY podocyte cells do not express levels of Tau protein detectable with Tau 12 antibody on a western blot. This is in spite of a strong signal detection on SH-SY5Y neuroblastoma cells.

Of the podocyte-specific markers in Figure 3.1F, only synaptopodin was detected at the protein level, and this was not differentially expressed between the two groups.

In conclusion, treating differentiated podocytes with 100 µM tBHP for 24 hours induces cellular oxidative stress as measured by increased peroxidised lipids and carbonylated protein. This was further confirmed by transcriptomic evidence of activation of genes involved in the NRF2/KEAP1 pathway, and proteomic analysis highlighting upregulation of NRF2-regulated HMOX1 and oxidative stress pathway associated proteins. Oxidative stress

induction also upregulates the expression of *MAPT* at the mRNA level along with other genes associated with RNA-binding. Functional changes are suggested by the altered expression of podocyte-specific markers such as synaptopodin and nephrin as well as IL-6 signalling. These results indicate a model *in vitro* system to explore pathways of potential relevance to DKD.

3.2.4 A flow cytometric method to quantify oxidative stress

The most common method for determining oxidative stress in live cells is to measure carbonylated protein. Typically, this is done by immunoblotting of cell lysates with an antibody recognising 2,4-dinitrophenylhydrazine (DNPH). The same antibody is also used for immunofluorescence methods (Reznick and Packer, 1994) (Levine et al., 1994). Both approaches are at best semi-quantitative. Moreover, since neither of these methods distinguish live from dead or dying cells, differences in cell death could influence the assay. For this project, knowing that the tBHP treatment affects cell viability (Figure 3.1A/D), it would be important to measure oxidative stress specifically in live cells. An optimal platform would be more quantitative than western blotting or immunofluorescence, while versatile enough to quantify multiple proteins simultaneously in live cells.

I therefore designed a modified flow cytometric method based on the quantification of carbonylated protein as an established surrogate for oxidative stress (see Methods 2.6.12). Using flow cytometry permits counter staining and gating for live cells prior to assessing carbonylated protein levels. This is an advance on conventional immunoblot methods.

Aim 3b. The relationship between NRF2 and oxidative stress in podocytes

3.2.5 NRF2 inhibition using CRISPR-dCAS9

The transcriptomics analyses confirmed that the anti-oxidant NRF2/KEAP1 pathway is activated in response to tBHP and also indicated an increase in *MAPT*, raising the question of whether these genes are co-regulated or interacting during the oxidative stress response, which I will further explore in Chapter 4. To better understand NRF2-dependent and -independent cellular responses in podocytes, I tested the effect of knockdown of *NFE2L2*, in the context of the cellular response to oxidative stress. Podocytes were transduced with a lentivirally-packaged catalytically inactivated 'dead' Cas9 fused to a Kruppel-associated box repressor with one of five different guide RNAs targeting the *NFE2L2* promotor region, or an empty vector as control, and subjected to antibiotic selection, to obtain five independent podocyte cell lines identified as LentiKRAB_NRF2_1, 2, 3, 4 or 5 respectively and a control line known as LentiKRAB_NRF2_0 (Thakore et al., 2015).

I set the threshold for significant decrease in expression as a fold change ≤ 0.5 relative to control cells. With this as a baseline, although there was an overall decrease in the expression of the NRF2 regulating gene *KEAP1* in LentiKRAB_NRF2_1, 2, 3, 4 or 5 cells compared to the control cells, this decrease was above the set threshold of ≤ 0.5 (Figure 3.6A). However, a decrease in expression of *NFE2L2*, of between 50-80% compared to control, was observed in LentiKRAB_NRF2 lines 3, 4 and 5 (Figure 3.6B), indicating successful knockdown. A smaller but still significant reduction in *NFE2L2* was also detected in LentiKRAB_NRF2 lines 1 and 2 relative to the LentiKRAB_NRF2_Ctrl cell line.

The effect of NRF2 downregulation on oxidative stress was then assessed by quantifying the level of basal oxidative stress under normal culture conditions. Only LentiKRAB_NRF2_3

and 4 lines had less basal oxidative stress than control NRF2_0 cells. (p values of 0.003 and 0.036, respectively) (Figure 3.6C). Next, the podocyte cells were treated with 100 μM tBHP for 24 hours, and oxidative stress was measured by carbonylated protein, by DNPH immunoblot and by DNPH flow cytometry, to validate the flow cytometry assay (see Materials and Methods) and to measure the effect of NRF2 knockdown on response to oxidative stress. Comparison across the two methods showed consistent results, validating the flow-based system (Figure 3.6D and E).

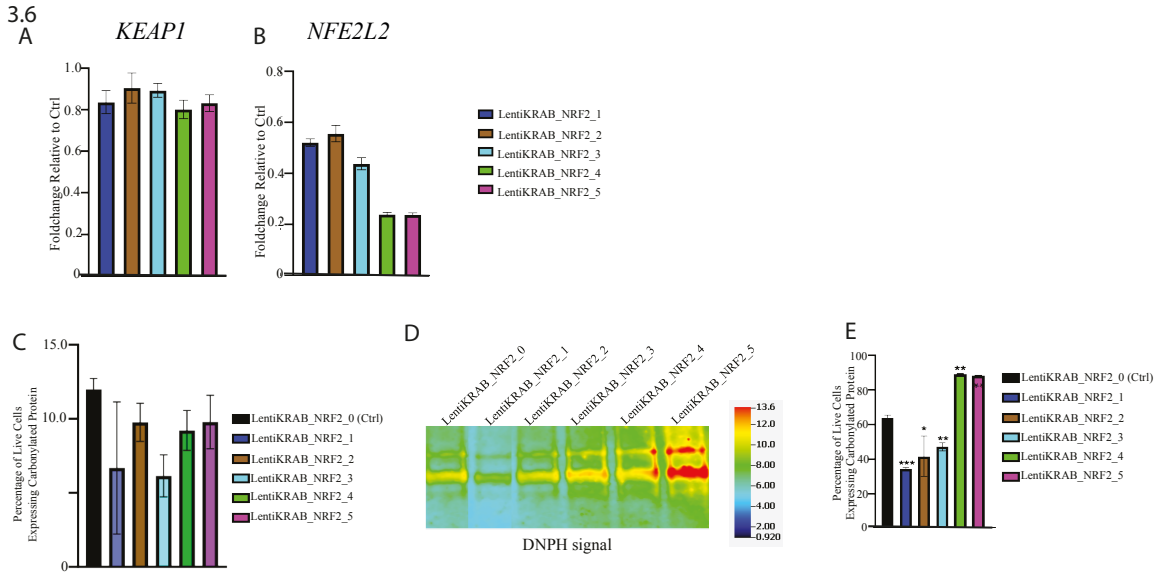

Figure 3.6 Inhibition of NRF2 with CRISPR-dCAS9 in podocytes. **A** Fold change in KEAP1 expression of LentiKRAB_NRF2_1 to 5 compared to Ctrl (LentiKRAB_NRF2_0) measured by qPCR **B** Fold change in NRF2 expression of LentiKRAB_NRF2_1 to 5 compared to Ctrl (LentiKRAB_NRF2_0) by qPCR. **C** Flow cytometrically quantified basal carbonylated protein in live LentiKRAB_NRF2_0 to 5 cells in the absence of tBHP **D** Oxyblot western blotting for DNPH in LentiKRAB_NRF2_0 to 5 cell lines treated with tBHP. with intensity bar on the right. **E** Flow cytometrically quantified carbonylated protein in live cells exposed to tBHP. * P<0.05, ** p<0.01, *** p<0.001. Error bars represent standard deviation.

The cell lines with the largest decreases in *NFE2L2* mRNA expression LentiKRAB_NRF2_4 and 5, exhibited increased oxidative stress, consistent with the established protective function of NRF2 in the antioxidant response. In contrast, a lower reduction in *NFE2L2* expression, around 50% in LentiKRAB_NRF2_1 to 3, unexpectedly appears to be associated with

protection against oxidative stress (Figure 3.6B and 3.6E). Thus, the effect on oxidative stress in the edited cell lines appears to be dependent on the extent of *NRF2* knockdown, although this result cannot fully exclude clonal effects, or off target effects beyond the targeted CRISPR interference.

The flow cytometry-based assay for proportion of live cells expressing carbonylated protein was used as the read out for oxidative stress for the experiments described in the remainder of this chapter and in Chapter 4.

3.2.6 NRF2 activation using CRISPR-dCAS9

Since NRF2 activates antioxidant pathways, priming the cells by increasing *NFE2L2* via CRISPR-CAS9 might be expected to protect the cells against oxidative stress. To increase NRF2 expression I used the CRISPR synergistic activation mediator system (CRISPR SAM), in which a dead Cas9 targets transcriptional activators at the *NFE2L2* promotor (Thakore et al., 2015). Five different guides were cloned into the CRISPR SAM plasmid, to generate lentivirus with which podocytes were transduced, generating five independent cell lines named LentiSamv2_NRF2_1 to 5. The control cell line, LentiSamv2_NRF2_0, was transduced with virus generated from the empty plasmid.

I set the threshold for significant increase in expression as a fold change of ≥1.5 relative to the control cells. In comparison to control, all five cell lines had an increase in expression of both *KEAP1* and *NFE2L2* (Figure 3.7A/B). However, although the increase in expression of *NFE2L2* was above the threshold for all the cell lines, the increase in *KEAP1* expression was above the set threshold for LentiSamv2_NRF2_2 to 5. The extent of *KEAP1* increase appears to correlate with the degree of *NFE2L2* increase.

While the correlation between *KEAP1* and *NFE2L2* at the RNA level could suggest positive feedback of NRF2 to *KEAP1* (Figure 3.7A and B), the increase in *KEAP1* mRNA may simply reflect the established role of KEAP1 in down regulating NRF2 in response to oxidative stress, though this was not observed with NRF2 inhibition by CRISPR-KRAB, even in cell lines with increased stress (Figure 3.6).

Despite the known function of NRF2 as an antioxidant regulator, in response to tBHP treatment all five edited cell lines showed increased proportion of cells expressing carbonylated protein relative to control (Figure 3.7C). This increase in carbonylated protein was unexpected, and could potentially be due to some off-target effects of gene editing or to toxicity induced by supraphysiological levels of NRF2. To understand whether this was specific to the genetic manipulation, pharmacological induction of NRF2 was explored.

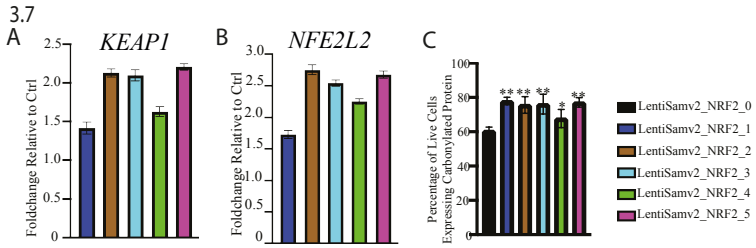

Figure 3.7 Effect of NRF2 activation by CRISPR-dCAS9 in podocytes on oxidative stress response. **A** Fold change in KEAP1 expression in LentiSamv2_NRF2_1 to 5 cell lines compared with control cell line Lentisamv2_NRF2_0 measured by qPCR. **B** Change in NRF2 expression in podocytes activated for NRF2 expression by CRISPR-dCAS9 by qPCR. **C** Proportion of carbonylated protein expressing cells for Lentisamv2_NRF2_0 to 5 cell lines in response to 100 μM tBHP, measured by flow cytometry gated for live cells. * $p<0.05$, **$p<0.01$. Results from three replicate experiments. Error bars represent standard deviation.

3.2.7 Pharmacological induction of NRF2 expression in podocytes

In order to avoid genetic manipulation, and to evaluate dosing effects, I primed the podocyte cells with the NRF2 inducer 1-[2-cyano-3-,12-dioxooleana-1,9(11)-dien-28-oyl] imidazole (CDDO-Im) prior to the induction of oxidative stress. Western blot for both NRF2 and the downstream protein HMOX1 in cell lysate, following 6 hours exposure to CDDO-Im (10 to 40 nM), or DMSO control, demonstrated dose-dependent increases in expression of both proteins indicating successful induction of functional NRF2 (Figure 3.8A).

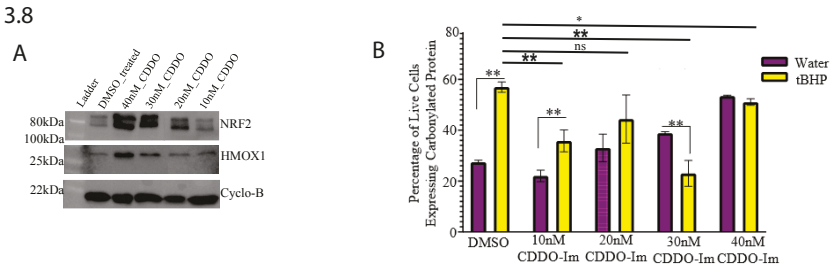

Figure 3.8 CDDO-Im priming of podocytes and response to tBHP treatment. **A** western blot showing effect of 6-hour exposure to 10-40 nM CDDO-Im on expression of NRF2 and HMOX1 with Cyclophilin-B (Cyclo-B) as loading control. **B** Flow cytometry measurement of carbonylated protein expressed by live podocytes treated with wither DMSO or CDDO-Im for 6 hours and then treated with either water or 100 μM tBHP for 18 hours. *p<0.05, **p<0.01, ns = not significant. Displayed result one of three replicates. Error bars represent standard deviation.

At concentrations of CDDO-Im above 10 nM, cells showed increased oxidative stress under standard culture conditions compared to the DMSO control, in a dose-dependent manner (Figure 3.8B). However, following tBHP treatment the proportion of cells exhibiting oxidative stress was lower with 10 nM, 30 nM or 40 nM CDDO-Im compared to DMSO control, consistent with the function of NRF2 as an antioxidant, though this effect was not observed with 20 nM CDDO-Im. Uniquely with 30 nM CDDO-Im, oxidative stress also decreased with tBHP exposure relative to resting conditions. These results were consistent over three independent experiments (Figure 3.8B).

Taken together the results of the CRISPR-dCAS9 and CDDO-Im NRF2 manipulations indicated that both suppression and upregulation of NRF2 can result in an increase in the level of oxidative stress in podocytes under resting conditions. However, either low levels of NRF2 inhibition or 30 nM CDDO-Im pharmacological NRF2 upregulation appear protective from oxidative injury induced by tBHP. The mechanism for these observations, or how a primed state of upregulated or suppressed NRF2 influences response to oxidative injury, is unclear. I therefore explored the pathways modulated by oxidative stress and NRF2 further using MS proteomics.

Aim 3C. Assessing the biological pathways disrupted in response to podocyte oxidative stress with NRF2 modulation

By comparing the biological pathways involved in cellular response to oxidative injury, with and without NRF2 modulation, I hypothesised that oxidative stress pathways could be designated as NRF2 dependent or independent. I designed a mass spectrometry proteomics experiment that compared the conditions described in Table 3.1.

3.2.8 Proteomics defines novel NRF2-regulated or candidate antioxidant proteins.

To explore NRF2-dependent and -independent antioxidant response pathways as potential therapeutic targets for DKD, I wanted to understand how manipulation of NRF2, under physiological conditions or with induction of oxidative stress, would alter podocyte cellular processes. To this end I explored the impact on the proteome of CDDO-Im NRF2 upregulation and CRISPR-dCAS9 NRF2 inhibition.

The finding that 50% *NFE2L2* down regulation appeared to reduce oxidative stress was unexpected (Figure 3.6). Likewise, NRF2 induction was expected to be protective against tBHP injury, but this varied by CDDO-Im dose, being most evident at 30 nM CDDO-Im. Taken together these results might indicate complex or bimodal effects of NRF2, though some non-NRF2 related perturbation shared between the stress resistant cell lines cannot be excluded.

I chose to study the LentiKRAB-NRF2-1 cells and CDDO-Im at 30 nM concentration since both these conditions protected from protein carbonylation (Figure 3.6 and Figure 3.8). This approach focused on potential protective pathways, and aimed to minimise confounding

factors, by comparison of populations with similar levels of oxidative stress. The proteomic experiment was designed to answer three questions: firstly, what pathways are altered in podocytes under oxidative stress (this analysis is described above in section 3.2.3.4), secondly, can novel NRF2-regulated proteins be defined, and finally, are there cellular proteomic changes following tBHP treatment, common to both the CDDO-Im 30 nM and LentiKRAB-NRF2 treatments in comparison to WT cells, thereby suggesting candidate (non-NRF2 driven) antioxidant targets?

For the second question, to explore whether these protein changes are NRF2 driven, I cross-referenced the proteins altered by tBHP treatment in unmanipulated podocytes (Condition 1 versus Condition 2) with the set similarly altered by tBHP treatment following NRF2 upregulation with CDDO-Im and altered in an opposing direction by NRF2 inhibition. Bidirectional consequences with NRF2 up and down regulation suggest NRF2-regulated proteins, but also suggest these may not be responsible for the reduction in oxidative stress with tBHP observed in both these cell lines compared to WT.

For the third question, I identified proteins modulated by oxidative stress in WT podocytes, but unchanged or changing in an opposing direction in both CDDO-Im treated and LentiKRAB_NRF2-1 cells with stress compared to resting. This aimed to identify candidate non-NRF2 regulated proteins with potential as antioxidant targets.

CDDO-Im may have non-NRF2 mediated effects, since the similar drug Bardoxolone Methyl inhibits NFkB as well as activating NRF2 (Chin et al., 2014). One strategy to determine potential off-target effects of CDDO-Im would have been to compare CDDO-Im to CRISPR NRF2 induction. However, I rejected this strategy because all five LentiSAM cell lines

resulted in increased oxidative stress compared to control, raising questions about biological relevance (Figure 3.7C).

Triplicates of each of the cell lines of interest and conditions shown in Table 3.1 were submitted together as part of a single experimental design with all the samples run simultaneously via mass spectrometry, allowing comparisons between any of the groups analysed here. Gene names are used as a standardised nomenclature representing the detected proteins.

3.2.9 NRF2-modulated proteins in the oxidative stress response

The next analysis examined how NRF2 influences the podocyte proteome in the context of oxidative stress induced by 100 μM tBHP, in order to detect candidate NRF2-mediated proteins in the stress response. I focused on changes in protein abundance in CDDO-Im treated cells with tBHP (Condition 4) versus DMSO control with tBHP (Condition 2), which are reversed, when NRF2 is suppressed, i.e. in LentiKRAB_NRF2_1 cells exposed to tBHP (condition 8) versus control LentiKRAB_NRF2_0 exposed to tBHP (condition 6).

LentiKRAB_NRF2_1, with 50% decrease in *NFE2L2* expression, showed less cell death and oxidative stress relative to the control cell line LentiKRAB_NRF2_0 in response to tBHP (Figure 3.6). After tBHP treatment, 28 proteins were downregulated in the LentiKRAB_NRF2_1 cell line (condition 8) relative to the LentiKRAB_NRF2_0 cells (condition 6) while 19 were upregulated. The upregulated genes included NRF2's downstream target HMOX1 despite the inhibition of NRF2 in the LentiKRAB_NRF2_1 line (Figure 3.6). This could suggest some NRF2-independent *HMOX1* activation (Kirby et al., 2018) (Kang et al., 2014) (Wright et al., 2009). However, since the suppression of NRF2 was

measured by mRNA and under normal culture conditions, it is possible that with tBHP, the LentiKRAB_NRF2_1 cells, despite lower 'resting' NRF2, might have an enhanced NRF2 response to oxidative stress relative to LentiKRAB_NRF2_0 controls.

Fifty-seven proteins were upregulated while 51 were downregulated in the CDDO-Im with tBHP cells (Condition 4) relative to the DMSO control with tBHP-treated cells (Condition 2).

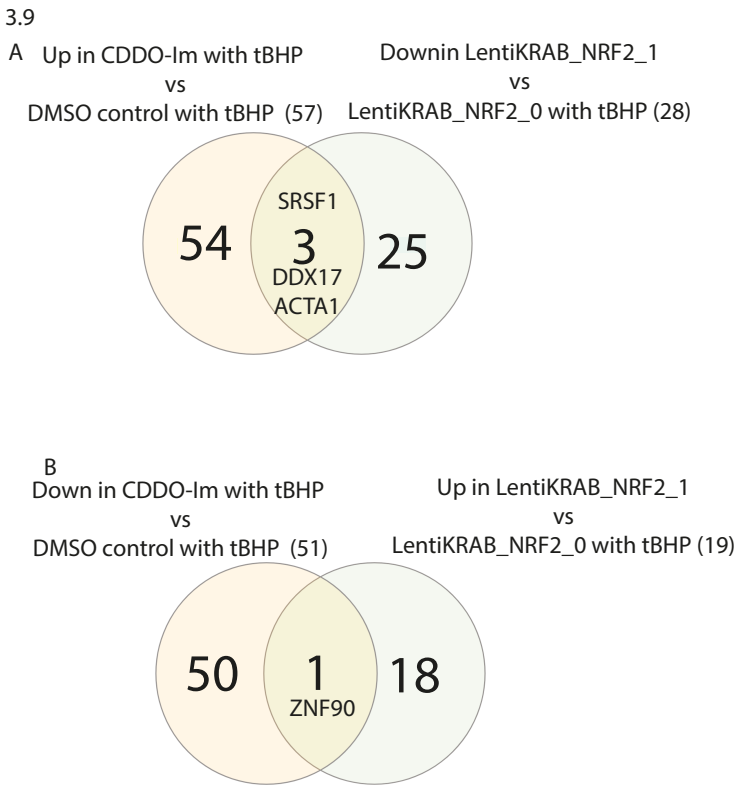

Figure 3.9 Venn diagram to show overlapping proteins between condition 4 vs 2 and condition 8 vs 6. A Proteins upregulated in condition 4 vs. 2 but down regulated under conditions 8 vs 6. B Proteins downregulated in condition 4 vs 2 but upregulated under conditions 8 vs 6. Condition 4 vs 2 = cells primed with CDDO before tBHP versus cells primed with DMSO before tBHP. Condition 8 vs 6 = tBHP-treated LentiKRAB_NRF2_1 versus tBHP-treated LentiKRAB_NRF2_0 (See Table 3.1 for conditions).

Therefore, to identify the NRF2-dependent proteins, I analysed those proteins with a bidirectional expression under NRF2 repression or activation when compared to tBHP-

treated control cells. Four proteins met these criteria (Figure 3.9A): DDX17, ACTA1 and SRSF2, were positively correlated with NRF2 levels, indicating NRF2 could upregulate these proteins. Conversely the results suggest ZNF90 might be supressed by NRF2 (Figure 3.9B).

Dead box RNA helicase 17 (*DDX17*) mRNA increases with NRF2 induction using sulforaphane in monocyte-derived dendritic cells (Vierbuchen et al., 2023), consistent with my findings. ACTA1, actin alpha 1, encodes the dominant actin subtype in adult skeletal muscle filaments, aiding muscle contraction, with lower expression in streptozocin-induced diabetic rats (Yamazaki et al., 2012). Within the kidney, ACTA1 is expressed in podocytes, where a dynamic actin cytoskeletal structure is central to function in the glomerular filtration barrier (Rinschen et al., 2018). In an *in vitro* Schwann cell model of diabetic peripheral neuropathy, NRF2 expression increases expression of ACTA1 via increased expression of HIF1a, promoting cell survival and proliferation (Chen et al., 2023). Serine and arginine rich splicing factor 2 (SRSF2) and Zinc finger protein 90 have not previously been linked to NRF2 to my knowledge, and therefore these represent novel targets of NRF2 in renal oxidative stress in the podocyte.

Finally, I explored the third question above: possible shared oxidative stress response/protective pathways in the NRF2 knockdown and overexpression cell lines. For this I identified proteins similarly upregulated or downregulated in both Condition 4 and Condition 8 relative to tBHP alone (Condition 6 or 2 controls respectively). The NRF2 downstream target proteins HMOX 1 and LCP1 were more abundant, and SHMT1 was less abundant, in both 8 versus 6 and 4 versus 2 (Figure 3.10 A and B). While increased HMOX1 might be expected in the CDDO-Im treated cells, the similar rise in the NRF2-inhibited cell line could be due to NRF2-independent HMOX1 regulation or some priming of the stress response as previously discussed. Elevation of this known antioxidant factor might explain the unexpected protective effect of CRISPR inhibition of NRF2 with LentiKRAB_NRF2_1. Lymphocyte cytosolic protein 1 (LCP1) is a ROS-regulated protein that induces high cellular adhesion, promotes actin binding and the assembly of actin (Koide et al., 2017) (Balta et al., 2019). Serine hydroxy methyltransferase 1 (SHMT1), suppressed in both low and high NRF2 states with tBHP versus tBHP alone, catalyses the one-carbon reversible reaction central to redox regulation and the synthesis of methionine and purines within the cytoplasm, and is downregulated under hypoxic conditions in LNT-229 and G55 cells (Pikman et al., 2022) (Locasale, 2013) (Engel et al., 2020). Hence, HMOX1, LCP1 and SHMT1 are potentially

acting as ‘NRF2 independent’ antioxidant response proteins.

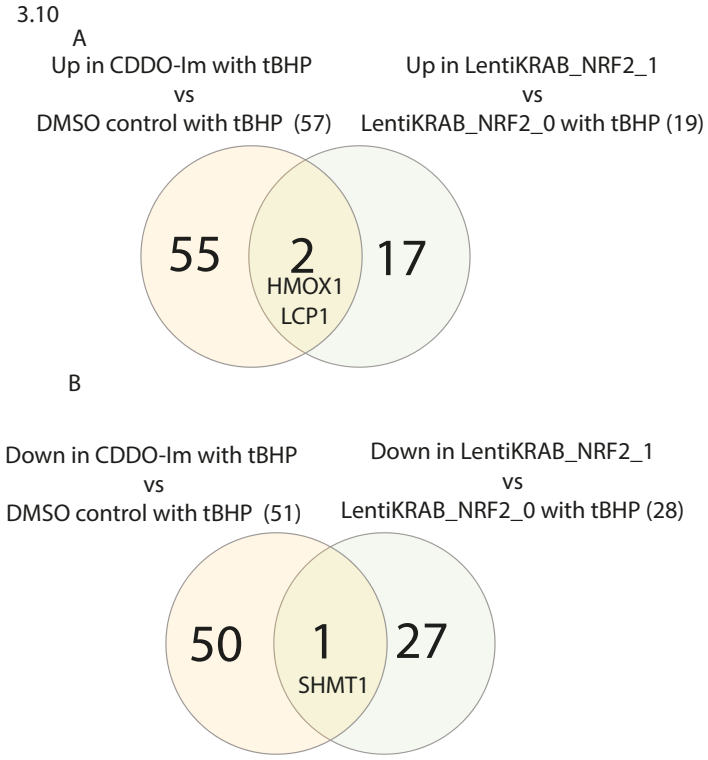

Figure 3.13 Proteins differentially expressed in podocytes in response to NRF2 modulation. Venn diagram of proteins overlapping between **A** those upregulated in cells treated with CDDO-Im and tBHP versus tBHP alone (condition 4 vs 2) and also upregulated in LentiKRAB_NRF2_1 cell treated with tBHP vs LentiKRAB_NRF2_0 controls treated with tBHP (Condition 8 vs 6) **B** As in A but downregulated in both comparisons.

3.3 Summary

In this chapter I show that with exposure to tBHP at 100 μM for 24 hours, oxidative stress can be induced in differentiated immortalised human podocytes, alongside reduced levels of key podocyte-specific proteins nephrin and synaptopodin. I validated a novel adaptation of the assay for carbonylated protein using flow cytometry to quantitate oxidative injury.

Applying transcriptomic and proteomic approaches, I identified biological pathways dysregulated in podocytes in response to oxidative stress including RNA- and DNA-binding and the antioxidant NRF2/KEAP1 pathway. I also showed that at the transcriptomic level, *MAPT* expression in podocytes is increased in response to oxidative stress.
I then modulated NRF2 expression in the cells both pharmacologically and through CRISPR-dCAS9 gene editing to explore the effects of NRF2 manipulation on the podocyte oxidative stress response. I found dose-dependent effects on oxidative stress, with increased protein carbonylation in the context of 80% reduction in NRF2 but reduced oxidative injury with ~ 50% reduction in NRF2 levels, following tBHP, compared to WT.

CRISPR activation of NRF2 unexpectedly increased protein carbonylation. While this could be genetic confounding, a similar, and dose dependent, increased in oxidative stress under normal culture conditions was found with pharmacological NRF2 activation with CDDO-Im. However, this was not the case following treatment with tBHP, where at a dose of 30 nM, CDDO-Im reduced carbonylated protein compared to cells in which NRF2 was not manipulated. Contrasting the effects of oxidative stress induction on cells with increased or suppressed NRF2 highlighted four proteins that appear NRF2 regulated during the response to oxidative stress. Two of these proteins, ACTA1 and DDX17, have been linked to oxidative stress and the NRF2 pathway in other cell types, which is supportive of my results, and that ZNF90 and SRSF2 as novel NRF2 target proteins.

Chapter 4

The role of Tau in neuroblastoma cell oxidative stress response

4.1 Introduction

In Chapter 3, I found that *MAPT* expression increased at the transcriptomic level in response to oxidative stress in human immortalised podocytes *in vitro* (Figure 3.3D). These findings, and the existing data suggesting a link between Tau and oxidative stress, particularly in Nrf2 deficient mice, provided justification to continue to investigate this potential association (Violet et al., 2014). I had hypothesised that the absence of Tau protein would increase the susceptibility of the cells to oxidative stress induction leading to increased cell death and high protein carbonylation. However, at the protein level, Tau was not detectable in the human podocyte cell line (Figure 3.5D) so I studied the effect of *MAPT* deletion in a the neuronal cell line, SH-SY5Y, that expresses high levels of Tau protein in the context of both basal culture conditions and induced oxidative stress.

SH-SY5Y cells are neuroblast-like cells subcloned from the neuroblastoma cell line SK-N-SH, generated from the bone metastasis of a tumour of the neural crest element of the sympathetic nervous system, in a 4-year old child in 1973 (Biedler et al., 1978, Biedler et al., 1973). SH-SY5Y cells have been pivotal to neuronal research because of their human origin, ease of maintenance and expression of neuronal cell characteristics, such as acetylcholinesterase and muscarinic receptors (Kovalevich and Langford, 2013) (Adem et al., 1987). They also express Tau within the cell body, nucleoli and neurites (LoPresti et al., 1992).

A recent study described the knockout (KO) of the Tau gene *MAPT* in SH-SY5Y cells, reporting an effect on p53 and cell fate (Sola et al., 2020a). In this chapter, I assessed Tau expression in these cells (designated 232P), and found evidence suggestive of persistent expression of a truncated Tau protein. Therefore, I used CRISPR-Cas9 gene editing to generate two clones of a novel full *MAPT* KO SH-SY5Y line, designated $MAPT^{-/-A2}$ and $MAPT^{-/-A4}$ that did not express any Tau protein. I made phenotypic comparisons between WT, the partial KO 232P and full *MAPT* KO in the context of oxidative stress induction (Figure 4.1).

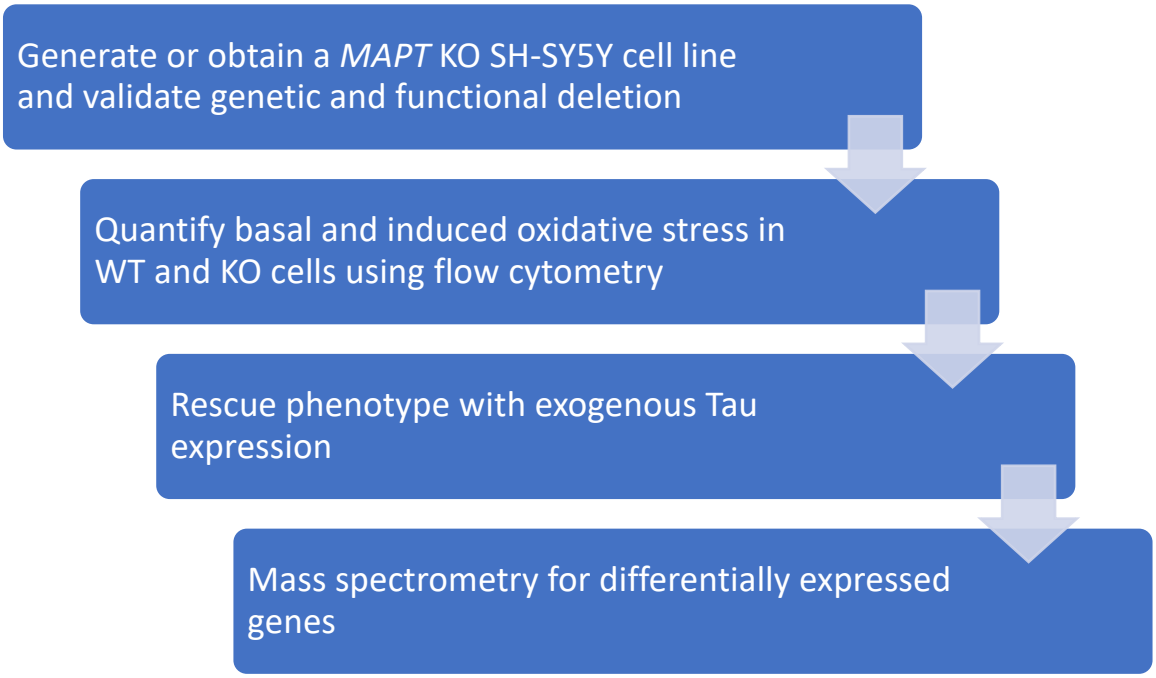

Figure 4.1 Chapter 4 Experimental Outline.

4.2 Results

4.2.1 Targeting exon 1 with CRISPR/Cas9 does not fully remove *MAPT* expression

The *MAPT* KO SH-SY5Y 232P cell line was obtained from the authors (Sola et al., 2020a). 232P was generated by targeting exon 1 of the *MAPT* gene using CRISPR-Cas9 gene editing, producing a 515 bp insertion and a 1 bp insertion (Sola et al., 2020a). I investigated the expression of Tau by western blot on lysates generated from these cells alongside WT SH-SY5Y cell lysates, and the immortalised human podocytes described in Chapter 3 using the N-terminal Tau 12 and C-terminal Tau 46 antibodies. The absence of a detectable Tau signal in the podocytes corroborated the results from the proteomics and western blotting previously shown in Figure 3.5. The WT 232P cells, while showing no signal with the N-terminal Tau 12 antibody, had a detectable band with Tau 46 of approximately 70 kDa (Figure 4.2A and B), which could be consistent with the 515 bp insertion and a form of the Tau protein missing the Tau 12 epitope.

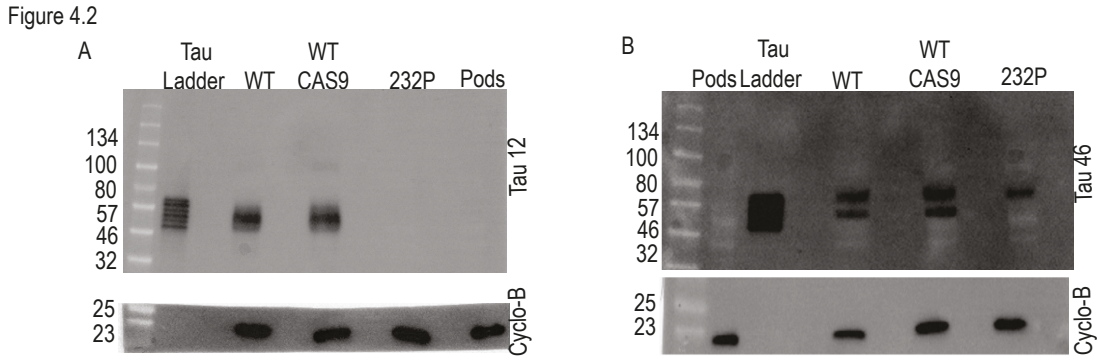

Figure 4.2 Western blotting to show expression of Tau in 232P cell line. Lysates from 232P, WT SH-SY5Y cells (WT), unedited WT SH-SY5Y cells expressing CAS9 but no sgRNA (WT CAS9), and podocytes (Pods) were run alongside the recombinant Tau ladder. **A** is a blot stained with the N-terminal Tau 12 antibody while **B** is the C-terminal Tau 46 antibody. Cyclophilin B (Cyclo-B) was used as loading control, expected size 23 kDa.

One possibility is that the 70 kDa band detected by Tau 46 may represent an epitope on the neuron-specific microtubule associated protein 2 (MAP2) that has a similar sequence to the C-terminus of the Tau protein (Boban et al., 2019a) (Kosik et al., 1988b). However, although

cultured podocytes express MAP2 this 70 kDa band is absent in the lysates obtained from these cells (Figure 4.2B) (Smoyer and Mundel, 1998).

In addition, we used fluorescent in situ hybridisation (FISH) to test for aneuploidy for chromosome 17q21.31. This showed that 76% of the 232P cells were triploid while 19.5% were tetraploid or higher, indicating aneuploidy levels higher than the also predominantly triploid parental SH-SY5Y line (Figure 4.3).

Figure 4.3

A

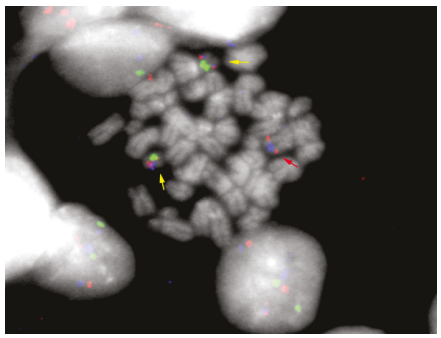

B

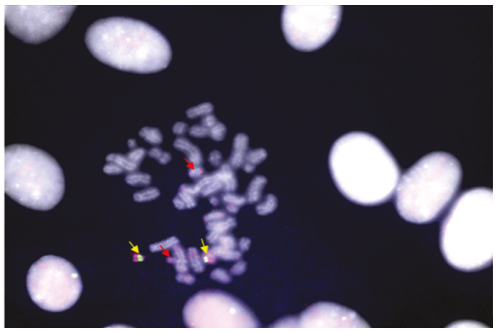

C

	1 signal per cell	2 signals per cell	3 signals per cell	4 signals per cell	5 signals per cell
SHSY5Y	-	28%	71%	1%	
232P	-	3.90%	76.40%	17.60%	1.90%

Figure 4.3 Fluorescent in situ hybridisation results for WT and 232P SH-SY5Y cells. A is a metaphase spread from WT SH-SY5Y cells. **B** is a metaphase spread for 232P cells. Yellow arrows represent the two normal *MAPT* copies on chromosome 17. The red arrows show translocated derivatives. **C** shows the results of the copy number analysis of the *MAPT* locus according to the number of signals observed per cell**.** (FISH data generated by Daniela Moralli)

To better characterise the genomic editing of *MAPT* in 232P, PCR was performed on genomic DNA from 232P and WT SH-SY5Y cells, using a forward primer 137 bp upstream of the first exon 1 nucleotide and reverse primer 220 bp downstream of exon 2's last nucleotide (232gPCR primer pair). Two larger bands were detected in 232P but not in WT cells. The largest band corresponds to the size (1,055 bp) expected in the case of a 515 bp insertion as reported in the original paper (Sola et al., 2020a) (Figure 4.4A red asterisks).

Two bands below 600 bp were present in both the WT and the 232P cell lines (Figure 4.4A black and yellow asterisks). The band of approximately 400 bp was smaller than expected for WT *MAPT*, but confirmed by sequencing to align to a region in exon 7 of the MAPT gene, suggesting some off-target amplification, while the larger band of approximately 550 bp aligned to the targeted N-terminal region of the MAPT gene including exon 1 and intron 2 in both WT and 232P cells. Comparison of this sequence in 232P to WT cells showed that this allele in 232P cells had a single cytosine insertion just before the PAM site, expected to introduce a frameshift. From the sequence, this frameshift is predicted to result in a stop codon within exon 1. No WT sequence was detected.

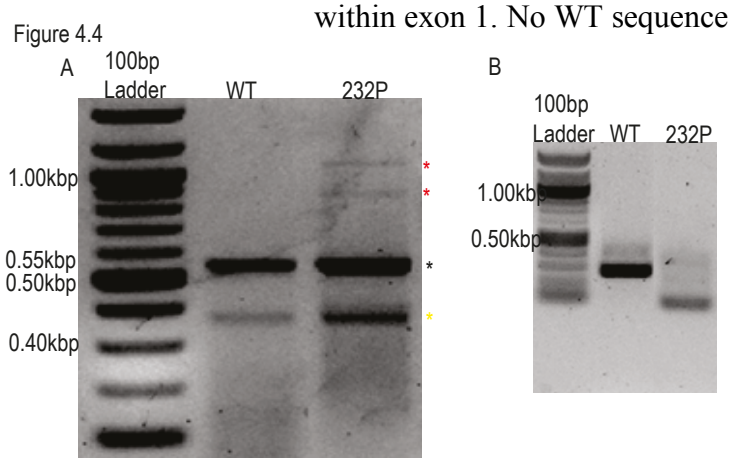

Figure 4.4 gDNA PCR and RT-PCR comparing 232P cells with WT SH-SY5Y cell. A WT (WT) and 232P genomic DNA were amplified using the 232gPCR primer pair and run on a 1% agarose gel alongside a 100bp ladder. Tau band (*) and non-specific band (*) detected in both the WT cells the 232P cells. Two larger bands were only detected in the 232P cells (*). **B** Using the 232rtPCR primer pair which targets the 0N3R isoform specifically, two amplicons of 300 and ~80bp were observed for the WT and the 232P cells respectively.

To understand how these edits influence the RNA transcripts, cDNA from 232P and WT cells was analysed using reverse transcription PCR (RT-PCR) with the 232rtPCR primer pair (Materials and Methods). A band of approximately 300 bp was seen for the WT cells but this was absent or very faint in the 232P cells which showed a smaller band of less than 100 bp

not present in WT (Figure 4.4B). Sequencing of these bands showed that in 232P the 5'UTR is spliced to exon 4 thus skipping the intervening exon 1. Thus, in the 232P cell line targeting exon 1 has resulted in expression of an RNA transcript that lacks the N-terminal region of the *MAPT* gene. However, if the C-terminal Tau 46 antibody is specific to Tau protein, then it appears that the loss of exon 1, with its transcription start site, is insufficient to fully inhibit gene expression and protein translation, which could suggest the existence of alternative start sites.

The possibility of an alternate start site is supported by experiments targeting *MAPT* using morpholinos against functional regions, including the start codon, splice donor sites and splice acceptor sites, in which cells lacking the start codon still expressed Tau. When targeting exon 1, the 5'UTR spliced directly onto exon 4 in the SH-SY5Y cells with some persistent Tau protein expression, although a 77% decrease relative to the WT untargeted cells (Sud et al., 2014a).

The large Tau isoform, known as Big Tau, is the result of the inclusion of exon 4a (753 bp) as well as exons 2 (87 bp) and 3 (86 bp). In the SH-SY5Y cells, treatment with okadaic acid enhances the expression of this isoform (Boban et al., 2019a). In the absence of a credible start site in exons 2, 3 or 4, I hypothesised that on disrupting exon 1's transcription start site, an alternative start site in exon 4a may allow for generation of a truncated protein devoid of the N-terminal exons 1, 2, 3 and 4, with their combined size of 372 bp. Instead, a protein with intact sequence downstream from exon 4a would be detectable using an antibody targeting the C-terminus.

Therefore, I concluded that an editing approach that targeted exon 1 and exon 4a together might generate a more complete deletion of Tau. Using CRISPR-Cas9 with two guide RNAs,

this could occur in two ways. Firstly, both the known start site in exon 1 and the proposed start site in exon 4a could be disrupted by indels around each of the two PAM sites, detectable using primer pairs specific to each targeted site. Secondly, it could also be possible for a large deletion between the two sites to take place, as has been previously reported with a dual guide CRISPR-CAS9 gene editing approach (Spagnuolo and Blenner, 2021).

4.2.2 Dual guide CRISPR/Cas9 to delete *MAPT* in SH-SY5Y cells

As shown in Figure 4.3A most of WT SH-SY5Y cells (71%) are triploid for the *MAPT* gene and 28% are diploid. This mixed population of cells were transduced with lentivirus to generate a cell line expressing an inducible Cas9, known as SH-SY5Y-CAS9. Following treatment with doxycycline for 72 hours Cas9 mRNA expression increased approximately 10-fold in comparison with uninduced SH-SY5Y-CAS9 cells (Figure 4.5A). Subsequently, the induced cells were simultaneously transfected with both exon 1 and exon 4a guides. Single clones of the transfected cells were expanded and tested at the genomic, transcriptomic and proteomic levels for *MAPT* expression.

4.2.2.1 Genomic PCR shows a large deletion and indels in two SH-SY5Y clones transfected with dual sgRNA guides

Genomic long-range PCR was performed on clones expanded after transfection, using a forward primer upstream of the exon 1 sgRNA guide and a reverse primer downstream of the 4a guide. A 22 kb band in WT DNA corresponding to the region of interest was also observed faintly in the edited DNA lines, but two clones also had a smaller band of about 550 bp absent in the WT (Figure 4.5B). These clones were designated as $MAPT^{-/-A2}$ and $MAPT^{-/-A4}$.

The 550 bp band was sequenced and aligned to the reference genome. This confirmed that in *MAPT*$^{-/-A2}$ and *MAPT*$^{-/-A4}$ a deletion between the exon 1 and exon 4a PAM sites was present (Figure 4.5C). The SH-SY5Y cells are triploid for the *MAPT* gene (Figure 4.3), and the 22,000 bp amplicon expected and observed in the WT cells were also seen in *MAPT*$^{-/-A2}$ and *MAPT*$^{-/-A4}$. Therefore, to test whether this larger band is an unedited allele or contains indels around the individual guides, primers specific to each of the exons were used to amplify the regions around the two PAM sites.

Sequence analysis of 22 kb PCR amplicons from *MAPT*$^{-/-A2}$ and *MAPT*$^{-/-A4}$, predicted that both cell lines shared a 1 bp insertion after the exon 1 sgRNA PAM site with a distribution of approximately 50%. The remaining 50% of the distribution was accounted for by a 9 bp deletion. No WT alleles were observed. A similar analysis using exon 4a primers also showed a 1 bp and a 3 bp insertion accounting for 43% and 46% of the edit distribution, plus a possible 2 bp insertion accounting for 2% of the distribution. Both *MAPT*$^{-/-A2}$ and *MAPT*$^{-/-A4}$ shared very similar editing profiles indicating they are likely to be subclones from the same parent cell.

Thus, using a dual set of guides within exons 1 and 4a led to a large deletion alongside smaller indels, both frameshift and in frame, with no WT alleles in either *MAPT*$^{-/-A2}$ and *MAPT*$^{-/-A4}$.

Assessment of off-target editing using whole genome sequencing (WGS) was performed on *MAPT*$^{-/-A2}$ and WT cells to corroborate the results of the Sanger sequencing and to screen for off-target edits which could potentially affect the results of any assays carried out on the

cells. Since large indels are possible with dual guide CRISPR editing, a long range WGS approach was used (PacBio HiFi sequencing).

After alignment to the reference human genome (GRCh38) and variant calling (Methods), private insertion or deletion (indel) variants that were called in *MAPT*$^{-/-A2}$ but not in WT were filtered and then reviewed manually based on read alignment patterns visualised with Integrative Genomics Viewer (IGV) to select for mutations caused by CRISPR-CAS9 (Thorvaldsdottir et al., 2013).

Four variants (all non-coding) met all of the following criteria and were selected as private homozygous mutations: (i) *MAPT*$^{-/-A2}$ genotyped as homozygous for the alternative allele (1/1) and WT genotyped as homozygous for the reference allele (0/0); (ii) allele depth (AD) = 0 for the reference allele in *MAPT*$^{-/-A2}$; (iii) AD = 0 for the alternative allele in WT.

Seven indel variants (three exonic, including the desired variant in *MAPT*) met all of the following criteria and were selected as private heterozygous variants: (i) AD = 0 for the alternative allele in WT; (ii) AD $\geqslant$ 2 for the alternative allele in A2 (iii) located within 30 kb distance from one of 495 in silico predicted CRISPR-CAS9 target sites with four or less mismatches identified using CRISPOR (Figure 4.6A) (Concordet and Haeussler, 2018).

Among these 11 private variants in *MAPT*$^{-/-A2}$, manual review confirmed that none of the homozygous variants and only two heterozygous variants, were sufficiently supported by read alignment patterns. Most variants that were considered false positives were caused by imbalanced sampling during sequencing, i.e. different haplotypes were sampled for WT and *MAPT*$^{-/-A2}$ cell lines, evident by the distribution of cis variants on the same reads.

The two heterozygous supported variants comprised the desired variant in *MAPT* (Figure 4.6B-D), and a 46.6 kb deletion that removed one copy of the ADAM29 coding exon.

Figure 4.6

A

B

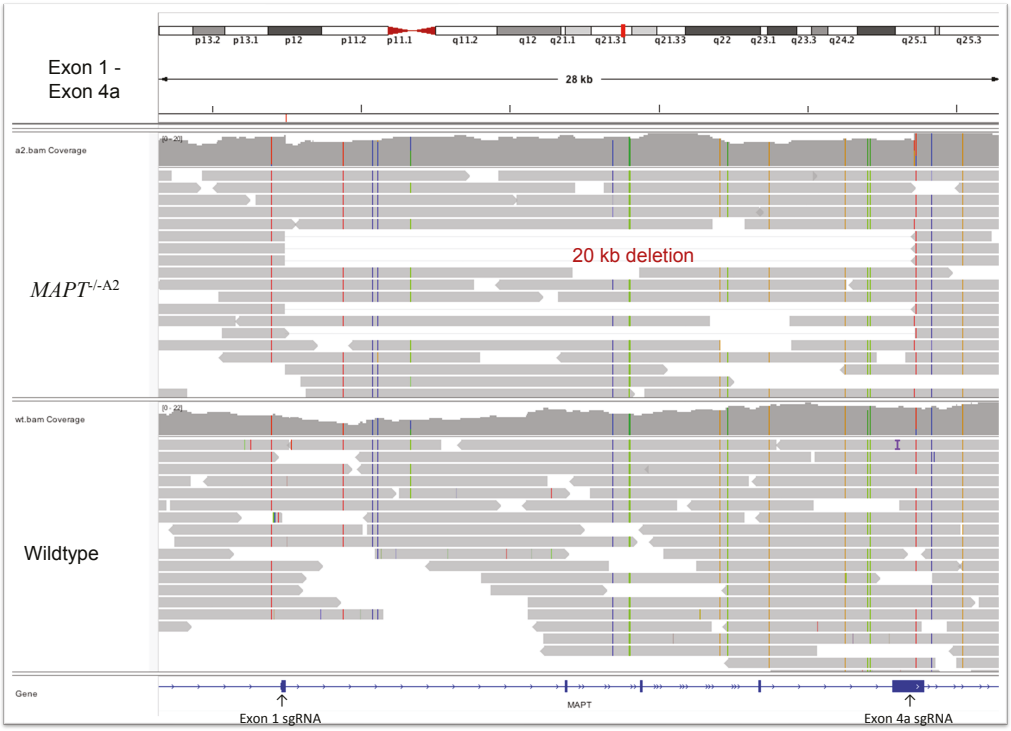

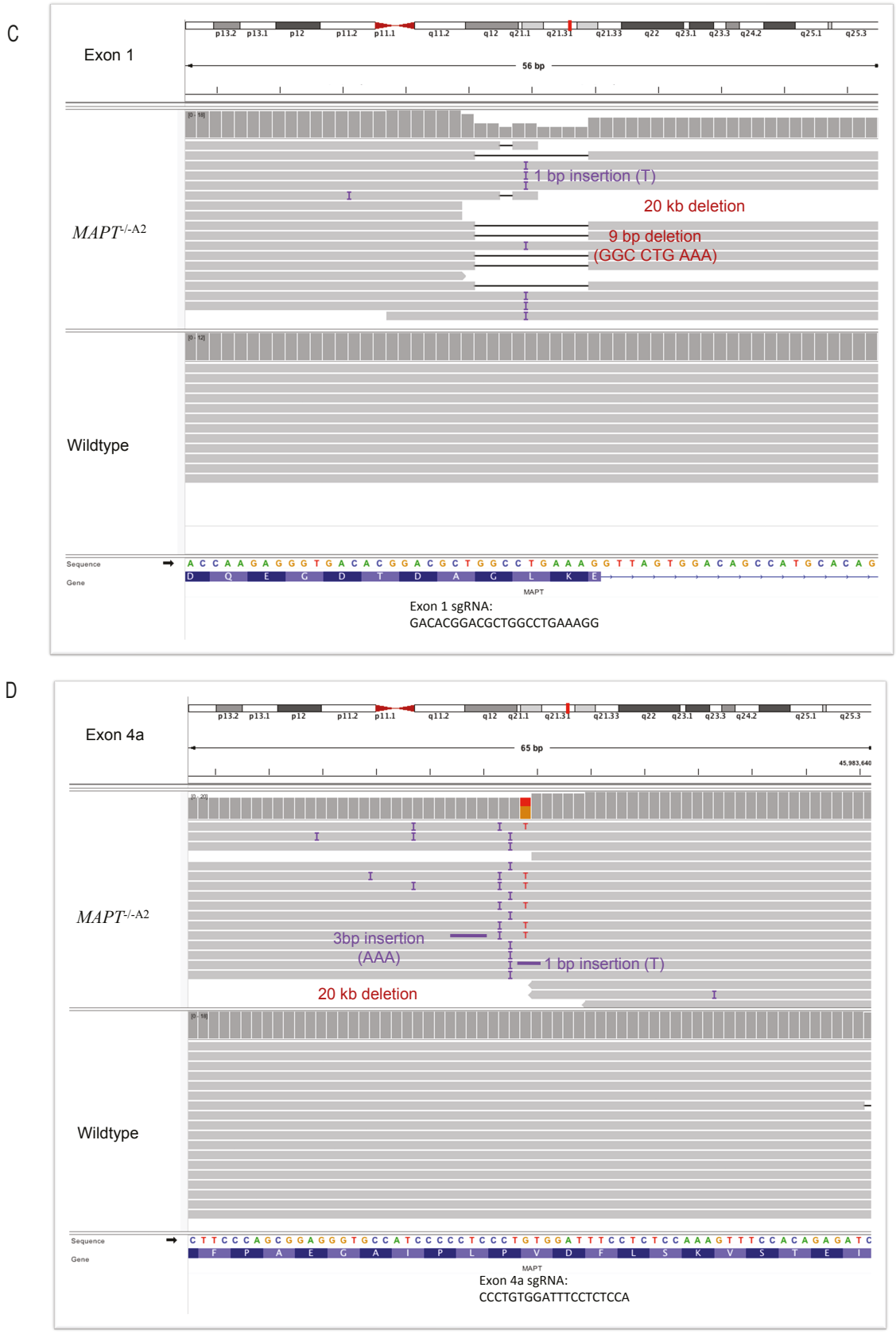

Figure 4.6 Whole genome sequencing result of clone *MAPT*$^{-/-A2}$ in comparison with WT SH-SY5Y cells. A shows the location of variants in ***MAPT***$^{-/-A2}$ within 30 kb of *in silico* predicted off-target sites **B** shows Integrated Genomics Viewer (IGV) visualisation for a ~20 kb deletion between exon 1 PAM site and exon 4a PAM site. **C** In comparison to the WT

cells, *MAPT*$^{-/-A2}$ cells have two smaller indel events at exon 1 on different alleles: a 9 bp deletion and a 1 bp insertion after the PAM site of exon 1. **D** At the exon 4a PAM site, there is a 3 bp insertion and 1 bp insertion in trans, independent of the ~20 kb deletion. (Analysis of whole genome sequencing data by Jiayuan Zhang)

ADAM29 is a member of a family of type 1 transmembrane proteins involved in cellular adhesion, fusion and transduction (Alonso et al., 2018b). It is known to contribute to cell survival and neuronal cell differentiation, with decreased expression leading to cellular apoptosis (Alonso et al., 2018b). Notably the KO clones had no differences in cell survival compared to the WT. There was no evidence that the deletion of one copy of ADAM29 had a phenotypic effect.

4.2.2.2 Undetectable Tau in MAPT$^{-/-A2}$ and MAPT$^{-/-A4}$ with N-terminal or C-terminal antibodies

MAPT$^{-/-A2}$ and *MAPT*$^{-/-A4}$ protein lysates were interrogated using the N-terminal Tau 12 antibody and the C-terminal Tau 46 antibody. In contrast to the 232P cells, no protein was detectable by either of the two antibodies in *MAPT*$^{-/-A2}$ or *MAPT*$^{-/-A4}$ (Figure 4.7). In conclusion, the two clones *MAPT*$^{-/-A2}$ and *MAPT*$^{-/-A4}$, generated by targeting the triploid SH-SY5Y cell line in both exon 1 and exon 4a, do not express detectable Tau protein due to a combination of indels and a large deletion in the Tau gene. To control for clonal effects, both clones were used in subsequent phenotyping experiments.

4.2.3 *MAPT*$^{-/-A2}$ and *MAPT*$^{-/-A4}$ clones have decreased tubulin polymerisation compared to WT SH-SY5Y cells or the 232P cell line

The role of Tau in promoting and maintaining microtubule polymerisation is well-established (Hernandez-Vega et al., 2017). Clones *MAPT*$^{-/-A2}$ and *MAPT*$^{-/-A4}$ were investigated for tubulin

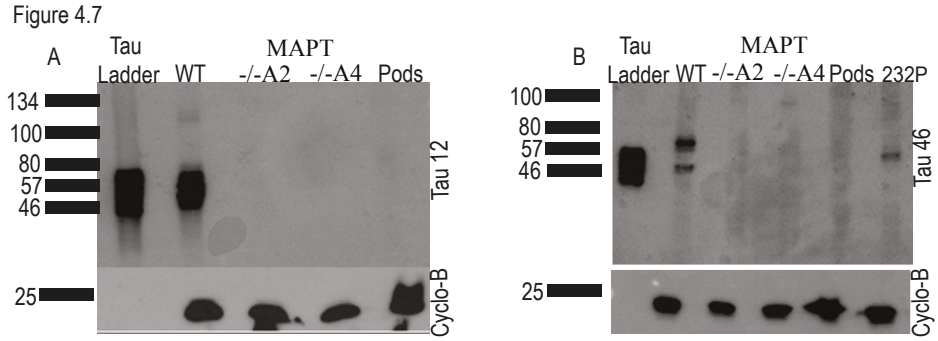

Figure 4.7 Western Blot of WT SH-SY5Y lysate compared with 232P cell line, *MAPT*$^{-/-A2}$ and *MAPT* $^{-/-A4}$ clones and podocytes. A Lysates from WT SH-SY5Y cells (WT), *MAPT*$^{-/-A2}$, *MAPT* $^{-/-A4}$ and podocytes (Pods) were run alongside the recombinant Tau ladder. The blot was probed with N-terminal Tau 12 antibody and cyclophilin-B (Cyclo-B) as the loading control. **B** The 232P cell line was also included in the lysates for the western alongside the WT, podocytes, *MAPT*$^{-/-A2}$, *MAPT* $^{-/-A4}$ clones. Here, the blot was probed with Tau 46 antibody targeting the C-terminus.

polymerisation in comparison with WT SH-SY5Y cells and the 232P cell line. Using both western blots and immunofluorescence, polymerised and free tubulin were quantified.

By western blot (Figure 4.8A), the signal intensity was less for the *MAPT*$^{-/-A2}$ and *MAPT*$^{-/-A4}$ cell lines compared to the WT cells. The 232P cells, while showing a decrease in comparison to the WT cells, was not as low as in either *MAPT*$^{-/-A2}$ and *MAPT*$^{-/-A4}$.

This observation was confirmed by immunofluorescence measurement of polymerised tubulin. By immunofluorescence, while no signal is detected in either *MAPT*$^{-/-A2}$ or *MAPT*$^{-/-A4}$ for polymerised tubulin, both the WT and the 232P cells show comparable intensity (Figure 4.8B). This indicates that in the absence of Tau expression in *MAPT*$^{-/-A2}$ and *MAPT*$^{-/-A4}$, there is a reduction in proportion and abundance of polymerised tubulin, suggesting a defect in Tau-mediated tubulin polymerisation.

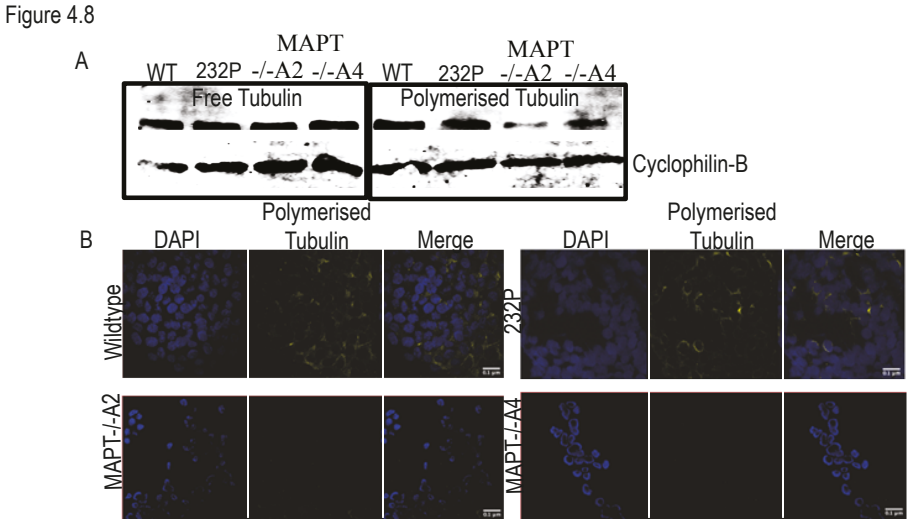

Figure 4.8 Western blot and immunofluorescence images comparing polymerised tubulin expression in WT (WT), 232P, *MAPT*$^{-/-A2}$, *MAPT* $^{-/-A4}$ SH-SY5Y clones. A Lysates for free and polymerised tubulin were extracted from all the four cell lines. The resulting blot was probed using anti-tubulin antibody with cyclophilin-B as the loading control. **B** Cells cultured on coverslips were treated with an extraction buffer to remove the free tubulin leaving behind the polymerised tubulin before fixation and staining. The nucleus is stained with DAPI (blue), polymerised tubulin is in yellow.

4.2.4 Oxidative stress in *MAPT*$^{-/-A2}$ and *MAPT*$^{-/-A4}$

Based on the finding that *MAPT* expression increased in podocytes under conditions of oxidative stress (Chapter 3), the *MAPT*$^{-/-A2}$ and *MAPT*$^{-/-A4}$ cells were investigated for oxidative stress under normal 'basal' culture conditions, and for their response to tBHP-dependent oxidative stress induction, compared to the WT and the 232P cell lines.

Under basal standard culture conditions, the proportion of live cells was equivalent between the Tau mutant and WT lines (Fig 4.9A, 'untreated' black circles). However, the proportion of cells expressing carbonylated protein was higher in *MAPT*$^{-/-A2}$ and *MAPT*$^{-/-A4}$ compared with the WT, despite no measured loss of cell viability, though unchanged in the 232P cells (Figure 4.9B, 'untreated' black circles).

In response to treatment with 15 μM tBHP to induce oxidative stress, there was an increase in cell death in all lines. *MAPT*$^{-/-A2}$ and *MAPT*$^{-/-A4}$, but not 232P, had higher levels of cell death than WT (Figure 4.9A, treated). All four cell lines exhibited increased oxidative stress, as measured by proportion of cells expressing carbonylated protein, in response to tBHP compared to the basal condition. The proportion of cells with carbonylated protein after tBHP treatment was higher in *MAPT*$^{-/-A2}$ and *MAPT*$^{-/-A4}$ compared to WT cells, but not in 232P compared to WT (Figure 4.9B, treated). Taken together these findings indicated that *MAPT*$^{-/-A2}$ and *MAPT*$^{-/-A4}$ SH-SY5Y cells have an enhanced basal and induced level of oxidative stress.

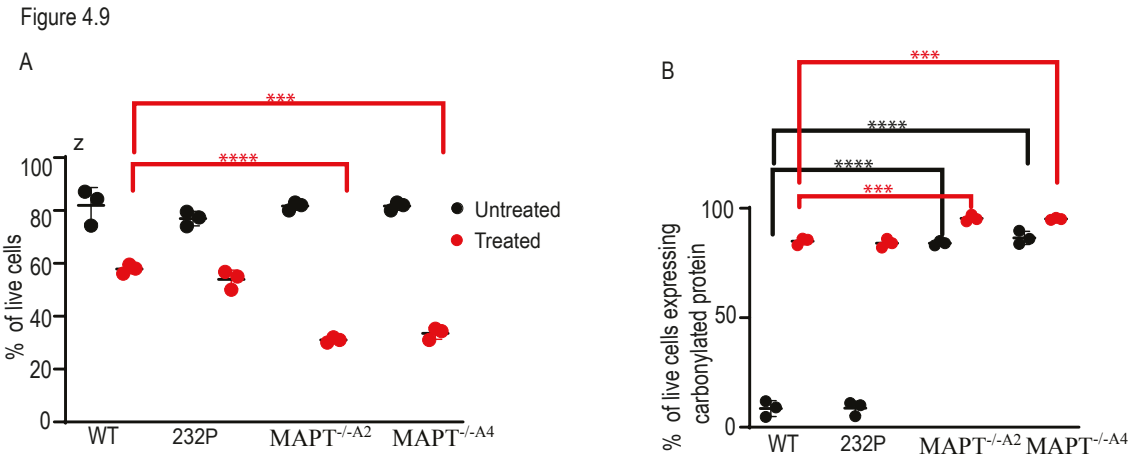

Figure 4.9 Absence of Tau increases oxidative stress and cell death in SH-SY5Y cells. WT, 232P, *MAPT*$^{-/-A2}$ and *MAPT* $^{-/-A4}$ cells were treated with 15 μM tBHP (treated **red** circles) or water (untreated **black** circles**)** for 24 hours. Cells were harvested, stained with live/dead stain and derivatised with DNPH before staining with anti-DNP antibodies for carbonylated protein, assayed by flow cytometry. **A** Percentage of live cells. **B** Percentage of live cells expressing carbonylated protein, gated by DNP expression. (* $p<0.05$, ** $p<0.01$, *** $p<0.001$)

4.2.5 Rescue of Tau expression in *MAPT*$^{-/-A2}$ and *MAPT*$^{-/-A4}$ reversed the oxidative stress signature

To test whether the oxidative stress phenotype in the *MAPT*$^{-/-A2}$ and *MAPT*$^{-/-A4}$ cells could be explained by factors other than the absence of Tau, I next re-expressed Tau in these cells, since rescue of the oxidative stress phenotype by Tau overexpression would support a Tau specific effect.

Figure 4.10

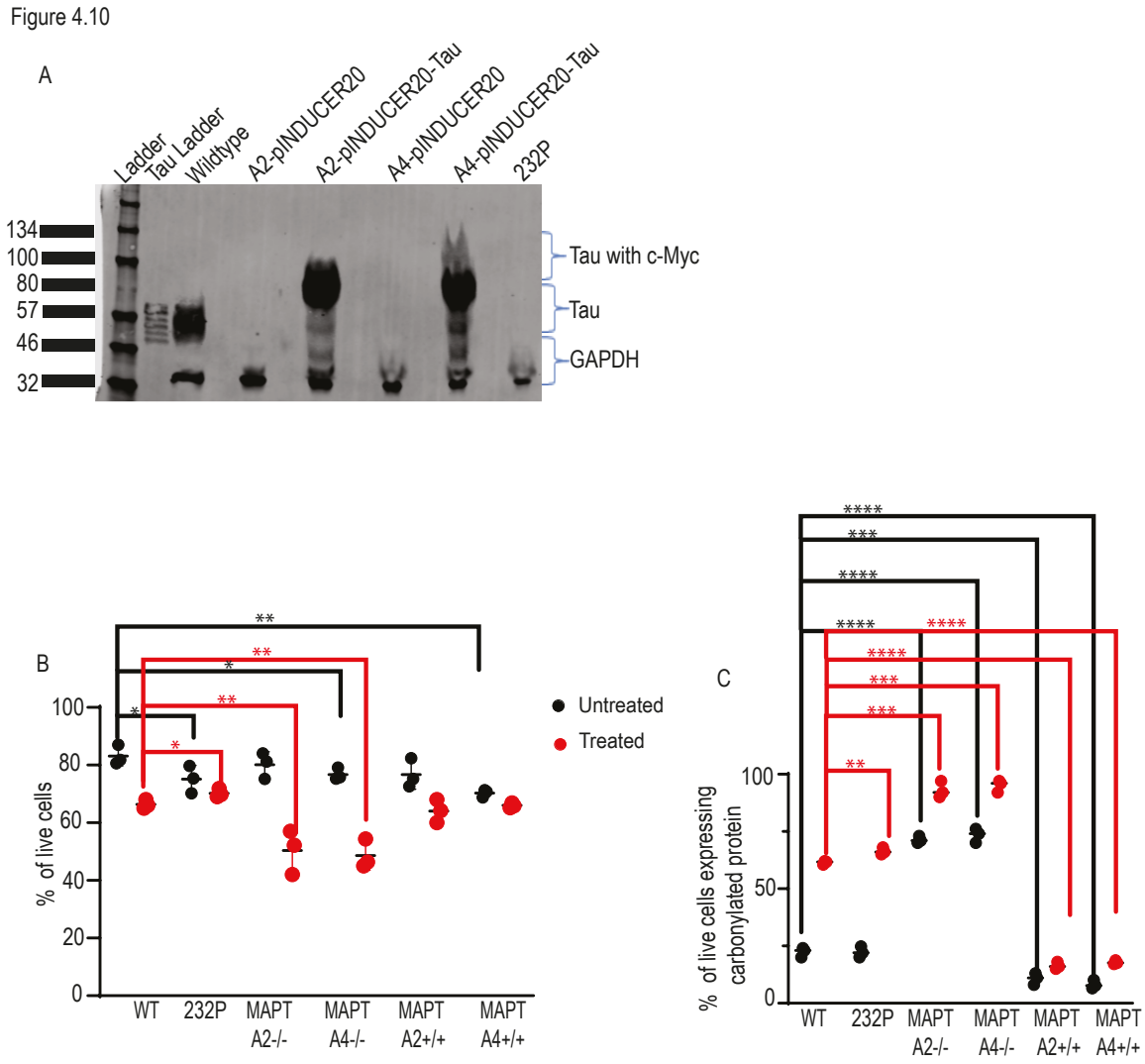

Figure 4.10 Tau rescue with pINDUCER20-Tau reverses oxidative stress signature in clones A2 and A4 cells. A *MAPT*$^{-/-A2}$ and *MAPT* $^{-/-A4}$ cells were transduced with either pINDUCER20-Tau or pINDUCER20 followed by induction with doxycycline. Both *MAPT*$^{-/-A2}$ and *MAPT* $^{-/-A4}$ cells with pINDUCER20-Tau express Tau at a larger size than the WT due to the c-Myc tag. **B** WT (WT), 232P, *MAPT*$^{-/-A2}$ and *MAPT* $^{-/-A4}$ cells transduced with pINDUCER20 or pINDUCER20-Tau were treated with 15 µM tBHP for 24 hours or water. Percentage of live cells in treated and untreated cells. In **black** is the control and in red is the tBHP-treated cells. **C** Percentage of live cells expressing carbonylated protein gated by DNP expression. (* p<0.05, ** p<0.01, *** p<0.001, ****p<0.0001)

MAPT$^{-/-A2}$ and *MAPT*$^{-/-A4}$ cells were transduced with a lentiviral construct to express the Tau-441 isoform with a c-Myc tag under a tetracycline inducible ubiquitin C promotor (pINDUCER20-Tau), or an empty vector control (pINDUCER20) (Meerbrey et al., 2011). Multiple Tau isoforms exist, and alternative splicing of exons 2, 3 and 10 have been associated with tauopathies with evidence of isoform-specific protein interactions (Hutton et al., 1998) (Malkani et al., 2006) (Terada et al., 2005) (Liu et al., 2016, Trabzuni et al., 2012). It has been postulated that increased inclusion of exon 3 could increase protection against oxidative stress (Wang and Mandelkow, 2016). Tau-441 was chosen as the exogenously expressed isoform since it includes exons 2, 3 and 10.

Transduction of *MAPT*$^{-/-A2}$ and *MAPT*$^{-/-A4}$ cells with pINDUCER20-Tau and subsequent induction with doxycycline leads to Tau expression (Figure 4.10A). The size of the Tau protein as determined by probing with Tau12 is higher than observed in the WT cells because of the c-Myc tag. *MAPT*$^{-/-A2}$ and *MAPT*$^{-/-A4}$ cells transduced with control pINDUCER20 did not show expression of Tau. As expected, the N-terminal Tau12 antibody did not detect Tau in the 232P cells (Figure 4.10A).

In response to tBHP, cell death increased in the *MAPT*$^{-/-A2}$ and *MAPT*$^{-/-A4}$ cells lacking Tau expression compared to WT, as seen previously (Figure 4.9A, treated), but remained equivalent to WT following tBHP treatment in induced pINDUCER20-Tau cells (Figure 4.10B, treated).

Under basal conditions, *MAPT*$^{-/-A2}$ and *MAPT*$^{-/-A4}$ transduced with pINDUCER20-Tau had lower proportions of cells with oxidative stress than WT cells (Figure 4.10C, untreated). In comparison, control pINDUCER20 *MAPT*$^{-/-A2}$ and *MAPT*$^{-/-A4}$ cells exhibited a larger

proportion of carbonylated protein-expressing cells than WT as previously observed (Figure 4.10C, untreated).

Moreover, with tBHP treatment, the pINDUCER20-Tau *MAPT*$^{-/-A2}$ and *MAPT*$^{-/-A4}$ also showed lower proportions of cells with oxidative stress compared to *MAPT*$^{-/-A2}$ and *MAPT*$^{-/-A4}$, and compared to WT treated or untreated cells, demonstrating a complete rescue of the oxidative stress phenotype in *MAPT*$^{-/-A2}$ and *MAPT*$^{-/-A4}$ by reinstating Tau expression (Figure 4.10C, treated). These control rescue findings confirm that the increase in oxidative stress in *MAPT*$^{-/-A2}$ and *MAPT*$^{-/-A4}$ neuronal cells is due to absence of Tau protein implying that Tau is required for protection from oxidative injury, at least in the *in vitro* cultured SH-SY5Y cell line.

4.2.6 NRF2 and KEAP1 expression increases in the absence of Tau

Since NRF2 is a key regulator of the intracellular oxidative stress response, the impact of loss of Tau on NRF2 expression and localisation was investigated.

NRF2 was undetectable by immunofluorescence in the WT and 232P cells under the usual culture conditions. By contrast, nuclear and cytoplasmic NRF2 were detected in *MAPT*$^{-/-A2}$ and *MAPT*$^{-/-A4}$ consistent with the observed increased oxidative stress (Figure 4.11). The percentage of live cells expressing the NRF2 repressor KEAP1 by flow cytometry increased in *MAPT*$^{-/-A2}$ and *MAPT*$^{-/-A4}$, but not 232P, when compared with WT (Figure 4.12A).

Figure 4.11

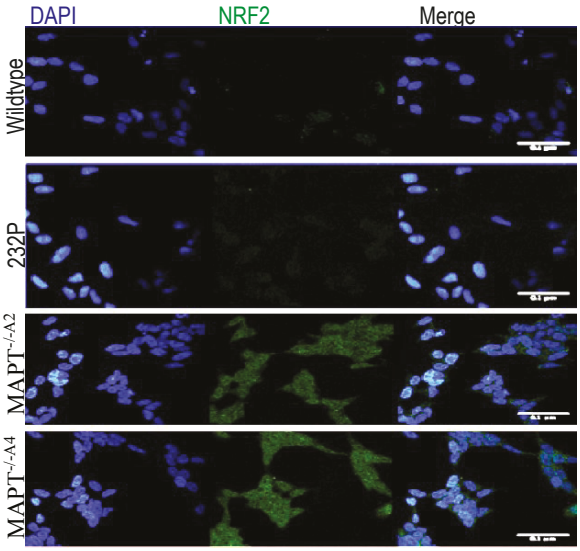

Figure 4.11 NRF2 localisation in SH-SY5Y cell lines with or without detectable Tau expression. WT (WT), 232P cells, *MAPT*$^{-/-A2}$ and *MAPT* $^{-/-A4}$ immunofluorescence are shown with DAPI nuclear staining shown in blue, NRF2 stained in green.

4.2.7 Polymerisation of tubulin with Paclitaxel does not rescue the stress phenotype in *MAPT*$^{-/-}$ cells

Since the KO cells had diminished polymerised tubulin (Figure 4.8), I tested whether loss of the tubulin polymerisation function of Tau contributes to the oxidative stress phenotype. If this was the case, I hypothesised that by enhancing the polymerised tubulin within these cells the oxidative stress signature could be reversed.

Tubulin polymerisation was induced by treating both KO cell lines, the WT cells, and the rescued KO cells with Paclitaxel at 1 nM for 24 hours. Paclitaxel is a chemotherapeutic that causes a mitotic block by stabilising microtubules (Carlier and Pantaloni, 1983). *MAPT*$^{-/-A2}$ and *MAPT*$^{-/-A4}$ cells were found to have an elevated proportion of cells with protein carbonylation compared to WT, not reversed with Paclitaxel treatment. Indeed, the percentage of cells with oxidative stress was increased in the *MAPT*$^{-/-}$ paclitaxel groups

relative to untreated *MAPT*$^{-/-}$ lines. This increased sensitivity to Paclitaxel in *MAPT*$^{-/-A2}$ and *MAPT*$^{-/-A4}$ cells, resulting in oxidative stress, was fully rescued in the pINDUCER20-Tau *MAPT*$^{-/-A2}$ and *MAPT*$^{-/-A4}$ (*MAPT*$^{+/+}$) cell lines (Figure 4.12B).

Figure 4.12

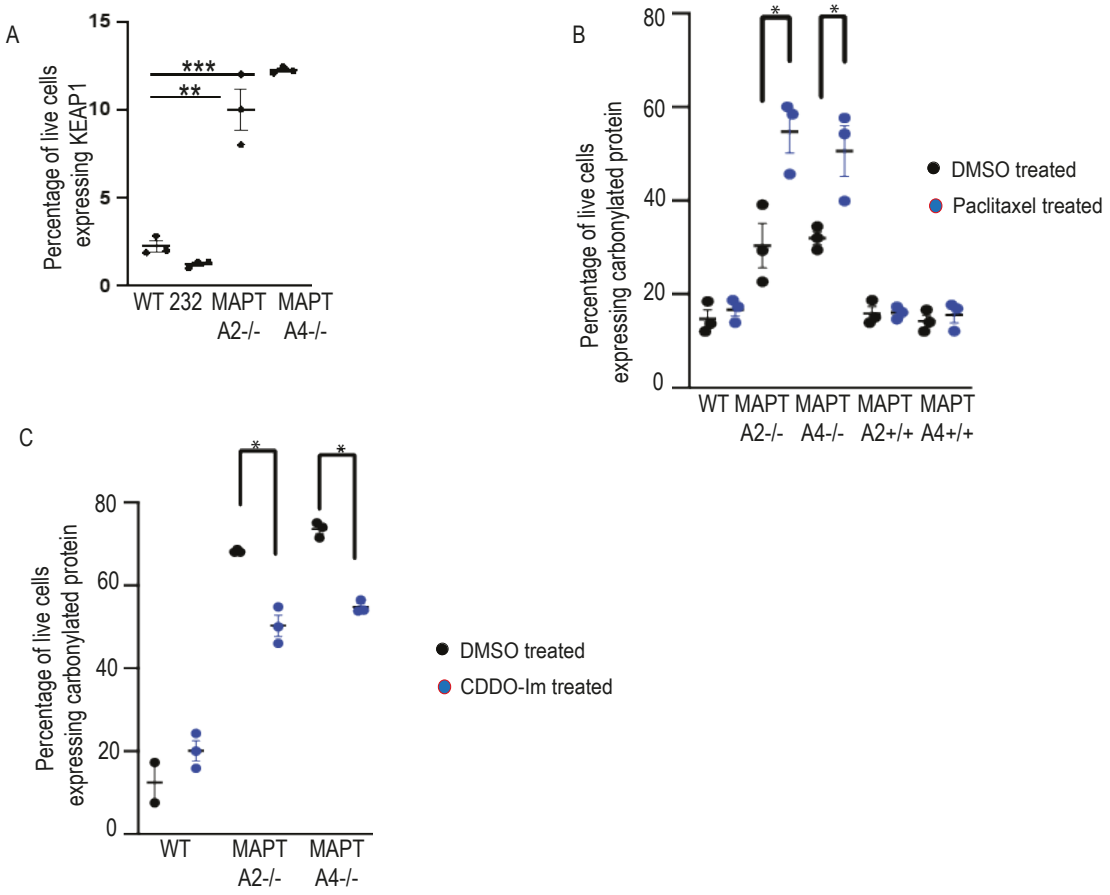

Figure 4.12 Effect of Tau manipulation on NRF2-dependent pathways. A Expression of KEAP1 Protein in SH-SY5Y cell lines**.** WT (WT), 232P, *MAPT*$^{-/-A2}$ and *MAPT* $^{-/-A4}$ cells were compared for their expression of KEAP1 using flow cytometry (** p<0.01, *** p<0.001) **B** Paclitaxel at 1nM for 24 hours exacerbates the redox imbalance in *MAPT* KO cell lines**.** WT (WT), *MAPT*$^{-/-A2}$, *MAPT*$^{-/-A2}$ with Tau-441-Myc, *MAPT* $^{-/-A4}$ and *MAPT* $^{-/-A4}$ with Tau-441-Myc cells were either treated with 1 nM Paclitaxel or DMSO as a vehicle control for 24 hours. In **black** is the DMSO control and in **blue** is the Paclitaxel treated cells. (*p<0.0.05). **C** 100 nM CDDO-Im for 24 hours partially rescues the oxidative stress phenotype in *MAPT* KO cells. WT (WT), *MAPT*$^{-/-A2}$ and *MAPT* $^{-/-A4}$ cells were either treated with 100nM CDDO-Im or DMSO as a vehicle control for 24 hours. In **black** is the control and in **blue** is the tBHP-treated cells. (*p<0.0.05)

4.2.8 *MAPT*$^{-/-A2}$ and *MAPT*$^{-/-A4}$ cell lines show decreased expression of microtubule and tubulin binding proteins alongside modifications in RNA and cadherin binding proteins in comparison to WT.

To understand pathways that are altered in the absence of Tau, the *MAPT*$^{-/-A2}$ and *MAPT*$^{-/-A4}$ proteome, without tBHP (untreated), was compared with WT cells untreated. The replicates that had most commonality according to Figure 4.15B were compared such that all the replicates of the WT cells treated with water vehicle control, all the replicates of *MAPT*$^{-/-A2}$ and replicates 1, 2 and 3 of the *MAPT*$^{-/-A4}$ treated with water were analysed.

Three hundred and five proteins were upregulated in *MAPT*$^{-/-A2}$ untreated, and 463 in *MAPT*$^{-/-A4}$, in comparison to WT untreated, and 174 of these were shared in both MAPT KO clones, most of which were RNA- and cadherin-binding proteins (Figure 4.14A and C). Ninety-six proteins were downregulated in *MAPT*$^{-/-A2}$ compared to WT, and 225 in *MAPT*$^{-/-A4}$ compared to WT, 40 of these were shared, confirming the loss of Tau function, and subsequent down regulation of other proteins that interact with microtubules, tubulin and actin such as Neurofilament Heavy Polypeptide (NEFH), Kinesin Family Member 1A (KIF1A) and Leucine-Rich Pentatricopeptide Repeat Motif-containing (LRPPRC) proteins. Nevertheless, the most downregulated molecular pathway was RNA binding (Figure 4.14B and D).

4.2.9 Dissecting differentially expressed proteins in the *MAPT*$^{-/-A2}$ and *MAPT*$^{-/-A4}$ cell lines in comparison to WT in the context of oxidative stress induction

The proteomic signature of RNA- and cadherin-binding in the untreated Tau KO cells compared to WT mirrors the findings in the tBHP treated WT cells. This may reflect the increased basal oxidative stress observed in the *MAPT*$^{-/-A2}$ and *MAPT*$^{-/-A4}$ cell lines (Figure 4.9A/B). To compare cell populations with similar levels of oxidative stress and focus on the

Figure 4.14

Figure 4.14 Differentially expressed proteins in response to loss of *MAPT* expression in SH-SY5Y cells. A Venn diagram of proteins upregulated in both *MAPT*$^{-/-A2}$ and *MAPT* $^{-/-A4}$ with water control in comparison with WT SH-SY5Y cells with water control. **B** Venn diagram of proteins downregulated in both *MAPT*$^{-/-A2}$ and *MAPT* $^{-/-A4}$ with water in

comparison with WT SH-SY5Y cells with water. **C** Top ten pathways with the most overlap with the proteins upregulated in both *MAPT*$^{-/-A2}$ and *MAPT* $^{-/-A4}$ in comparison with WT SH-SY5Y cells as shown in A **D** Top ten pathways with the most overlap with the proteins downregulated in both *MAPT*$^{-/-A2}$ and *MAPT* $^{-/-A4}$ in comparison with WT SH-SY5Y cells as shown in B.

differences due to loss of Tau, I compared the *MAPT*$^{-/-A2}$ and *MAPT*$^{-/-A4}$ cells without tBHP treatment to tBHP treated WT cells. Differences between these groups should be due to Tau, though I could not exclude effects of tBHP beyond oxidative stress induction, or residual differences in the level of oxidative stress contributing to the set of differentially-expressed proteins. In order to enrich for Tau effects, I focused on those proteins with expression altered in opposing directions in the WT tBHP group versus *MAPT* KO cells at basal conditions. I also required that the protein was differentially expressed in both *MAPT* KO lines.

One hundred and seventy-four proteins were upregulated in both KO cell lines without tBHP compared to WT BHP treated cells, and 35 of these were also downregulated in WT cells treated with tBHP compared to WT untreated cells, suggesting that the observed upregulation in Tau KO cells is not a function of tBHP treatment, and may therefore indicate a Tau deletion mediated effect (Figure 4.15A). Likewise, 40 proteins were downregulated in the both KO cell without tBHP compared to WT tBHP treated cells, and 21 of these were also upregulated in WT cells treated with tBHP compared to WT untreated cells (Figure 4.15B). A list of these proteins is shown in Tables 4.1 and 4.2 with highlighted biological pathways and molecular functions shown in Tables 4.3 and 4.4.

Figure 4.15

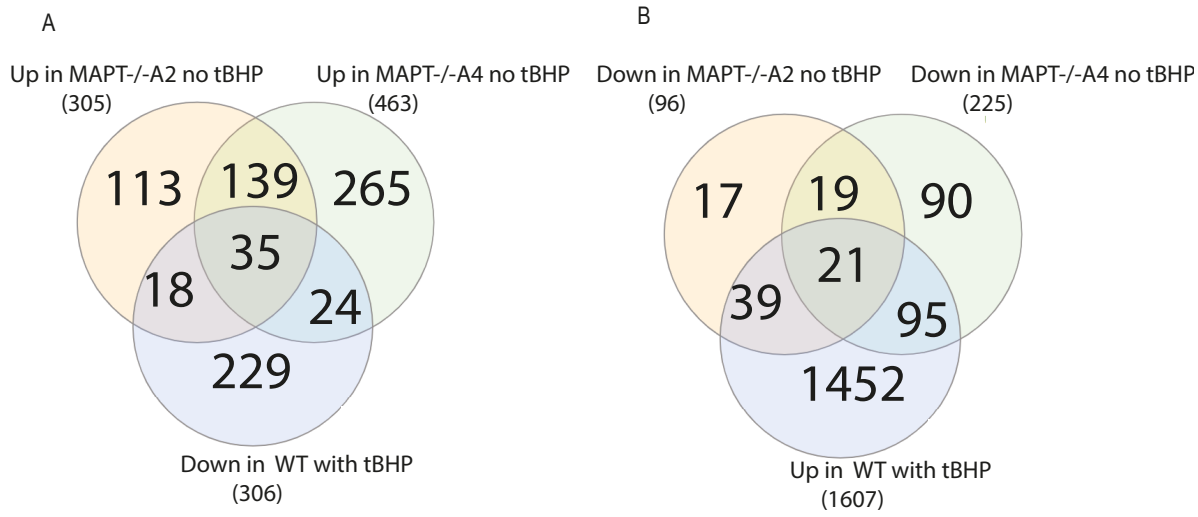

Figure 4.15 Differentially-expressed proteins in *MAPT* KO SH-SY5Y cells in comparison to WT SH-SY5Y cells treated with 15 μM tBHP for 24 hours. A Venn diagram of proteins upregulated in both *MAPT*$^{-/-A2}$ and *MAPT* $^{-/-A4}$ but downregulated in WT cells treated with tBHP in comparison with WT SH-SY5Y cells. **B** Venn diagram of proteins downregulated in both *MAPT*$^{-/-A2}$ and *MAPT* $^{-/-A4}$ but upregulated in WT cells treated with tBHP in comparison with WT SH-SY5Y cells.

Table 4.1 : Proteins upregulated in knockout clones but dowregulated widltype cells treated with tBHP

AHCTF1	DNAJB5	HDLBP	PABPC1	SND1	AHCTF1	DNAJB5
AIFM1	DYNC1H1	HNRNPM	PDIA3	SSB	AIFM1	DYNC1H1
CCDC86	ECH1	HSPA5	PHB2	TPR	CCDC86	ECH1
COPA	EEF1A1	LDHB	PLEC	TRAP1	COPA	EEF1A1
COPB2	EFTUD2	MACROH2A1	PURA	VASP	COPB2	EFTUD2

Table 4.2 : Proteins downregulated in knockout clones but dowregulated widltype cells treated with tBHP

AASDHPPT	EIF3A	INA	MVP	NUP210	PRPF4B	PHIP
CHGB	GANAB	ITGA2	MYH9	OGDH	SPTBN1	VARS1
DYNC1H1	HPCAL1	LRPPRC	MYL12A	PDIA6	STRA6	VGF

Table 4.3 : Top 5 pathways deregulated by differentially expressed genes in tables 4.4 and 4.5

Term	Overlapping genes
Oxidative Phosphorylation	LDHB, AIFM1, ECH1, OGDH, PHB2, LRPPRC
Mitotic Spindle	DYNC1H1, MYH9, LRPPRC, SPTBN1
Hypoxia	HSPA5, HDLBP, MYH9, ENO1
Glycolysis	COPB2, HSPA5, HDLBP, ENO1
Peroxisome	MVP, ECH1, PABPC1

Table 4.4 : Top 5 molecular functions deregulated by differentially expressed genes in tables 4.4 and 4.5

Term	Overlapping genes
RNA Binding (GO:0003723)	PDIA3, DYNC1H1, SSB, DDX27, HDLBP, PRPF4B, ENO1, SND1, LRPPRC, EEF1A1, EFTUD2, HNRNPM, PURA, GANAB, ZNF638, TPR, MYH9, CCDC86, PABPC1, SPTBN1, GCN1, PLEC
Cadherin Binding (GO:0045296)	VASP, HSPA5, YWHAB, HDLBP, MYH9, ENO1, SND1, SPTBN1, GCN1, PLEC
mRNA Binding (GO:0003729)	HNRNPM, SSB, ZNF638, TPR, HDLBP, PABPC1, LRPPRC
Ankyrin Binding (GO:0030506)	SPTBN1, PLEC
Poly(U) RNA Binding (GO:0008266)	SSB, PABPC1

4.3 Summary

The aim of this research was to investigate the role of Tau in oxidative stress by manipulating a cell line with robust expression of the *MAPT* gene, SH-SY5Y. In an SH-SY5Y cell line previously reported to be a *MAPT* KO I found expression of a truncated version of the Tau protein potentially detectable with the C-terminal antibody, Tau 46 (Figure 4.2). Therefore, using CRISPR-CAS9 gene editing, I generated two new cell lines in which Tau expression is undetectable either with N-terminal or C-terminal antibodies. Basal oxidative stress, as quantified by the proportion of cells expressing carbonylated protein, is higher than in these Tau KO cells in the WT, alongside reduced tubulin polymerisation. Upon rescuing the KO cells by inducing Tau overexpression in them, both the basal and induced oxidative stress signature observed in the KO cells were fully reversed indicating that the increased oxidative stress phenotype is due to loss of Tau (Figure 4.9).

To establish a possible mechanism by which Tau could be influencing oxidative stress in the SH-SY5Y cells, I measured the NRF2 levels in the KO cells in comparison to the WT and furthermore treated the KO cell lines with the NRF2 activator, CDDO-Im. The incomplete rescue of the oxidative stress phenotype in the CDDO-Im treated KO cells suggests that Tau's role in oxidative stress is either not, or only partially dependent, on NRF2 (Figure 4.12).

Finally, I used MS proteomics to identify proteins whose expression differed in the KO cells treated with water (with high oxidative stress) relative to the tBHP-treated WT cells whose oxidative stress levels were also high. This identified 56 altered proteins with opposing effects with Tau deletion compared to oxidative stress in the presence of Tau. These can be considered candidate Tau-regulated proteins that may be important in the antioxidant

response, of which 50% are involved in RNA binding while 20% are involved in cadherin binding (Figure 4.14).

Chapter 5

Modelling Oxidative Stress in Kidney Organoids

5.1 Introduction

An aim of this project was to investigate the role of Tau in DKD. In Chapter 3, I found that in response to oxidative stress induction using tBHP, differentiated human podocytes expressed increased mRNA levels of the Tau gene *MAPT*. The association between *MAPT* expression and oxidative stress could not be investigated any further with the immortalised human podocyte cell line because neither the podocytes in their resting state nor those treated with tBHP expressed Tau protein at a level detectable with western blotting or immunofluorescence. This contrasts with findings in mice, where the Tau4R isoform is detectable in podocytes in vivo (Valles-Saiz et al., 2022). Thus, further work in Chapter 4 with deletion of *MAPT* was completed on human neuronal cells that express high levels of Tau. These results supported a role for Tau in the oxidative stress response in SH-SY5Y cells, but the question remains as to the role of Tau in human DKD. In this Chapter I aimed to establish a toolkit to investigate the role of Tau in a human kidney model.

As described in Chapter 1, kidney organoids provide 3-dimensional self-organising multicellular structures that can mimic tissue level development and some function (Takasato et al., 2015). Manipulation of Tau in renal organoids could circumvent the lack of detectable Tau in immortalised podocytes and provide a model system that represents both glomerular and tubular components of the nephron.

As prerequisite steps towards this aim, it is necessary to better understand Tau mRNA expression in healthy human kidney, to establish an in-house protocol to generate and characterise kidney organoids from human induced pluripotent stem cells (hIPSCs) and to measure their expression of Tau protein.

Methods to induce and quantify oxidative stress in the organoids are then explored, and the gene editing approach developed in Chapter 4 to delete *MAPT* in neuronal cells applied to the

iPSCs, to establish a platform for future work exploring the function of Tau in the context of oxidative injury in the diabetic kidney.

5.2 Results

5.2.1 *MAPT* is expressed in human kidney in the proximal tubule and podocytes.

To establish the cell type-specific expression of the Tau encoding gene *MAPT* in the human kidney, a human kidney single nuclei RNA sequencing (snRNA-Seq) dataset was analysed, generated from a single healthy renal biopsy core. SnRNA-Seq can provide better representation of glomerular cell types than scRNA-Seq, in which glomerular cells, already only 3-5% of renal cortex cell types, are relatively depleted due to their poor dissociation under scRNA-Seq lysis protocols, as well as reducing artefactual stress signatures (Wu et al., 2019).

The snRNA-Seq dataset comprised 5,162 nuclei, and clustered into 23 populations represented by uniform manifold approximation and projection (UMAP) (Figure 5.1A). The proximal tubule is divided into segments S1-3 based on microscopic appearance and function. Eighty to 90% of filtered glucose is reabsorbed in the most proximal segment, S1, via the sodium glucose co-transporter 2, SGLT2, encoded by *SLC5A2*, S2 has the highest levels of the organic anion transporter 1, *SLC22A6*, and amino acid transport occurs in S3 via AGT1 encoded by *SLC7A13*. Such markers allow annotation of the proximal tubule clusters by segment. *MAPT* mRNA was expressed predominantly in the proximal tubular clusters, and found in all three segments, though most abundantly in S1 (Figure 5.1B). While this is evidence of mRNA-level renal expression, the Human Protein Atlas database also supports a proximal tubular and glomerular distribution of Tau protein (Figure 5.1C) (Uhlen et al., 2015)

5.1

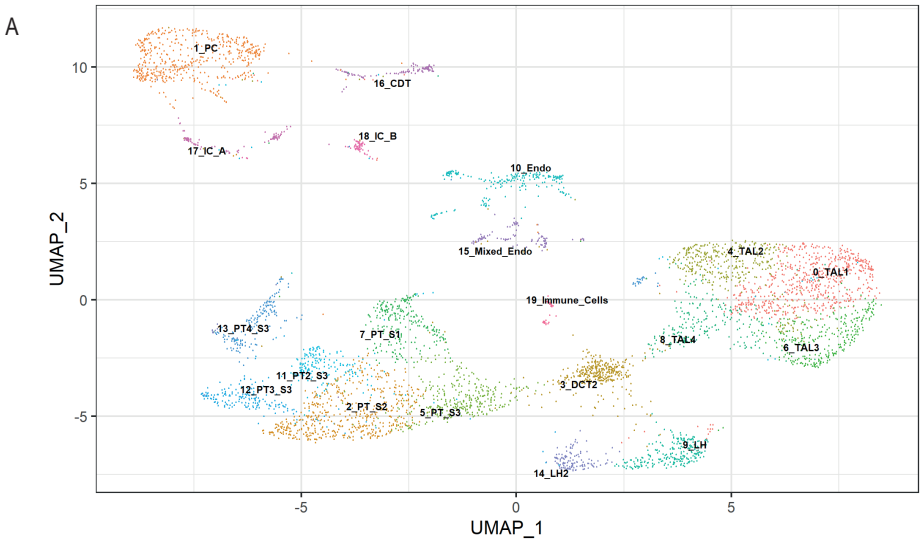
A
1_PC
16_CDT
18_IC_B
17_IC_A
10_Endo
15_Mixed_Endo
4_TAL2
0_TAL1
19_Immune_Cells
13_PT4_S3
7_PT_S1
8_TAL4
6_TAL3
11_PT2_S3
12_PT3_S3
3_DCT2
2_PT_S2
5_PT_S3
9_LH
14_LH2
UMAP_2
UMAP_1
10
5
0
-5
-5
0
5

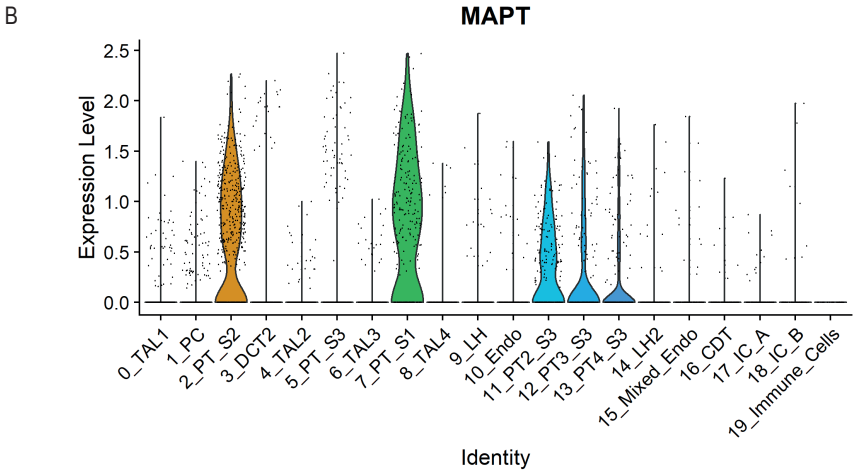
B
MAPT
Expression Level
2.5
2.0
1.5
1.0
0.5
0.0
0_TAL1
1_PC
2_PT_S2
3_DCT2
4_TAL2
5_PT_S3
6_TAL3
7_PT_S1
8_TAL4
9_LH
10_Endo
11_PT2_S3
12_PT3_S3
13_PT4_S3
14_LH2
15_Mixed_Endo
16_CDT
17_IC_A
18_IC_B
19_Immune_Cells
Identity

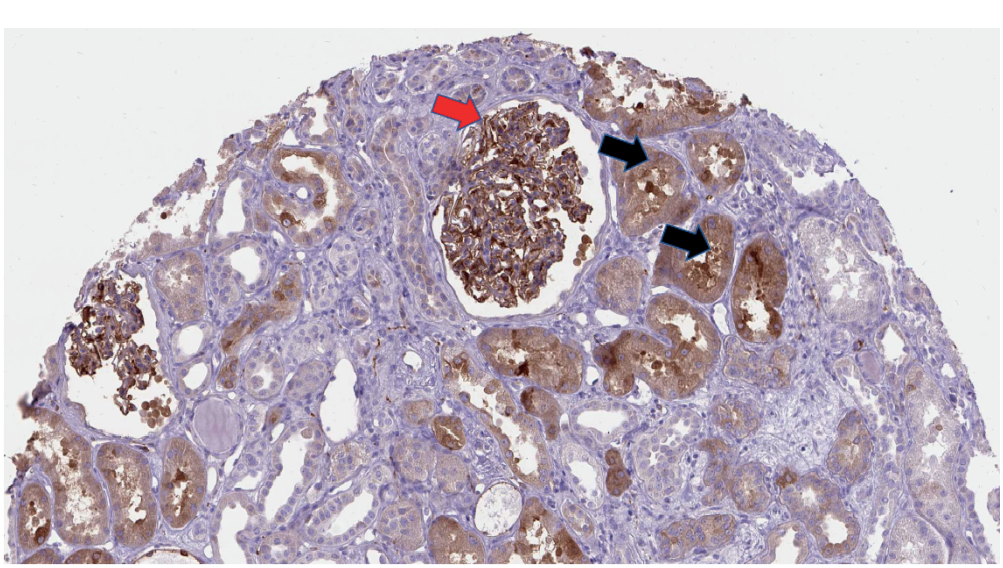
C

Figure 5.1 A. Uniform manifold approximation and projection (UMAP) of nuclei identified by snRNA-Seq in healthy human kidney, with annotated clusters. PC = principal cell (of collecting duct), PT = proximal tubule, annotated by segment (S1-3). DCT = distal convoluted tubule, LH= loop of Henle, TAL = thick ascending loop, IC = intercalated cells (type A or B), CDT = collecting duct. Endo = endothelial (mixed endo population includes podocytes and mesangial cells), **B**.Violin plot showing expression of *MAPT* across snRNA clusters. **C.** Protein expression of Tau in kidney from the Human Protein Atlas (https://www.proteinatlas.org/) following incubation with antibody HPA069570. Red arrow represents Tau in the glomeruli. Black arrows indicating Tau protein in the proximal tubules. (snRNA-Seq data analyses completed by Jessica Kepple)

5.2.2 Differentiation of kidney organoids from human induced pluripotent stem cells.

As a baseline prior to hiPSC differentiation, I assessed the expression of nephrin, synaptopodin and WT1, as podocyte specific markers, GATA binding protein-3 (GATA-3) for the distal tubule, E-cadherin for epithelial cells, and SRY-Box Transcription factor 17 (SOX17) for endothelial cells, in hIPSCs and compared this to differentiated immortalised human podocyte cells as a positive control for the podocyte markers. As expected, undifferentiated hiPSCs expressed very low or undetectable levels of synaptopodin, GATA-3, E-cadherin and SOX17, with some non-specific weak staining for nephrin in comparison with podocytes, which were positive for nephrin, synaptopodin, WT1 and E-cadherin, with some SOX17 fluorescence suggesting some non-specific binding with this antibody, and negative staining for tubular marker GATA3. This established a baseline for later phenotyping of the differentiated organoids (Figure 5.2A to E).

To generate renal organoids iPSCs were cultured in a matrigel and exposed to sequential treatment of growth factors CHIR99021, a highly selective inhibitor of glycogen synthase kinase (GSK-3) that acts as a Wingless/Integrated (Wnt) activator, and fibroblast growth factor 9 (FGF9), and transferred to a transwell system(Takasato et al., 2016, Takasato et al., 2015).

Initial attempts to replicate the published organoid protocol in-house did not reproduce the morphology or the markers anticipated. Therefore, further optimisation of the protocol was

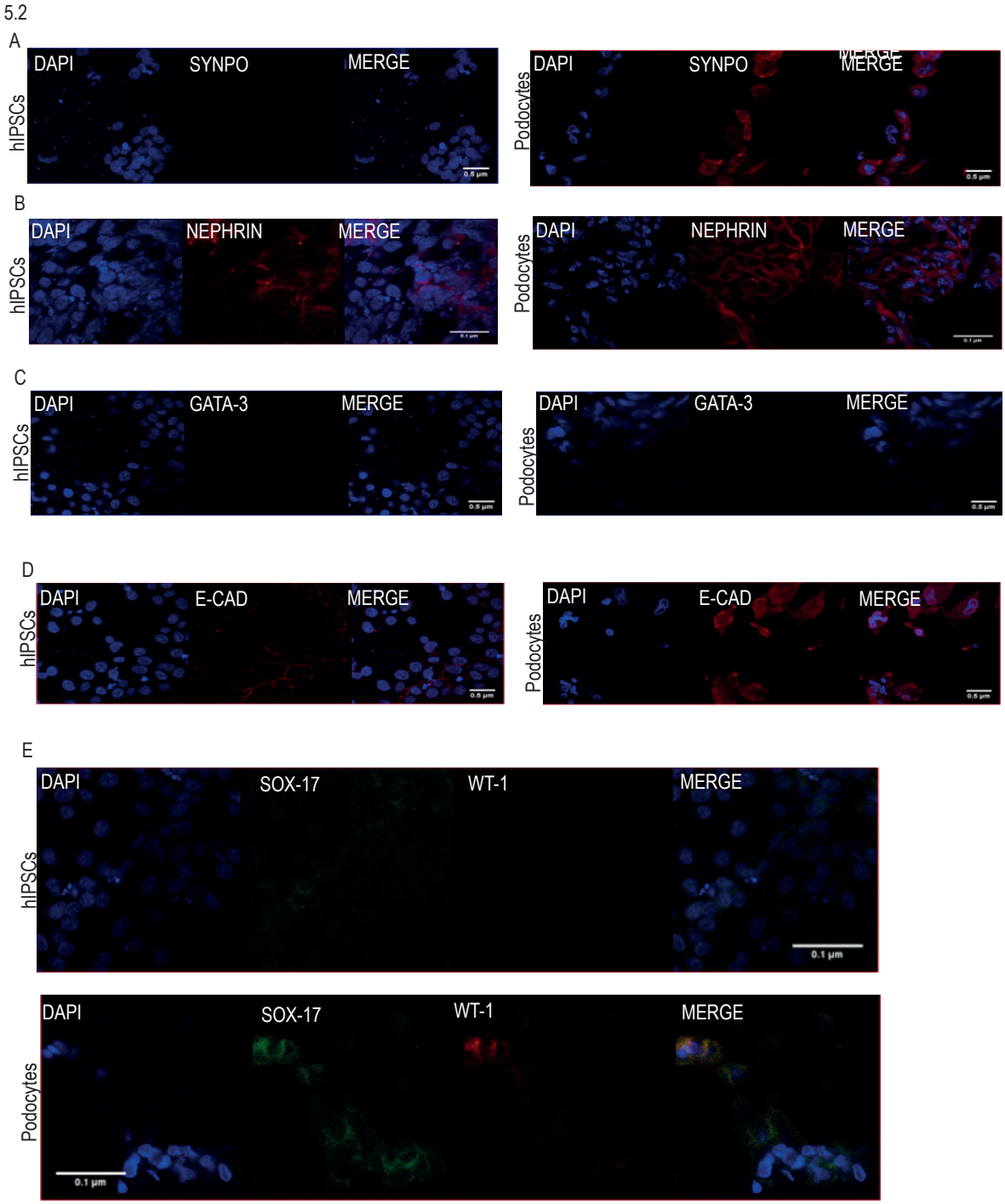

Figure 5.2 Expression of podocyte and endothelia markers in undifferentiated human induced pluripotent stem cells (hiPSCs) and differentiated immortalised human podocytes. DAPI is used for nuclear staining. **A –** synaptopodin (SYNPO) B – nephrin **C** – GATA binding protein 3 (GATA-3) **D** – E-cadherin (E-Cad) **E –** SRY-box 17 (SOX 17) and Wilms tumour protein (WT1).

undertaken, with support from the Lennon group (University of Manchester). It was found that while the transwell membrane on which the hiPSCs are seeded for differentiation are supplied with four different membranes, successful organoid production required the hydrophilic Polytetrafluoroethylene (PTFE). We also found that the protein free hybridoma used as a supplement for the culture media requires titration for each batch to identify the appropriate concentration for differentiation. Depending on the batch, a concentration between 1% and 10% could be required. Moreover, we reduced the number of organoids per transwell from ten to four as larger numbers of organoids per transwell inhibited differentiation.

5.2.3 Kidney organoids express kidney markers.

Using this revised protocol (Methods), the organoids developed changes in structure with increasing patterning and definition between days 3, 5 and 10 of differentiation (Figure 5.3A). After 30 days of differentiation, organoids were stained with a panel of antibodies against the following kidney protein markers: SOX17, nephrin, synaptopodin, GATA-3 and E-cadherin, plus LDL-receptor related protein 2 (LRP2) as a proximal tubular marker. The IF results indicated a complex structure with *de novo* expression of kidney-specific markers, not present in the iPSCs prior to differentiation (Figure 5.3B-E). Nephrin and synaptopodin, podocyte-specific markers, were co-localised (Figure 5.3B).

The epithelial marker E-cadherin stained well defined tubular structures, with weak GATA-3 staining suggesting these might be distal tubule/collecting duct (Figure 5.3C). In other regions, E-cadherin was detected in less well-defined structures independent of GATA-3 (Figure 5.3D). LRP2 encodes the protein megalin, and the observed LRP2 positivity in the organoids suggested proximal tubular differentiation. (Figure 5.3E). Overall, the IF results

indicate successful generation of kidney organoids with evidence of both glomerular and tubular tissue representation.

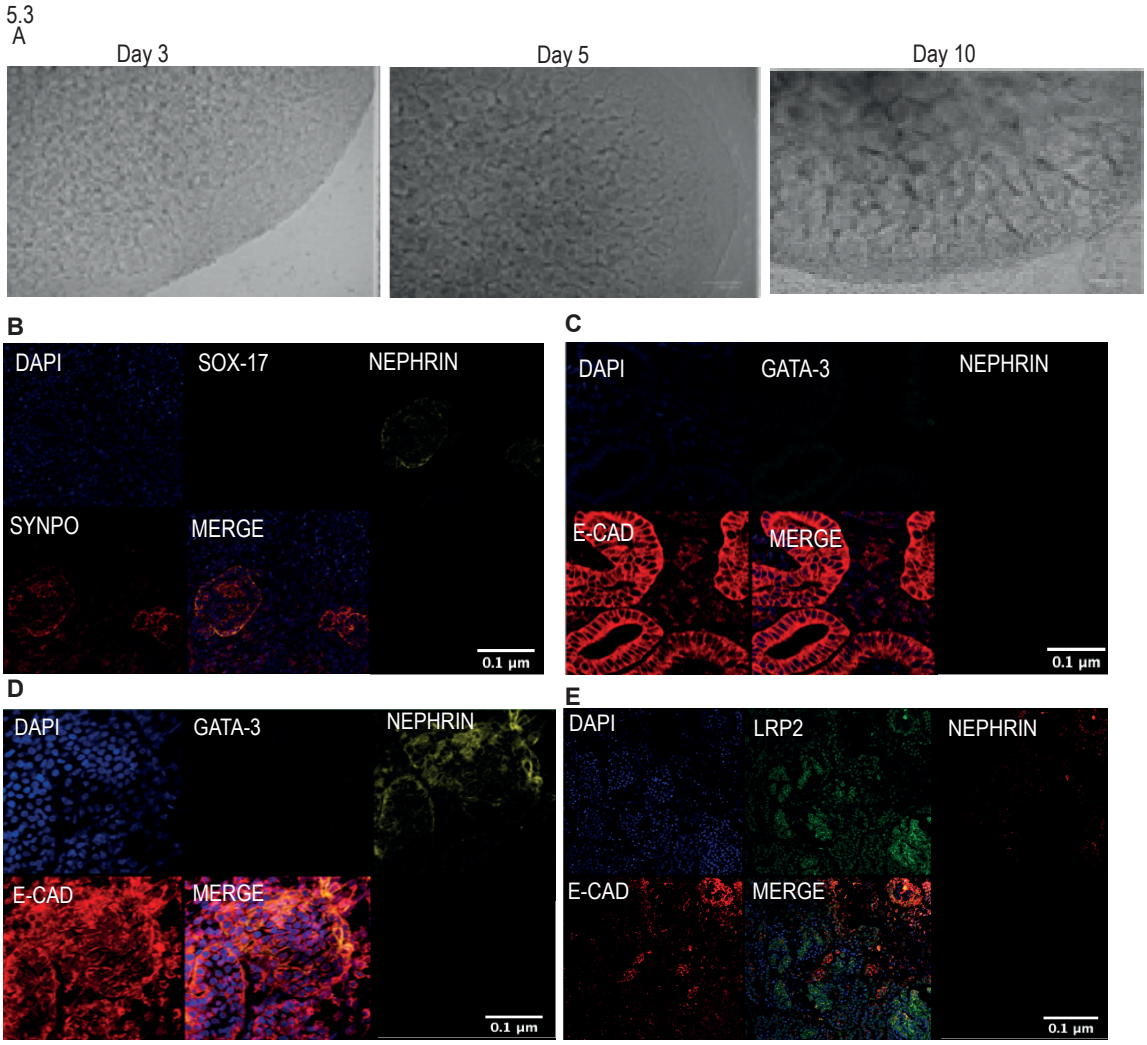

Figure 5.3 Structural changes in hiPSCs with differentiation into kidney organoids **A** Early changes in cell patterning during organoid differentiation. All images taken with 20x objective. Days represent the number of days following CHIR99021 treatment and transfer into transwell plates. **B-D** Expression of podocyte-specific markers in kidney organoids. 30-day differentiated kidney organoids stained with **B –** SRY-box 17 (SOX 17), nephrin and synaptopodin (SYNPO), **C –** GATA-3, nephrin and E-Cad, **D –** low density lipoprotein-related protein 2 (LRP2), nephrin and E-Cad. Diamidino-2-phnenylindole (DAPI) is used in all the images for staining the nuclei. (Organoids generated by Phalguni Rath, staining performed by Belinda Ameyaw)

5.2.4 Kidney organoids express Tau

I then assessed if the renal organoids express Tau. Based on the human kidney snRNA-seq and Human Protein Atlas data it was hypothesised that Tau protein might be detected within the podocytes and/or proximal tubules. IF with the C-terminal Tau antibody, Tau 46, detected

Tau protein in the kidney organoids that co-localised with the podocyte-specific marker nephrin, but not the proximal tubule protein LRP2 (Figure 5.4), However, the widespread peripheral distribution of nephrin in these organoids was not typical for glomeruli and so non-specific staining or immature development cannot be excluded. These findings confirm Tau expression in the kidney organoids, and suggest this might localise with glomerular structures. The lack of Tau co-localisation with the proximal tubular marker LRP2 may indicate that Tau is absent from the organoid proximal tubule, which could be due to some incomplete differentiation of the proximal tubule cell type in the organoid, or the early embryonic stage. Kidney organoid proximal tubule cells represent an immature developmental stage, with only low expression of the main water transport channel *Aqp1* and organic anion transporters (Wilson et al., 2022).

Treatment of kidney organoids with tBHP shows increased oxidative stress.

To establish a platform for the study of oxidative stress it was necessary to optimise an assay to both induce and then measure stress in the organoids. Kidney organoids were tested for their response to two concentrations of tBHP, 50 µM or 200 µM for 24 hours, compared to equivalent concentrations of DMSO. As in the previous chapters, a DNP-based test was used as a surrogate read-out for oxidative stress. By IF, both concentrations of tBHP-induced increased oxidative stress in the organoids in comparison to control, with the highest intensity with 200 µM tBHP (Figure 5.5). Two hundred µM tBHP for 24 hours induced widespread cellular oxidative stress, However E-cadherin and nephrin intensity appeared largely unchanged between the control organoids and those treated with tBHP, with tubular structures still visible (Figure 5.6).

5.4

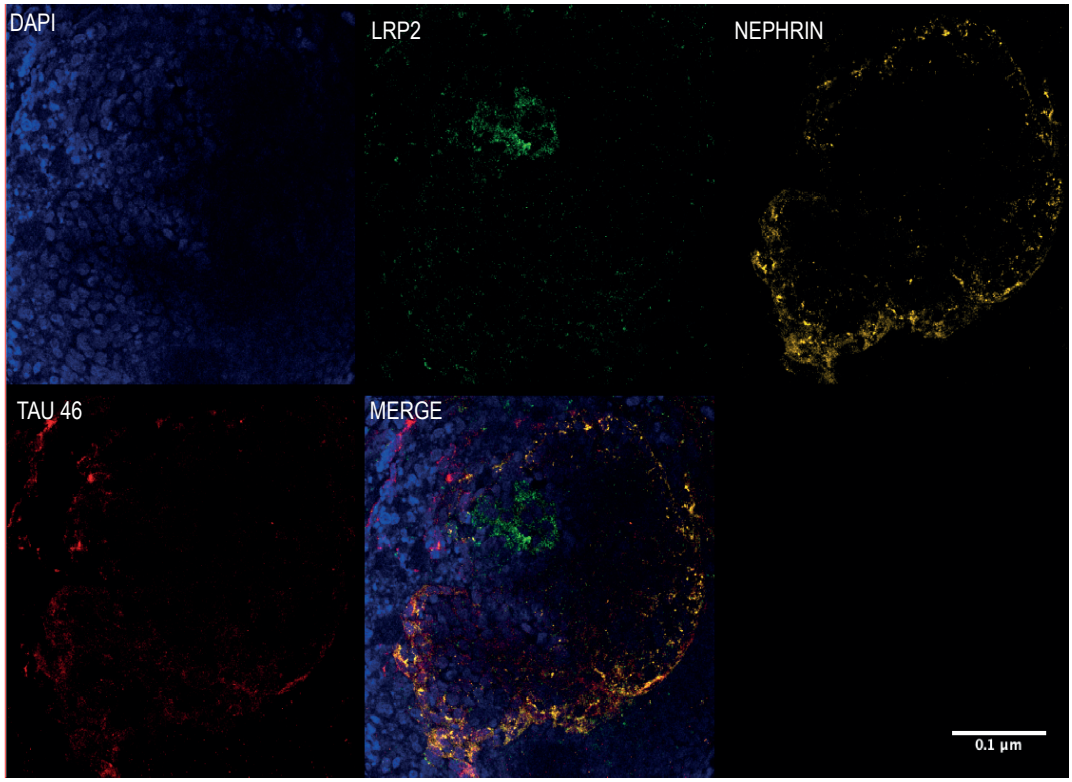

Figure 5.4 *MAPT* expression in kidney organoids. 30-day differentiated kidney organoids stained with Diamidino-2-phnenylindole (DAPI) for the nuclei, low density lipoprotein-related protein 2 (LRP2) for the proximal tubule, nephrin for the glomerular and Tau 46 for the Tau protein. All four stains combined to create the merged image.

5.2.5 Neuronal cells differentiated from *MAPT*$^{-/-}$ hiPSCs do not express WT Tau protein.

A future aim is to determine the effect of loss of Tau on the response to oxidative stress in kidney organoids. This requires both a kidney organoid oxidative stress protocol, as described above, and the generation of organoids with deletion of *MAPT*. For the latter, hiPSCs were edited using the dual guide CRISPR-CAS9 gene editing described in Chapter 4, but with the second sgRNA in exon 4a replaced with a sgRNA targeting exon 7. This amendment to the editing approach was required due to loss of edits with hiPSC passage using the exon 1 and 4a pair.

To make an initial assessment of the deletion efficacy, the edited hiPSCs were expanded into colonies from isolated single-cells and then differentiated into neuronal cells. Neuronal cells

provide a useful tool to check deletion because of their high WT expression of Tau protein. Four WT and four edited clones were assessed by western blot (WB). All four WT clones expressed a detectable band between 32 kDa and 57 kDa with either an N-terminal antibody, Tau 12 (Figure 5.7A) or a C-terminal antibody, DAKO A0024 (Figure 5.7B). In contrast, the four clones in which gene editing was performed lost these signals. Instead, smaller bands between 22 kDa and 25 kDa were observed in these clones alongside a weak band above 60 kDa. These blots indicate absence of the full-length WT Tau protein in the edited organoids.

5.3 Summary

I have established a set of tools for future work to explore the function of Tau in the human kidney, building on the evidence from Chapter 4 that Tau has a role in the oxidative stress response in neuronal cells. Firstly, I found evidence of Tau expression in healthy human kidney, in proximal tubule and glomeruli. Next, we established a protocol to generate kidney organoids from hiPSC cells, and showed that these cells form tubular and glomerular structures, and express Tau, which appears to be co-localised to the podocyte-specific marker nephrin. By IF I showed that oxidative stress can be induced and quantified in these organoids with preservation of tissue structure and differentiation markers. Finally, I confirmed the generation of $Tau^{-/-}$ organoids. Together these experiments provide a strong basis to translate the neuronal Tau findings to a model more relevant to DKD.

5.5

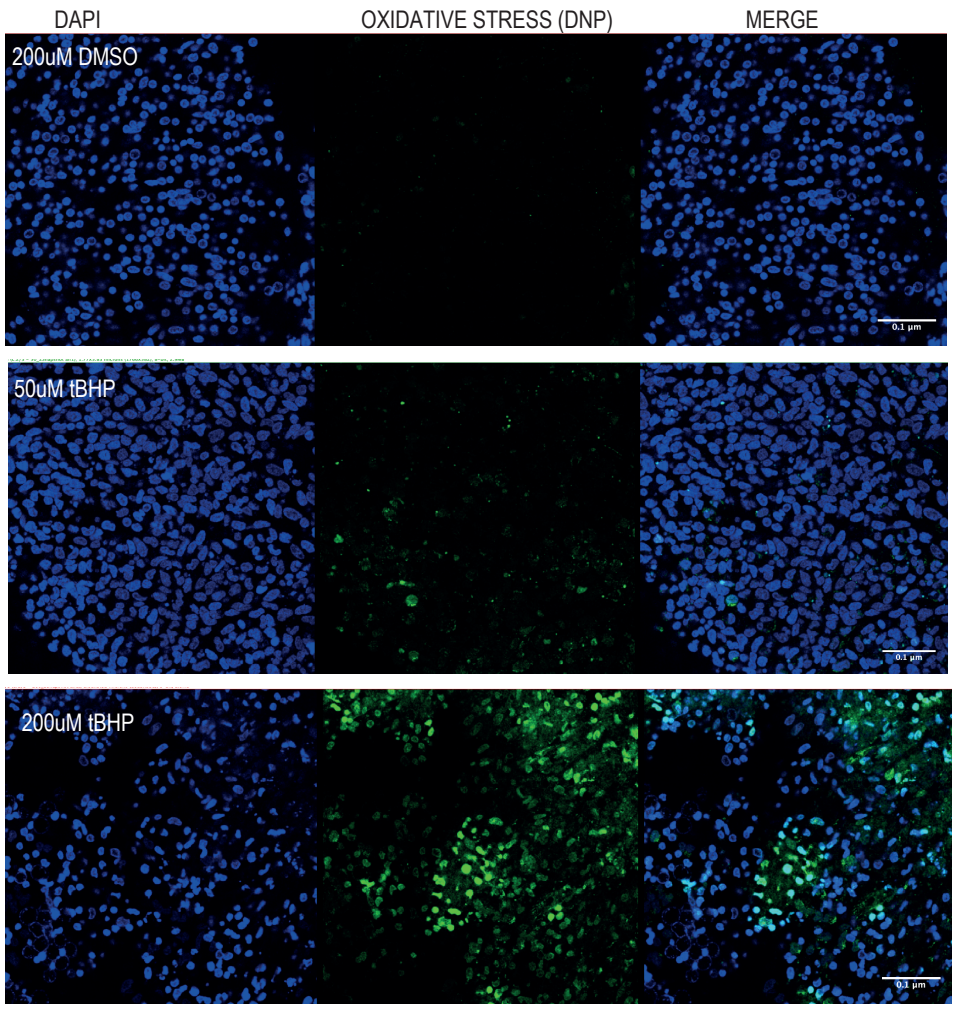

Figure 5.5 Response of kidney organoids to oxidative stress. Differentiated kidney organoids treated with either 200 µM dimethyl sulfoxide (DMSO) – untreated, 50uM tert-butyl hydroperoxide (tBHP) or 200 µM tBHP for 24 hours. Oxidative stress indicated in green by 2 ,4 Dinitrophenol (DNP) antibody.

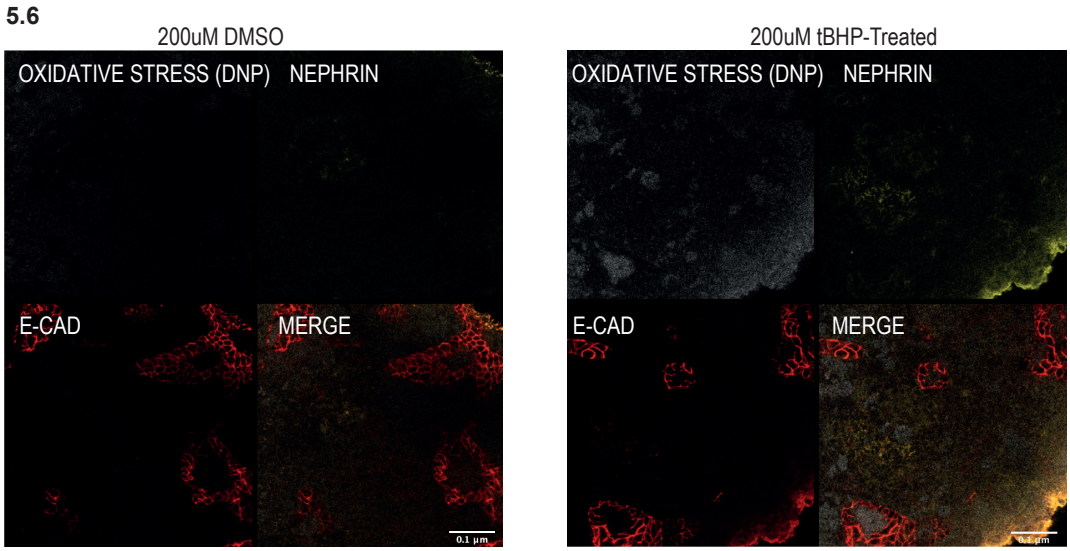

Figure 5.6 Effect of 200 µM tBHP for 24 hours on morphology of kidney organoids. Differentiated kidney organoids treated with either 200 µM of dimethyl sulfoxide (DMSO) or 200 µM tert-butyl hydroperoxide (tBHP) were stained with 2,4 Dinitrophenol (DNP), nephrin and E-cadherin (E-Cad) with the final image a merge of the three individual stains.

5.7

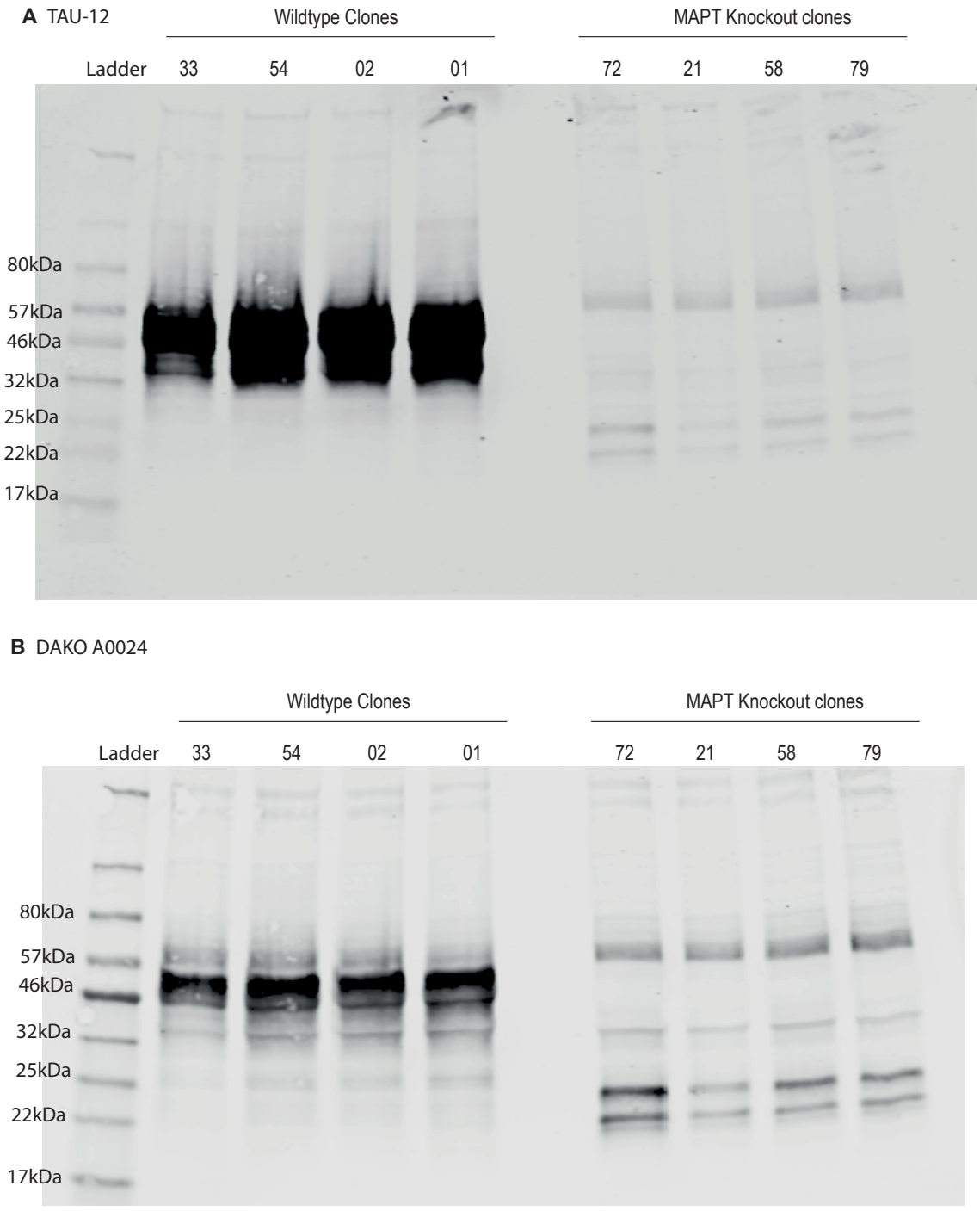

Figure 5.7 Western blot of *MAPT* KO human induced pluripotent stem cells (hiPSCs) – 10,000 cells per lane, differentiated into neuronal cells. **A** N-terminal Tau 12 and **B** C-terminal Dako A0024 fluorescent blots for 4 independent WT and *MAPT* KO clones. Tau expression within the kidney. (Western Blotting undertaken by Phalguni Rath)

Chapter 6
Discussion

6.1 Introduction

The aims of this project were to explore the effects of oxidative stress in renal podocytes as model for diabetic kidney disease, to test the hypothesis that Tau protein has a functional role in the oxidative stress response, and to explore new models to study renal oxidative injury.

To this end, in Chapter 3 I established a model to induce oxidative stress in immortalised human podocytes using tBHP, and using this model, investigated alternative proteins within the NRF2-KEAP1 pathway that could be druggable targets to diabetes-dependent oxidative stress. Podocyte RNA-seq identified increased *MAPT* transcription in oxidatively-stressed podocytes relative to water vehicle control cells. However, since Tau protein expression in immortalised human podocyte cells was below the level of detection, an alternative strategy was required to further explore the observed association between oxidative stress and Tau.

Therefore, in Chapter 4, I used the neuroblastoma cell line SH-SY5Y, which expresses high levels of Tau, to study how the loss of Tau affected response to oxidative stress. Oxidative stress was elevated in *MAPT* KO cells compared to WT, a phenotype rescued by exogenous expression of Tau. By MS proteomics, both tBHP and loss of Tau alter the expression of RNA-binding proteins. Within the context of high oxidative stress, a group of 56 proteins correlated specifically with the loss of Tau, and could thus represent newly-identified Tau-regulated proteins relevant to the antioxidant response.

In Chapter 5, I returned to diabetes and the kidney, establishing a kidney organoid system to test genetic drivers of the antioxidant response. In kidney organoids generated from hiPSCs, expressing glomerular and tubular markers, I induced and quantified oxidative stress. I

suggest in future studies the use of these organoids to test the impact of Tau loss on these cell structures and morphology, and susceptibility to oxidative stress.

In this discussion, I will explore the implications, limitations and future opportunities presented by the findings presented in this thesis.

6.2 Oxidative stress modelling and NRF2 modulation

6.3.1 An oxidative stress model in human podocytes

Much of the work in this thesis depends upon in vitro induction of oxidative stress in cell lines. More work will be needed to establish whether these findings can be extrapolated to other cell types, or to *in vivo* physiology. Despite this caveat, the *in vitro* model provides an efficient and readily manipulatable system to test cellular responses.

One important consideration was the method of stress induction. Oxidative stress can be induced by compromising the cell's defence mechanisms or increasing by the generation of oxidising agents. Inhibition of cellular defence can be attempted by RNA interference to suppress superoxide dismutase or by pharmacologically inhibiting glutathione with buthionine sulfoximine (Kim et al., 2010, Martin et al., 2009a, Martin et al., 2009b). Despite good specificity, the former can be time-consuming while the latter has a short window of activity due to clearance (Koch and Hill, 2017). Therefore, induction using oxidising agents is more commonly used to induce stress, deploying a range of agents including heavy metals, ionising radiation, paraquat, hydrogen peroxide, glutamate, potassium bromate or tBHP (Goffart et al., 2021) (Wang et al., 2019). Aside their varying mechanisms of action, factors including their toxicity to handle, stability and off-target effects are important considerations in choosing a mode of inducing oxidative stress in a cell model. For instance, hydrogen peroxide, a commonly used inducer of oxidative stress in cellular models and convenient to

use, works by stimulating Fenton reaction between the peroxide and the Fe^{2+} ions to generate hydroxide free radicals (Ransy et al., 2020). However, the hydrogen peroxide in the cell medium is removed by cells over time, at a rate dependent on cells type and density, introducing experimental variability (Wagner et al., 2013).

For this study, tBHP, a stable analogue of hydrogen peroxide, metabolised within the cells by cytochrome P450 or haemoglobin into unstable free radical intermediates, including as tert-butoxyl and methyl radicals, was selected as an agent previously used in podocytes, with minimal toxicity in handling and chemically stable under cell culturing conditions (Hix et al., 2000, Minotti et al., 1986, Anderson et al., 1967). tBHP treatment is stable for up to 24 hours, and achieved induction of stress and downregulation of podocyte specific gene expression. The choice of stress induction agent may influence the nature of the stress response. A comparison of tBHP and hydrogen peroxide in the human cancer cell line HepG2 found that only tBHP increased the levels of superoxide dismutase and glutathione peroxidase (Slamenova et al., 2013). Therefore, it is possible that some effects observed in this thesis might not be replicated with other oxidative agents. However, tBHP has broad mechanisms of action, mirroring *in vivo* oxidative injury pathways, including inhibition of NADPH resulting in the depletion of antioxidant glutathione, production of radicals that initiate lipid peroxidation, reduction of the mitochondrial membrane potential and DNA damage by single stranded breaks. These mechanisms mimic the mitochondrial glutathione loss and consequent mitochondrial stress observed in DKD (Wedel et al., 2020, Wang et al., 2019, Zavodnik et al., 1998) (Davies, 1989) (Brownlee, 2001).

Measurement of carbonylated protein or lipid peroxidation, and the results of the podocyte transcriptomic analysis, confirmed effective induction of stress. Following 24 hours of

exposure to 100 μM tBHP, in addition to NRF2-KEAP1 pathway activation, DNA-binding proteins are upregulated, and cholesterol biosynthesis and sterol deregulation pathways were downregulated due to decreased expression of two rate-limiting enzymes 3-hydroxy-3-methylglutaryl-coenzyme A reductase (HMGCR) and squalene monooxygenase (SQLE) (Xu et al., 2023, Stormo et al., 2012). The latter finding is consistent with inhibition of NADPH, the reducing agent for synthesis of lipids, including cholesterol.

The strongest finding from the transcriptomic analysis was that induction of oxidative stress in the podocytes results in dysregulation of RNA-binding proteins. RNA-binding proteins have been linked to paraquat sensitivity and response to oxidative stress in Jurkat cells, including those involved in translation initiation such as eIF4G1 (Turner and Turner, 2021). Consistent with this, tBHP increased podocyte eIF4GI expression in the present study. The function of RNA-binding proteins in the oxidative stress response remains unclear. However, one hypothesis is a link to their role in the formation of stress granules.

Stress granules are part of a cell's first line of defence against stress. They are non-membranous organelles containing RNA-binding proteins and stalled pre-initiation translation complexes such as T-cell intracellular antigen 1 (TIA1), GTPase-activating protein-binding protein 1 (G3BP1) and polyadenylate-binding protein 1 (PABP1) (Marcelo et al., 2021). Increased stress granules are found in diseases such as amyotrophic lateral sclerosis, frontotemporal lobar degeneration, and Alzheimer's disease, and could act as sites for pathological protein aggregation (Wolozin and Ivanov, 2019, Fan and Leung, 2016, Marcelo et al., 2021). Their formation requires downregulation of NLR Family Pyrin Domain Containing 3 (NLRP3) and upregulation of DEAD-Box Helicase 3 X-Linked (DDX3X) (Samir et al., 2019). Notably in the podocyte transcriptome, oxidative stress induced

upregulation of NLRP3 and downregulation of DDX3X. This could suggest impaired stress granule formation, and further experiments to quantify stress granules and their contents could illuminate the functional consequences of RNA-binding protein changes in oxidative stress.

A novel finding in the stressed podocytes was increased *MAPT* expression, alongside upregulation of other microtubule-interacting genes such as *TUBB, TUBB4A* and *KIF1A,* in response to tBHP. Murine *Mapt* KOs have an exaggerated oxidative stress response compared to WT mice, supporting a role for Tau in oxidative stress response (Violet et al., 2014). The results from the transcriptomic data are the first evidence of such an association in a human cell line. However, Tau was not amongst the differentially-expressed proteins in stressed podocytes. Indeed, Tau protein was not detected in the podocyte cell line by the N-terminal antibody (Tau 12) or the C-terminal antibody (Tau 46) western blotting, indicating that Tau protein is very weakly or not at all present in the cells. This might reflect low rates of translation, rapid degradation, or novel isoforms lacking the antibody epitopes.

Mapt mRNA and Tau protein have been reported in the rat kidney at a level approximately 30% of that found in the brain (Alonso et al., 2018b). In human tissues stained with anti-Tau antibodies, medium to high levels of Tau are found within both glomeruli and tubules (Ponten et al., 2008). Mouse kidneys interrogated for Tau using a GFP reporter showed expression of the Tau4R protein isoform within glomerular podocytes based on immunofluorescence localisation (Valles-Saiz et al., 2022). Thus *in vivo* data suggested that there is renal, and potentially, podocyte Tau expression.

While lack of Tau protein could be specific to the cultured cell line, examination of human kidney snRNA-seq data suggested that *MAPT* mRNA in the kidney is predominantly found in the proximal tubule. Nevertheless, since oxidative stress and podocyte injury are both central

to DKD, the podocyte cell line provided a model to explore NRF2-KEAP1 pathways and potential druggable targets for renal antioxidant therapy.

6.2.2 Modulation of NRF2 in podocytes using CDDO-Im and CRISPR-dCAS9 suggests the effects of NRF2 may be both dose and stress context dependent.

Clinical trials of the NRF2 agonist Bardoxolone in DKD and chronic kidney disease patients, while suggesting positive effects on the slope of eGFR, have not been successful, in part due to safety concerns including an increased risk of cardiac failure (Nangaku et al., 2020, de Zeeuw et al., 2013, Pergola et al., 2011). Identifying alternative targetable NRF2 pathway genes could provide effective approaches to protect from oxidative stress. The proteomic dataset generated here provide a starting point.

The results of CRISPR/Cas9 inhibition of NRF2 suggested that while robust inhibition led to increasing oxidative stress, more modest downregulation resulted in reductions in oxidative stress relative to WT cells. The consequences of upregulating NRF2, both genetically and pharmacologically in podocytes were also somewhat unexpected: CRISPR activation of the NRF2 gene in all five cell lines had significantly higher oxidative stress than the control cell line, despite NRF2's role as an antioxidant. This could be due to some off target or otherwise toxic effects of the CRISPR SAM activation system, or might indicate that excessive NRF2 is itself damaging. Some ROS activity is required in cells, in the kidney for example, ROS is required for solute and water reabsorption and vessel wall tension (Munoz et al., 2018) (Ishimoto et al., 2018). Thus, it is conceivable that both too little, and too much, antioxidant activity can be pathological.

Consistent with this possibility, using CDDO-Imidazole, a drug similar to Bardoxolone, which upregulates NRF2, under resting conditions there was a dose-dependent increase in stress. By contrast, CDDO-Im protected podocytes against tBHP-dependent oxidative stress in a reproducible bimodal pattern, reaching maximum protection at 30 nM for 6 hours. These findings suggest that the level of oxidative stress before introducing an NRF2 agonist could influence the outcome of the treatment in a complex and potentially unpredictable manner.

To quantify oxidative stress in cells I developed a flow cytometric oxidative stress assay. Redox imbalance generates many markers including superoxides, hydroxyl radicals, hydrogen peroxides, peroxidised lipids, damaged DNA and carbonylated proteins. With half-lives ranging from 10^{-9} seconds to days, the stability of these molecules influences their suitability as stress read-outs (Sies, 1993).

These molecules can be quantified by methods including comet assays, which involve quantification of oxidation of guanine to 8-oxo-7,8-dihydro-2′-deoxyguanosine (8OHdG or 8-oxodG); derivatization of the carbonyl group with 2,4-dinitrophenylhydrazine to form a dinitrophenylhydrazone (DNP) or malondialdehyde (MDA) readouts as surrogates for lipid peroxidation, each with its own limitations in levels of accuracy, reproducibility and specificity (Murphy et al., 2022) (Muruzabal et al., 2021) (Hawkins et al., 2009). The lipid peroxidation MDA assay utilises thiobarbituric acid reactive substances (TBARS), which interact with other organic molecules aside the intended aldehydes, limiting specificity (Yin and Porter, 2003) (Lapenna et al., 2001). Carbonylated proteins are arguably the gold standard for oxidative stress quantification due to their stability, with many semi-quantitative readouts available (Luddi et al., 2020, Dalle-Donne et al., 2003). Accumulation of

carbonylated protein aggregates can lead to toxicity and ultimately cell death, and has been linked to disease progression in diseases including CKD, diabetes and Alzheimer's (Fedorova et al., 2014). Here, the versatility of flow cytometry for single cell multi-parametric analysis was combined with the confidence of quantifying carbonylated protein with DNP-derivatisation.

Quantitation of per live cell oxidative stress can reveal heterogeneity within a cell population. I compared a maximum of three markers at a time. However, there is potential to design a more extensive panel. This could be applied to study the effect of oxidative stress on proteins linked to some of the pathways highly dysregulated in response to tBHP including stress granule proteins, RNA-binding proteins and DNA-interacting proteins.

6.3 Tau as an antioxidant in neuronal cells

6.3.1 Tau deletion in neuronal cells

Because podocytes had no detectable Tau protein, a neuronal cell line, SH-SY5Y, known to express high levels of Tau was chosen to model the effects of Tau deletion. Tau's canonical role is to bind tubulin to facilitate the assembly and stabilisation of microtubule structure (Weingarten et al., 1975) (Alonso et al., 1994a) (Alonso et al., 2018a). However, several lines of evidence suggested an association with oxidative stress. In mice, KO of the *Mapt* gene enhanced both basal and hyperthermia-induced oxidative stress (Violet et al., 2014). Moreover, an antioxidant response element within intron 1 of the MAPT gene has been reported to interact with NRF2, and while oxidative stress induced by hyperoxia increased *Mapt* expression, this effect was lost in *Nrf2* KO mice (Wang et al., 2016a). Taken together, these reports suggest a possible role for Tau in oxidative stress response in mice.

Mapt has also been implicated in DKD: *Mapt* KO mice may have reduced creatinine clearance compared to WT mice and have disrupted glomerular microtubules (Valles-Saiz et al., 2022). In biopsies of DKD patients, there is a decrease in *MAPT* expression in the tubulointerstitium. Given these findings, and the finding in Chapter 3 that *MAPT* expression increased in human podocytes *in vitro* under oxidative stress, I investigated the effect of knocking out the *MAPT* gene on basal and induced oxidative stress.

In the *MAPT* KO mice targeting exon 1 singularly appeared to be an effective strategy in eliminating Tau expression *in* vivo (Sud et al., 2014b). However, in the SH-SY5Y neuroblastoma cells, an existing cell line with an exon 1 indel generated a truncated protein whose function, at least in terms of tubulin polymerisation and redox homeostasis, was equivalent to WT cells. An explanation for this may lie in the gene editing methods adopted: in the mice, a replacement-type or ends-out targeting vector containing a PGK-neo cassette in the same transcriptional orientation as the Tau gene and a PGK-tk cassette on the upstream side of the construct was employed such that exon 1 was substituted for by the PGK-neo cassette leaving the rest of the gene intact but not translated (Gong and Golic, 2003). In contrast, CRISPR-CAS9 was used to edit the 232P cells. Increasingly, mRNA dysregulation, chromosome instability and exon skipping have been highlighted as limitations of the CRISPR-CAS9 (Tuladhar et al., 2019) (Rayner et al., 2019). The skipping of exons has been previously reported in a case where multiple oligonucleotides were used to reduce *MAPT* mRNA expression and Tau protein levels (Sud et al., 2014b).

In 232P cells, it appears that by targeting exon 1 singularly, the resulting indel led to the exclusion of this exon but the generation of a truncated protein. Hence, an N-terminal antibody with an epitope within exon 1 did not detect Tau in the 232P cells whereas a C-

terminal antibody did. It is possible that a different exon 1 edit could have a more effective outcome, for example by inducing frameshift and nonsense mediated decay. However. identifying suitable guides can be challenging.

Mapt KO mice generated by targeting exon 1 have no detectable Tau using several antibodies including Tau 12 and Tau 46 (Harada et al., 1994a) (Petry et al., 2014) (Dawson et al., 2001). In principle, cells could be isolated from these mice and primary cells cultured for further analysis. However, murine models do not always recapitulate human disease physiology, and the *Mapt* KO mice do not exhibit an overt neuronal phenotype, with subtle defects only with ageing in certain strains and no convincing evidence for renal impairment.

To circumvent this limitation, a dual guide CRISPR/Cas9 approach was used targeting exons 1 and 4a simultaneously to generate a new full KO of the MAPT gene in human SH-SY5Y cells. In this way, the anticipated outcome is a deletion between the two PAM sites (Canver et al., 2014). Because the SH-SY5Y cells were shown to be triploid for *MAPT* expression (Figure 4.3), a deletion on all three alleles was unlikely but the prospect of a combination of edits resulting in the inhibition of Tau expression was expected to be enhanced by this approach. Deletion of a large region can, however, increase the risk of unwanted off target edits (Chen et al., 2014). To screen for this a global assessment was performed using long range whole genome sequencing, designed so that over half of all data are in reads greater than 20 kb, to detect large deletions (Rhoads and Au, 2015). The Pacbio sequencing analysis confirmed the results of the gene editing observed using Sanger sequencing. This analysis did not detect any homozygous edits in coding genes, but did identify one probable heterozygous off-target edit in the *ADAM29* gene. ADAM29 belongs to a family of membrane-anchored glycoproteins that mediate cell matrix interactions with no known link to oxidative stress

response (Edwards et al., 2009, Chen and Wang, 2018). Overall the long-range sequencing findings gave confidence in the specificity of the CRISPR editing.

The approach of using dual guides to target *MAPT* provides a large deletion between the two guides, but also resulted in alleles without a large deletion. These smaller edits still appeared to have disrupted Tau expression, as evidenced by western blot for both C and N terminal Tau. Alongside a decrease in polymerised tubulin, the absence of Tau increased both basal and induced oxidative stress in the neuroblastoma cell line (Figure 4.9). Consistent with this the NRF2-KEAP1 pathway was activated in the KOs, with many of the proteins upregulated in the KO cells also increased in WT SH-SY5Y cells treated with tBHP.

Several Tau antibodies exist, targeting different Tau domains or to detect Tau proteins with specific post-translational modifications including phosphorylation (Flores-Rodríguez et al., 2015) (McHugh et al., 2015). Tau 12 and Tau 46 are specific antibodies targeting the proximal part of the N-terminal domain and the most distal segment of the C-terminal domain, respectively (Flores-Rodríguez et al., 2015). Hence, they were used as confirmatory antibodies for Tau expression. However, the Tau 46 antibody also cross-reacts with MAP2 (Kosik et al., 1988a) (Boban et al., 2019b), due to shared sequences between MAP2 and Tau within their most carboxy terminals at the Tau 46 binding site (Kosik et al., 1988a). In mice, deletion of Tau is compensated by increased expression of other MAP proteins including MAP2 (Harada et al., 1994) ((Ma et al., 2014). The WT SH-SY5Y lysate had two distinct bands, the smaller of which disappeared in the 232P cell lysate. However, no signal was detected with Tau 46 antibody in the immortalised podocytes, either for the Tau band or the upper band thought to correspond to MAP2 (Figure 4.2B). Neither band was detectable in the $MAPT^{-/-A2}$ and $MAPT^{-/-A4}$ lysates, and since the guide RNAs used here do not target

sequences in MAP2, the possibility remains that the persistent 232P band with Tau 46 is Tau specific, which could explain the 232P cell's phenotypic similarity with WT SH-SY5Y cells.

The phenotypes observed in the absence of Tau were restored with exogenous Tau expression, confirming a Tau-specific effect. Thus, this work provides strong evidence that Tau is required in redox homeostasis in SH-SY5Y neuroblastoma cells.

6.3.2 Interpretation of effect of modulation of tubulin polymerisation on the *MAPT* deletion oxidative stress phenotype

Based on the differentially expressed proteins within the MAPT$^{-/-A2}$ and MAPT$^{-/-A4}$ clones, some observations can be made about the impact of loss on Tau on the SH-SY5Y neuroblastoma cells. Firstly, loss of Tau changes the expression of proteins involved in maintaining the microtubule, cytoskeleton and tubulin interaction. This association, together with the decrease in polymerised tubulin in MAPT$^{-/-A2}$ and MAPT$^{-/-A4}$ clones suggests microtubule disruption as a candidate instigator for redox imbalance.

Oxidative stress has a negative effect on microtubule integrity and tubulin structure (Goldblum et al., 2021) (Lee et al., 2005) (Drum et al., 2016) (Valen et al., 1999). Microtubule and tubulin interacting proteins such as KIF1A, TUBA1A and MAP1B were dysregulated in the *MAPT*$^{-/-}$ clones compared to WT, and polymerised tubulin decreased in the absence of Tau, consistent with the idea that loss of Tau could drive redox imbalance via a dysfunctional microtubular system. The overexpressed Tau used to rescue, Tau-441, contains all four microtubule binding exons, and in our model restores tubulin polymerisation to levels comparable to the WT. However, demonstrating targeting microtubule function to

test this idea is challenging, because the agents available have broad-ranging or poorly understood mechanisms of action.

When Paclitaxel, a known microtubule-stabilising drug, was added to the KO cells, this restored tubulin polymerisation, but the oxidative stress phenotype persisted. This could suggest that Tau's involvement in oxidative stress may be independent of its function in tubulin polymerisation. However, non-specific cell toxicity due to Paclitaxel cannot be excluded. Paclitaxel's potency is not limited to the polymerisation of tubulin, it belongs to a family of drugs which include colchicine, nocodazole and rotenone, all of which are fundamentally cytoskeletal drugs (Dutta et al., 2022). They do, however, have other biological roles related to oxidative stress induction. For instance, rotenone enhances the formation of reactive oxygen species through its strong inhibition of the mitochondrial respiratory chain's complex I (Palmer et al., 1968) (Heinz et al., 2017). Similarly, Paclitaxel increases oxidative stress and apoptosis by increasing the activation of JNK and p38 (Meshkini and Yazdanparast, 2012) (Faridi et al., 2017) (Zhao et al., 2019, Ramanathan et al., 2005). Priming cells with antioxidants that do not act on tubulin polymerisation decreases the effect Paclitaxel has on redox disruption (Ramanathan et al., 2005) (Faridi et al., 2017). Thus, the observed oxidative stress with Paclitaxel could be downstream of increased tubulin polymerisation or occur independently. The present data could therefore suggest that the loss of Tau may be make the cells more vulnerable to Paclitaxel-induced oxidative stress, rather than addressing the question of tubulin function in the Tau antioxidant pathway.

The stress response with loss of Tau was only partly rescued by upregulation of NRF2, and so the mechanism by which Tau acts as an antioxidant remains to be answered. A further observation from the Tau deletion proteomics is altered expression of RNA-binding proteins,

stress granule formation and tight junctional proteins with loss of Tau, but these signatures are also features of increased oxidative stress. Hence, further experimental work will be required to delineate the mechanism by which Tau modulates the oxidative stress response.

While Tau's canonical role is to bind tubulin, to facilitate the assembly and stabilisation of microtubule structure, increasingly other Tau functions are recognised (Weingarten et al., 1975) (Alonso et al., 1994a, Alonso et al., 2018a). For instance, there is evidence from *in vitro* models to show a decrease in protein synthesis and ribosomal biogenesis mediated by the N-terminal domain of the human Tau protein (Evans et al., 2021).

With oxidative stress implicated in cancer, diabetes, and Alzheimer's disease, an antioxidant role for Tau could be relevant for our understanding of the pathobiology of Tauopathies and other chronic diseases.

In the $MAPT^{-/-A2}$ and $MAPT^{-/-A4}$ clones, the increase in carbonylated protein under normal culture conditions suggests that the cells are in redox imbalance even without exogenous oxidative stressors. In this context, the proteomics highlights decreased expression in the predominantly RNA-binding proteins PHIP, CCAR1, SRRT, PCBP2, PRPF4 and EIF3A in the $MAPT^{-/-A2}$ and $MAPT^{-/-A4}$ cells compared to WT, with all these genes increasing in expression with overexpression of Tau in SH-SY5Y cells (Montalbano et al., 2021). Tau binds to DNA with residues in the proline-rich and the microtubule-binding domains (Wei et al., 2008). In the Tau 441, Tau1-255 and Tau256-441 isoforms the RNA-interacting region is located at the N-terminus, in proline-rich domains between residues 1 and 255 (Geeth Gunawardana et al., 2015). Based on this the 232P cells lacking just the exon 1 might interact similarly to the WT with nucleic acids, while the $MAPT^{-/-A2}$ and $MAPT^{-/-A4}$ would have lost this function. If RNA-binding proteins are important in redox homeostasis this could explain

the differences observed in the MAPT$^{-/-A2}$ and MAPT$^{-/-A4}$ cells in comparison to either the WT or the 232P cells. However, since in the WT SH-SY5Y cells oxidative stress induction in the presence of Tau is also accompanied by a disruption in the RNA-binding proteins, the RNA binding signature may simply reflect non-specific effects of increased oxidative stress.

While treatment of SH-SY5Y cells with tBHP has been previously reported, this is the first time the global proteome has been assessed in this cell line (Drummond et al., 2017) (Cai et al., 2016). The finding of RNA-binding modulation with stress could be linked to dysfunction in organelles which have a unique composition of mRNA and RNA-binding proteins (Decker and Parker, 2012) (Hubstenberger et al., 2017) (Stroberg and Schnell, 2017, West et al., 2016).

The formation of non-membranous organelles such as processing-bodies, paraspeckles and stress granules is observed in neurodegenerative diseases such as amyotrophic lateral sclerosis (ALS), Creutzfeldt-Jakob disease, frontotemporal lobar degeneration and Alzheimer's disease (Harley et al., 2021) (Vanderweyde et al., 2012) (Liu-Yesucevitz et al., 2010). This may act as a countermeasure to cellular stress through the generation of translationally repressed mRNAs, proteins related to mRNA decay and the maintenance of proteins that protect against oxidative stress such as heat shock proteins (Stroberg and Schnell, 2017) (Vanderweyde et al., 2012) (Gilks et al., 2004, Chernov et al., 2009).

As is the case for podocytes, the WT SH-SY5Y cells upregulate expression of proteins related to stress granule formation in response to tBHP treatment, likely as an attempt to protect against oxidative injury. For example, the cytotoxic granule associated RNA-binding protein TIA1, with its Prion-like aggregation domain, together with PABPC1, which

promotes the stability and translation of polyadenylated mRNAs, are upregulated in the WT cells treated with tBHP compared to untreated WT (Gilks et al., 2004) (Kedersha et al., 1999). Tau has also been proposed to regulate the expression of TIA1. In brain tissues from mouse Tau KOs, the TAI interactome is disrupted and key RNA-binding proteins such as EWSR1, SNRNP70 and RPL7 are dysregulated in comparison to the WT (Vanderweyde et al., 2016). In addition, overexpression of TIA1 potentiates the increased levels of Tau phosphorylation seen with Tau overexpression on exposure to arsenite to induce oxidative stress (Vanderweyde et al., 2012). Conversely, TIA1 inhibition decreases the accumulation of Tau oligomers, suggesting a bi-directional relationship between the proteins (Apicco et al., 2018).

Neither the KO cells treated with tBHP nor their vehicle controls show increases in expression of stress granule-related proteins compared to WT cells. However, the EIF3A protein, required for the assembly of stress granules in the human cell line U2OS (Ohn et al., 2008) , is downregulated in the $MAPT^{-/-A2}$ and $MAPT^{-/-A4}$ KO cell lines with or without tBHP (Vanderweyde et al., 2012) which could be consistent with a putative defect in stress granule formation mechanisms in the absence of Tau. In summary, it is possible Tau mediates an antioxidant protective effect by promoting stress granule formation, perhaps via alterations in RNA-binding proteins.

The finding that in human neuronal cells *in vitro*, Tau has a role in the oxidative injury response, is important given the central role of oxidative injury in many disease pathologies, including DKD, and the importance of Tau in neurodegenerative disease. In tauopathies such as Alzheimer's disease, redox imbalance occurs alongside the hyperphosphorylation of Tau into neurofibrillary tangles and the formation of amyloid-beta-containing plaques: patients

show increased expression of oxidative stress markers including oxidised and nitrous advanced glycation elements, and the peroxidised lipid surrogate isoprostane 8,12-iso-iP$F_{2\alpha}$-VI in cerebrospinal fluids relative to healthy individuals (Batkulwar et al., 2018) (Pratico et al., 2000b).

Murine experiments support a link between these arms of disease pathophysiology: in mice whose amyloid beta and Tau proteins had been modified to reflect both frontotemporal dementia and Alzheimer's disease, deviations from redox homeostasis occurred with alterations in the oxidative phosphorylation system (Rhein et al., 2009a). However, the relationship between Tau and oxidative response remains poorly understood. For example, it is not known whether the resulting redox imbalance is the outcome of a gain-of-function by hyperphosphorylated Tau or the loss of physiological Tau function. Future experiments to measure oxidative stress in neuronal cell lines with mutated or hyperphosphorylated Tau could address these questions. Additionally, experiments in other cell lines, in primary cells or in more complex multicellular models such as organoids will be required to understand if the findings extrapolate to other tissues and to the *in vivo* setting, particularly in the context of DKD.

6.4 Exploring oxidative stress and Tau expression in kidney organoids

In Chapter 5, I developed tools that can be used to ask if Tau has a role in oxidative stress response in a kidney organoid. Kidney organoids should reflect the complexity of the kidney, expressing important markers of the both glomerular and tubular cell types. Achieving this was challenging due to the sensitivity of the protocol to batch number of reagents, type of membrane and number of organoids per membrane. Protocols were developed in collaboration with the Lennon Lab, Wellcome Centre for Matrix Biology,

University of Manchester, based on the method described by Takasato et al (Takasato et al., 2015). One challenge was identifying the right conditions under which differentiation into specific kidney tissues or cells was enhanced. Depending on the duration and dosage of FGF9 or CHIR99021, the cellular landscape of the kidney organoid could vary (Wu et al., 2018) (Takasato et al., 2015). This raises potential issues of experimental variability and limits the potential to scale up organoid experiments.

Even when successfully differentiated, kidney organoids are comparable to foetal kidneys within the first or second trimester of development, (Khoshdel-Rad et al., 2022, Takasato et al., 2015, Wu et al., 2018), and, therefore, cannot fully recapitulate the environment of adult chronic kidney disease such as DKD. Nevertheless, organoids provide an opportunity to test oxidative stress in a multi-cellular renal context, amenable to genetic modification. This is useful for exploration of Tau agnostic to which renal cell types are most important.

Recently, new approaches have been proposed to increase the cellular complexity of kidney organoids. These include co-culturing the organoids with other cell lines or altering the environmental cues within which the organoids grow to promote maturity. For instance, by growing hiPSCs to a monolayer followed by a three-dimensional microenvironment and applying defined renal inductive signals including CHIR 99021, FGF9a and activin A, organoids reflective of the second-trimester of human foetal kidneys with a more complex structure were generated (Garreta et al., 2019). Alternatively, using a combination of fluidic shear stress and coculture with human endothelial cells, vascularisation of kidney organoids and maturity of tubular epithelia has been described (Homan et al., 2019).

These advances suggest possible strategies for future work to establish a more complex and biologically relevant organoid system with which to address the effect of genetic changes, including loss of Tau, on responses to oxidative stress.

The organoid protocol established in Chapter 5, nevertheless, appears sufficient for the next steps for this project, to differentiate *MAPT* KO hiPSCs into kidney organoids and test whether this modulates the oxidative stress response. One important test is to confirm that the Tau is deleted in the KO hiPSCs, Since Tau protein expression is not detectable in the iPSCs this can be confirmed at the protein level only after differentiation, as shown in Chapter 5 in neuronal cells. WT kidney organoids express Tau but further work is needed to explore cellular localisation. In future work the KO organoids can be assessed for Tau expression, to confirm renal organoid deletion, and for their expression of key kidney markers including nephrin, e-cadherin and GATA-3, and assessed for any Tau-dependent effects on structure and morphology under standard culture conditions.

WT and *MAPT* KO kidney organoids could be treated with tBHP at the tested concentration of 200 nM for 24 hours, to interrogate the effect of the oxidative stress induction on the structure and viability of the organoids with and without Tau protein. As with the SH-SY5Y cells, Tau protein could be reintroduced into hiPSCs to determine if this would rescue the phenotype observed with the loss of Tau protein expression.

A global assessment of transcriptomic and protein expression with and without Tau protein in response to tBHP-dependent oxidative stress in organoids would be instructive in identifying pathways and proteins critical to oxidative stress response pathway in the kidney, and highlight possible mechanisms by which Tau might affect these responses. This could include

use of scRNA-seq and recently-developed spatial transcriptomic and proteomic approaches, with the goal of identifying genes, proteins and pathways of importance in human DKD.

Overall, the results from this work highlight new candidate NRF2-regulated proteins within the podocyte oxidative stress response that could be therapeutic targets relevant to DKD, reveal a new role for Tau in the anti-oxidant response in neuronal cells *in vitro*, and initiate the development of further models to explore Tau and oxidative stress in a complex renal organoid system.

Appendix

The first step in developing the flow cytometric protocol was to assess if using the live/dead stain NIR zombie, I could segregate live podocytes from dead podocytes. For this, I treated 12-day differentiated podocytes with 100 μM tBHP for 24 hours or with water as a control. Cells from each condition were divided into two groups, one group was incubated with PBS as an unstained compensation control. The second group from each experimental condition was then pooled and stained with NIR zombie at 4°C before rinsing the cells with PBS as following the protocol described previously in the methods. The mixed population of conditions ensured that both dead and live cells were in the pool of cells being assessed for live/dead staining. The unstained compensation control and the NIR zombie cells were sorted and analysed with the gating parameters as shown below in Appendix 1.1.

Following multiple replicating results of Appendix 1.1, podocytes were treated with tBHP or water for control as previously described. After 24 hours, the cells from both conditions were stained as above for live/dead cell populations. Then, cells were for each experimental condition were either derivatised with DNP as described in the methods or incubated with 2M hydrochloric acid (no derivatisation). Cells were then incubated with anti-DNP antibody and FITC 488 secondary antibody (Method) before sorting. The compensation conditions were no staining, NIR Zombie only, DNP with FITC 488 and FITC 488 secondary antibody only. As shown in Appendix 1.2, in both tBHP treated and water treated cells, there are significantly low number of cells with oxidative stress as detectable by DNP derivatisation. Instead, derivatisation increases this ration significantly although in the tBHP treated cells, there are approximately twice as many cells in the DNP positive pool compared with those in the water treated cells.

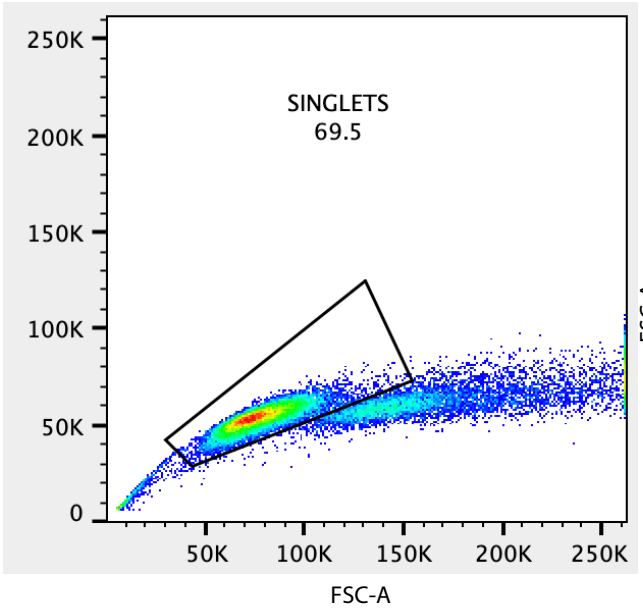
SINGLETS
69.5
FSC-H
FSC-A
250K
200K
150K
100K
50K
0
50K
100K
150K
200K
250K

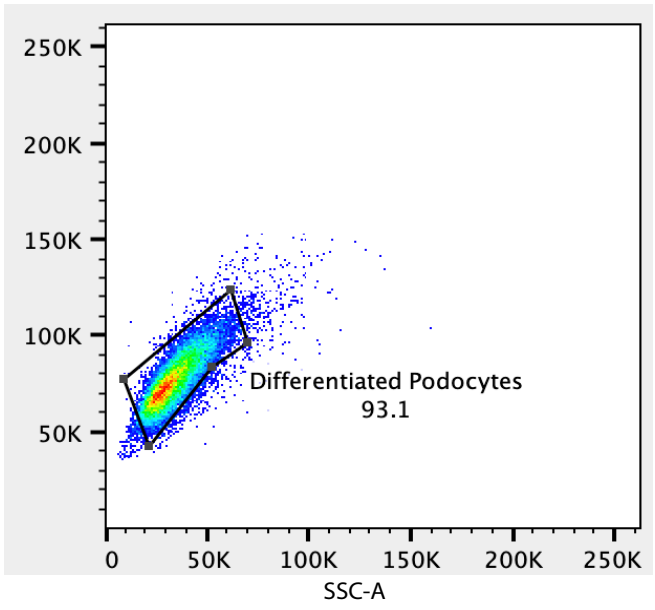
Differentiated Podocytes
93.1
FSC-A
SSC-A
250K
200K
150K
100K
50K
0
50K
100K
150K
200K
250K

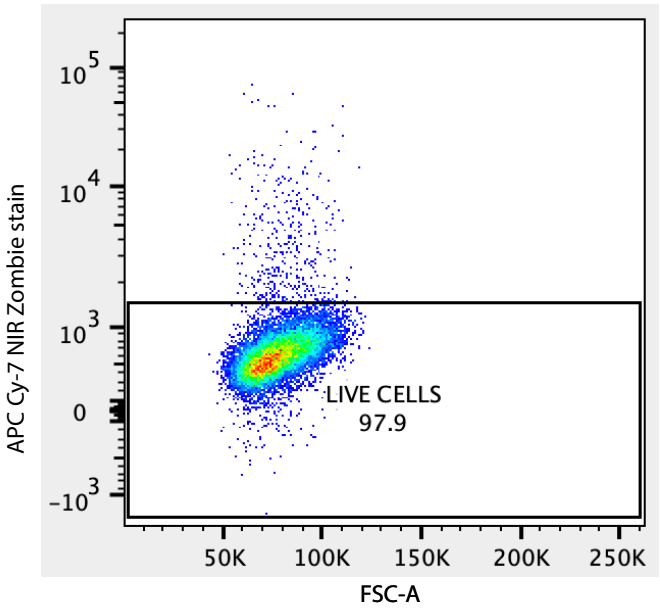
LIVE CELLS
97.9
APC Cy-7 NIR Zombie stain
FSC-A
10^5
10^4
10^3
0
-10^3
50K
100K
150K
200K
250K

Appendix 1.1 FACs gating strategy to identify live podocytes. Sorting gates to assess the podocyte cell size, granularity and viability to exclude debris and define singlets and live cells.

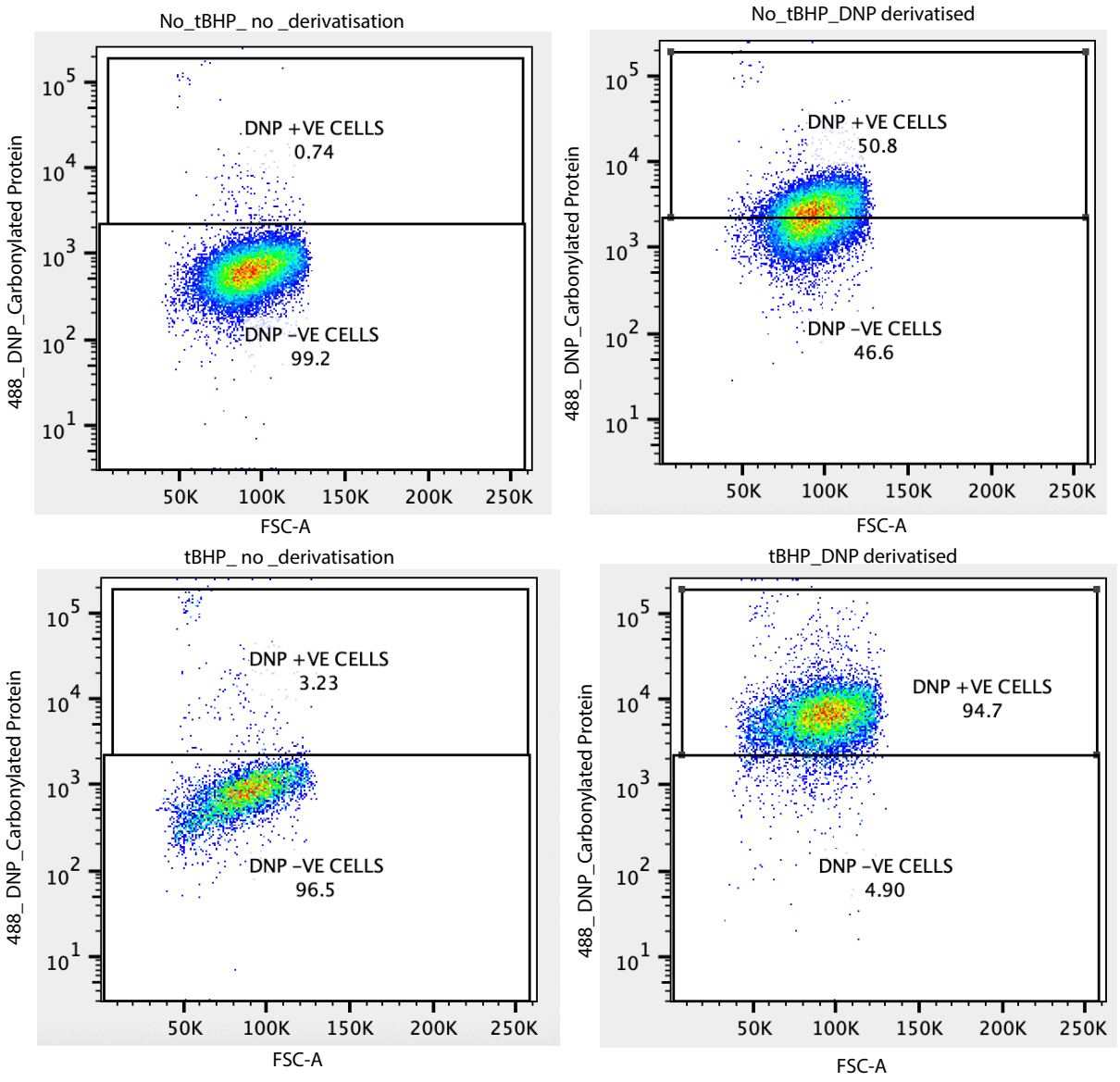

Appendix 1.2 FACs comparison of DNP derivatisation on podocytes treated with tBHP with those treated with water. Left panel represents underivatized cells either treated with tBHP or water. Right panel represents cells derivatised with DNP after either tBHP or water treatment. All cells were gated for singlets and live cell populations as shown previously in Appendix 1.1

Comparison of oxidative stress with increasing glucose in differentiated podocytes

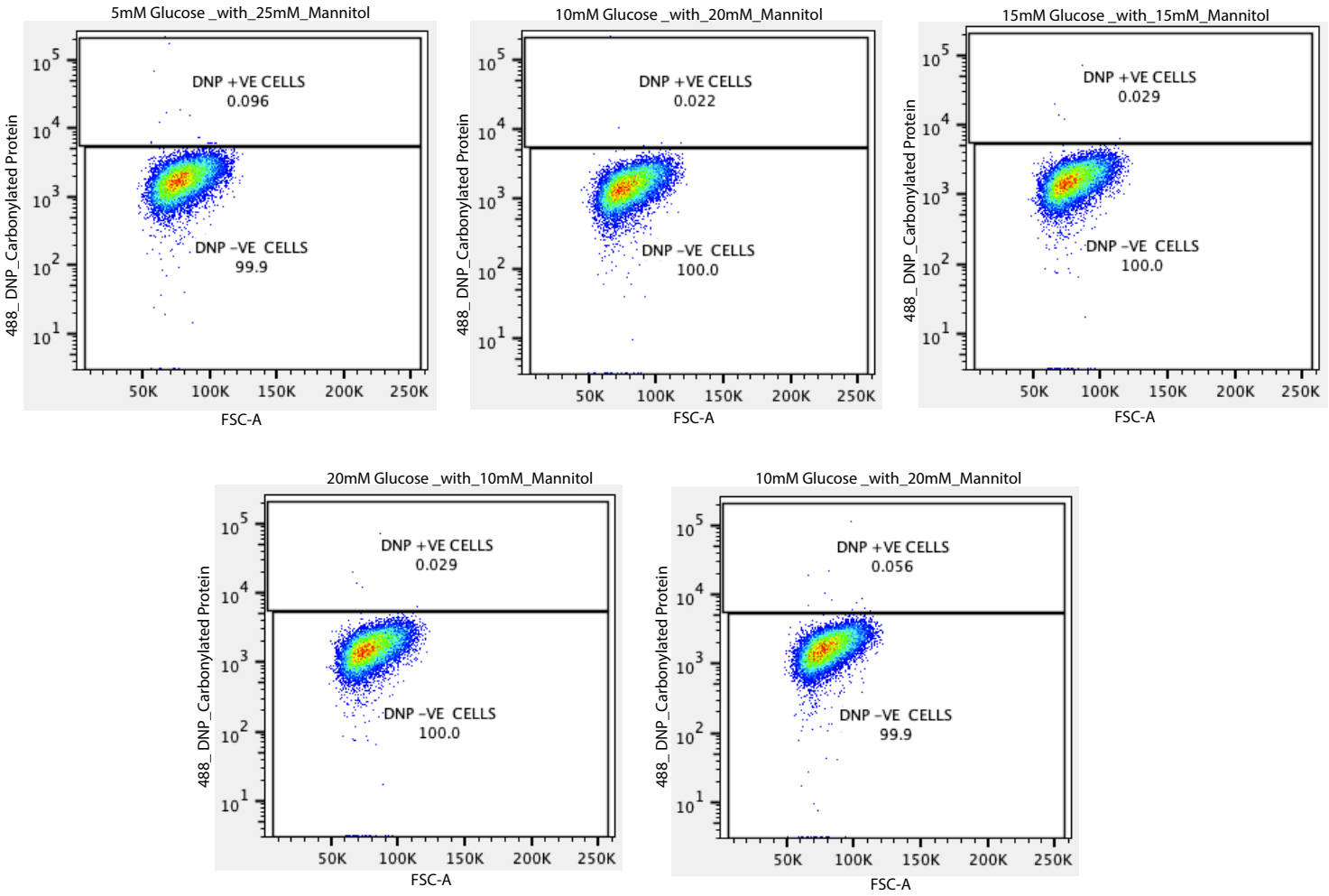

Appendix 1.3 FACs comparison of carbonylated protein in normoglycaemic (5 mM) with 25 mM mannitol podocytes against increasing concentrations of glucose.

Bibliography

1. ABDERRAZAK, A., SYROVETS, T., COUCHIE, D., EL HADRI, K., FRIGUET, B., SIMMET, T. & ROUIS, M. 2015. NLRP3 inflammasome: from a danger signal sensor to a regulatory node of oxidative stress and inflammatory diseases. Redox Biol, 4, 296-307.
2. ADEM, A., MATTSSON, M. E., NORDBERG, A. & PAHLMAN, S. 1987. Muscarinic receptors in human SH-SY5Y neuroblastoma cell line: regulation by phorbol ester and retinoic acid-induced differentiation. Brain Res, 430, 235-42.
3. AFKARIAN, M., SACHS, M. C., KESTENBAUM, B., HIRSCH, I. B., TUTTLE, K. R., HIMMELFARB, J. & DE BOER, I. H. 2013. Kidney disease and increased mortality risk in type 2 diabetes. J Am Soc Nephrol, 24, 302-8.
4. AHMED, S. M., LUO, L., NAMANI, A., WANG, X. J. & TANG, X. 2017. Nrf2 signaling pathway: Pivotal roles in inflammation. Biochim Biophys Acta Mol Basis Dis, 1863, 585-597.
5. ALONSO, A. C., ZAIDI, T., GRUNDKE-IQBAL, I. & IQBAL, K. 1994b. Role of abnormally phosphorylated tau in the breakdown of microtubules in Alzheimer disease. Proc Natl Acad Sci U S A, 91, 5562-6.
6. ALONSO, A. D., COHEN, L. S., CORBO, C., MOROZOVA, V., ELIDRISSI, A., PHILLIPS, G. & KLEIMAN, F. E. 2018b. Hyperphosphorylation of Tau Associates With Changes in Its Function Beyond Microtubule Stability. Front Cell Neurosci, 12, 338.
7. ALONSO, A., COHEN, L. S., CORBO, C., MOROZOVA, V., ELIDRISSI, A., PHILLIPS, G. & KLEIMAN, F. E. 2018a. Hyperphosphorylation of Tau Associates with changes in its function beyond microtubule stability. Frontiers in Cellular Neuroscience, 12.
8. ALONSO, A., ZAIDI, T., GRUNDKE-IQBAL, I. & IQBAL, K. 1994a. Role of abnormally phosphorylated tau in the breakdown of microtubules in Alzheimer disease (microtbule assembly/ associated proteins/cytoskeletal protein pathloy/dephosphorylation/paired hdeical flets). Proc. Nati. Acad. Sci. USA, 91, 5562-5566.
9. ALPERS, C. E. & HUDKINS, K. L. 2011. Mouse models of diabetic nephropathy. Curr Opin Nephrol Hypertens, 20, 278-84.
10. ALSAAD, K. O. & HERZENBERG, A. M. 2007. Distinguishing diabetic nephropathy from other causes of glomerulosclerosis: an update. J Clin Pathol, 60, 18-26.
11. ALTAVILLA, D., SAITTA, A., CUCINOTTA, D., GALEANO, M., DEODATO, B., COLONNA, M., TORRE, V., RUSSO, G., SARDELLA, A., URNA, G., CAMPO, G. M., CAVALLARI, V., SQUADRITO, G. & SQUADRITO, F. 2001. Inhibition of lipid peroxidation restores impaired vascular endothelial growth factor expression and stimulates wound healing and angiogenesis in the genetically diabetic mouse. Diabetes, 50, 667-74.
12. ANDERSON, J., LEE, H. A. & TOMLINSON, R. W. 1967. Some metabolic aspects of idiopathic hypercalciuria. Nephron, 4, 129-38.
13. ANDREWS, P. M. 1981. Investigations of cytoplasmic contractile and cytoskeletal elements in the kidney glomerulus. Kidney Int, 20, 549-62.
14. APICCO, D. J., ASH, P. E. A., MAZIUK, B., LEBLANG, C., MEDALLA, M., AL ABDULLATIF, A., FERRAGUD, A., BOTELHO, E., BALLANCE, H. I., DHAWAN, U., BOUDEAU, S., CRUZ, A. L., KASHY, D., WONG, A., GOLDBERG, L. R., YAZDANI, N., ZHANG, C., UNG, C. Y., TRIPODIS, Y., KANAAN, N. M., IKEZU, T., COTTONE, P., LESZYK, J., LI, H., LUEBKE, J., BRYANT, C. D. & WOLOZIN, B. 2018. Reducing the RNA binding protein TIA1 protects against tau-mediated neurodegeneration in vivo. Nature Neuroscience, 21, 72-82.
15. AWAD, A. S., KINSEY, G. R., KHUTSISHVILI, K., GAO, T., BOLTON, W. K. & OKUSA, M. D. 2011. Monocyte/macrophage chemokine receptor CCR2 mediates diabetic renal injury. Am J Physiol Renal Physiol, 301, F1358-66.

16. BACHMANN, S., BELL, M., KLIMEK, J. & ZEMPEL, H. 2021. Differential Effects of the Six Human TAU Isoforms: Somatic Retention of 2N-TAU and Increased Microtubule Number Induced by 4R-TAU. Front Neurosci, 15, 643115.
17. BAKRIS, G. L., AGARWAL, R., ANKER, S. D., PITT, B., RUILOPE, L. M., ROSSING, P., KOLKHOF, P., NOWACK, C., SCHLOEMER, P., JOSEPH, A., FILIPPATOS, G. & INVESTIGATORS, F.-D. 2020. Effect of Finerenone on Chronic Kidney Disease Outcomes in Type 2 Diabetes. N Engl J Med, 383, 2219-2229.
18. BALTA, E., HARDT, R., LIANG, J., KIRCHGESSNER, H., ORLIK, C., JAHRAUS, B., HILLMER, S., MEUER, S., HUBNER, K., WABNITZ, G. H. & SAMSTAG, Y. 2019. Spatial oxidation of L-plastin downmodulates actin-based functions of tumor cells. Nat Commun, 10, 4073.
19. BANDAY, A. A. & LOKHANDWALA, M. F. 2011. Oxidative stress causes renal angiotensin II type 1 receptor upregulation, Na+/H+ exchanger 3 overstimulation, and hypertension. Hypertension, 57, 452-9.
20. BARBIER, P., ZEJNELI, O., MARTINHO, M., LASORSA, A., BELLE, V., SMET-NOCCA, C., TSVETKOV, P. O., DEVRED, F. & LANDRIEU, I. 2019. Role of Tau as a Microtubule-Associated Protein: Structural and Functional Aspects. Front Aging Neurosci, 11, 204.
21. BARKER, D. J. 1990. The fetal and infant origins of adult disease. BMJ, 301, 1111.
22. BATKULWAR, K., GODBOLE, R., BANARJEE, R., KASSAAR, O., WILLIAMS, R. J. & KULKARNI, M. J. 2018. Advanced Glycation End Products Modulate Amyloidogenic APP Processing and Tau Phosphorylation: A Mechanistic Link between Glycation and the Development of Alzheimer's Disease. ACS Chemical Neuroscience, 9, 988-1000.
23. BEISSWENGER, P. J. & SPIRO, R. G. 1973. Studies on the Human Glomerular Basement Membrane: Composition, Nature of the Carbohydrate Units and Chemical Changes in Diabetes Mellitus. Diabetes, 22, 180-193.
24. BETTERIDGE, D. J. 2000. What Is Oxidative Stress?
25. BIEDLER, J. L., HELSON, L. & SPENGLER, B. A. 1973. Morphology and growth, turoigenicity and cytogenetics of human neuroblastoma cells in continuous culture. Cancer research, 33, 2643-2652.
26. BIEDLER, J. L., ROFFLER-TARLOV, S., SCHANCHNER, M. & FREEDMAN, L. S. 1978. Multipler neurotransmitter synthesis by human neuroblastoma cell lines and clones. Cancer research, 38, 3751-3757.
27. BOBAN, M., , BABIĆ LEKO, M., , MIŠKIĆ, T., , HOF, P. R., , ŠIMIĆ, G. & 2019a. Human neuroblastoma SH-SY5Y cells treated with okadaic acid express phosphorylated high molecular weight tau-immunoreactive protein species. Elsevier B.V.
28. BOBAN, M., BABIC LEKO, M., MISKIC, T., HOF, P. R. & SIMIC, G. 2019b. Human neuroblastoma SH-SY5Y cells treated with okadaic acid express phosphorylated high molecular weight tau-immunoreactive protein species. J Neurosci Methods, 319, 60-68.
29. BOHRER, M. P., BAYLIS, C., HUMES, H. D., GLASSOCK, R. J., ROBERTSON, C. R. & BRENNER, B. M. 1978. Permselectivity of the glomerular capillary wall. Facilitated filtration of circulating polycations. J Clin Invest, 61, 72-8.
30. BOUTE, N., GRIBOUVAL, O., ROSELLI, S., BENESSY, F., LEE, H., FUCHSHUBER, A., DAHAN, K., GUBLER, M.-C., NIAUDET, P. & ANTIGNAC, C. 2000. NPHS2, encoding the glomerular protein podocin, is mutated in autosomal recessive steroid-resistant nephrotic syndrome. Nature Genetics, 24, 349-354.
31. BOVERIS, A., OSHINO, N. & CHANCE, B. 1972. The Cellular Production of Hydrogen Peroxide. Biochem. J.
32. BRAMBLETT, G. T., GOEDERT, M., JAKES, R., MERRICK, S. E., TROJANOWSKI, J. Q. & LEE, V. M. 1993. Abnormal tau phosphorylation at Ser396 in Alzheimer's disease

recapitulates development and contributes to reduced microtubule binding. Neuron, 10, 1089-99.
33. BRANCATI, F. L., WHELTON, P. K., RANDALL, B. L., NEATON, J. D., STAMLER, J. & KLAG, M. J. 1997. Risk of end-stage renal disease in diabetes mellitus: a prospective cohort study of men screened for MRFIT. Multiple Risk Factor Intervention Trial. JAMA, 278, 2069-74.
34. BRENNER, B. M., COOPER, M. E., DE ZEEUW, D., KEANE, W. F., MITCH, W. E., PARVING, H. H., REMUZZI, G., SNAPINN, S. M., ZHANG, Z., SHAHINFAR, S. & INVESTIGATORS, R. S. 2001. Effects of losartan on renal and cardiovascular outcomes in patients with type 2 diabetes and nephropathy. N Engl J Med, 345, 861-9.
35. BRILL, A., CHAUHAN, A. K., CANAULT, M., WALSH, M. T., BERGMEIER, W. & WAGNER, D. D. 2009. Oxidative stress activates ADAM17/TACE and induces its target receptor shedding in platelets in a p38-dependent fashion. Cardiovasc Res, 84, 137-44.
36. BROWNLEE, M. 2001. Biochemistry and molecular cell biology of diabetic complications. Nature, 414, 813-20.
37. BROWNLEE, M. 2005. The pathobiology of diabetic complications: a unifying mechanism. Diabetes, 54, 1615-25.
38. BULL, K. R., MASON, T., RIMMER, A. J., CROCKFORD, T. L., SILVER, K. L., BOURIEZ-JONES, T., HOUGH, T. A., CHAUDHRY, S., ROBERTS, I. S., GOODNOW, C. C. & CORNALL, R. J. 2014. Next-generation sequencing to dissect hereditary nephrotic syndrome in mice identifies a hypomorphic mutation in Lamb2 and models Pierson's syndrome. J Pathol, 233, 18-26.
39. BURKE, A. P., KOLODGIE, F. D., ZIESKE, A., FOWLER, D. R., WEBER, D. K., VARGHESE, P. J., FARB, A. & VIRMANI, R. 2004. Morphologic findings of coronary atherosclerotic plaques in diabetics: a postmortem study. Arterioscler Thromb Vasc Biol, 24, 1266-71.
40. CAI, L., WANG, L. F., PAN, J. P., MI, X. N., ZHANG, Z., GENG, H. J., WANG, J. H., HU, S. H., ZHANG, W., GAO, Q., WU, W. T. & LUO, H. M. 2016. Neuroprotective Effects of Methyl 3,4-Dihydroxybenzoate against TBHP-Induced Oxidative Damage in SH-SY5Y Cells. Molecules, 21.
41. CANVER, M. C., BAUER, D. E., DASS, A., YIEN, Y. Y., CHUNG, J., MASUDA, T., MAEDA, T., PAW, B. H. & ORKIN, S. H. 2014. Characterization of genomic deletion efficiency mediated by clustered regularly interspaced palindromic repeats (CRISPR)/cas9 nuclease system in mammalian cells. Journal of Biological Chemistry, 289, 21312-21324.
42. CARLIER, M. F. & PANTALONI, D. 1983. Taxol effect on tubulin polymerization and associated guanosine 5'-triphosphate hydrolysis. Biochemistry, 22, 4814-22.
43. CARMINES, P. K., OHISHI, K. & IKENAGA, H. 1996. Functional impairment of renal afferent arteriolar voltage-gated calcium channels in rats with diabetes mellitus. The Journal of clinical investigation, 98, 2564-71.
44. CASTELLANI, R., SMITH, M. A., RICHEY, P. L., KALARIA, R., GAMBETTI, P. & PERRY, G. 1995. Evidence for oxidative stress in Pick disease and corticobasal degeneration. Brain Res, 696, 268-71.
45. CERIELLO, A. & MOTZ, E. 2004. Is oxidative stress the pathogenic mechanism underlying insulin resistance, diabetes, and cardiovascular disease? The common soil hypothesis revisited. Arterioscler Thromb Vasc Biol, 24, 816-23.
46. CERIELLO, A., MOROCUTTI, A., MERCURI, F., QUAGLIARO, L., MORO, M., DAMANTE, G. & VIBERTI, G. C. 2000. Defective intracellular antioxidant enzyme production in type 1 diabetic patients with nephropathy. Diabetes, 49, 2170-7.
47. CHANG, J. H. & GURLEY, S. B. 2012. Assessment of diabetic nephropathy in the Akita mouse. Methods Mol Biol, 933, 17-29.

48. CHANG, R. L., UEKI, I. F., TROY, J. L., DEEN, W. M., ROBERTSON, C. R. & BRENNER, B. M. 1975. Permselectivity of the glomerular capillary wall to macromolecules. II. Experimental studies in rats using neutral dextran. Biophysical Journal, 15, 887-906.
49. CHEN, E. Y., TAN, C. M., KOU, Y., DUAN, Q., WANG, Z., MEIRELLES, G. V., CLARK, N. R. & MA'AYAN, A. 2013a. Enrichr: interactive and collaborative HTML5 gene list enrichment analysis tool. BMC Bioinformatics, 14, 128.
50. CHEN, E. Y., TAN, C. M., KOU, Y., DUAN, Q., WANG, Z., MEIRELLES, G. V., CLARK, N. R. & MA'AYAN, A. 2013b. Enrichr: interactive and collaborative HTML5 gene list enrichment analysis tool. BMC bioinformatics, 14, 128-128.
51. CHEN, H. & WANG, S. 2018. Clinical significance of adam29 promoting the invasion and growth of gastric cancer cells in vitro. Oncology Letters, 16, 1483-1490.
52. CHEN, J., LI, G., LIU, X., CHEN, K., WANG, Y., QIN, J. & YANG, F. 2023. Delivery of miR-130a-3p Through Adipose-Derived Stem Cell-Secreted EVs Protects Against Diabetic Peripheral Neuropathy via DNMT1/NRF2/HIF1alpha/ACTA1 Axis. Mol Neurobiol, 60, 3678-3694.
53. CHEN, X., XU, F., ZHU, C., JI, J., ZHOU, X., FENG, X. & GUANG, S. 2014. Dual sgRNA-directed gene knockout using CRISPR/Cas9 technology in Caenorhabditis elegans. Scientific Reports, 4.
54. CHERNEY, D. Z. I., MILLER, J. A., SCHOLEY, J. W., BRADLEY, T. J., SLORACH, C., CURTIS, J. R., DEKKER, M. G., NASRALLAH, R., HÉBERT, R. L. & SOCHETT, E. B. 2008. The effect of cyclooxygenase-2 inhibition on renal hemodynamic function in humans with type 1 diabetes. Diabetes, 57, 688-695.
55. CHERNEY, D. Z. I., PERKINS, B. A., SOLEYMANLOU, N., MAIONE, M., LAI, V., LEE, A., FAGAN, N. M., WOERLE, H. J., JOHANSEN, O. E., BROEDL, U. C. & VON EYNATTEN, M. 2014. Renal hemodynamic effect of sodium-glucose cotransporter 2 inhibition in patients with type 1 diabetes mellitus. Circulation, 129, 587-597.
56. CHERNOV, K. G., BARBET, A., HAMON, L., OVCHINNIKOV, L. P., CURMI, P. A. & PASTRÉ, D. 2009. Role of microtubules in stress granule assembly: Microtubule dynamical instability favors the formation of micrometric stress granules in cells. Journal of Biological Chemistry, 284, 36569-36580.
57. CHIN, M. P., REISMAN, S. A., BAKRIS, G. L., O'GRADY, M., LINDE, P. G., MCCULLOUGH, P. A., PACKHAM, D., VAZIRI, N. D., WARD, K. W., WARNOCK, D. G. & MEYER, C. J. 2014. Mechanisms contributing to adverse cardiovascular events in patients with type 2 diabetes mellitus and stage 4 chronic kidney disease treated with bardoxolone methyl. Am J Nephrol, 39, 499-508.
58. CHOPRA, M., BESWICK, H., CLAPPERTON, M., DARGIE, H. J., SMITH, W. E. & MCMURRAY, J. 1992. Antioxidant effects of angiotensin-converting enzyme (ACE) inhibitors: free radical and oxidant scavenging are sulfhydryl dependent, but lipid peroxidation is inhibited by both sulfhydryl- and nonsulfhydryl-containing ACE inhibitors. J Cardiovasc Pharmacol, 19, 330-40.
59. CLAVAGUERA, F., BOLMONT, T., CROWTHER, R. A., ABRAMOWSKI, D., FRANK, S., PROBST, A., FRASER, G., STALDER, A. K., BEIBEL, M., STAUFENBIEL, M., JUCKER, M., GOEDERT, M. & TOLNAY, M. 2009. Transmission and spreading of tauopathy in transgenic mouse brain. Nat Cell Biol, 11, 909-13.
60. COLLABORATORS, G. B. D. D. 2023. Global, regional, and national burden of diabetes from 1990 to 2021, with projections of prevalence to 2050: a systematic analysis for the Global Burden of Disease Study 2021. Lancet, 402, 203-234.
61. COMBES, A. N., ZAPPIA, L., ER, P. X., OSHLACK, A. & LITTLE, M. H. 2019. Single-cell analysis reveals congruence between kidney organoids and human fetal kidney. Genome Med, 11, 3.

62. CONCORDET, J. P. & HAEUSSLER, M. 2018. CRISPOR: intuitive guide selection for CRISPR/Cas9 genome editing experiments and screens. Nucleic Acids Res, 46, W242-W245.
63. COWARD, R. J., WELSH, G. I., YANG, J., TASMAN, C., LENNON, R., KOZIELL, A., SATCHELL, S., HOLMAN, G. D., KERJASCHKI, D., TAVARE, J. M., MATHIESON, P. W. & SALEEM, M. A. 2005. The human glomerular podocyte is a novel target for insulin action. Diabetes, 54, 3095-102.
64. CUADRADO, A., ROJO, A. I., WELLS, G., HAYES, J. D., COUSIN, S. P., RUMSEY, W. L., ATTUCKS, O. C., FRANKLIN, S., LEVONEN, A. L., KENSLER, T. W. & DINKOVA-KOSTOVA, A. T. 2019. Therapeutic targeting of the NRF2 and KEAP1 partnership in chronic diseases. Nat Rev Drug Discov, 18, 295-317.
65. DAHLGREN, C. & KARLSSON, A. 1999. Respiratory burst in human neutrophils. Journal of Immunological Methods.
66. DALLE-DONNE, I., ROSSI, R., GIUSTARINI, D., MILZANI, A. & COLOMBO, R. 2003. Protein carbonyl groups as biomarkers of oxidative stress. Clinica Chimica Acta. Elsevier.
67. DANE, M. J. C., VAN DEN BERG, B. M., LEE, D. H., BOELS, M. G. S., TIEMEIER, G. L., AVRAMUT, M. C., VAN ZONNEVELD, A. J., VAN DER VLAG, J., VINK, H. & RABELINK, T. J. 2015. A microscopic view on the renal endothelial glycocalyx. American Journal of Physiology-Renal Physiology, 308, F956-F966.
68. DAVID, D. C., HAUPTMANN, S., SCHERPING, I., SCHUESSEL, K., KEIL, U., RIZZU, P., RAVID, R., DROSE, S., BRANDT, U., MULLER, W. E., ECKERT, A. & GOTZ, J. 2005. Proteomic and functional analyses reveal a mitochondrial dysfunction in P301L tau transgenic mice. J Biol Chem, 280, 23802-14.
69. DAVIES, M. J. 1989. Detection of peroxyl and alkoxyl radicals produced by reaction of hydroperoxides with rat liver microsomal fractions. Biochem J, 257, 603-6.
70. DAWSON, H., FERREIRA, A., EYSTER, V. M., GHOSHAL, N., BINDER, I. L. & VITEK, P. M. 2001. Inhibition of Neuronal Maturation in Primary Hippocampal Neurons from Tau Deficient Mice. Journal of Cell Science, 114, 1179-1187.
71. DE ZEEUW, D., AKIZAWA, T., AUDHYA, P., BAKRIS, G. L., CHIN, M., CHRIST-SCHMIDT, H., GOLDSBERRY, A., HOUSER, M., KRAUTH, M., LAMBERS HEERSPINK, H. J., MCMURRAY, J. J., MEYER, C. J., PARVING, H. H., REMUZZI, G., TOTO, R. D., VAZIRI, N. D., WANNER, C., WITTES, J., WROLSTAD, D., CHERTOW, G. M. & INVESTIGATORS, B. T. 2013. Bardoxolone methyl in type 2 diabetes and stage 4 chronic kidney disease. N Engl J Med, 369, 2492-503.
72. DECKER, C. J. & PARKER, R. 2012. P-bodies and stress granules: Possible roles in the control of translation and mRNA degradation. Cold Spring Harbor Perspectives in Biology, 4.
73. DELEO, F. R. & QUINN, M. T. 1996. Assembly of the phagocyte NADPH oxidase: Molecular interaction of oxidase proteins. Journal of Leukocyte Biology. Federation of American Societies for Experimental Biology.
74. DEWANGAN, N. 2023. Nephron- Definition, Structure, Physiology, Functions [Online]. Available: https://microbenotes.com/nephron-structure-functions/ [Accessed 15/01/2024 2024].
75. DIGBY, J. L. M., VANICHAPOL, T., PRZEPIORSKI, A., DAVIDSON, A. J. & SANDER, V. 2020. Evaluation of cisplatin-induced injury in human kidney organoids. Am J Physiol Renal Physiol, 318, F971-F978.
76. DING, T., CHEN, W., LI, J., DING, J., MEI, X. & HU, H. 2017. High Glucose Induces Mouse Mesangial Cell Overproliferation via Inhibition of Hydrogen Sulfide Synthesis in a TLR-4-Dependent Manner. Cell Physiol Biochem, 41, 1035-1043.

77. DOI, T., HATTORI, M., AGODOA, L. Y., SATO, T., YOSHIDA, H., STRIKER, L. J. & STRIKER, G. E. 1990. Glomerular lesions in nonobese diabetic mouse: before and after the onset of hyperglycemia. Lab Invest, 63, 204-12.
78. DOUBLIER, S., SALVIDIO, G., LUPIA, E., RUOTSALAINEN, V., VERZOLA, D., DEFERRARI, G. & CAMUSSI, G. 2003. Nephrin Expression Is Reduced in Human Diabetic Nephropathy. Diabetes, 52, 1023-1030.
79. DRUM, B. M. L., YUAN, C., LI, L., LIU, Q., WORDEMAN, L. & SANTANA, L. F. 2016. Oxidative stress decreases microtubule growth and stability in ventricular myocytes. Journal of Molecular and Cellular Cardiology, 93, 32-43.
80. DRUMMOND, N. J., DAVIES, N. O., LOVETT, J. E., MILLER, M. R., COOK, G., BECKER, T., BECKER, C. G., MCPHAIL, D. B. & KUNATH, T. 2017. A synthetic cell permeable antioxidant protects neurons against acute oxidative stress. Sci Rep, 7, 11857.
81. DU, C., WENG, X., HU, W., LV, Z., XIAO, H., DING, C., GYABAAH, O. A., XIE, H., ZHOU, L., WU, J. & ZHENG, S. 2015. Hypoxia-inducible MiR-182 promotes angiogenesis by targeting RASA1 in hepatocellular carcinoma. J Exp Clin Cancer Res, 34, 67.
82. DUANN, P. & LIN, P. H. 2017. Mitochondria Damage and Kidney Disease. Adv Exp Med Biol, 982, 529-551.
83. DUTTA, S., BOSE, D., GHOSH, S. & CHAKRABARTI, A. 2022. Spectrin: an alternate target for cytoskeletal drugs. Journal of Biomolecular Structure and Dynamics.
84. EDWARDS, D. R., HANDSLEY, M. M. & PENNINGTON, C. J. 2009. The ADAM metalloproteinases. Molecular Aspects of Medicine.
85. EID, A. A., GORIN, Y., FAGG, B. M., MAALOUF, R., BARNES, J. L., BLOCK, K. & ABBOUD, H. E. 2009. Mechanisms of podocyte injury in diabetes: role of cytochrome P450 and NADPH oxidases. Diabetes, 58, 1201-11.
86. ELBATREEK, M. H., PACHADO, M. P., CUADRADO, A., JANDELEIT-DAHM, K. & SCHMIDT, H. 2019. Reactive Oxygen Comes of Age: Mechanism-Based Therapy of Diabetic End-Organ Damage. Trends Endocrinol Metab, 30, 312-327.
87. ENGEL, A. L., LORENZ, N. I., KLANN, K., MUNCH, C., DEPNER, C., STEINBACH, J. P., RONELLENFITSCH, M. W. & LUGER, A. L. 2020. Serine-dependent redox homeostasis regulates glioblastoma cell survival. Br J Cancer, 122, 1391-1398.
88. EVANS, H. T., TAYLOR, D., KNEYNSBERG, A., BODEA, L. G. & GOTZ, J. 2021. Altered ribosomal function and protein synthesis caused by tau. Acta Neuropathol Commun, 9, 110.
89. FAN, A. C. & LEUNG, A. K. 2016. RNA Granules and Diseases: A Case Study of Stress Granules in ALS and FTLD. Adv Exp Med Biol, 907, 263-96.
90. FAN, Z., WIRTH, A. K., CHEN, D., WRUCK, C. J., RAUH, M., BUCHFELDER, M. & SAVASKAN, N. 2017. Nrf2-Keap1 pathway promotes cell proliferation and diminishes ferroptosis. Oncogenesis, 6, e371.
91. FARIDI, U., ALATAWI, F. & MOSTAFA, M. 2017. Protective role of tocopherol and ascorbic acid in taxol-treated human erythrocytes in vitro. Toxicology Research and Application, 1, 239784731770581-239784731770581.
92. FEDOROVA, M., BOLLINENI, R. C. & HOFFMANN, R. 2014. Protein carbonylation as a major hallmark of oxidative damage: update of analytical strategies. Mass Spectrom Rev, 33, 79-97.
93. FIORETTO, P. & MAUER, M. 2007. Histopathology of Diabetic Nephropathy. Seminars in Nephrology, 27, 195-207.
94. FIORETTO, P., STEFFES, M. W. & MAUER, M. 1994. Glomerular Structure in Nonproteinuric IDDM Patients With Various Levels of Albuminuria. DIABETES.
95. FLORES-RODRÍGUEZ, P., ONTIVEROS-TORRES, M. A., CÁRDENAS-AGUAYO, M. C., LUNA-ARIAS, J. P., MERAZ-RÍOS, M. A., VIRAMONTES-PINTOS, A.,

HARRINGTON, C. R., WISCHIK, C. M., MENA, R., FLORÁN-GARDUÑO, B. & LUNA-MUÑOZ, J. 2015. The relationship between truncation and phosphorylation at the C-terminus of tau protein in the paired helical filaments of Alzheimer's disease. Frontiers in Neuroscience, 9.
96. FLORIAN, J. A., KOSKY, J. R., AINSLIE, K., PANG, Z., DULL, R. O. & TARBELL, J. M. 2003. Heparan Sulfate Proteoglycan Is a Mechanosensor on Endothelial Cells. Circulation Research, 93.
97. FLYVBJERG, A., BENNETT, W. F., RASCH, R., KOPCHICK, J. J. & SCARLETT, J. A. 1999. Inhibitory Effect of a Growth Hormone Receptor Antagonist (G120K-PEG) on Renal Enlargement, Glomerular Hypertrophy, and Urinary Albumin Excretion in Experimental Diabetes in Mice. DIABETES.
98. FLYVBJERG, A., FRYSTYK, J., THORLACIUS-USSING, O. & □RSKOV, H. 1989. Somatostatin analogue administration prevents increase in kidney somatomedin C and initial renal growth in diabetic and uninephrectomized rats. Diabetologia, 32, 261-265.
99. FREEDMAN, B. S., BROOKS, C. R., LAM, A. Q., FU, H., MORIZANE, R., AGRAWAL, V., SAAD, A. F., LI, M. K., HUGHES, M. R., WERFF, R. V., PETERS, D. T., LU, J., BACCEI, A., SIEDLECKI, A. M., VALERIUS, M. T., MUSUNURU, K., MCNAGNY, K. M., STEINMAN, T. I., ZHOU, J., LEROU, P. H. & BONVENTRE, J. V. 2015. Modelling kidney disease with CRISPR-mutant kidney organoids derived from human pluripotent epiblast spheroids. Nat Commun, 6, 8715.
100. FUKAMI, K., YAMAGISHI, S., COUGHLAN, M. T., HARCOURT, B. E., KANTHARIDIS, P., THALLAS-BONKE, V., OKUDA, S., COOPER, M. E. & FORBES, J. M. 2014. Ramipril inhibits AGE-RAGE-induced matrix metalloproteinase-2 activation in experimental diabetic nephropathy. Diabetol Metab Syndr, 6, 86.
101. FUKUDA, A., MINAKAWA, A., KIKUCHI, M., SATO, Y., NAGATOMO, M., NAKAMURA, S., MIZOGUCHI, T., FUKUNAGA, N., SHIBATA, H., NAIK, A. S., WIGGINS, R. C. & FUJIMOTO, S. 2020. Urinary podocyte mRNAs precede microalbuminuria as a progression risk marker in human type 2 diabetic nephropathy. Sci Rep, 10, 18209.
102. GALICIA-GARCIA, U., BENITO-VICENTE, A., JEBARI, S., LARREA-SEBAL, A., SIDDIQI, H., URIBE, K. B., OSTOLAZA, H. & MARTIN, C. 2020. Pathophysiology of Type 2 Diabetes Mellitus. Int J Mol Sci, 21.
103. GAMA, R. M., KALYESUBULA, R., FABIAN, J. & MAHALINGASIVAM, V. 2021. NICE takes ethnicity out of estimating kidney function. BMJ, 374, n2159.
104. GARRETA, E., PRADO, P., STANIFER, M. L., MONTEIL, V., MARCO, A., ULLATE-AGOTE, A., MOYA-RULL, D., VILAS-ZORNOZA, A., TARANTINO, C., ROMERO, J. P., JONSSON, G., ORIA, R., LEOPOLDI, A., HAGELKRUYS, A., GALLO, M., GONZALEZ, F., DOMINGO-PEDROL, P., GAVALDA, A., DEL POZO, C. H., HASAN ALI, O., VENTURA-AGUIAR, P., CAMPISTOL, J. M., PROSPER, F., MIRAZIMI, A., BOULANT, S., PENNINGER, J. M. & MONTSERRAT, N. 2022. A diabetic milieu increases ACE2 expression and cellular susceptibility to SARS-CoV-2 infections in human kidney organoids and patient cells. Cell Metab, 34, 857-873 e9.
105. GARRETA, E., PRADO, P., TARANTINO, C., ORIA, R., FANLO, L., MARTI, E., ZALVIDEA, D., TREPAT, X., ROCA-CUSACHS, P., GAVALDA-NAVARRO, A., COZZUTO, L., CAMPISTOL, J. M., IZPISUA BELMONTE, J. C., HURTADO DEL POZO, C. & MONTSERRAT, N. 2019. Fine tuning the extracellular environment accelerates the derivation of kidney organoids from human pluripotent stem cells. Nat Mater, 18, 397-405.
106. GEETH GUNAWARDANA, C., MEHRABIAN, M., WANG, X., MUELLER, I., LUBAMBO, I. B., JONKMAN, J. E. N., WANG, H. & SCHMITT-ULMS, G. 2015. The

Human Tau Interactome: Binding to the Ribonucleoproteome, and Impaired Binding of the Proline-to-Leucine Mutant at Position 301 (P301L) to Chaperones and the Proteasome* □ S. Molecular and Cellular Proteomics, 14, 3000-3014.
107. GHEITH, O., FAROUK, N., NAMPOORY, N., HALIM, M. & AL-OTAIBI, T. 2016a. Diabetic kidney disease: world wide difference of prevalence and risk factors. Journal of Nephropharmacology J Nephropharmacol, 5, 49-56.
108. GHEITH, O., FAROUK, N., NAMPOORY, N., HALIM, M. A. & AL-OTAIBI, T. 2016b. Diabetic kidney disease: world wide difference of prevalence and risk factors. J Nephropharmacol, 5, 49-56.
109. GILKS, N., KEDERSHA, N., AYODELE, M., SHEN, L., STOECKLIN, G., DEMBER, L. & ANDERSON, P. 2004. Stress Granule Assembly is Mediated by Prion-like Aggregation of TIA-1. Molecular Biology of the Cell, 15, 5383-5398.
110. GOFFART, S., TIKKANEN, P., MICHELL, C., WILSON, T. & POHJOISMAKI, J. 2021. The Type and Source of Reactive Oxygen Species Influences the Outcome of Oxidative Stress in Cultured Cells. Cells, 10.
111. GOLDBLUM, R. R., MCCLELLAN, M., WHITE, K., GONZALEZ, S. J., THOMPSON, B. R., VANG, H. X., COHEN, H., HIGGINS, L. A., MARKOWSKI, T. W., YANG, T. Y., METZGER, J. M. & GARDNER, M. K. 2021. Oxidative stress pathogenically remodels the cardiac myocyte cytoskeleton via structural alterations to the microtubule lattice. Developmental Cell, 56, 2252-2266.e6.
112. GONG, W. J. & GOLIC, K. G. 2003. Ends-out, or replacement, gene targeting in Drosophila. PNAS March.
113. GRAY, S. P., DI MARCO, E., OKABE, J., SZYNDRALEWIEZ, C., HEITZ, F., MONTEZANO, A. C., DE HAAN, J. B., KOULIS, C., EL-OSTA, A., ANDREWS, K. L., CHIN-DUSTING, J. P., TOUYZ, R. M., WINGLER, K., COOPER, M. E., SCHMIDT, H. H. & JANDELEIT-DAHM, K. A. 2013. NADPH oxidase 1 plays a key role in diabetes mellitus-accelerated atherosclerosis. Circulation, 127, 1888-902.
114. GUIMARÃES, M. A. M., NIKOLOVSKI, J., PRATT, L. M., GREIVE, K. & COMPER, W. D. 2003. Anomalous fractional clearance of negatively charged Ficoll relative to uncharged Ficoll. American Journal of Physiology-Renal Physiology, 285, F1118-F1124.
115. GUO, Z. J., NIU, H. X., HOU, F. F., ZHANG, L., FU, N., NAGAI, R., LU, X., CHEN, B. H., SHAN, Y. X., TIAN, J. W., NAGARAJ, R. H., XIE, D. & ZHANG, X. 2008. Advanced oxidation protein products activate vascular endothelial cells via a RAGE-mediated signaling pathway. Antioxid Redox Signal, 10, 1699-712.
116. GUPTA, M., PANDEY, S., RUMMAN, M., SINGH, B. & MAHDI, A. A. 2023. Molecular mechanisms underlying hyperglycemia associated cognitive decline. IBRO Neuroscience Reports. Elsevier B.V.
117. GUZMAN, J., JAUREGUI, A. N., MERSCHER-GOMEZ, S., MAIGUEL, D., MURESAN, C., MITROFANOVA, A., DIEZ-SAMPEDRO, A., SZUST, J., YOO, T. H., VILLARREAL, R., PEDIGO, C., MOLANO, R. D., JOHNSON, K., KAHN, B., HARTLEBEN, B., HUBER, T. B., SAHA, J., BURKE, G. W., 3RD, ABEL, E. D., BROSIUS, F. C. & FORNONI, A. 2014. Podocyte-specific GLUT4-deficient mice have fewer and larger podocytes and are protected from diabetic nephropathy. Diabetes, 63, 701-14.
118. HARADA, A., OGUCHI, K., OKABE, S., KUNO, J., TERADA, S., OHSHIMA, T., SATO-YOSHITAKE, R., TAKEI, Y., NODA, T. & HIROKAWA, N. 1994a. Altered microtubule organization in small-calibre axons of mice lacking tau protein. Nature, 369.
119. HARADA, A., OGUCHI, K., OKABE, S., KUNO, J., TERADA, S., OHSHIMA, T., SATO-YOSHITAKE, R., TAKEI, Y., NODA, T. & HIROKAWA, N. 1994b. Altered

microtubule organization in small-calibre axons of mice lacking tau protein. Nature, 369, 488-91.
120. HARALDSSON, B., NYSTROM, J. & DEEN, W. M. 2008. Properties of the glomerular barrier and mechanisms of proteinuria. Physiol Rev, 88, 451-87.
121. HARJUTSALO, V. & GROOP, P. H. 2014. Epidemiology and risk factors for diabetic kidney disease. Advances in Chronic Kidney Disease. W.B. Saunders.
122. HARLEY, J., CLARKE, B. E. & PATANI, R. 2021. The interplay of rna binding proteins, oxidative stress and mitochondrial dysfunction in als. Antioxidants. MDPI.
123. HARVEY, J. N., EDMUNDSON, A. W., JAFFA, A. A., MARTIN, L. L. & MAYFIELD, R. K. 1992. Renal excretion of kallikrein and eicosanoids in patients with type 1 (insulin-dependent) diabetes mellitus. Relationship to glomerular and tubular function. Diabetologia, 35, 857-62.
124. HARVEY, S. J., JARAD, G., CUNNINGHAM, J., ROPS, A. L., VAN DER VLAG, J., BERDEN, J. H., MOELLER, M. J., HOLZMAN, L. B., BURGESS, R. W. & MINER, J. H. 2007. Disruption of Glomerular Basement Membrane Charge through Podocyte-Specific Mutation of Agrin Does Not Alter Glomerular Permselectivity. The American Journal of Pathology, 171, 139-152.
125. HAWKINS, C. L., MORGAN, P. E. & DAVIES, M. J. 2009. Quantification of protein modification by oxidants. Free Radical Biology and Medicine.
126. HE, B., CHEN, P., ZAMBRANO, S., DABAGHIE, D., HU, Y., MOLLER-HACKBARTH, K., UNNERSJO-JESS, D., KORKUT, G. G., CHARRIN, E., JEANSSON, M., BINTANEL-MORCILLO, M., WITASP, A., WENNBERG, L., WERNERSON, A., SCHERMER, B., BENZING, T., ERNFORS, P., BETSHOLTZ, C., LAL, M., SANDBERG, R. & PATRAKKA, J. 2021. Single-cell RNA sequencing reveals the mesangial identity and species diversity of glomerular cell transcriptomes. Nat Commun, 12, 2141.
127. HE, F. F., BAO, D., SU, H., WANG, Y. M., LEI, C. T., ZHANG, C. Y., YE, C., TANG, H., WAN, C., YOU, C. Q., ZHANG, J., XIONG, J. & ZHANG, C. 2018. IL-6 increases podocyte motility via MLC-mediated focal adhesion impairment and cytoskeleton disassembly. J Cell Physiol, 233, 7173-7181.
128. HE, Y., ZENG, M. Y., YANG, D., MOTRO, B. & NUNEZ, G. 2016. NEK7 is an essential mediator of NLRP3 activation downstream of potassium efflux. Nature, 530, 354-7.
129. HEINZ, S., FREYBERGER, A., LAWRENZ, B., SCHLADT, L., SCHMUCK, G. & ELLINGER-ZIEGELBAUER, H. 2017. Mechanistic Investigations of the Mitochondrial Complex i Inhibitor Rotenone in the Context of Pharmacological and Safety Evaluation. Scientific Reports, 7.
130. HERMAN-EDELSTEIN, M., THOMAS, M. C., THALLAS-BONKE, V., SALEEM, M., COOPER, M. E. & KANTHARIDIS, P. 2011. Dedifferentiation of immortalized human podocytes in response to transforming growth factor-β: A model for diabetic podocytopathy. Diabetes, 60, 1779-1788.
131. HERNANDEZ-VEGA, A., BRAUN, M., SCHARREL, L., JAHNEL, M., WEGMANN, S., HYMAN, B. T., ALBERTI, S., DIEZ, S. & HYMAN, A. A. 2017. Local Nucleation of Microtubule Bundles through Tubulin Concentration into a Condensed Tau Phase. Cell Rep, 20, 2304-2312.
132. HERRINGTON, W. G., ALEGRE-DIAZ, J., WADE, R., GNATIUC, L., RAMIREZ-REYES, R., HILL, M., SOLANO-SANCHEZ, M., BAIGENT, C., LEWINGTON, S., COLLINS, R., TAPIA-CONYER, R., PETO, R., KURI-MORALES, P. & EMBERSON, J. R. 2018. Effect of diabetes duration and glycaemic control on 14-year cause-specific mortality in Mexican adults: a blood-based prospective cohort study. Lancet Diabetes Endocrinol, 6, 455-463.

133. HIX, S., KADIISKA, M. B., MASON, R. P. & AUGUSTO, O. 2000. In vivo metabolism of tert-butyl hydroperoxide to methyl radicals. EPR spin-trapping and DNA methylation studies. Chem Res Toxicol, 13, 1056-64.
134. HOFER, M. & LUTOLF, M. P. 2021. Engineering organoids. Nat Rev Mater, 6, 402-420.
135. HOMAN, K. A., GUPTA, N., KROLL, K. T., KOLESKY, D. B., SKYLAR-SCOTT, M., MIYOSHI, T., MAU, D., VALERIUS, M. T., FERRANTE, T., BONVENTRE, J. V., LEWIS, J. A. & MORIZANE, R. 2019. Flow-enhanced vascularization and maturation of kidney organoids in vitro. Nat Methods, 16, 255-262.
136. HORLBECK, M. A., GILBERT, L. A., VILLALTA, J. E., ADAMSON, B., PAK, R. A., CHEN, Y., FIELDS, A. P., PARK, C. Y., CORN, J. E., KAMPMANN, M. & WEISSMAN, J. S. 2016. Compact and highly active next-generation libraries for CRISPR-mediated gene repression and activation. Elife, 5.
137. HUBSTENBERGER, A., COUREL, M., BÉNARD, M., SOUQUERE, S., ERNOULT-LANGE, M., CHOUAIB, R., YI, Z., MORLOT, J. B., MUNIER, A., FRADET, M., DAUNESSE, M., BERTRAND, E., PIERRON, G., MOZZICONACCI, J., KRESS, M. & WEIL, D. 2017. P-Body Purification Reveals the Condensation of Repressed mRNA Regulons. Molecular Cell, 68, 144-157.e5.
138. HUDKINS, K. L., PICHAIWONG, W., WIETECHA, T., KOWALEWSKA, J., BANAS, M. C., SPENCER, M. W., MUHLFELD, A., KOELLING, M., PIPPIN, J. W., SHANKLAND, S. J., ASKARI, B., RABAGLIA, M. E., KELLER, M. P., ATTIE, A. D. & ALPERS, C. E. 2010. BTBR Ob/Ob mutant mice model progressive diabetic nephropathy. J Am Soc Nephrol, 21, 1533-42.
139. HUNG, S. Y. & FU, W. M. 2017. Drug candidates in clinical trials for Alzheimer's disease. Journal of Biomedical Science. BioMed Central Ltd.
140. HUTTON, M., LENDON, C. L., RIZZU, P., BAKER, M., FROELICH, S., HOULDEN, H., PICKERING-BROWN, S., CHAKRAVERTY, S., ISAACS, A., GROVER, A., HACKETT, J., ADAMSON, J., LINCOLN, S., DICKSON, D., DAVIES, P., PETERSEN, R. C., STEVENS, M., DE GRAAFF, E., WAUTERS, E., VAN BAREN, J., HILLEBRAND, M., JOOSSE, M., KWON, J. M., NOWOTNY, P., CHE, L. K., NORTON, J., MORRIS, J. C., REED, L. A., TROJANOWSKI, J., BASUN, H., LANNFELT, L., NEYSTAT, M., FAHN, S., DARK, F., TANNENBERG, T., DODD, P. R., HAYWARD, N., KWOK, J. B. J., SCHOFIELD, P. R., ANDREADIS, A., SNOWDEN, J., CRAUFURD, D., NEARY, D., OWEN, F., OOSTRA, B. A., HARDY, J., GOATE, A., VAN SWIETEN, J., MANN, D., LYNCH, T. & HEUTINK, P. 1998. Association of missense and 5-splice-site mutations in tau with the inherited dementia FTDP-17. Nature, 393, 702-705.
141. ICHIMURA, K., MIYAZAKI, N., SADAYAMA, S., MURATA, K., KOIKE, M., NAKAMURA, K., OHTA, K. & SAKAI, T. 2015. Three-dimensional architecture of podocytes revealed by block-face scanning electron microscopy. Sci Rep, 5, 8993.
142. IKEGAMI, S., HARADA, A. & HIROKAWA, N. 2000. Muscle weakness, hyperactivity, and impairment in fear conditioning in tau-deficient mice. Neurosci Lett, 279, 129-32.
143. IMASAWA, T., OBRE, E., BELLANCE, N., LAVIE, J., IMASAWA, T., RIGOTHIER, C., DELMAS, Y., COMBE, C., LACOMBE, D., BENARD, G., CLAVEROL, S., BONNEU, M. & ROSSIGNOL, R. 2017. High glucose repatterns human podocyte energy metabolism during differentiation and diabetic nephropathy. FASEB journal : official publication of the Federation of American Societies for Experimental Biology, 31, 294-307.
144. ISHIMOTO, Y., TANAKA, T., YOSHIDA, Y. & INAGI, R. 2018. Physiological and pathophysiological role of reactive oxygen species and reactive nitrogen species in the kidney. Clin Exp Pharmacol Physiol, 45, 1097-1105.

145. JEFFERSON, J. A., SHANKLAND, S. J. & PICHLER, R. H. 2008. Proteinuria in diabetic kidney disease: a mechanistic viewpoint. Kidney Int, 74, 22-36.
146. JHA, J. C., GRAY, S. P., BARIT, D., OKABE, J., EL-OSTA, A., NAMIKOSHI, T., THALLAS-BONKE, V., WINGLER, K., SZYNDRALEWIEZ, C., HEITZ, F., TOUYZ, R. M., COOPER, M. E., SCHMIDT, H. H. & JANDELEIT-DAHM, K. A. 2014. Genetic targeting or pharmacologic inhibition of NADPH oxidase nox4 provides renoprotection in long-term diabetic nephropathy. J Am Soc Nephrol, 25, 1237-54.
147. JOHNSTONE, M. T., CREAGER, S. J., SCALES, K. M., CUSCO, J. A., LEE, B. K. & CREAGER, M. A. 1993. Impaired endothelium-dependent vasodilation in patients with insulin-dependent diabetes mellitus. Circulation, 88, 2510-6.
148. JUNAID, R., WAHID, M., WASEEM, F. S., HABIB, R. & HASAN, A. 2021. Effect of glucose mediated oxidative stress on apoptotic gene expression in gingival mesenchymal stem cells. BMC Oral Health, 21, 653.
149. KAKU, H. & ROTHSTEIN, T. L. 2020. FAIM Is a Non-redundant Defender of Cellular Viability in the Face of Heat and Oxidative Stress and Interferes With Accumulation of Stress-Induced Protein Aggregates. Frontiers in Molecular Biosciences, 7.
150. KANG, J., JEONG, M. G., OH, S., JANG, E. J., KIM, H. K. & HWANG, E. S. 2014. A FoxO1-dependent, but NRF2-independent induction of heme oxygenase-1 during muscle atrophy. FEBS Lett, 588, 79-85.
151. KEDERSHA, N. L., GUPTA, M., LI, W., MILLER, I. & ANDERSON, P. 1999. RNA-binding Proteins TIA-1 and TIAR Link the Phosphorylation of eIF-2 to the Assembly of Mammalian Stress Granules. The Journal of Cell Biology.
152. KESTILÄ, M., LENKKERI, U., MÄNNIKKÖ, M., LAMERDIN, J., MCCREADY, P., PUTAALA, H., RUOTSALAINEN, V., MORITA, T., NISSINEN, M., HERVA, R., KASHTAN, C. E., PELTONEN, L., HOLMBERG, C., OLSEN, A. & TRYGGVASON, K. 1998. Positionally Cloned Gene for a Novel Glomerular Protein—Nephrin—Is Mutated in Congenital Nephrotic Syndrome. Molecular Cell, 1, 575-582.
153. KHOSHDEL-RAD, N., AHMADI, A. & MOGHADASALI, R. 2022. Kidney organoids: current knowledge and future directions. Cell Tissue Res, 387, 207-224.
154. KIM, J. W., SAHM, H., YOU, J. & WANG, M. 2010. Knock-down of superoxide dismutase 1 sensitizes cisplatin-resistant human ovarian cancer cells. Anticancer Res, 30, 2577-81.
155. KIRBY, R. J., DIVLIANSKA, D. B., WHIG, K., BRYAN, N., MORFA, C. J., KOO, A., NGUYEN, K. H., MALONEY, P., PEDDIBHOTLA, S., SESSIONS, E. H., HERSHBERGER, P. M., SMITH, L. H. & MALANY, S. 2018. Discovery of Novel Small-Molecule Inducers of Heme Oxygenase-1 That Protect Human iPSC-Derived Cardiomyocytes from Oxidative Stress. J Pharmacol Exp Ther, 364, 87-96.
156. KLESSENS, C. Q. F., ZANDBERGEN, M., WOLTERBEEK, R., BRUIJN, J. A., RABELINK, T. J., BAJEMA, I. M. & DHT, I. J. 2017. Macrophages in diabetic nephropathy in patients with type 2 diabetes. Nephrol Dial Transplant, 32, 1322-1329.
157. KOCH, R. E. & HILL, G. E. 2017. An assessment of techniques to manipulate oxidative stress in animals. Functional Ecology, 31, 9-21.
158. KOIDE, N., KASAMATSU, A., ENDO-SAKAMOTO, Y., ISHIDA, S., SHIMIZU, T., KIMURA, Y., MIYAMOTO, I., YOSHIMURA, S., SHIIBA, M., TANZAWA, H. & UZAWA, K. 2017. Evidence for Critical Role of Lymphocyte Cytosolic Protein 1 in Oral Cancer. Sci Rep, 7, 43379.
159. KOSIK, K. S., ORECCHIO, D., TROJANOWSKI, J. Q., M-Y LEE, V. & LEE, G. 1988a. Epitopes That Span the Tau Molecule Are Shared with Paired Helical Filaments. Neuron.

160. KOSIK, K. S., ORECCHIO, L. D., BINDER, L., TROJANOWSKI, J. Q., LEE, V. M. & LEE, G. 1988b. Epitopes that span the tau molecule are shared with paired helical filaments. Neuron, 1, 817-25.
161. KOSTOVSKA, I., TOSHESKA-TRAJKOVSKA, K., TOPUZOVSKA, S., CEKOVSKA, S., SPASOVSKI, G., KOSTOVSKI, O. & LABUDOVIC, D. 2020. Urinary nephrin is earlier, more sensitive and specific marker of diabetic nephropathy than microalbuminuria. Journal of medical biochemistry, 39, 83-90.
162. KOVALEVICH, J. & LANGFORD, D. 2013. Considerations for the use of SH-SY5Y neuroblastoma cells in neurobiology. Methods Mol Biol, 1078, 9-21.
163. KOYE, D. N., MAGLIANO, D. J., NELSON, R. G. & PAVKOV, M. E. 2018. The Global Epidemiology of Diabetes and Kidney Disease. Adv Chronic Kidney Dis, 25, 121-132.
164. KRIZ, W., HACKENTHAL, E., NOBILING, R., SAKAI, T. & ELGER, M. A role for podocytes to counteract capillary wall distension. Kidney International, 1994. Nature Publishing Group, 369-376.
165. KULESHOV, M. V., JONES, M. R., ROUILLARD, A. D., FERNANDEZ, N. F., DUAN, Q., WANG, Z., KOPLEV, S., JENKINS, S. L., JAGODNIK, K. M., LACHMANN, A., MCDERMOTT, M. G., MONTEIRO, C. D., GUNDERSEN, G. W. & MA'AYAN, A. 2016. Enrichr: a comprehensive gene set enrichment analysis web server 2016 update. Nucleic Acids Res, 44, W90-7.
166. KWIATKOWSKI, T. J., BOSCO, D. A., LECLERC, A. L., TAMRAZIAN, E., VANDERBURG, C. R., RUSS, C., DAVIS, A., GILCHRIST, J., KASARSKIS, E. J., MUNSAT, T., VALDMANIS, P., ROULEAU, G. A., HOSLER, B. A., CORTELLI, P., DE JONG, P. J., YOSHINAGA, Y., HAINES, J. L., PERICAK-VANCE, M. A., YAN, J., TICOZZI, N., SIDDIQUE, T., MCKENNA-YASEK, D., SAPP, P. C., HORVITZ, H. R., LANDERS, J. E. & BROWN, R. H. 2009. Mutations in the FUS/TLS gene on chromosome 16 cause familial amyotrophic lateral sclerosis. Science, 323, 1205-1208.
167. LAN, J., ZHENG, J., FENG, J. & PENG, W. 2020. Nrf2 mediates the antinociceptive activity of dexmedetomidine in an acute inflammatory visceral pain rat model by activating the NF-kappaB sensor. Cell Biochem Funct, 38, 97-105.
168. LANGHAM, R., KELLY, D., COX, A., THOMSON, N., HOLTHÖFER, H., ZAOUI, P., PINEL, N., CORDONNIER, D. & GILBERT, R. 2002. Proteinuria and the expression of the podocyte slit diaphragm protein, nephrin, in diabetic nephropathy: Effects of angiotensin converting enzyme inhibition. Diabetologia, 45, 1572-1576.
169. LAPENNA, D., CIOFANI, G., PIERDOMENICO, S. D., GIAMBERARDINO, M. A. & CUCCURULLO, F. 2001. Original Contribution Reaction Conditions affecting the Relationship between Thiobarbituric Acid Reactivity and Lipid Peroxides in Human Plasma. Free Radical Biology and Medicine, 31, 331-335.
170. LASAGNI, L., LAZZERI, E., SHANKLAND, S. J., ANDERS, H. J. & ROMAGNANI, P. 2013. Podocyte mitosis - a catastrophe. Curr Mol Med, 13, 13-23.
171. LAY, A. C., HURCOMBE, J. A., BETIN, V. M. S., BARRINGTON, F., ROLLASON, R., NI, L., GILLAM, L., PEARSON, G. M. E., OSTERGAARD, M. V., HAMIDI, H., LENNON, R., WELSH, G. I. & COWARD, R. J. M. 2017. Prolonged exposure of mouse and human podocytes to insulin induces insulin resistance through lysosomal and proteasomal degradation of the insulin receptor. Diabetologia, 60, 2299-2311.
172. LEE, C. F., LIU, C. Y., HSIEH, R. H. & WEI, Y. H. Oxidative stress-induced depolymerization of microtubules and alteration of mitochondrial mass in human cells. Annals of the New York Academy of Sciences, 2005. New York Academy of Sciences, 246-254.

173. LEE, J. S., CHANG, P. Y., ZHANG, Y., KIZER, J. R., BEST, L. G. & HOWARD, B. V. 2017. Triglyceride and HDL-C Dyslipidemia and Risks of Coronary Heart Disease and Ischemic Stroke by Glycemic Dysregulation Status: The Strong Heart Study. Diabetes Care, 40, 529-537.
174. LEE, S. J., BORSTING, E., DECLEVES, A. E., SINGH, P. & CUNARD, R. 2012. Podocytes express IL-6 and lipocalin 2/ neutrophil gelatinase-associated lipocalin in lipopolysaccharide-induced acute glomerular injury. Nephron Exp Nephrol, 121, e86-96.
175. LEITER, E. H. 1982. Multiple low-dose streptozotocin-induced hyperglycemia and insulitis in C57BL mice: influence of inbred background, sex, and thymus. Proc Natl Acad Sci U S A, 79, 630-4.
176. LENKKERI, U., MÄNNIKKÖ, M., MCCREADY, P., LAMERDIN, J., GRIBOUVAL, O., NIAUDET, P., ANTIGNAC, C., KASHTAN, C. E., HOLMBERG, C., OLSEN, A., KESTILÄ, M. & TRYGGVASON, K. 1999. Structure of the Gene for Congenital Nephrotic Syndrome of the Finnish Type (NPHS1) and Characterization of Mutations. The American Journal of Human Genetics, 64, 51-61.
177. LETO, T. L. & GEISZT, M. 2006. Role of Nox family NADPH oxidases in host defense. Antioxid Redox Signal, 8, 1549-61.
178. LEVEY, A. S., STEVENS, L. A., SCHMID, C. H., ZHANG, Y. L., CASTRO, A. F., 3RD, FELDMAN, H. I., KUSEK, J. W., EGGERS, P., VAN LENTE, F., GREENE, T., CORESH, J. & CKD, E. P. I. 2009. A new equation to estimate glomerular filtration rate. Ann Intern Med, 150, 604-12.
179. LEVINE, R. L., WILLIAMS, J. A., STADTMAN, E. R. & SHACTER, E. 1994. Carbonyl assays for determination of oxidatively modified proteins. Methods Enzymol, 233, 346-57.
180. LEWIS, E. J., HUNSICKER, L. G., BAIN, R. P. & ROHDE, R. D. 1993. The effect of angiotensin-converting-enzyme inhibition on diabetic nephropathy. The Collaborative Study Group. N Engl J Med, 329, 1456-62.
181. LI, J. H., HUANG, X. R., ZHU, H. J., OLDFIELD, M., COOPER, M., TRUONG, L. D., JOHNSON, R. J. & LAN, H. Y. 2004. Advanced glycation end products activate Smad signaling via TGF-β-dependent and -independent mechanisms: implications for diabetic renal and vascular disease. The FASEB Journal, 18, 176-178.
182. LI, S., LIU, Y., HE, Y., RONG, W., ZHANG, M., LI, L., LIU, Z. & ZEN, K. 2020. Podocytes present antigen to activate specific T cell immune responses in inflammatory renal disease. J Pathol, 252, 165-177.
183. LIU, C., SONG, X., NISBET, R. & GÖTZ, J. 2016. Co-immunoprecipitation with Tau isoform-specific antibodies reveals distinct protein interactions and highlights a putative role for 2N Tau in disease. Journal of Biological Chemistry, 291, 8173-8188.
184. LIU, R., REN, Y., GARVIN, J. L. & CARRETERO, O. A. 2004. Superoxide enhances tubuloglomerular feedback by constricting the afferent arteriole. Kidney Int, 66, 268-74.
185. LIU, Y., LV, Y., ZHANG, T., HUANG, T., LANG, Y., SHENG, Q., LIU, Y., KONG, Z., GAO, Y., LU, S., YANG, M., LUAN, Y., WANG, X. & LV, Z. 2023. T cells and their products in diabetic kidney disease. Front Immunol, 14, 1084448.
186. LIU-YESUCEVITZ, L., BILGUTAY, A., ZHANG, Y. J., VANDERWYDE, T., CITRO, A., MEHTA, T., ZAARUR, N., MCKEE, A., BOWSER, R., SHERMAN, M., PETRUCELLI, L. & WOLOZIN, B. 2010. Tar DNA binding protein-43 (TDP-43) associates with stress granules: Analysis of cultured cells and pathological brain tissue. PLoS ONE, 5.
187. LOBO, V., PATIL, A., PHATAK, A. & CHANDRA, N. 2010. Free radicals, antioxidants and functional foods: Impact on human health. Pharmacognosy Reviews.
188. LOCASALE, J. W. 2013. Serine, glycine and one-carbon units: cancer metabolism in full circle. Nat Rev Cancer, 13, 572-83.

189. LOPRESTI, P., POLUHA, W., POLUHA, D. K., DRINKWATER, E. & ROSS, A. H. 1992. Neuronal differentiation triggered by blocking cell proliferation. Cell Growth Differ, 3, 627-35.
190. LOVSHIN, J. A., BOULET, G., LYTVYN, Y., LOVBLOM, L. E., BJORNSTAD, P., FAROOQI, M. A., LAI, V., CHAM, L., TSE, J., ORSZAG, A., SCARR, D., WEISMAN, A., KEENAN, H. A., BRENT, M. H., PAUL, N., BRIL, V., PERKINS, B. A. & CHERNEY, D. Z. 2018. Renin-angiotensin-aldosterone system activation in long-standing type 1 diabetes. JCI Insight, 3.
191. LOW, J. H., LI, P., CHEW, E. G. Y., ZHOU, B., SUZUKI, K., ZHANG, T., LIAN, M. M., LIU, M., AIZAWA, E., RODRIGUEZ ESTEBAN, C., YONG, K. S. M., CHEN, Q., CAMPISTOL, J. M., FANG, M., KHOR, C. C., FOO, J. N., IZPISUA BELMONTE, J. C. & XIA, Y. 2019. Generation of Human PSC-Derived Kidney Organoids with Patterned Nephron Segments and a De Novo Vascular Network. Cell Stem Cell, 25, 373-387 e9.
192. LUDDI, A., GOVERNINI, L., CAPALDO, A., CAMPANELLA, G., DE LEO, V., PIOMBONI, P. & MORGANTE, G. 2020. Characterization of the age-dependent changes in antioxidant defenses and protein's sulfhydryl/carbonyl stress in human follicular fluid. Antioxidants, 9, 1-16.
193. MAEDA, K., MEHTA, H., DREVETS, D. A. & COGGESHALL, K. M. 2010. IL-6 increases B-cell IgG production in a feed-forward proinflammatory mechanism to skew hematopoiesis and elevate myeloid production. Blood, 115, 4699-706.
194. MAGEE, G. M., BILOUS, R. W., CARDWELL, C. R., HUNTER, S. J., KEE, F. & FOGARTY, D. G. 2009. Is hyperfiltration associated with the future risk of developing diabetic nephropathy? A meta-analysis. Diabetologia, 52, 691-697.
195. MALKANI, R., D'SOUZA, I., GWINN-HARDY, K., SCHELLENBERG, G. D., HARDY, J. & MOMENI, P. 2006. A MAPT mutation in a regulatory element upstream of exon 10 causes frontotemporal dementia. Neurobiology of Disease, 22, 401-403.
196. MARCELO, A., KOPPENOL, R., DE ALMEIDA, L. P., MATOS, C. A. & NOBREGA, C. 2021. Stress granules, RNA-binding proteins and polyglutamine diseases: too much aggregation? Cell Death Dis, 12, 592.
197. MARCOTTE, D., ZENG, W., HUS, J. C., MCKENZIE, A., HESSION, C., JIN, P., BERGERON, C., LUGOVSKOY, A., ENYEDY, I., CUERVO, H., WANG, D., ATMANENE, C., ROECKLIN, D., VECCHI, M., VIVAT, V., KRAEMER, J., WINKLER, D., HONG, V., CHAO, J., LUKASHEV, M. & SILVIAN, L. 2013. Small molecules inhibit the interaction of Nrf2 and the Keap1 Kelch domain through a non-covalent mechanism. Bioorg Med Chem, 21, 4011-9.
198. MARTIN, C. E. & JONES, N. 2018. Nephrin Signaling in the Podocyte: An Updated View of Signal Regulation at the Slit Diaphragm and Beyond. Front Endocrinol (Lausanne), 9, 302.
199. MARTIN, I., JONES, M. A. & GROTEWIEL, M. 2009a. Manipulation of Sod1 expression ubiquitously, but not in the nervous system or muscle, impacts age-related parameters in Drosophila. FEBS Lett, 583, 2308-14.
200. MARTIN, I., JONES, M. A., RHODENIZER, D., ZHENG, J., WARRICK, J. M., SEROUDE, L. & GROTEWIEL, M. 2009b. Sod2 knockdown in the musculature has whole-organism consequences in Drosophila. Free Radic Biol Med, 47, 803-13.
201. MATHIESON, P. W. 2012. The podocyte cytoskeleton in health and in disease. Clin Kidney J, 5, 498-501.
202. MATHUR, R., BHASKARAN, K., EDWARDS, E., LEE, H., CHATURVEDI, N., SMEETH, L. & DOUGLAS, I. 2004. Clinical Practice Research Datalink. BMJ Open, 7, 14444-14444.

203. MAY, C. J., SALEEM, M. & WELSH, G. I. 2014. Podocyte dedifferentiation: a specialized process for a specialized cell. Front Endocrinol (Lausanne), 5, 148.
204. MCHUGH, K. P., SQUIBB, B.-M., MOROZOVA, O. & COLBY, D. W. 2015. Convergent Replication of Mouse Synthetic Prion Strains View project.
205. MEERBREY, K. L., HU, G., KESSLER, J. D., ROARTY, K., LI, M. Z., FANG, J. E., HERSCHKOWITZ, J. I., BURROWS, A. E., CICCIA, A., SUN, T., SCHMITT, E. M., BERNARDI, R. J., FU, X., BLAND, C. S., COOPER, T. A., SCHIFF, R., ROSEN, J. M., WESTBROOK, T. F. & ELLEDGE, S. J. 2011. The pINDUCER lentiviral toolkit for inducible RNA interference in vitro and in vivo. Proc Natl Acad Sci U S A, 108, 3665-70.
206. MESHKINI, A. & YAZDANPARAST, R. 2012. Involvement of oxidative stress in taxol-induced apoptosis in chronic myelogenous leukemia K562 cells. Experimental and Toxicologic Pathology, 64, 357-365.
207. MINOTTI, G., BORRELLO, S., PALOMBINI, G. & GALEOTTI, T. 1986. Cytochrome P-450 deficiency and resistance to t-butyl hydroperoxide of hepatoma microsomal lipid peroxidation. Biochim Biophys Acta, 876, 220-5.
208. MISHRA, R., EMANCIPATOR, S. N., KERN, T. & SIMONSON, M. S. 2005. High glucose evokes an intrinsic proapoptotic signaling pathway in mesangial cells. Kidney Int, 67, 82-93.
209. MONTALBANO, M., JAWORSKI, E., GARCIA, S., ELLSWORTH, A., MCALLEN, S., ROUTH, A. & KAYED, R. 2021. Tau Modulates mRNA Transcription, Alternative Polyadenylation Profiles of hnRNPs, Chromatin Remodeling and Spliceosome Complexes. Frontiers in Molecular Neuroscience, 14.
210. MORGAN, P. E., DEAN, R. T. & DAVIES, M. J. 2002. Inactivation of cellular enzymes by carbonyls and protein-bound glycation/glycoxidation products. Arch Biochem Biophys, 403, 259-69.
211. MUKRASCH, M. D., BIBOW, S., KORUKOTTU, J., JEGANATHAN, S., BIERNAT, J., GRIESINGER, C., MANDELKOW, E. & ZWECKSTETTER, M. 2009. Structural polymorphism of 441-residue tau at single residue resolution. PLoS Biol, 7, e34.
212. MULDER, G. M., MELENHORST, W. B., CELIE, J. W., KLOOSTERHUIS, N. J., HILLEBRANDS, J. L., PLOEG, R. J., SEELEN, M. A., VISSER, L., VAN DIJK, M. C. & VAN GOOR, H. 2012. ADAM17 up-regulation in renal transplant dysfunction and non-transplant-related renal fibrosis. Nephrol Dial Transplant, 27, 2114-22.
213. MULLARKEY, C. J., EDELSTEIN, D. & BROWNLEE, M. 1990. Free radical generation by early glycation products: a mechanism for accelerated atherogenesis in diabetes. Biochem Biophys Res Commun, 173, 932-9.
214. MUNDEL, P., GILBERT, P. & KRIZ, W. 1991. Podocytes in glomerulus of rat kidney express a characteristic 44 KD protein. Journal of Histochemistry & Cytochemistry, 39, 1047-1056.
215. MUNDEL, P., HEID, H. W., MUNDEL, T. M., KRÜGER, M., REISER, J. & KRIZ, W. 1997. Synaptopodin: An Actin-associated Protein in Telencephalic Dendrites and Renal Podocytes. Journal of Cell Biology, 139, 193-204.
216. MUNOZ, M., MARTINEZ, M. P., LOPEZ-OLIVA, M. E., RODRIGUEZ, C., CORBACHO, C., CARBALLIDO, J., GARCIA-SACRISTAN, A., HERNANDEZ, M., RIVERA, L., SAENZ-MEDINA, J. & PRIETO, D. 2018. Hydrogen peroxide derived from NADPH oxidase 4- and 2 contributes to the endothelium-dependent vasodilatation of intrarenal arteries. Redox Biol, 19, 92-104.
217. MURPHY, M. P., BAYIR, H., BELOUSOV, V., CHANG, C. J., DAVIES, K. J. A., DAVIES, M. J., DICK, T. P., FINKEL, T., FORMAN, H. J., JANSSEN-HEININGER, Y., GEMS, D., KAGAN, V. E., KALYANARAMAN, B., LARSSON, N. G., MILNE, G. L., NYSTRÖM, T., POULSEN, H. E., RADI, R., VAN REMMEN, H., SCHUMACKER, P. T.,

THORNALLEY, P. J., TOYOKUNI, S., WINTERBOURN, C. C., YIN, H. & HALLIWELL, B. 2022. Guidelines for measuring reactive oxygen species and oxidative damage in cells and in vivo. Nature Metabolism, 4, 651-662.
218. MURUZABAL, D., COLLINS, A. & AZQUETA, A. 2021. The enzyme-modified comet assay: Past, present and future. Food and Chemical Toxicology. Elsevier Ltd.
219. MUSAH, S., MAMMOTO, A., FERRANTE, T. C., JEANTY, S. S. F., HIRANO-KOBAYASHI, M., MAMMOTO, T., ROBERTS, K., CHUNG, S., NOVAK, R., INGRAM, M., FATANAT-DIDAR, T., KOSHY, S., WEAVER, J. C., CHURCH, G. M. & INGBER, D. E. 2017. Mature induced-pluripotent-stem-cell-derived human podocytes reconstitute kidney glomerular-capillary-wall function on a chip. Nat Biomed Eng, 1.
220. NAGATA, M., NAKAYAMA, K., TERADA, Y., HOSHI, S. & WATANABE, T. 1998. Cell cycle regulation and differentiation in the human podocyte lineage. Am J Pathol, 153, 1511-20.
221. NANGAKU, M., KANDA, H., TAKAMA, H., ICHIKAWA, T., HASE, H. & AKIZAWA, T. 2020. Randomized Clinical Trial on the Effect of Bardoxolone Methyl on GFR in Diabetic Kidney Disease Patients (TSUBAKI Study). Kidney Int Rep, 5, 879-890.
222. NATH, K. A. 1992. Tubulointerstitial changes as a major determinant in the progression of renal damage. Am J Kidney Dis, 20, 1-17.
223. NAVARRO-MUNOZ, M., IBERNON, M., PEREZ, V., ARA, J., ESPINAL, A., LOPEZ, D., BONET, J. & ROMERO, R. 2011. Messenger RNA expression of B7-1 and NPHS1 in urinary sediment could be useful to differentiate between minimal-change disease and focal segmental glomerulosclerosis in adult patients. Nephrol Dial Transplant, 26, 3914-23.
224. NING, L., SULEIMAN, H. Y. & MINER, J. H. 2020. Synaptopodin Is Dispensable for Normal Podocyte Homeostasis but Is Protective in the Context of Acute Podocyte Injury. J Am Soc Nephrol, 31, 2815-2832.
225. NISHIKAWA, T., EDELSTEIN, D., DU, X. L., YAMAGISHI, S., MATSUMURA, T., KANEDA, Y., YOREK, M. A., BEEBE, D., OATES, P. J., HAMMES, H. P., GIARDINO, I. & BROWNLEE, M. 2000. Normalizing mitochondrial superoxide production blocks three pathways of hyperglycaemic damage. Nature, 404, 787-90.
226. NORDQUIST, L., LAI, E. Y., SJÖQUIST, M., PATZAK, A. & PERSSON, A. E. G. 2008. Proinsulin C-peptide constricts glomerular afferent arterioles in diabetic mice. A potential renoprotective mechanism. American Journal of Physiology-Regulatory, Integrative and Comparative Physiology, 294, R836-R841.
227. OHN, T., KEDERSHA, N., HICKMAN, T., TISDALE, S. & ANDERSON, P. 2008. A functional RNAi screen links O-GlcNAc modification of ribosomal proteins to stress granule and processing body assembly. Nature Cell Biology, 10, 1224-1231.
228. OOHIRA, A., WIGHT, T. N. & BORNSTEIN, P. 1983. Sulfated proteoglycans synthesized by vascular endothelial cells in culture. Journal of Biological Chemistry, 258, 2014-2021.
229. OSICKA, T. M., PRATT, L. M. & COMPER, W. D. 1996. Glomerular capillary wall permeability to albumin and horseradish peroxidase. Nephrology, 2, 199-212.
230. PAGTALUNAN, M. E., MILLER, P. L., JUMPING-EAGLE, S., NELSON, R. G., MYERS, B. D., RENNKE, H. G., COPLON, N. S., SUN, L. & MEYER, T. W. 1997. Podocyte loss and progressive glomerular injury in type II diabetes. J Clin Invest, 99, 342-8.
231. PALMER, G., HORGAN, D. J., TISDALE, H., SINGER, T. P. & BEINERT, H. 1968. Studies on the Respiratory Chain-linked Reduced Nicotinamide Adenine Dinucleotide Dehydrogenase. Journal of Biological Chemistry, 243, 844-847.
232. PAVENSTADT, H., KRIZ, W. & KRETZLER, M. 2003. Cell biology of the glomerular podocyte. Physiol Rev, 83, 253-307.

233. PENNO, G., ORSI, E., SOLINI, A., BONORA, E., FONDELLI, C., TREVISAN, R., VEDOVATO, M., CAVALOT, F., GRUDEN, G., LAVIOLA, L., NICOLUCCI, A., PUGLIESE, G., RENAL, I. & CARDIOVASCULAR EVENTS STUDY, G. 2020. Renal hyperfiltration is independently associated with increased all-cause mortality in individuals with type 2 diabetes: a prospective cohort study. BMJ Open Diabetes Res Care, 8.
234. PERGOLA, P. E., RASKIN, P., TOTO, R. D., MEYER, C. J., HUFF, J. W., GROSSMAN, E. B., KRAUTH, M., RUIZ, S., AUDHYA, P., CHRIST-SCHMIDT, H., WITTES, J., WARNOCK, D. G. & INVESTIGATORS, B. S. 2011. Bardoxolone methyl and kidney function in CKD with type 2 diabetes. N Engl J Med, 365, 327-36.
235. PETRIE, J. R., GUZIK, T. J. & TOUYZ, R. M. 2018. Diabetes, Hypertension, and Cardiovascular Disease: Clinical Insights and Vascular Mechanisms. Can J Cardiol, 34, 575-584.
236. PETRY, F. R., PELLETIER, J. O., BRETTEVILLE, A., MORIN, F., CALON, F. E., ḾEBERT, S. S., WHITTINGTON, R. A. & PLANEL, E. 2014. Specificity of anti-Tau antibodies when analyzing mice models of Alzheimer's disease: Problems and solutions. PLoS ONE, 9.
237. PIKMAN, Y., OCASIO-MARTINEZ, N., ALEXE, G., DIMITROV, B., KITARA, S., DIEHL, F. F., ROBICHAUD, A. L., CONWAY, A. S., ROSS, L., SU, A., LING, F., QI, J., ROTI, G., LEWIS, C. A., PUISSANT, A., VANDER HEIDEN, M. G. & STEGMAIER, K. 2022. Targeting serine hydroxymethyltransferases 1 and 2 for T-cell acute lymphoblastic leukemia therapy. Leukemia, 36, 348-360.
238. POLLAK, M. R., QUAGGIN, S. E., HOENIG, M. P. & DWORKIN, L. D. 2014. The glomerulus: the sphere of influence. Clin J Am Soc Nephrol, 9, 1461-9.
239. PONTEN, F., JIRSTROM, K. & UHLEN, M. 2008. The Human Protein Atlas--a tool for pathology. J Pathol, 216, 387-93.
240. PRATICO, D., CLARK, C. M., LEE, V. M. Y., TROJANOWSKI, J. Q., ROKACH, J. & FITZGERALD, G. A. 2000b. Increased 8,12-iso-iPF2?-VI in Alzheimer's disease: Correlation of a noninvasive index of lipid peroxidation with disease severity. Annals of Neurology, 48, 809-812.
241. PRATICO, D., CLARK, C. M., LEE, V. M., TROJANOWSKI, J. Q., ROKACH, J. & FITZGERALD, G. A. 2000a. Increased 8,12-iso-iPF2alpha-VI in Alzheimer's disease: correlation of a noninvasive index of lipid peroxidation with disease severity. Ann Neurol, 48, 809-12.
242. PRESTON, R., STUART, H. M. & LENNON, R. 2019. Genetic testing in steroid-resistant nephrotic syndrome: why, who, when and how? Pediatr Nephrol, 34, 195-210.
243. PRZEPIORSKI, A., VANICHAPOL, T., ESPIRITU, E. B., CRUNK, A. E., PARASKY, E., MCDANIELS, M. D., EMLET, D. R., SALISBURY, R., HAPP, C. L., VERNETTI, L. A., MACDONALD, M. L., KELLUM, J. A., KLEYMAN, T. R., BATY, C. J., DAVIDSON, A. J. & HUKRIEDE, N. A. 2022. Modeling oxidative injury response in human kidney organoids. Stem Cell Res Ther, 13, 76.
244. QI, Z., FUJITA, H., JIN, J., DAVIS, L. S., WANG, Y., FOGO, A. B. & BREYER, M. D. 2005. Characterization of susceptibility of inbred mouse strains to diabetic nephropathy. Diabetes, 54, 2628-37.
245. RAMANATHAN, B., JAN, K. Y., CHEN, C. H., HOUR, T. C., YU, H. J. & PU, Y. S. 2005. Resistance to paclitaxel is proportional to cellular total antioxidant capacity. Cancer Research, 65, 8455-8460.
246. RANSY, C., VAZ, C., LOMBES, A. & BOUILLAUD, F. 2020. Use of H(2)O(2) to Cause Oxidative Stress, the Catalase Issue. Int J Mol Sci, 21.
247. RAYNER, E., DURIN, M.-A., THOMAS, R., MORALLI, D., O'CATHAIL, S. M., TOMLINSON, I., GREEN, C. M. & LEWIS, A. 2019. CRISPR-Cas9 Causes Chromosomal

Instability and Rearrangements in Cancer Cell Lines, Detectable by Cytogenetic Methods. The CRISPR Journal, 2, 406-416.
248. REICHARD, J. F., MOTZ, G. T. & PUGA, A. 2007. Heme oxygenase-1 induction by NRF2 requires inactivation of the transcriptional repressor BACH1. Nucleic Acids Research, 35, 7074-7086.
249. RESENDE, R., MOREIRA, P. I., PROENCA, T., DESHPANDE, A., BUSCIGLIO, J., PEREIRA, C. & OLIVEIRA, C. R. 2008. Brain oxidative stress in a triple-transgenic mouse model of Alzheimer disease. Free Radic Biol Med, 44, 2051-7.
250. REUTENS, A. T., JANDELEIT-DAHM, K., THOMAS, M., SALIM, A., DE LIVERA, A. M., BACH, L. A., COLMAN, P. G., DAVIS, T. M. E., EKINCI, E. I., FULCHER, G., HAMBLIN, P. S., KOTOWICZ, M. A., MACISAAC, R. J., MORBEY, C., SIMMONS, D., SOLDATOS, G., WITTERT, G., WU, T., COOPER, M. E. & SHAW, J. E. 2020. A physician-initiated double-blind, randomised, placebo-controlled, phase 2 study evaluating the efficacy and safety of inhibition of NADPH oxidase with the first-in-class Nox-1/4 inhibitor, GKT137831, in adults with type 1 diabetes and persistently elevated urinary albumin excretion: Protocol and statistical considerations. Contemp Clin Trials, 90, 105892.
251. REZNICK, A. Z. & PACKER, L. 1994. Oxidative damage to proteins: spectrophotometric method for carbonyl assay. Methods Enzymol, 233, 357-63.
252. RHEIN, V., SONG, X., WEISNER, A., ITTNER, L., BAYSANG, G., MEIER, F., OZMEN, L., BLUETHMANN, H., DROSE, S., BRANDT, U., SAVASKAN, E., CZECH, C., GOTZ, J. & ECKERT, A. 2009a. Amyloid-and tau synergistically impair the oxidative phosphorylation system in triple transgenic Alzheimer's disease mice. PNAS, 106, 20057-20062.
253. RHEIN, V., SONG, X., WIESNER, A., ITTNER, L. M., BAYSANG, G., MEIER, F., OZMEN, L., BLUETHMANN, H., DROSE, S., BRANDT, U., SAVASKAN, E., CZECH, C., GOTZ, J. & ECKERT, A. 2009b. Amyloid-beta and tau synergistically impair the oxidative phosphorylation system in triple transgenic Alzheimer's disease mice. Proc Natl Acad Sci U S A, 106, 20057-62.
254. RHOADS, A. & AU, K. F. 2015. PacBio Sequencing and Its Applications. Genomics, Proteomics and Bioinformatics. Beijing Genomics Institute.
255. RINSCHEN, M. M., GODEL, M., GRAHAMMER, F., ZSCHIEDRICH, S., HELMSTADTER, M., KRETZ, O., ZAREI, M., BRAUN, D. A., DITTRICH, S., PAHMEYER, C., SCHRODER, P., TEETZEN, C., GEE, H., DAOUK, G., POHL, M., KUHN, E., SCHERMER, B., KUTTNER, V., BOERRIES, M., BUSCH, H., SCHIFFER, M., BERGMANN, C., KRUGER, M., HILDEBRANDT, F., DENGJEL, J., BENZING, T. & HUBER, T. B. 2018. A Multi-layered Quantitative In Vivo Expression Atlas of the Podocyte Unravels Kidney Disease Candidate Genes. Cell Rep, 23, 2495-2508.
256. RITCHIE, M. E., PHIPSON, B., WU, D., HU, Y., LAW, C. W., SHI, W. & SMYTH, G. K. 2015. limma powers differential expression analyses for RNA-sequencing and microarray studies. Nucleic Acids Res, 43, e47.
257. ROJO, A. I., PAJARES, M., RADA, P., NUNEZ, A., NEVADO-HOLGADO, A. J., KILLIK, R., VAN LEUVEN, F., RIBE, E., LOVESTONE, S., YAMAMOTO, M. & CUADRADO, A. 2017. NRF2 deficiency replicates transcriptomic changes in Alzheimer's patients and worsens APP and TAU pathology. Redox Biol, 13, 444-451.
258. ROMERO, D. M., POIRIER, K., BELVINDRAH, R., MOUTKINE, I., HOULLIER, A., LEMOING, A. G., PETIT, F., BOLAND, A., COLLINS, S. C., SOIZA-REILLY, M., YALCIN, B., CHELLY, J., DELEUZE, J. F., BAHI-BUISSON, N. & FRANCIS, F. 2022. Novel role of the synaptic scaffold protein Dlgap4 in ventricular surface integrity and neuronal migration during cortical development. Nature Communications, 13.

259. ROMERO, M., ORTEGA, A., IZQUIERDO, A., LOPEZ-LUNA, P. & BOSCH, R. J. 2010. Parathyroid hormone-related protein induces hypertrophy in podocytes via TGF- 1 and p27Kip1: implications for diabetic nephropathy. Nephrology Dialysis Transplantation, 25, 2447-2457.
260. RUF, B., CATANIA, V. V., WABITSCH, S., MA, C., DIGGS, L. P., ZHANG, Q., HEINRICH, B., SUBRAMANYAM, V., CUI, L. L., POUZOLLES, M., EVANS, C. N., CHARI, R., SAKAI, S., OH, S., BARRY, C. E., 3RD, BARBER, D. L. & GRETEN, T. F. 2021. Activating Mucosal-Associated Invariant T Cells Induces a Broad Antitumor Response. Cancer Immunol Res, 9, 1024-1034.
261. RUGGENENTI, P., PORRINI, E. L., GASPARI, F., MOTTERLINI, N., CANNATA, A., CARRARA, F., CELLA, C., FERRARI, S., STUCCHI, N., PARVANOVA, A., ILIEV, I., DODESINI, A. R., TREVISAN, R., BOSSI, A., ZALETEL, J. & REMUZZI, G. 2012. Glomerular Hyperfiltration and Renal Disease Progression in Type 2 Diabetes. Diabetes Care, 35, 2061-2068.
262. SAGAR, A., ARIF, E., SOLANKI, A. K., SRIVASTAVA, P., JANECH, M. G., KIM, S. H., LIPSCHUTZ, J. H., KWON, S. H., ASHISH & NIHALANI, D. 2017. Targeting Neph1 and ZO-1 protein-protein interaction in podocytes prevents podocyte injury and preserves glomerular filtration function. Sci Rep, 7, 12047.
263. SALEEM, M. A., O'HARE, M. J., REISER, J., COWARD, R. J., INWARD, C. D., FARREN, T., XING, C. Y., NI, L., MATHIESON, P. W. & MUNDEL, P. 2002. A conditionally immortalized human podocyte cell line demonstrating nephrin and podocin expression. J Am Soc Nephrol, 13, 630-638.
264. SALEM, R. M., TODD, J. N., SANDHOLM, N., COLE, J. B., CHEN, W. M., ANDREWS, D., PEZZOLESI, M. G., MCKEIGUE, P. M., HIRAKI, L. T., QIU, C., NAIR, V., DI LIAO, C., CAO, J. J., VALO, E., ONENGUT-GUMUSCU, S., SMILES, A. M., MCGURNAGHAN, S. J., HAUKKA, J. K., HARJUTSALO, V., BRENNAN, E. P., VAN ZUYDAM, N., AHLQVIST, E., DOYLE, R., AHLUWALIA, T. S., LAJER, M., HUGHES, M. F., PARK, J., SKUPIEN, J., SPILIOPOULOU, A., LIU, A., MENON, R., BOUSTANY-KARI, C. M., KANG, H. M., NELSON, R. G., KLEIN, R., KLEIN, B. E., LEE, K. E., GAO, X., MAUER, M., MAESTRONI, S., CARAMORI, M. L., DE BOER, I. H., MILLER, R. G., GUO, J., BORIGHT, A. P., TREGOUET, D., GYORGY, B., SNELL-BERGEON, J. K., MAAHS, D. M., BULL, S. B., CANTY, A. J., PALMER, C. N. A., STECHEMESSER, L., PAULWEBER, B., WEITGASSER, R., SOKOLOVSKA, J., ROVITE, V., PIRAGS, V., PRAKAPIENE, E., RADZEVICIENE, L., VERKAUSKIENE, R., PANDURU, N. M., GROOP, L. C., MCCARTHY, M. I., GU, H. F., MOLLSTEN, A., FALHAMMAR, H., BRISMAR, K., MARTIN, F., ROSSING, P., COSTACOU, T., ZERBINI, G., MARRE, M., HADJADJ, S., MCKNIGHT, A. J., FORSBLOM, C., MCKAY, G., GODSON, C., MAXWELL, A. P., KRETZLER, M., SUSZTAK, K., COLHOUN, H. M., KROLEWSKI, A., PATERSON, A. D., GROOP, P. H., RICH, S. S., HIRSCHHORN, J. N., FLOREZ, J. C. & SUMMIT CONSORTIUM, D. E. R. G. G. C. 2019. Genome-Wide Association Study of Diabetic Kidney Disease Highlights Biology Involved in Glomerular Basement Membrane Collagen. J Am Soc Nephrol, 30, 2000-2016.
265. SAMIR, P., KESAVARDHANA, S., PATMORE, D. M., GINGRAS, S., MALIREDDI, R. K. S., KARKI, R., GUY, C. S., BRIARD, B., PLACE, D. E., BHATTACHARYA, A., SHARMA, B. R., NOURSE, A., KING, S. V., PITRE, A., BURTON, A. R., PELLETIER, S., GILBERTSON, R. J. & KANNEGANTI, T. D. 2019. DDX3X acts as a live-or-die checkpoint in stressed cells by regulating NLRP3 inflammasome. Nature, 573, 590-594.
266. SANDHOLM, N., COLE, J. B., NAIR, V., SHENG, X., LIU, H., AHLQVIST, E., VAN ZUYDAM, N., DAHLSTROM, E. H., FERMIN, D., SMYTH, L. J., SALEM, R. M., FORSBLOM, C., VALO, E., HARJUTSALO, V., BRENNAN, E. P., MCKAY, G. J.,

ANDREWS, D., DOYLE, R., LOOKER, H. C., NELSON, R. G., PALMER, C., MCKNIGHT, A. J., GODSON, C., MAXWELL, A. P., GROOP, L., MCCARTHY, M. I., KRETZLER, M., SUSZTAK, K., HIRSCHHORN, J. N., FLOREZ, J. C., GROOP, P. H. & CONSORTIUM, G. 2022. Genome-wide meta-analysis and omics integration identifies novel genes associated with diabetic kidney disease. Diabetologia, 65, 1495-1509.
267. SAULNIER, P. J., GAND, E., RAGOT, S., DUCROCQ, G., HALIMI, J. M., HULIN-DELMOTTE, C., LLATY, P., MONTAIGNE, D., RIGALLEAU, V., ROUSSEL, R., VELHO, G., SOSNER, P., ZAOUI, P., HADJADJ, S. & GROUP, S. S. 2014. Association of serum concentration of TNFR1 with all-cause mortality in patients with type 2 diabetes and chronic kidney disease: follow-up of the SURDIAGENE Cohort. Diabetes Care, 37, 1425-31.
268. SAXENA, S., TYAGI, I., AGRAWAL, U., AMITABH, V. & JAIN, A. K. 2008. Thickness of glomerular and tubular basement membranes in preclinical and clinical stages of diabetic nephropathy. Indian Journal of Nephrology, 18, 64-64.
269. SCANLON, P. H. 2008. Article Commentary: The English national screening programme for sight-threatening diabetic retinopathy. Journal of Medical Screening, 15, 1-4.
270. SCHENK, L. K., OUSINGSAWAT, J., SKRYABIN, B. V., SCHREIBER, R., PAVENSTADT, H. & KUNZELMANN, K. 2018. Regulation and Function of TMEM16F in Renal Podocytes. Int J Mol Sci, 19.
271. SCHIFFER, M., BITZER, M., ROBERTS, I. S., KOPP, J. B., TEN DIJKE, P., MUNDEL, P. & BÖTTINGER, E. P. 2001. Apoptosis in podocytes induced by TGF-beta and Smad7. The Journal of clinical investigation, 108, 807-16.
272. SCHNELLMANN, R. G. 1988. Mechanisms of t-butyl hydroperoxide-induced toxicity to rabbit renal proximal tubules. Am J Physiol, 255, C28-33.
273. SCHWARZ, K., SIMONS, M., REISER, J., SALEEM, M. A., FAUL, C., KRIZ, W., SHAW, A. S., HOLZMAN, L. B. & MUNDEL, P. 2001. Podocin, a raft-associated component of the glomerular slit diaphragm, interacts with CD2AP and nephrin. J Clin Invest, 108, 1621-9.
274. SCURT, F. G., MENNE, J., BRANDT, S., BERNHARDT, A., MERTENS, P. R., HALLER, H., CHATZIKYRKOU, C. & COMMITTEE, R. S. 2019. Systemic Inflammation Precedes Microalbuminuria in Diabetes. Kidney Int Rep, 4, 1373-1386.
275. SHANKLAND, S. J. & WOLF, G. 2000. Cell cycle regulatory proteins in renal disease: role in hypertrophy, proliferation, and apoptosis. Am J Physiol Renal Physiol, 278, F515-29.
276. SHI, Y. & VANHOUTTE, P. M. 2017. Macro- and microvascular endothelial dysfunction in diabetes. J Diabetes, 9, 434-449.
277. SHIH, N. Y., LI, J., COTRAN, R., MUNDEL, P., MINER, J. H. & SHAW, A. S. 2001. CD2AP localizes to the slit diaphragm and binds to nephrin via a novel C-terminal domain. Am J Pathol, 159, 2303-8.
278. SHIMOMURA, H. & SPIRO, R. G. 1987. Studies on Macromolecular Components of Human Glomerular Basement Membrane and Alterations in Diabetes: Decreased Levels of Heparan Sulfate Proteoglycan and Laminin. Diabetes, 36, 374-381.
279. SIES, H. 2000. WHAT IS OXIDATIVE STRESS?
280. SINGH, A., FRIDÉN, V., DASGUPTA, I., FOSTER, R. R., WELSH, G. I., TOOKE, J. E., HARALDSSON, B., MATHIESON, P. W. & SATCHELL, S. C. 2011. High glucose causes dysfunction of the human glomerular endothelial glycocalyx. American Journal of Physiology-Renal Physiology, 300, F40-F48.
281. SLAMENOVA, D., KOZICS, K., HUNAKOVA, L., MELUSOVA, M., NAVAROVA, J. & HORVATHOVA, E. 2013. Comparison of biological processes induced in HepG2 cells by tert-butyl hydroperoxide (t-BHP) and hydroperoxide (H2O2): The influence of carvacrol. Mutat Res, 757, 15-22.

282. SLYNE, J., SLATTERY, C., MCMORROW, T. & RYAN, M. P. 2015. New developments concerning the proximal tubule in diabetic nephropathy: in vitro models and mechanisms. Nephrol Dial Transplant, 30 Suppl 4, iv60-7.
283. SMITH, M. A., PERRY, G., RICHEY, P. L., SAYRE, L. M., ANDERSON, V. E., BEAL, M. F. & KOWALL, N. 1996. Oxidative damage in Alzheimer's. Nature, 382, 120-1.
284. SMOYER, W. E. & MUNDEL, P. 1998. Regulation of podocyte structure during the development of nephrotic syndrome. J Mol Med (Berl), 76, 172-83.
285. SOLA, M., , MAGRIN, C., , PEDRIOLI, G., , PINTON, S., , SALVADÈ, A., , PAPIN, S., , PAGANETTI, P. & 2020a. Tau affects P53 function and cell fate during the DNA damage response. Nature Research.
286. SOLA, M., MAGRIN, C., PEDRIOLI, G., PINTON, S., SALVADÈ, A., PAPIN, S. & PAGANETTI, P. 2020b. Tau affects P53 function and cell fate during the DNA damage response. Communications Biology, 3.
287. SPAGNUOLO, M. & BLENNER, M. 2021. Gene Excision by Dual-Guide CRISPR-Cas9. Methods Mol Biol, 2307, 85-94.
288. SPRITZ, R. A., STRUNK, K., SUROWY, C. S., HOCH, S. O., BARTON, D. E. & FRANCKE, U. 1987. The human U1-70K snRNP protein: cDNA cloning, chromosomal localization, expression, alternative splicing and RNA-binding. Nucleic Acids Research, 15, 10373-10391.
289. STEIN, B. & YANG, M. X. 1995. Repression of the interleukin-6 promoter by estrogen receptor is mediated by NF-kappa B and C/EBP beta. Molecular and Cellular Biology, 15, 4971-4979.
290. STORMO, C., KRINGEN, M. K., GRIMHOLT, R. M., BERG, J. P. & PIEHLER, A. P. 2012. A novel 3-hydroxy-3-methylglutaryl-coenzyme A reductase (HMGCR) splice variant with an alternative exon 1 potentially encoding an extended N-terminus. BMC Mol Biol, 13, 29.
291. STRIMMER, K. 2008. fdrtool: a versatile R package for estimating local and tail area-based false discovery rates. Bioinformatics, 24, 1461-2.
292. STROBERG, W. & SCHNELL, S. 2017. On the origin of non-membrane-bound organelles, and their physiological function. Journal of Theoretical Biology, 434, 42-49.
293. SUD, R., , GELLER, E. T., , SCHELLENBERG, G. D. & 2014a. Antisense-mediated exon skipping decreases Tau protein expression: A potential therapy for tauopathies. Nature Publishing Group.
294. SUD, R., GELLER, E. T. & SCHELLENBERG, G. D. 2014b. Antisense-mediated exon skipping decreases Tau protein expression: A potential therapy for tauopathies. Molecular Therapy - Nucleic Acids, 3.
295. SUGAHARA, M., PAK, W. L. W., TANAKA, T., TANG, S. C. W. & NANGAKU, M. 2021. Update on diagnosis, pathophysiology, and management of diabetic kidney disease. Nephrology (Carlton), 26, 491-500.
296. SULTAN, A., NESSLANY, F., VIOLET, M., BÉGARD, S., LOYENS, A., TALAHARI, S., MANSUROGLU, Z., MARZIN, D., SERGEANT, N., HUMEZ, S., COLIN, M., BONNEFOY, E., BUÉE, L. & GALAS, M. C. 2011. Nuclear Tau, a key player in neuronal DNA protection. Journal of Biological Chemistry, 286, 4566-4575.
297. SUN, H., SAEEDI, P., KARURANGA, S., PINKEPANK, M., OGURTSOVA, K., DUNCAN, B. B., STEIN, C., BASIT, A., CHAN, J. C. N., MBANYA, J. C., PAVKOV, M. E., RAMACHANDARAN, A., WILD, S. H., JAMES, S., HERMAN, W. H., ZHANG, P., BOMMER, C., KUO, S., BOYKO, E. J. & MAGLIANO, D. J. 2022. IDF Diabetes Atlas: Global, regional and country-level diabetes prevalence estimates for 2021 and projections for 2045. Diabetes Res Clin Pract, 183, 109119.

298. SUN, M., SONG, H., YE, Y., YANG, Q., XU, X., ZHU, X., ZHANG, J., SHI, S., WANG, J. & LIU, Z. 2019. Differential toxicities of triptolide to immortalized podocytes and the podocytes in vivo. Biomed Pharmacother, 109, 2375-2386.
299. SUSZTAK, K., RAFF, A. C., SCHIFFER, M. & BOTTINGER, E. P. 2006. Glucose-induced reactive oxygen species cause apoptosis of podocytes and podocyte depletion at the onset of diabetic nephropathy. Diabetes, 55, 225-33.
300. SYNTHEGO 2019. Synthego Performance Analysis.
301. SZABADFI, K., PINTER, E., REGLODI, D. & GABRIEL, R. 2014. Neuropeptides, trophic factors, and other substances providing morphofunctional and metabolic protection in experimental models of diabetic retinopathy. Int Rev Cell Mol Biol, 311, 1-121.
302. TAKASATO, M., ER, P. X., CHIU, H. S. & LITTLE, M. H. 2016. Generation of kidney organoids from human pluripotent stem cells. Nat Protoc, 11, 1681-92.
303. TAKASATO, M., ER, P. X., CHIU, H. S., MAIER, B., BAILLIE, G. J., FERGUSON, C., PARTON, R. G., WOLVETANG, E. J., ROOST, M. S., CHUVA DE SOUSA LOPES, S. M. & LITTLE, M. H. 2015. Kidney organoids from human iPS cells contain multiple lineages and model human nephrogenesis. Nature, 526, 564-8.
304. TAN, Y., WANG, B., KEUM, J. S. & JAFFA, A. A. 2005. Mechanisms through which bradykinin promotes glomerular injury in diabetes. Am J Physiol Renal Physiol, 288, F483-92.
305. TANG, S. C. W. & YIU, W. H. 2020. Innate immunity in diabetic kidney disease. Nat Rev Nephrol, 16, 206-222.
306. TANG, S., LEUNG, J. C., ABE, K., CHAN, K. W., CHAN, L. Y., CHAN, T. M. & LAI, K. N. 2003. Albumin stimulates interleukin-8 expression in proximal tubular epithelial cells in vitro and in vivo. J Clin Invest, 111, 515-27.
307. TANG, W. H., MARTIN, K. A. & HWA, J. 2012. Aldose reductase, oxidative stress, and diabetic mellitus. Front Pharmacol, 3, 87.
308. TEO, Z. L., THAM, Y. C., YU, M., CHEE, M. L., RIM, T. H., CHEUNG, N., BIKBOV, M. M., WANG, Y. X., TANG, Y., LU, Y., WONG, I. Y., TING, D. S. W., TAN, G. S. W., JONAS, J. B., SABANAYAGAM, C., WONG, T. Y. & CHENG, C. Y. 2021. Global Prevalence of Diabetic Retinopathy and Projection of Burden through 2045: Systematic Review and Meta-analysis. Ophthalmology, 128, 1580-1591.
309. TERADA, S., ISHIZU, H., ISHIGURO, K., TANABE, Y., ITOH, N., YASUTAKE, K., FURUBAYASHI, A., KITAMURA, Y. & KURODA, S. 2005. Exon 3 insert of tau protein in neurodegenerative diseases. Acta Neuropathologica, 110, 12-18.
310. THAKORE, P. I., D'IPPOLITO, A. M., SONG, L., SAFI, A., SHIVAKUMAR, N. K., KABADI, A. M., REDDY, T. E., CRAWFORD, G. E. & GERSBACH, C. A. 2015. Highly specific epigenome editing by CRISPR-Cas9 repressors for silencing of distal regulatory elements. Nat Methods, 12, 1143-9.
311. THE, E.-K. C. G., HERRINGTON, W. G., STAPLIN, N., WANNER, C., GREEN, J. B., HAUSKE, S. J., EMBERSON, J. R., PREISS, D., JUDGE, P., MAYNE, K. J., NG, S. Y. A., SAMMONS, E., ZHU, D., HILL, M., STEVENS, W., WALLENDSZUS, K., BRENNER, S., CHEUNG, A. K., LIU, Z. H., LI, J., HOOI, L. S., LIU, W., KADOWAKI, T., NANGAKU, M., LEVIN, A., CHERNEY, D., MAGGIONI, A. P., PONTREMOLI, R., DEO, R., GOTO, S., ROSSELLO, X., TUTTLE, K. R., STEUBL, D., PETRINI, M., MASSEY, D., EILBRACHT, J., BRUECKMANN, M., LANDRAY, M. J., BAIGENT, C. & HAYNES, R. 2023. Empagliflozin in Patients with Chronic Kidney Disease. N Engl J Med, 388, 117-127.
312. THORVALDSDOTTIR, H., ROBINSON, J. T. & MESIROV, J. P. 2013. Integrative Genomics Viewer (IGV): high-performance genomics data visualization and exploration. Brief Bioinform, 14, 178-92.

313. TONNEIJCK, L., MUSKIET, M. H. A., SMITS, M. M., VAN BOMMEL, E. J., HEERSPINK, H. J. L., VAN RAALTE, D. H. & JOLES, J. A. 2017. Glomerular Hyperfiltration in Diabetes: Mechanisms, Clinical Significance, and Treatment. Journal of the American Society of Nephrology : JASN, 28, 1023-1039.
314. TOYODA, M., NAJAFIAN, B., KIM, Y., CARAMORI, M. L. & MAUER, M. 2007. Podocyte detachment and reduced glomerular capillary endothelial fenestration in human type 1 diabetic nephropathy. Diabetes, 56, 2155-2160.
315. TRABZUNI, D., WRAY, S., VANDROVCOVA, J., RAMASAMY, A., WALKER, R., SMITH, C., LUK, C., GIBBS, J. R., DILLMAN, A., HERNANDEZ, D. G., AREPALLI, S., SINGLETON, A. B., COOKSON, M. R., PITTMAN, A. M., DE SILVA, R., WEALE, M. E., HARDY, J. & RYTEN, M. 2012. MAPT expression and splicing is differentially regulated by brain region: Relation to genotype and implication for tauopathies. Human Molecular Genetics, 21, 4094-4103.
316. TRIPATHI, B. K., ANDERMAN, M. F., BHARGAVA, D., BOCCUZZI, L., QIAN, X., WANG, D., DURKIN, M. E., PAPAGEORGE, A. G., DE MIGUEL, F. J., POLITI, K., WALTERS, K. J., DOROSHOW, J. H. & LOWY, D. R. 2021. Inhibition of cytoplasmic EZH2 induces antitumor activity through stabilization of the DLC1 tumor suppressor protein. Nat Commun, 12, 6941.
317. TRONCOSO BRINDEIRO, C. M., FALLET, R. W., LANE, P. H. & CARMINES, P. K. 2008. Potassium channel contributions to afferent arteriolar tone in normal and diabetic rat kidney. American journal of physiology. Renal physiology, 295, F171-8.
318. TSAI, R. M., MILLER, Z., KOESTLER, M., ROJAS, J. C., LJUBENKOV, P. A., ROSEN, H. J., RABINOVICI, G. D., FAGAN, A. M., COBIGO, Y., BROWN, J. A., JUNG, J. I., HARE, E., GELDMACHER, D. S., NATELSON-LOVE, M., MCKINLEY, E. C., LUONG, P. N., CHUU, E. L., POWERS, R., MUMFORD, P., WOLF, A., WANG, P., SHAMLOO, M., MILLER, B. L., ROBERSON, E. D. & BOXER, A. L. 2020. Reactions to Multiple Ascending Doses of the Microtubule Stabilizer TPI-287 in Patients with Alzheimer Disease, Progressive Supranuclear Palsy, and Corticobasal Syndrome: A Randomized Clinical Trial. JAMA Neurology, 77, 215-224.
319. TULADHAR, R., YEU, Y., TYLER PIAZZA, J., TAN, Z., RENE CLEMENCEAU, J., WU, X., BARRETT, Q., HERBERT, J., MATHEWS, D. H., KIM, J., HYUN HWANG, T. & LUM, L. 2019. CRISPR-Cas9-based mutagenesis frequently provokes on-target mRNA misregulation. Nature Communications, 10.
320. TURNER, D. J. & TURNER, M. 2021. RNA Binding Proteins As Regulators of Oxidative Stress Identified by a Targeted CRISPR-Cas9 Single Guide RNA Library. CRISPR J, 4, 427-437.
321. UHLEN, M., FAGERBERG, L., HALLSTROM, B. M., LINDSKOG, C., OKSVOLD, P., MARDINOGLU, A., SIVERTSSON, A., KAMPF, C., SJOSTEDT, E., ASPLUND, A., OLSSON, I., EDLUND, K., LUNDBERG, E., NAVANI, S., SZIGYARTO, C. A., ODEBERG, J., DJUREINOVIC, D., TAKANEN, J. O., HOBER, S., ALM, T., EDQVIST, P. H., BERLING, H., TEGEL, H., MULDER, J., ROCKBERG, J., NILSSON, P., SCHWENK, J. M., HAMSTEN, M., VON FEILITZEN, K., FORSBERG, M., PERSSON, L., JOHANSSON, F., ZWAHLEN, M., VON HEIJNE, G., NIELSEN, J. & PONTEN, F. 2015. Proteomics. Tissue-based map of the human proteome. Science, 347, 1260419.
322. VALEN, G., SONDÉN, A., VAAGE, J., MALM, E., THOMAS, B. & KJELLSTR¨OM, K. O. 1999. Original Contribution HYDROGEN PEROXIDE INDUCES ENDOTHELIAL CELL ATYPIA AND CYTOSKELETON DEPOLYMERIZATION.
323. VALLES-SAIZ, L., PEINADO-CAHUCHOLA, R., AVILA, J. & HERNANDEZ, F. 2022. Microtubule-associated protein tau in murine kidney: role in podocyte architecture. Cell Mol Life Sci, 79, 97.

324. VAN DEN BERG, C. W., KOUDIJS, A., RITSMA, L. & RABELINK, T. J. 2020. In Vivo Assessment of Size-Selective Glomerular Sieving in Transplanted Human Induced Pluripotent Stem Cell-Derived Kidney Organoids. J Am Soc Nephrol, 31, 921-929.
325. VAN ZUYDAM, N. R., AHLQVIST, E., SANDHOLM, N., DESHMUKH, H., RAYNER, N. W., ABDALLA, M., LADENVALL, C., ZIEMEK, D., FAUMAN, E., ROBERTSON, N. R., MCKEIGUE, P. M., VALO, E., FORSBLOM, C., HARJUTSALO, V., FINNISH DIABETIC NEPHROPATHY, S., PERNA, A., RURALI, E., MARCOVECCHIO, M. L., IGO, R. P., JR., SALEM, R. M., PERICO, N., LAJER, M., KARAJAMAKI, A., IMAMURA, M., KUBO, M., TAKAHASHI, A., SIM, X., LIU, J., VAN DAM, R. M., JIANG, G., TAM, C. H. T., LUK, A. O. Y., LEE, H. M., LIM, C. K. P., SZETO, C. C., SO, W. Y., CHAN, J. C. N., HONG KONG DIABETES REGISTRY THEME-BASED RESEARCH SCHEME PROJECT, G., ANG, S. F., DORAJOO, R., WANG, L., CLARA, T. S. H., MCKNIGHT, A. J., DUFFY, S., WARREN, GENETICS OF KIDNEYS IN DIABETES STUDY, G., PEZZOLESI, M. G., CONSORTIUM, G., MARRE, M., GYORGY, B., HADJADJ, S., HIRAKI, L. T., DIABETES, C., COMPLICATIONS TRIAL /EPIDEMIOLOGY OF DIABETES, I., COMPLICATIONS RESEARCH, G., AHLUWALIA, T. S., ALMGREN, P., SCHULZ, C. A., ORHO-MELANDER, M., LINNEBERG, A., CHRISTENSEN, C., WITTE, D. R., GRARUP, N., BRANDSLUND, I., MELANDER, O., PATERSON, A. D., TREGOUET, D., MAXWELL, A. P., LIM, S. C., MA, R. C. W., TAI, E. S., MAEDA, S., LYSSENKO, V., TUOMI, T., KROLEWSKI, A. S., RICH, S. S., HIRSCHHORN, J. N., FLOREZ, J. C., DUNGER, D., PEDERSEN, O., HANSEN, T., ROSSING, P., REMUZZI, G., MICRO, S. U. M. F., MACROVASCULAR HARD ENDPOINTS FOR INNOVATIVE DIABETES TOOLS, C., BROSNAN, M. J., PALMER, C. N. A., GROOP, P. H., COLHOUN, H. M., GROOP, L. C. & MCCARTHY, M. I. 2018. A Genome-Wide Association Study of Diabetic Kidney Disease in Subjects With Type 2 Diabetes. Diabetes, 67, 1414-1427.
326. VANDERWEYDE, T., APICCO, D. J., YOUMANS-KIDDER, K., ASH, P. E. A., COOK, C., LUMMERTZ DA ROCHA, E., JANSEN-WEST, K., FRAME, A. A., CITRO, A., LESZYK, J. D., IVANOV, P., ABISAMBRA, J. F., STEFFEN, M., LI, H., PETRUCELLI, L. & WOLOZIN, B. 2016. Interaction of tau with the RNA-Binding Protein TIA1 Regulates tau Pathophysiology and Toxicity. Cell Reports, 15, 1455-1466.
327. VANDERWEYDE, T., YU, H., VARNUM, M., LIU-YESUCEVITZ, L., CITRO, A., IKEZU, T., DUFF, K. & WOLOZIN, B. 2012. Contrasting pathology of the stress granule proteins TIA-1 and G3BP in Tauopathies. Journal of Neuroscience, 32, 8270-8283.
328. VERZOLA, D., CAPPUCCINO, L., D'AMATO, E., VILLAGGIO, B., GIANIORIO, F., MIJ, M., SIMONATO, A., VIAZZI, F., SALVIDIO, G. & GARIBOTTO, G. 2014. Enhanced glomerular Toll-like receptor 4 expression and signaling in patients with type 2 diabetic nephropathy and microalbuminuria. Kidney Int, 86, 1229-43.
329. VIERBUCHEN, T., AGARWAL, S., JOHNSON, J. L., GALIA, L., LEI, X., STEIN, K., OLAGNIER, D., GAEDE, K. I., HERZMANN, C., HOLM, C. K., HEINE, H., PAI, A., O'HARA HALL, A., HOEBE, K. & FITZGERALD, K. A. 2023. The lncRNA LUCAT1 is elevated in inflammatory disease and restrains inflammation by regulating the splicing and stability of NR4A2. Proc Natl Acad Sci U S A, 120, e2213715120.
330. VIOLET, M., DELATTRE, L., TARDIVEL, M., SULTAN, A., CHAUDERLIER, A., CAILLIEREZ, R., TALAHARI, S., NESSLANY, F., LEFEBVRE, B., BONNEFOY, E., BUEE, L. & GALAS, M. C. 2014. A major role for Tau in neuronal DNA and RNA protection in vivo under physiological and hyperthermic conditions. Front Cell Neurosci, 8, 84.

331. VOLPE, C. M. O., VILLAR-DELFINO, P. H., DOS ANJOS, P. M. F. & NOGUEIRA-MACHADO, J. A. 2018. Cellular death, reactive oxygen species (ROS) and diabetic complications. Cell Death Dis, 9, 119.
332. WADA, T., TOMOSUGI, N., NAITO, T., YOKOYAMA, H., KOBAYASHI, K., HARADA, A., MUKAIDA, N. & MATSUSHIMA, K. 1994. Prevention of proteinuria by the administration of anti-interleukin 8 antibody in experimental acute immune complex-induced glomerulonephritis. J Exp Med, 180, 1135-40.
333. WAGNER, B. A., WITMER, J. R., VAN 'T ERVE, T. J. & BUETTNER, G. R. 2013. An Assay for the Rate of Removal of Extracellular Hydrogen Peroxide by Cells. Redox Biol, 1, 210-217.
334. WANG, G., LAI, F. M.-M., LAI, K.-B., CHOW, K.-M., KWAN, B. C.-H., LI, P. K.-T. & SZETO, C.-C. 2008. Urinary messenger RNA expression of podocyte-associated molecules in patients with diabetic nephropathy treated by angiotensin-converting enzyme inhibitor and angiotensin receptor blocker. European Journal of Endocrinology, 158, 317-322.
335. WANG, J., SHEN, X., LIU, J., CHEN, W., WU, F., WU, W., MENG, Z., ZHU, M. & MIAO, C. 2020. High glucose mediates NLRP3 inflammasome activation via upregulation of ELF3 expression. Cell Death Dis, 11, 383.
336. WANG, L., TAO, T., SU, W., YU, H., YU, Y. & QIN, J. 2017. A disease model of diabetic nephropathy in a glomerulus-on-a-chip microdevice. Lab Chip, 17, 1749-1760.
337. WANG, X., CAMPBELL, M. R., LACHER, S. E., CHO, H. Y., WAN, M., CROWL, C. L., CHORLEY, B. N., BOND, G. L., KLEEBERGER, S. R., SLATTERY, M. & BELL, D. A. 2016a. A Polymorphic Antioxidant Response Element Links NRF2/sMAF Binding to Enhanced MAPT Expression and Reduced Risk of Parkinsonian Disorders. Cell Reports, 15, 830-842.
338. WANG, X., CAMPBELL, M. R., LACHER, S. E., CHO, H. Y., WAN, M., CROWL, C. L., CHORLEY, B. N., BOND, G. L., KLEEBERGER, S. R., SLATTERY, M. & BELL, D. A. 2016b. A Polymorphic Antioxidant Response Element Links NRF2/sMAF Binding to Enhanced MAPT Expression and Reduced Risk of Parkinsonian Disorders. Cell Rep, 15, 830-842.
339. WANG, Y. & MANDELKOW, E. 2016. Tau in physiology and pathology. Nat Rev Neurosci, 17, 5-21.
340. WANG, Y. J., WANG, X. Y., HAO, X. Y., YAN, Y. M., HONG, M., WEI, S. F., ZHOU, Y. L., WANG, Q., CHENG, Y. X. & LIU, Y. Q. 2019. Ethanol Extract of Centipeda minima Exerts Antioxidant and Neuroprotective Effects via Activation of the Nrf2 Signaling Pathway. Oxid Med Cell Longev, 2019, 9421037.
341. WANNER, N., HARTLEBEN, B., HERBACH, N., GOEDEL, M., STICKEL, N., ZEISER, R., WALZ, G., MOELLER, M. J., GRAHAMMER, F. & HUBER, T. B. 2014. Unraveling the role of podocyte turnover in glomerular aging and injury. J Am Soc Nephrol, 25, 707-16.
342. WEDEL, S., MARTIC, I., HRAPOVIC, N., FABRE, S., MADREITER-SOKOLOWSKI, C. T., HALLER, T., PIERER, G., PLONER, C., JANSEN-DURR, P. & CAVINATO, M. 2020. tBHP treatment as a model for cellular senescence and pollution-induced skin aging. Mech Ageing Dev, 190, 111318.
343. WEI, M., GASKILL, S. P., HAFFNER, S. M. & STERN, M. P. 1998. Effects of diabetes and level of glycemia on all-cause and cardiovascular mortality. The San Antonio Heart Study. Diabetes Care, 21, 1167-72.
344. WEI, Y., QU, M. H., WANG, X. S., CHEN, L., WANG, D. L., LIU, Y., HUA, Q. & HE, R. Q. 2008. Binding to the minor groove of the double-strand, Tau protein prevents DNA damage by peroxidation. PLoS ONE, 3.

345. WEIL, E. J., LEMLEY, K. V., MASON, C. C., YEE, B., JONES, L. I., BLOUCH, K., LOVATO, T., RICHARDSON, M., MYERS, B. D. & NELSON, R. G. 2012. Podocyte detachment and reduced glomerular capillary endothelial fenestration promote kidney disease in type 2 diabetic nephropathy. Kidney International, 82, 1010-1017.
346. WEINGARTEN, M. D., LOCKWOOD, A. H., HWO, S.-Y. & KIRSCHNER, M. W. 1975. A Protein Factor Essential for Microtubule Assembly (tau factor/tubulin/electron microscopy/phosphocellulose).
347. WELSH, G. I. & SALEEM, M. A. 2011. The podocyte cytoskeleton--key to a functioning glomerulus in health and disease. Nat Rev Nephrol, 8, 14-21.
348. WEST, J. A., MITO, M., KUROSAKA, S., TAKUMI, T., TANEGASHIMA, C., CHUJO, T., YANAKA, K., KINGSTON, R. E., HIROSE, T., BOND, C., FOX, A. & NAKAGAWA, S. 2016. Structural, super-resolution microscopy analysis of paraspeckle nuclear body organization. Journal of Cell Biology, 214.
349. WHICHER, C. A., O'NEILL, S. & HOLT, R. I. G. 2020. Diabetes in the UK: 2019. Diabet Med, 37, 242-247.
350. WILSON, S. B., HOWDEN, S. E., VANSLAMBROUCK, J. M., DORISON, A., ALQUICIRA-HERNANDEZ, J., POWELL, J. E. & LITTLE, M. H. 2022. DevKidCC allows for robust classification and direct comparisons of kidney organoid datasets. Genome Med, 14, 19.
351. WOLFF, S. P. & DEAN, R. T. 1987. Glucose autoxidation and protein modification. The potential role of 'autoxidative glycosylation' in diabetes. Biochem J, 245, 243-50.
352. WOLOZIN, B. & IVANOV, P. 2019. Stress granules and neurodegeneration. Nat Rev Neurosci, 20, 649-666.
353. WRIGHT, M. M., KIM, J., HOCK, T. D., LEITINGER, N., FREEMAN, B. A. & AGARWAL, A. 2009. Human haem oxygenase-1 induction by nitro-linoleic acid is mediated by cAMP, AP-1 and E-box response element interactions. Biochem J, 422, 353-61.
354. WU, H., KIRITA, Y., DONNELLY, E. L. & HUMPHREYS, B. D. 2019. Advantages of Single-Nucleus over Single-Cell RNA Sequencing of Adult Kidney: Rare Cell Types and Novel Cell States Revealed in Fibrosis. J Am Soc Nephrol, 30, 23-32.
355. WU, H., UCHIMURA, K., DONNELLY, E. L., KIRITA, Y., MORRIS, S. A. & HUMPHREYS, B. D. 2018. Comparative Analysis and Refinement of Human PSC-Derived Kidney Organoid Differentiation with Single-Cell Transcriptomics. Cell Stem Cell, 23, 869-881 e8.
356. XIE, Z., BAILEY, A., KULESHOV, M. V., CLARKE, D. J. B., EVANGELISTA, J. E., JENKINS, S. L., LACHMANN, A., WOJCIECHOWICZ, M. L., KROPIWNICKI, E., JAGODNIK, K. M., JEON, M. & MA'AYAN, A. 2021. Gene Set Knowledge Discovery with Enrichr. Curr Protoc, 1, e90.
357. XU, R., SONG, J., RUZE, R., CHEN, Y., YIN, X., WANG, C. & ZHAO, Y. 2023. SQLE promotes pancreatic cancer growth by attenuating ER stress and activating lipid rafts-regulated Src/PI3K/Akt signaling pathway. Cell Death Dis, 14, 497.
358. YAMAZAKI, S., YAMAJI, T., MURAI, N., YAMAMOTO, H., MATSUDA, T., PRICE, R. D. & MATSUOKA, N. 2012. FK1706, a novel non-immunosuppressive immunophilin ligand, modifies gene expression in the dorsal root ganglia during painful diabetic neuropathy. Neurol Res, 34, 469-77.
359. YANG, S., LI, S. & LI, X. J. 2018. Shortening the Half-Life of Cas9 Maintains Its Gene Editing Ability and Reduces Neuronal Toxicity. Cell Rep, 25, 2653-2659 e3.
360. YARIBEYGI, H., FARROKHI, F. R., BUTLER, A. E. & SAHEBKAR, A. 2019. Insulin resistance: Review of the underlying molecular mechanisms. J Cell Physiol, 234, 8152-8161.

361. YE, J., BEETZ, N., O'KEEFFE, S., TAPIA, J. C., MACPHERSON, L., CHEN, W. V., BASSEL-DUBY, R., OLSON, E. N. & MANIATIS, T. 2015. HnRNP U protein is required for normal pre-mRNA splicing and postnatal heart development and function. Proceedings of the National Academy of Sciences of the United States of America, 112, E3020-E3029.
362. YI, S. A., ZHANG, Y., RATHNAM, C., PONGKULAPA, T. & LEE, K. B. 2021. Bioengineering Approaches for the Advanced Organoid Research. Adv Mater, 33, e2007949.
363. YIM, M. B., YIM, H. S., LEE, C., KANG, S. O. & CHOCK, P. B. 2001. Protein glycation: creation of catalytic sites for free radical generation. Ann N Y Acad Sci, 928, 48-53.
364. YIN, H. & PORTER, N. A. 2003. Specificity of the ferrous oxidation of xylenol orange assay: Analysis of autoxidation products of cholesteryl arachidonate. Analytical Biochemistry, 313, 319-326.
365. YU, T., ROBOTHAM, J. L. & YOON, Y. 2006. Increased production of reactive oxygen species in hyperglycemic conditions requires dynamic change of mitochondrial morphology. Proc Natl Acad Sci U S A, 103, 2653-8.
366. ZAINUDDIN, A., CHUA, K. H., ABDUL RAHIM, N. & MAKPOL, S. 2010. Effect of experimental treatment on GAPDH mRNA expression as a housekeeping gene in human diploid fibroblasts. BMC Mol Biol, 11, 59.
367. ZANG, H., MATHEW, R. O. & CUI, T. 2020. The Dark Side of Nrf2 in the Heart. Frontiers in Physiology. Frontiers Media S.A.
368. ZAVODNIK, L. B., ZAVODNIK, I. B., NIEKURZAK, A., SZOSLAND, K. & BRYSZEWSKA, M. 1998. Activation of red blood cell glutathione peroxidase and morphological transformation of erythrocytes under the action of tert-butyl hydroperoxide. Biochem Mol Biol Int, 44, 577-88.
369. ZHANG, P., LIU, X., LI, H., CHEN, Z., YAO, X., JIN, J. & MA, X. 2017. TRPC5-induced autophagy promotes drug resistance in breast carcinoma via CaMKKbeta/AMPKalpha/mTOR pathway. Sci Rep, 7, 3158.
370. ZHANG, Y., WU, K. M., YANG, L., DONG, Q. & YU, J. T. 2022. Tauopathies: new perspectives and challenges. Mol Neurodegener, 17, 28.
371. ZHAO, H. J., WANG, S., CHENG, H., ZHANG, M. Z., TAKAHASHI, T., FOGO, A. B., BREYER, M. D. & HARRIS, R. C. 2006. Endothelial nitric oxide synthase deficiency produces accelerated nephropathy in diabetic mice. J Am Soc Nephrol, 17, 2664-9.
372. ZHAO, Y., ZENG, X., TANG, H., YE, D. & LIU, J. 2019. Combination of metformin and paclitaxel suppresses proliferation and induces apoptosis of human prostate cancer cells via oxidative stress and targeting the mitochondria-dependent pathway. Oncology Letters, 17, 4277-4284.
373. ZHOU, Y., CHANG, D. Y., LI, J., SHAN, Y., HUANG, X. Y., ZHANG, F., LUO, Q., XIONG, Z. Y., ZHAO, M. H., HOU, S. & CHEN, M. 2022. The role of Kimmelstiel-Wilson nodule in the kidney outcome in patients with diabetic kidney disease: A two-center retrospective cohort study. Diabetes Research and Clinical Practice, 190.
374. ZIEGLER, V., FREMTER, K., HELMCHEN, J., WITZGALL, R. & CASTROP, H. 2021. Mesangial cells regulate the single nephron GFR and preserve the integrity of the glomerular filtration barrier: An intravital multiphoton microscopy study. Acta Physiol (Oxf), 231, e13592.
375. ØSTERBY, R. 1972. Morphometric studies of the peripheral glomerular basement membrane in early juvenile diabetes I. Development of initial basement membrane thickening. Diabetologia, 8, 84-92.